Early Metal Complexes of Rigid Dianionic Ligands

Rare Earth and Group 4 Transition Metal Complexes of Rigid Dianionic Pincer Ligands

By

Kelly Sarah Anne Motolko, B.Sc. (Hons.)

A Thesis

Submitted to the School of Graduate Studies

in Partial Fulfilment of the Requirements

for the Degree

Doctor of Philosophy of Science

McMaster University

Doctor of Philosophy of Science (2017) McMaster University
(Department of Chemistry and Chemical Biology) Hamilton, Ontario

TITLE: Rare Earth and Group 4 Transition Metal Complexes of Rigid Dianionic Pincer Ligands

AUTHOR: Kelly Motolko, B.Sc. (Hons.)

SUPERVISOR: Dr. David J. H. Emslie

NUMBER OF PAGES: xlii, 191

Lay Abstract

Pincer ligands are defined as meridionally-coordinating tridentate ligands, and are typically mono-, di- or tri-anionic. This thesis is focused on the synthesis and reactivity of rigid dianionic pincer ligands with an NON- or POP-donor array, with particular emphasis on rare earth and group 4 transition metal complexes. This work explores the effect that these rigid ligands have on the reactivity of the resulting metal complexes and the thermal stability of the solid state structures. Both neutral and cationic mono alkyl complexes have been isolated, and several are highly active catalysts for intra- and intermolecular hydroamination or ethylene polymerization.

Abstract

The synthesis and electropositive metal (Y, Lu, La, Zr, Hf) chemistry of two rigid dianionic xanthene-based ligands, 4,5-bis(2,4,6-triisopropylanilido)--2,7-di-*tert*-butyl-9,9-dimethylxanthene (XN_2) and 4,5-bis(2,4,6-triisopropylphenylphosphido)-2,7-di-*tert*-butyl-9,9-dimethylxanthene (XP_2) have been explored.

The reaction of the pro-ligand H_2XN_2 with $[Y(CH_2SiMe_2R)_3(THF)_2]$ (R = Me or Ph) produced the monoalkyl yttrium complexes $[(XN_2)Y(CH_2SiMe_3)(THF)]\cdot(O(SiMe_3)_2)_x$ (**3**, x = 1-1.5) and $[(XN_2)Y(CH_2SiMe_2Ph)(THF)]\cdot(O(SiMe_3)_2)$ (**4**). Neutral **3** reacted with excess $AlMe_3$ to yield $[(XN_2)Y\{(\mu\text{-}Me)_2AlMe_2\}(THF)]\cdot O(SiMe_3)_2$ (**5**$\cdot O(SiMe_3)_2$), which is thermally robust, and transfer of the XN_2 ligand to aluminum was not observed. However, $[(XN_2)AlMe]\cdot(O(SiMe_3)_2)_{0.5}$ (**6**$\cdot(O(SiMe_3)_2)_{0.5}$) was synthesized via the reaction of H_2XN_2 with $AlMe_3$. Compounds **3**, **5** and **6** were characterized by X-ray crystallography, and neutral **3**, while being poorly active for ethylene polymerization, was highly active for both intra- and inter-molecular hydroamination with a variety of substrates.

The synthesis of the pro-ligand H_2XP_2 was achieved via reduction of 4,5--bis(2,4,6-triisopropylphenylchlorophosphino)-2,7-di-*tert*-butyl-9,9-dimethylxanthene (XP_2Cl_2; **7**). Double deprotonation of H_2XP_2 (**8**) with excess KH yielded the potassium salt, $[K_2XP_2(DME)_{2.5}]$ (**9**), which when stirred in THF followed by recrystallization from hexanes, produced the tetrametallic complex, $[K_4(XP_2)_2(THF)_4]$ (**10**) featuring a central K_4P_4 cage. The reaction of $[K_2XP_2(DME)_{2.5}]$ (**9**) with $[YI_3(THF)_{3.5}]$ yielded a mixture of products

including $[(XP_2)YI(THF)_2]$ (**11**) and tris(2,4,6-triisopropylphenylphosphinidene) (P_3Tripp_3); pure **11** could be isolated in low yield by extraction with a minimum volume of hexanes or $O(SiMe_3)_2$. In the solid state, complex **11** reveals a face-capped trigonal bipyramidal geometry at yttrium, in which the xanthene backbone is planar and adopts a large angle (85°) between the P(1)/C(4)/C(5)/P(2) and P(1)/Y/P(2) planes.

Due to the successful synthesis and hydroamination catalysis achieved with the XN_2 ligand in combination with yttrium, the chemistry of XN_2 was further explored using both smaller (Lu) and larger (La) rare earth elements. The alkane elimination reaction of H_2XN_2 with $[Lu(CH_2SiMe_3)_3(THF)_2]$, followed by crystallization from $O(SiMe_3)_2$, yielded $[(XN_2)Lu(CH_2SiMe_3)(THF)]\cdot(O(SiMe_3)_2)_{1.5}$ (**12**$\cdot(O(SiMe_3)_2)_{1.5}$). By contrast, lanthanum complexes of the XN_2 dianion were prepared by salt metathesis; treatment of H_2XN_2 with excess KH in DME produced the dipotassium salt, $[K_2(XN_2)(DME)_x]$ (**2**; $x =$ 2-2.5), and subsequent reaction with $[LaCl_3(THF)_3]$ afforded $[\{(XN_2)LaCl(THF)\}_x]\cdot(O(SiMe_3)_2)_{0.25x}$ (**13**$\cdot(O(SiMe_3)_2)_{0.25x}$; $x = 1$ or 2) after crystallization from $O(SiMe_3)_2$. Compound **13**$\cdot(O(SiMe_3)_2)_{0.25x}$ reacted with two equivalents of $LiCH_2SiMe_3$, to form the dialkyl-'ate' complex, $[Li(THF)_x][(XN_2)La(CH_2SiMe_3)_2]\cdot$Toluene$\cdot$LiCl (**14**$\cdot$Toluene$\cdot$LiCl; $x = 3$). Both **12** and **14** ($x = 4$) were structurally characterized by X-ray crystallography, and were evaluated as catalysts for intramolecular hydroamination. While compound **14** showed poor activity, the neutral lutetium alkyl complex, **12**, is highly active for both intramolecular hydroamination and more challenging intermolecular hydroamination. Like the yttrium analogue, **3**, reactions with unsymmetrical alkenes yielded Markovnikov products. Additionally, it is noteworthy that the activity of **12** surpassed that of **3** in the reaction of diphenylacetylene with 4-*tert*-butylbenzylamine.

The reaction of H_2XN_2 with $[Zr(NMe_2)_4]$, followed by crystallization from $O(SiMe_3)_2$, yielded $[(XN_2)Zr(NMe_2)_2]\cdot(O(SiMe_3)_2)_{0.5}$ (**15**$\cdot(O(SiMe_3)_2)_{0.5}$). The zirconium dimethyl complex $[(XN_2)ZrMe_2]$ (**16**) was accessed via two routes; either by treatment of **15**$\cdot(O(SiMe_3)_2)_{0.5}$ with excess $AlMe_3$, or by reaction of **15**$\cdot(O(SiMe_3)_2)_{0.5}$ with excess Me_3SiCl, affording $[(XN_2)ZrCl_2]$ (**17**), followed by the subsequent reaction of **17** with 2 equivalents of MeLi. The reaction of **16** with one equivalent of $B(C_6F_5)_3$ or $[CPh_3][B(C_6F_5)_4]$ yielded cationic [-$(XN_2)ZrMe][MeB(C_6F_5)_3]$ (**18**) and $[(XN_2)ZrMe(arene)][B(C_6F_5)_4]$ (**19**; arene = η^6-benzene, η^6-toluene or bromobenzene), respectively. Both **18** and **19** are active for ethylene polymerization under 1 atm of ethylene at 24 °C and 80 °C in toluene, with activities ranging from 23.5–883 kg/(mol·atm·h), yielding polymers with weight average molecular weights (M_w) of 71–88 kg/mol and polydispersities (M_w/M_n) of 3.94–4.67.

Acknowledgements

First and foremost I would like to thank my supervisor Dr. David J. H. Emslie, to whom I am indebted for providing a positive environment to grow as a chemist. I was very lucky to have a supervisor with such an enthusiasm for chemistry, who was always willing to read over and edit my work whether for a presentation, an application or my thesis. Thank you for sharing your knowledge, expertise, advice and for always being available to talk no matter what time of day. I know that through your guidance I have gained the research and leadership skills that will serve me well as I continue to take on new challenges.

I would like to thank all of the Emslie group members with whom I have had the opportunity to work, including Velislave Bacharova, Adam Pantaleo, Lilly Vo, Tara Dickie, Judy Tsao, Meera Mehta, Terry Chu, Katarina Paskaruk, Aathith Vasanthakumar, Kristopher Kolpin, Jeffrey Price, Nick Andreychuk, Majeda Al Hareri, Dr. Bradley Cowie, Dr. Carlos Cruz, Dr. Bala Vidjayacoumar, Dr. Preeti Chadha, Dr. Todd Whitehorne and Dr. Edwin Wong. I would like to especially thank Dr. Preeti Chadha and Dr. Edwin Wong for their guidance and leadership in helping me to become a more effective researcher and scientist. Additionally, I would like to extend my gratitude to Dr. Maria Ivanova, Jeffrey Price and Lucia Lee for the many coffee runs and conversations, not only about graduate work but life beyond the lab.

I am indebted to my Ph.D. committee members, Dr. Ignacio Vargas-Baca and Dr. Gary Schrobilgen for their invaluable mentorship. I am very grateful for all of the advice and support they provided, especially through the most trying points of my graduate career. In addition, I would like to extend my gratitude to the external examiner, Dr. Gino Lavoie, and the chair, Dr. Greg Slater, for their roles in administering my thesis defence.

I would like to thank Dr. Hilary Jenkins, Dr. Jim Britten and Victoria Jarvis from the McMaster Analytical X-ray Diffraction Facility for all of their help, not only pertaining to X-ray crystallography but also for all of the conversations, support and encouragement. I would also like to acknowledge the valuable contributions of the members of the other facilities, including Dr. Bob Berno, Dr. Dan Sorensen and Dr. Steve Kornic in the Nuclear Magnetic Resonance Facility, Dr. Steve Kornic and Megan Fair for assistance with elemental analysis, and Dr. Kirk Green and Dr. Fan Fei from the McMaster Regional Centre of Mass Spectrometry for sharing their knowledge and expertise.

I am also very grateful for the professors with whom I had the pleasure to work as a TA, including Dr. David Emslie, Dr. Alex Adronov, Dr. David Brock, Dr. Ignacio Vargas-Baca, and Dr. William Leigh. Through their guidance I was able to become a more effective educator and mentor. Additionally, I would like to thank Karen Neumann for all of the friendly chats between classes, and for all of the encouragement and support throughout my entire graduate career.

I would like to acknowledge the office staff of the Department of Chemistry and Chemical Biology, Jane Garneau Linda Spruce, Christine Cosgrove and Connie Carrabs; thank you for all of your kind remarks and expedited assistance with all of the administrative tasks that arose.

I would also like to thank the Department of Chemistry and Chemical Biology at McMaster University and the Government of Ontario for their generous financial support.

I am profoundly grateful to my parents, Michael and Kathryn Motolko and to my siblings, Alexander and Carolyn Joy for all of their support and encouragement. Whether through meals, wine, conversations or other countless acts, you've always been there to provide the help and support I needed.

Finally to my husband Travis: there are insufficient words to describe how thankful I am for you and for everything you have done. Even through living apart these last almost four years, you have always been there to support me in everything from my graduate career and beyond. I am very excited to see what the next chapter has in store and I know we can get through anything together.

Declaration of Academic Achievement

Dr. David J. H. Emslie was responsible for the synthesis of $[NBu_4][B(C_6F_5)_4]$. Terry Chu, a former 4th year undergraduate thesis student in the Emslie group was responsible for the initial synthesis of XP_2Cl_2 and H_2XP_2. Kristopher Kolpin, a current Ph.D. student in the Emslie group was responsible for the synthesis of $B(C_6F_5)_3$. Dr. Carlos Cruz, a former Ph.D. student in the Emslie group was responsible for the synthesis of 1-amino-2,2-diphenyl-4-pentene. Dr. Kirk Green and Dr. Fan Fei were responsible for performing all mass spectrometry experiments. Dr. Steve Kornic and Megan Fair from McMaster University, and Mr. Joseph Fornefeld from Midwest Microlab Inc. were responsible for performing elemental analysis for all samples. Nick Andreychuk, a current Ph.D. student in the Emslie group was responsible for performing the DSC experiments. Dr. D. W. Lester from the University of Warwick, Coventry, UK was responsible for the operation and analysis of all GPC samples. Dr. Hilary Jenkins and Dr. James Britten were responsible for crystal mounting, data acquisition, refinement and structure solution for single crystal X-ray diffraction experiments. All other results were obtained by myself, Kelly S. A. Motolko.

I was taught that the way of progress was neither swift nor easy. – Marie Curie

Table of Contents

List of Figures

List of Schemes

List of Tables

List of Abbreviations

General

$^\circ$	Degree(s)
$^\circ$C	Degree Celcius
K	Kelvin
η^n	Denotes the hapticity of the ligand, which is the coordination of a ligand to a metal center via delocalized charge distribution over a series of n atoms
κ^n	Denotes the denticity of the ligand, which refers to the number of donor groups in a single ligand, n, that bind to a central metal in a coordination complex
μ_n	Refers to a ligand that is bridging between n atoms
Anal. Calcd.	Calculated (Elemental) Analysis
equiv.	Equivalent(s)
h	Hour(s)
min	Minutes
g	Gram(s)
kg	Kilogram(s)
L	Liter(s)
mL	Milliliter(s)
mol	Mole(s)
mmol	Millimole(s)
M	Molarity (mol/L)
atm	Atmosphere(s)

General Cont.

ppm	Parts per million
THF	Tetrahydrofuran
Tol	Toluene
DME	1,2-Dimethoxyethane
MAO	Methylaluminoxane
fac	Facial
mer	Meridional
CIP	Contact Ion Pair
SSIP	Solvent-Separated Ion Pair
D	Deuterium
Ln	Lanthanide
An	Actinide
Pn	Pnictogen (N, P, As, Sb, Bi)
M	General Metal (Unless Otherwise Specified)

Substituents and	**Ligands**
Ar	Aryl
Dipp	2,6-Diisopropylphenyl (2,6-$^{i}Pr_2$-C_6H_3)
Tripp	2,4,6-Triisopropylphenyl (2,4,6-$^{i}Pr_3$-C_6H_2)
Mes	Mesityl (2,4,6-Me_3-C_6H_2)
Ind	Indenyl
Cp	Cyclopentadienyl
Cp*	Pentamethylcyclopentadienyl
Cyp	Cyclopentyl

Substituents and	**Ligands Cont.**
Et	Ethyl
^{i}Pr	Isopropyl
Me	Methyl
^{n}Bu	*n*-Butyl (n = Normal)
Ph	Phenyl
^{t}Bu	*t*-Butyl (*tert* = Tertiary)
R	Alkyl or Aryl Group (Unless Otherwise Specified)
Binap	2,2′-disubstituted-1,1′-binaphthyl
DPEPhos	Bis(2-(diphenylphosphino)phenyl)ether
Xanth	Xanthene
XBr_2	4,5-dibromo-2,7-di-*tert*-butyl-9,9-dimethyl-xanthene
BDPP	2,6-bis(2,6-diisopropylanilidomethyl)pyridine
XA_2	4,5-bis(2,6-diisopropyl-anilino)-2,7-di-*tert*-butyl-9,9-dimethylxanthene
XP_2	4,5-bis(2,4,6-triisopropylphenylphosphido)-2,7-di-*tert*-butyl-9,9-dimethylxanthene
XN_2	4,5-bis(2,4,6-triisopropyl-anilido)-2,7-di-*tert*-butyl-9,9-dimethylxanthene

Spectroscopy and	**Analytical Techniques**
Å	Angstrom
δ	NMR Chemical Shift (ppm)
Hz	Hertz
MHz	Megahertz
1D	One Dimensional
2D	Two Dimensional
NMR	Nuclear Magnetic Resonance
$\{^1H\}$	Proton Decoupled
COSY	Correlation Spectroscopy
DEPT	Distortionless Enhancement by Polarization Transfer
HMBC	Heteronuclear Multiple Bond Correlation
HSQC	Heteronuclear Single Quantum Coherence
s	Singlet
d	Doublet
sept	Septet
m	Multiplet
br.	Broad
J	Symbol for Coupling Constant
$^nJ_{\mathrm{X,Y}}$	Coupling Constant Between Nuclei X and Y; n = The Number of Bonds Separating X and Y
GC-MS	Gas Chromatography-Mass Spectrometry
DSC	Differential Scanning Calorimetry
GPC	Gel Permeation Chromatography

Spectroscopy and	**Analytical Techniques Cont.**
N_t	Turnover Frequency
M_n	Number Average Molecular Weight
M_w	Weight Average Molecular Weight
PDi	Polydispersity Index

List of Compounds

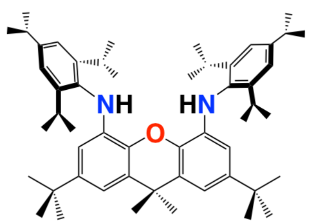

1

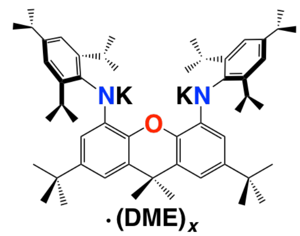

2

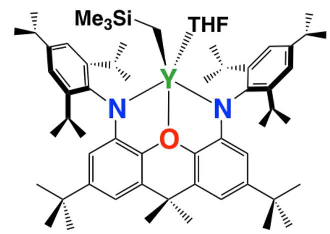

3

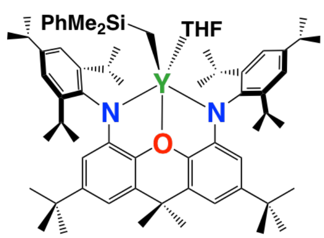

4

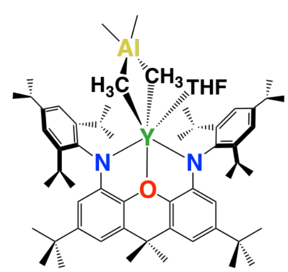

5

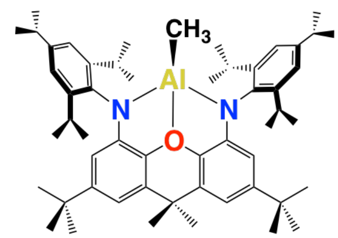

6

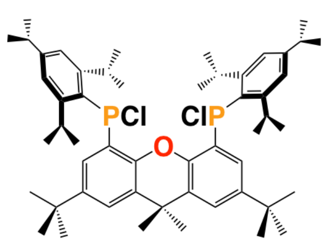

7

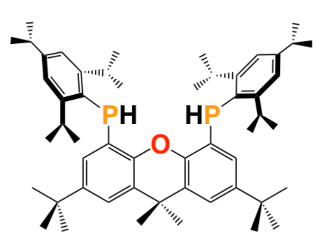

8

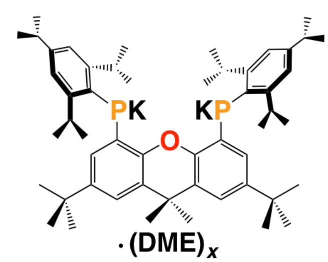

9

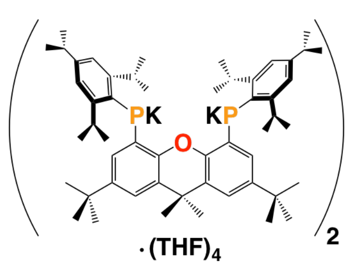

10

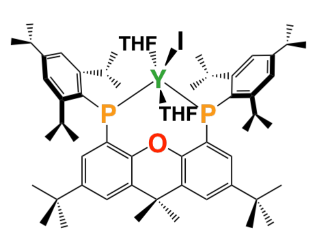

11

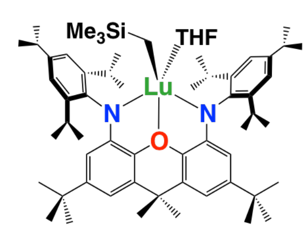

12

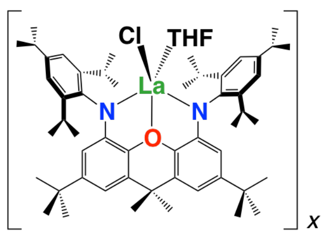 **13**	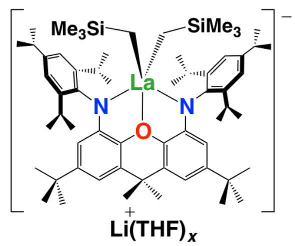 **14**	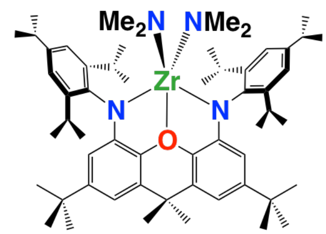 **15**
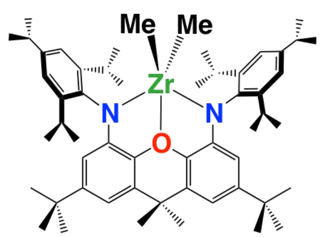 **16**	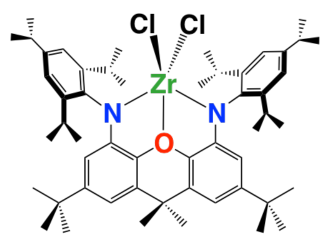 **17**	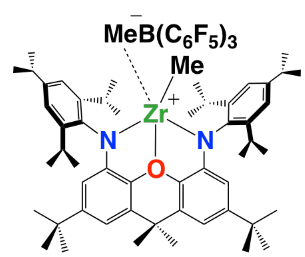 **18**
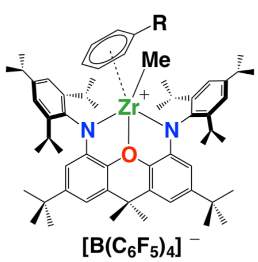 **19**	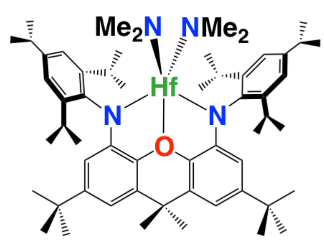 **20**	

Chapter 1

Introduction

1.1 Introduction to Rare Earth Metal Chemistry

The rare earth elements (REE) consist of the lanthanides (La–Yb in the periodic table) and the group 3 elements scandium, yttrium and lutetium. The lanthanide metals reside in what is commonly known as the *f*-block, which refers to the presence of *f*-orbitals. The general set of the *f*-orbitals, which are most commonly used, are seven-fold degenerate and include $f\mathrm{z}^3$, $f\mathrm{xz}^2$, $f\mathrm{yz}^2$, $f\mathrm{y}(3\mathrm{x}^2\text{-}\mathrm{y}^2)$, $f\mathrm{x}(\mathrm{x}^2\text{-}3\mathrm{y}^2)$, $f$xyz, and $f\mathrm{z}(\mathrm{x}^2\text{-}\mathrm{y}^2)$ (an alternative is the cubic set, which would be appropriate for cubic (O_h) symmetry).[1,2] However, an important characteristic of the lanthanides is that the 4*f*-orbitals have poor radial extension and are unavailable for covalent bonding. Consequently, the bonding is predominantly electrostatic/ionic in nature. The most common oxidation state for all the rare earth elements is M^{3+}, but there are examples in which rare earth elements have been found to display oxidation states of M^{2+} or M^{4+}.[3] For example, Cerium (Ce), and less commonly Praseodymium (Pr), Terbium

(Tb) have been known to exist as M^{4+}, while Samarium (Sm), Europium (Eu) and Ytterbium (Yb) exist as M^{2+} in a range of complexes.[1] It is noteworthy that the M^{2+} oxidation state is invariably highly reducing, while the M^{4+} oxidation state is strongly oxidizing. Therefore, the common mechanisms of oxidative addition and reductive elimination, which require a change of two units in the oxidation state, cannot easily occur. The predominant reactions for rare earth organometallic complexes are σ-bond methathesis and insertion mechanisms, in which the oxidation state is unchanged. The large M^{3+} cations are highly Lewis acidic and result in strong oxophilicity, which makes them prone to nucleophilic attack. As such they are extremely sensitive to air and moisture and require meticulous handling under an inert atmosphere.

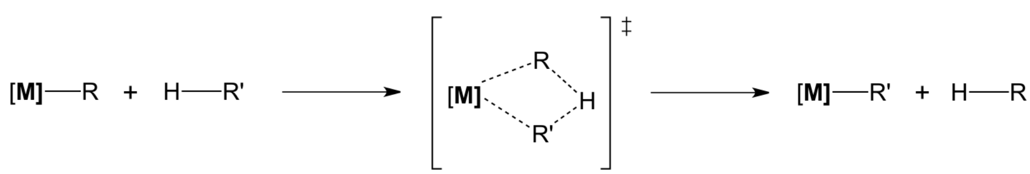

Scheme 1.1: The σ-Bond Methathesis Mechanism.

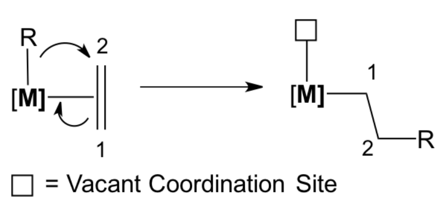

Scheme 1.2: The 1,2-Insertion Mechanism.

σ-Bond methathesis was first published in 1987 by Bercaw *et al.* and is described as a concerted process in which the oxidation state remains constant.

The general mechanism progresses through a 4-centered transition state, as shown in Scheme 1.1, and results in the formation of a new M–R bond.[4] Similarly, 1,2-insertion reactions (Scheme 1.2) also proceed through a 4-centered transition state and the metal oxidation state remains unchanged.[5] Through this process a coordinated unsaturated substrate, such as ethylene, inserts into a M–R bond, generating a vacant coordination site. This reaction is fundamentally important for olefin polymerization, particularly the Cossee-Arlman mechanism, as discussed further in Section 1.4.

Element (M^{3+})	Ionic Radii (Å)
Sc	0.745
Y	0.900
La	1.032
Ce	1.01
Pr	0.99
Nd	0.983
Pm	0.97
Sm	0.958
Eu	0.947
Gd	0.938
Tb	0.923
Dy	0.912
Ho	0.901
Er	0.890
Tm	0.880
Yb	0.868
Lu	0.861

Table 1.1: The Ionic Radii of the Rare Earth Elements (M^{3+}) with a Coordination Number of VI.[6]

Another significant characteristic of the lanthanides is the regular decrease of atomic and ionic radii across the series, termed the lanthanide contraction (Table 1.1). This is due to the poor shielding of the 4-*f* electrons; thus moving across the series from lanthanum to lutetium causes the effective nuclear charge to increase, resulting in the observed contraction.[1,2,5] The effects of the lanthanide contraction reach beyond the rare earth metals to the third row of the transition metal series, causing them to be very similar in size to those in the second row of the same triad. For example, the ionic radius of hafnium(IV) is very similar to that of zirconium(IV) (0.58 Å and 0.59 Å respectively).[6]

1.2 Pincer Ligands Utilized in the Synthesis of Rare Earth and Group 4 Transition Metal Alkyl Complexes

1.2.1 Introduction to Pincer Ligands

The term 'pincer' describes a class of tridentate ligands that are most often mono-, di- or tri-anionic and have the general architecture shown in Figure 1.1. The first pincer ligand was reported by Shaw and Moulton in 1976, and featured a 2,6-ortho-disubstituted monoanionic phenyl ring with phosphines as the flanking neutral donors.[7] However, this tridentate coordination mode or three-pronged strategy employed by pincer ligands dates back well beyond the 1970's to antiquity and ancient warfare tactics. Likely the first use of this three-pronged pincer strategy was performed by Hannibal in 216 BC, during the battle of Cannae, where he was able to defeat the formidable Roman army. The Roman army typically engaged a battle by concentrating their fighting force towards the center of the enemy's military line. Hannibal, however, anticipated this style of attack and organized his army specifically to reinforce his wings with additional military units. As Hannibal's army advanced, the two wings/flanking units engaged the sides of the Roman military line, while spontaneously advancing the center lines, resulting in the Romans being effectively surrounded, leading to Hannibal's victory.[8]

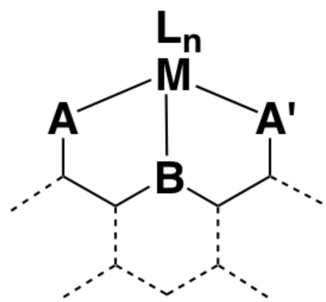

Figure 1.1: The General Architecture of a Pincer Ligand (A, A′ and B represent locations for varying donor groups).

This military tactic is consequently related to pincer-style ligand designs, where the metal center is effectively surrounded by the tridentate ligand structure (a three-pronged attack). Additionally, organizing the center line and flanking units in a specific way allows ligands to be customized for use against different armies (*in sensu hoc* metal centers), by way of altering the electronic or steric properties. Since the first report of pincer ligands in the 1970's, their use has flourished, leading to applications with metals across the periodic table.[9–13]

1.2.2 Ligand Attachment Methods

In organometallic chemistry, three common methods to attach an anionic ancillary ligand to a metal center are salt metathesis, alkane elimination and amine elimination (Scheme 1.3). In this thesis, each of these synthetic methods was used, where appropriate, to yield the complexes reported herein. Salt metathesis (Scheme 1.3, (a)) involves the reaction of an alkali metal salt of the ligand with a metal halide precursor, resulting in elimination of an alkali metal halide byproduct. Often the rare earth metal halide precursor exists as a THF adduct, which aids in solubility, and examples include $[LuCl_3(THF)_3]$, $[LaCl_3(THF)_3]$ and $[ZrCl_4(THF)_2]$. Interestingly, some rare earth metal halide precursors exist as ion pairs. For example, the yttrium trichloride analogue exists as the ion pair $[YCl_2(THF)_5][YCl_4(THF)_2]$, which is commonly written as $[YCl_3(THF)_{3.5}]$. The product generated from a salt metathesis reaction is a ligand-metal halide compound that can subsequently be reacted via standard techniques to form a variety of desired organometallic complexes. The drawback of this synthetic route is that the alkali metal halide byproduct can be difficult to remove and is often retained in the bulk material of the target complex. Alkane and amine elimination reactions avoid this problem, as metal-alkyl or metal-amido complexes are formed directly through these processes and are accompanied by volatile reaction byproducts, which are easily removed.

Amine elimination (Scheme 1.3, (b)) involves the reaction of a pro-ligand with a metal amido precursor, generating a ligand-metal amido complex with elimination of an amine byproduct. The metal amido complex can be converted to a variety of metal alkyl complexes in two steps, first via the reaction with Me_3SiCl generating a metal chloride complex followed by alkylation.[14,15] This multi-step synthesis to the desired metal alkyl complex can be a hindrance, as not only is it time consuming but each step also invites potential

$$[K_2(L)] + [MCl_3(THF)_3] \longrightarrow [(L)MCl(THF)_x] + 2\,KCl \quad (a)$$

$$[H_2(L)] + [M(NR_2)_4] \longrightarrow [(L)M(NR_2)_2] + 2\,HNR_2 \quad (b)$$

$$[H_2(L)] + [MR_3(THF)_2] \longrightarrow [(L)MR(THF)_x] + 2\,HR \quad (c)$$

Scheme 1.3: Commonly Employed Methods for Anionic Ligand Attachment (a) Salt Metathesis, (b) Amine Elimination, (c) Alkane Elimination.

synthetic issues and can result in low yields. Alternatively, the metal amido complex can be directly converted to a metal methyl complex, through the reaction with trimethylaluminum ($AlMe_3$).[16,17]

The final synthetic method, alkane elimination, is the most direct route as it generates ligand-metal alkyl complexes in a single step through the reaction of a pro-ligand with a metal alkyl precursor, with the elimination of alkane byproducts (Scheme 1.3, (c)). The drawback for this route is that there are a limited number of metal alkyl precursors available, especially for the rare earth metals, thus restricting the variety of complexes that can be synthesized via this method. The most common precursor for the rare earth metals is $[M(CH_2SiMe_3)_3(THF)_2]$,[18] which can be synthesized *in situ* or isolated. However, trialkyl complexes of this type are thermally unstable and consequently, they are not appropriate for alkane elimination reactions that require heating.

1.2.3 Introduction to the XN_2 and XP_2 Ligands Framework

The ligand architecture is vital in order to isolate thermally stable organometallic complexes. Key points to consider when designing a ligand scaffold are the steric bulk, donor elements and overall charge of the ligand.[12] In order to access highly reactive cationic alkyl species, the ligand should contain enough steric bulk to deter metal complex dimerization, be resistant to cyclometallation and nucleophilic attack, and should disfavor undesired coordination by donor solvents (eg. THF). However, too much steric bulk can negatively affect reactivity, thus a balance must be reached. The donor elements are an important factor to consider and can be selected in such a way as to be compatible with the chosen metal center. In general, metal centers described as being 'hard' will bond more favorably with 'hard' ligands, and 'soft' metal centers with 'soft' ligands. The terms hard and soft are related to polarizability; a hard species is less polarizable, while a soft species is more polarizable.[2] This dissertation focuses on early metals that are considered 'hard' and Lewis acidic, therefore hard donor elements (such as oxygen and nitrogen) are a suitable choice. Soft donor elements (such as phosphorus) are typically used in late transition metal chemistry to match with the less electropositive non-d^0 (soft) metals.

The overall charge of the ligand should also be considered when determining what kind of organometallic complex is desired. Dianionic ligands are of interest since they can generate neutral monoalkyl complexes with rare earth metals, which can be directly compared to analogous bis-cyclopentadienyl complexes. In addition, dianionic ligands can form neutral dialkyl complexes with group 4 transition metals, which can be used to generate cationic alkyl complexes. These complexes are highly successful as catalysts in the field of olefin polymerization (*vide infra*, Section 1.4).

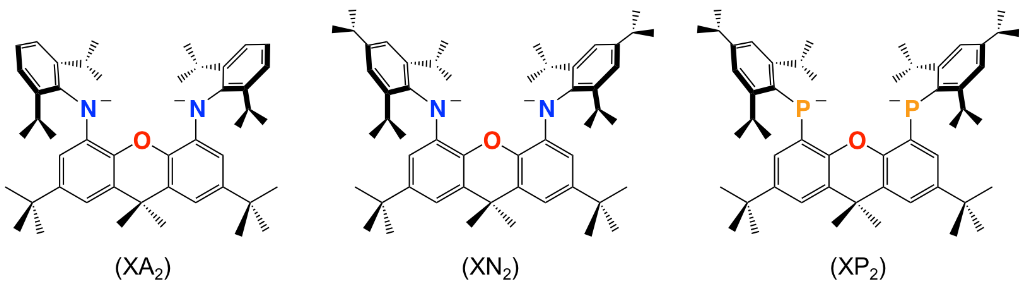

Figure 1.2: The XA_2, XN_2 and XP_2 Ligands.

The dianionic XN_2 and XP_2 ligands (Figure 1.2) are used for all research presented in this thesis, and they are designed for investigations with electropositive metals since they possess very suitable steric characteristics to encourage complex formation. Both ligands are rigid, enforcing a specific coordination environment and maximizing the effectiveness of the bulky triisopropylphenyl groups. The hard amido donors in the XN_2 ligand are ideally matched with the early metals on which this thesis is focused. In addition, it is of interest to explore the effect of the softer phosphido donors in the XP_2 ligand, which provide a direct comparison between the isolated complexes of these two ligands. Previously in the Emslie group, the related XA_2 ligand (Figure 1.2) was successfully employed in the syntheses of a variety of actinide(IV) complexes (thorium and uranium),[19–25] and expanding the scope of this ligand scaffold to other electropositive metals (rare earth and group 4) and altering the donor groups was compelling. The aryl groups were changed from 2,6-diisopropylphenyl, in the XA_2 ligand, to 2,4,6-triisopropylphenyl due to previous findings of aminyl radical formation upon oxidation of certain actinide(IV) complexes. It was hypothesized that the 2,4,6-triisopropylphenyl groups could aid in stabilizing such oxidized thorium and uranium complexes, since radical character can build up in the ortho and para positions of a diaryl aminyl radical ($NAr_2^{\cdot}$). The following sections discuss relevant literature examples of pincer ligands containing diamido and diphosphido donors, focusing on tridentate ligands that have been used to synthesize rare earth and group 4 transition metal complexes.

1.2.4 Reported Ligands Containing Bisamido Donors

Bisamido donor ligands are very common, especially in combination with rare earth and group 4 transition metals, and a wide range of architectures are known. Therefore, this section will focus on selected tridentate pincer and related ligands, which are most relevant for comparison with the XN_2 ligand (Figure 1.3). A key feature is that these ligands are more flexible than the XN_2 ligand, resulting in the possibility of coordinating to a metal center in either a facial (*fac*) or meridional (*mer*) coordination mode (Figure 1.4). The exception is the $(NNN)^{2-}$ ligand (Figure 1.3, (f)) which was designed specifically to only coordinate facially to a metal center.

Arguably the most pertinent to this discussion are the $(NON)^{2-}$ ligands synthesized by Schrock *et al.* (Figure 1.3, (a), (b) and (c)).[26–28] Both ligands (a) and (b) were used to synthesize dimethyl zirconium(IV) complexes and, in the solid state, the complex with ligand (a) was described as a twisted *fac*

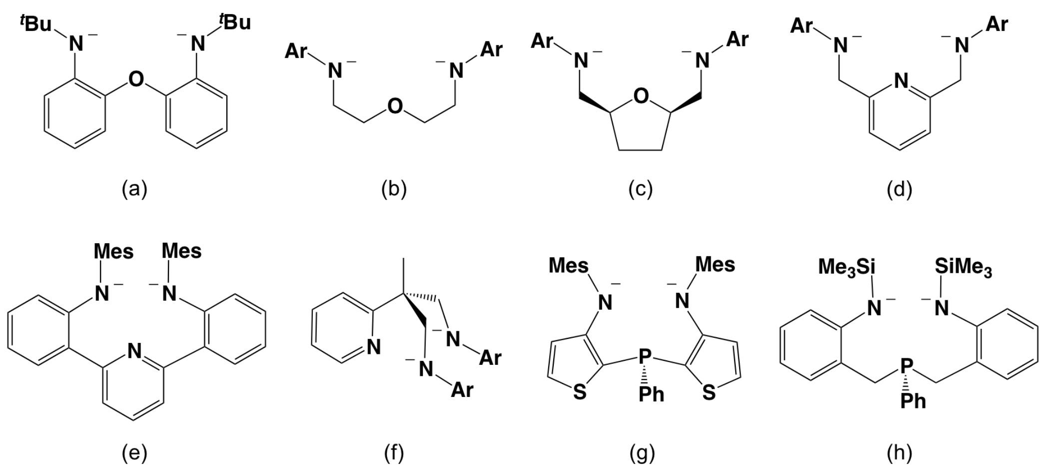

Figure 1.3: Select Previously Reported Diamido Pincer and Related Ligands.

coordination mode, although in solution from room temperature to –80 °C, the methyl groups are equivalent by NMR spectroscopy indicating apparent C_{2v} symmetry, while that with ligand (b) was reported to involve a *mer* type coordination mode.[26,27,29] Ligand (a) was also utilized for the synthesis of yttrium monoalkyl complexes ([(O{C_6H_4(N^{t}Bu)-*o*}$_2$)Y(R)(THF)]), in which a *mer* coordination mode was observed in the solid state.[30] It is noteworthy that in the solid state [(NON)ZrMe][MeB(C_6F_5)$_3$], utilizing the same ligand (NON = (a) in Figure 1.3), adopts a *fac* coordination mode. Ligand (c) was also utilized for the synthesis of a dimethyl zirconium(IV) complex, but unlike the previous examples, the ^{1}H NMR spectrum revealed two separate Zr–*Me* resonances, and in the solid state the geometry at zirconium is described as a distorted square-pyramid with methyl groups in apical and basal positions. It was proposed that the increased rigidity of this ligand restricts the pincers' flanking units causing the distortion away from the "ideal *mer*" coordination mode.[28]

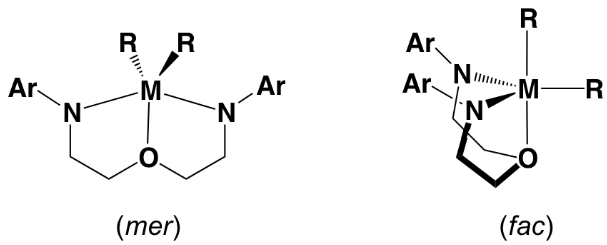

Figure 1.4: Meridional and Facial Coordination Modes of the ^{tBu}NON Ligand in 5-coordinate $[(\kappa^3\text{-}^{tBu}\text{NON})\text{MR}_2]$ Complexes.[27]

The $(\text{NNN})^{2-}$ ligand (Figure 1.3, (d)) was reported to form bis(dimethylamido) and dimethyl zirconium (IV) complexes and rare earth (M = Sc, Lu, Y, La) tetramethylaluminate complexes. In all cases, the ligand meridionally coordinates to the metal center based on NMR spectroscopy as well as X-ray crystallography.[31,32] The related ligand shown in Figure 1.3 (e), was also utilized for the synthesis of a bis(dimethylamido) zirconium (IV) complex and the solid state structure confirmed *mer* coordination of the ligand with a distorted trigonal-bipyramidal geometry at zirconium.[33] By contrast, the $(\text{NNN})^{2-}$ ligand (Figure 1.3, (f)) coordinates exclusively in the *fac* orientation if the pyridyl donor is bound to the metal. This was validated by the synthesis of bis(dimethylamido) and dimethyl zirconium (IV) complexes, as the ligand coordinated with *fac* geometry in both cases based on NMR spectroscopy and X-ray crystallography studies.[34–36] The $(\text{NPN})^{2-}$ ligands (Figure 1.3, (g) and (h)) were also used for the synthesis of bis(dimethylamido) zirconium(IV) complexes and in both cases the solid state structures revealed distorted trigonal-bipyramidal geometries with the ligand bound facially to the metal center.[37,38]

1.2.5 Reported Pincer Ligands Containing Two Phosphido Donors

Bisphosphido donor pincer ligands are extremely rare and to date there are only four that have been reported. The first two (Figure 1.5, (a) and (b)) were both reported to form bis(dimethylamido) zirconium(IV) complexes,[39,40] while ligands (c) and (d) (Figure 1.5) were used to synthesize alkali metal coordination compounds.[41]

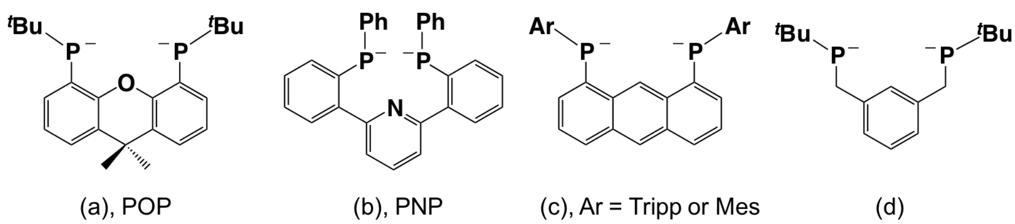

Figure 1.5: Previously Reported Bisphosphido Pincer Ligands.

The protio ligand, H_2(PNP), reported by Bercaw *et al.* exists as a mixture of *rac* and *meso* diastereomers in a 1:1 ratio, which is accompanied by two doublets in the ^{31}P NMR spectrum with a large one bond coupling constant observed ($^1J_{P,H}$ = 223-224 Hz). Double deprotonation with benzylpotassium in THF yielded the dimeric [((PNP)$K_2(THF)_3)_2$] salt, which resulted in a single resonance in the ^{31}P NMR spectrum, consistent with the formation of a single product. The [(PNP)Zr$(NMe_2)_2$] complex was synthesized from the reaction between the protio ligand and [Zr$(NMe_2)_4$] at room temperature after just 5 minutes in benzene.[39]

Similarly, the protio ligands (c) and (d) in Figure 1.5 were both reported as a mixture of *rac* and *meso* diastereomers in approximate 1:1 ratios, each with two signals in the ^{31}P NMR spectra, with $^{1}J_{P,H}$ coupling constants of 221-223 Hz for (c) and 194 Hz for (d). However, both protio ligands were unreactive towards amine and alkane elimination with zirconium(IV) precursors, even with elevated temperatures.[41]

By contrast, the protio ligand, H_2(POP), exists as a 2:3 ratio of *rac* and *meso* diastereomers, determined by the ^{1}H and ^{31}P NMR spectra. Double deprotonation with benzylpotassium in THF yielded K_2(POP), which was subsequently reacted with [$ZrCl_2(NMe_2)_2$(DME)] in THF to form [(POP)Zr-$(NMe_2)_2$].[40] It is of note that both [(PNP)Zr$(NMe_2)_2$] and [(POP)Zr$(NMe_2)_2$]-exhibited trigonal bipyramidal geometry in the solid state and displayed long Zr–P bonds, which led to the conclusion that no significant π-interactions occurred between the phosphido donors and the metal center.[39–41]

1.3 Introduction to Hydroamination

Hydroamination is the process in which a carbon-nitrogen bond is formed through the reaction between an N–H bond (amine) and an unsaturated carbon-carbon bond. This reaction is an atom-economical process and is industrially relevant as the products (amines and imines) are desirable and consequently there has been significant research to develop catalysts able to facilitate this process.[42–44] This discussion will focus exclusively on rare earth (Sc, Y, Lu, La) and group 4 (Ti, Zr, Hf) metal catalysis with respect to both intra- and inter-molecular hydroamination processes. Late transition metals, actinide, alkali and alkaline earth metals have also been explored, but they are beyond the scope of this thesis, and therefore will not be discussed in detail.

1.3.1 Intramolecular Hydroamination

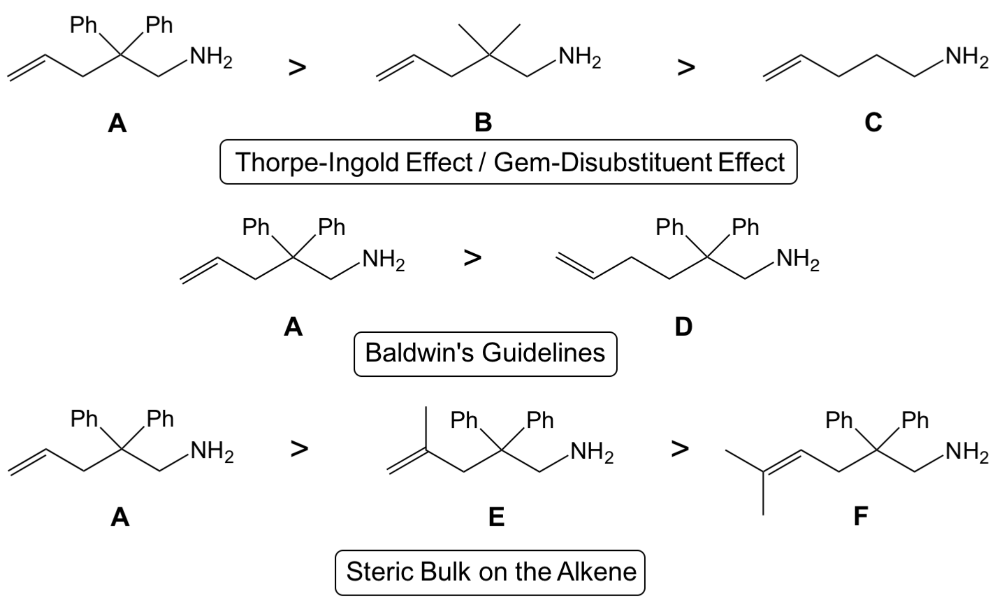

Figure 1.6: Selected Substrates Cyclized by Rare Earth and Group 4 Transition Metal Intramolecular Hydroamination Catalysts (Non-comprehensive). In Each Row, Substrates are Arranged in Order of Decreasing Reactivity Towards Cyclization.

Intramolecular hydramination involves a single substrate containing both an amine group and an unsaturated carbon-carbon bond. These so-called aminoalkene and aminoalkyne substrates can contain a wide range of additional features, which can either aid or hinder the ability of the N–C bond to form during hydroamination/cyclization. Figure 1.6 displays multiple examples of possible aminoalkene derivatives, with differing reactivity. This collection is not comprehensive, however it does provide a well-rounded collection of the kinds of intramolecular substrates employed. The reactivity of the aminoalkene is controlled by two main features; the Thorpe-Ingold effect/gem-disubstituent effect[45,46] and Baldwin's guideline for ring formation. Baldwin's guideline suggests that the ease of the reaction increases with decreasing ring size, as the formation of a 5-membered ring is favored over a 6-membered ring.[47] This is supported by the fact that cyclization of 1-amino-2,2-diphenyl-4-pentene (**A**) is more facile than 1-amino-2,2-diphenyl--5-hexene (**D**), which often requires more harsh experimental conditions such as increased catalyst loading, higher temperature and longer reaction times. The gem-disubstituent effect, also called the Thorpe-Ingold effect, describes the influence of additional groups on the alkyl chain, with respect to the reactivity of the substrate. Specifically, the addition of geminal groups on the aminoalkene decreases conformational freedom, promoting the likelihood of the alkene group adopting an appropriate orientation with the catalyst, thus promoting the reaction.[45,46,48] The accepted trend is that substrates containing geminal groups with increased steric bulk are more favorable compared to groups with minimal steric bulk, which are more favorable than the absence of geminal substitution altogether. Therefore, 1-amino-2,2-diphenyl-4-pentene (**A**) is more reactive than 1-amino-2,2-dimethyl-4-pentene (**B**), which is more reactive than 1-amino-4-pentene (**C**). In addition, substitution of the carbon-carbon double bond will have an effect on reactivity. Increasing the steric bulk around the alkene renders cyclization less favorable,[42,43,49–51] as it can hinder the formation of the transition state for C–N bond formation (*vide infra*).[48] For example, 1-amino-2,2-diphenyl-4-pentene (**A**) is more reactive than 1-amino-2,2-diphenyl-4-methyl-4-pentene (**E**), which is more reactive than 1-amino-2,2-diphenyl-5-methyl-4-hexene (**F**).

1.3.2 Intramolecular Hydroamination with Rare Earth Metal Catalysts

The mechanism for intramolecular hydroamination differs for rare earth and group 4 metal catalysts. The general mechanism for rare earth catalysts is described in Scheme 1.4, and begins with initiation of the catalyst by protonolysis of the metal amido or alkyl ligand by the aminoalkene substrate, forming a M–N bond. The next step requires the insertion of the alkene into the M–N bond. The resulting metal alkyl species undergoes protonolysis with a second aminoalkene, releasing the heterocyclic product and regenerating the active catalyst.[42,43,52]

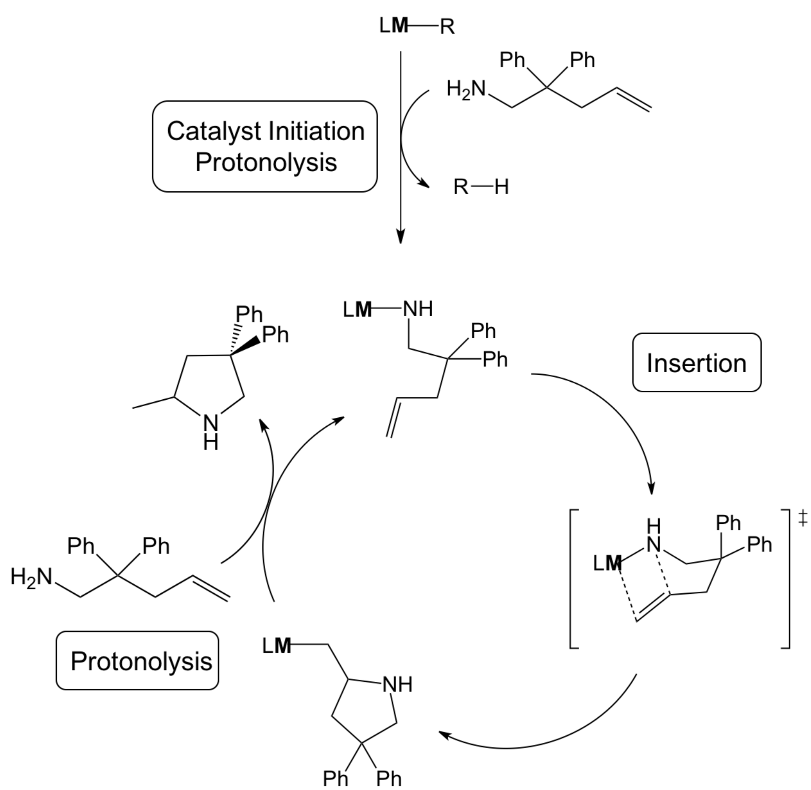

Scheme 1.4: General Mechanism for Rare Earth Metal Intramolecular Hydroamination Catalysis, (M = Rare Earth Metal).

Rare earth metal alkyl and amido complexes have been shown to be highly active catalysts for hydroamination reactions, typically exceeding that achievable with transition metal catalysts.[43] The rare earth metals are highly electrophilic and 'hard', which supports the mechanism proceeding through activation of the amine. In addition, M–C σ-bonds are highly reactive, which leads to increased reaction rates. If the metal was tightly bound to either the aminoalkene substrate or the heterocyclic product, the reaction rate would be substantially decreased.[43] In general, it has been established that the catalytic activity for alkene hydroamination increases with increasing ionic radius of the metal ion; La is more active than Y, which is more active than Lu (*vide infra*).[6,42] The drawback with these catalysts is their extreme air and moisture sensitivity, which requires all synthesis and handling in an inert atmosphere. In the literature, a wide range of active catalysts have been reported,[42–44,49] including metallocene and non-metallocene alkyl and amido complexes. However, the most relevant hydroamination catalysts to this thesis are those with dianionic ligands, yielding monoalkyl or monoamido rare earth metal complexes. Hydroamination reactions involving aminoalkynes, aminoallenes, and substrates containing multiple sites of unsaturation are beyond the scope of this thesis.

The use of rare earth metals for intramolecular hydroamination began in the late 1980's by Marks *et al.*[53,54] who published lanthanocene hydroamination of aminoalkenes. The problem encountered with metallocene complexes is that they can be sterically hindered with respect to the initial insertion of the aminoalkene substrate. Thus, the evolution of hydroamination catalyst designs moved towards less sterically hindered *ansa*-metallocene complexes, such as [$Me_2Si(C_5Me_4)_2Nd(CH(SiMe_3)_2)$] ((d) in Figure 1.7), and the more sterically-open, constrained geometry complexes, such as [$Me_2Si(C_5Me_4)(^tBu$-$N)Ln(CH(SiMe_3)_2)$] ((e) in Figure 1.7), which resulted in increased rates of cyclization.[42] The non-metallocene/post-metallocene complexes are particularly advantageous as they can be specifically designed and tuned to allow the metal to be more accessible to the incoming substrate, which generally results in greater catalytic activity. The first non-cyclopentadienyl hydroamination catalyst was reported in the late 1990's by Roesky *et al.*,[55] and this (aminotroponiminato)yttrium amide complex ((f) in Figure 1.7) did catalyze aminoalkyne cyclization. However, the catalytic activity was less than that of the previously reported lanthanocene catalysts.

Some of the most active rare earth catalysts for intramolecular hydroamination include those synthesized by Hultzsch *et al.*,[56] Schulz *et al.*,[57] Schafer *et al.*[58] and others.[42–44,59] A few examples, shown in Figure 1.7, include (a); (R)--[Y{Binol-$SiAr_3$}(o-$C_6H_4CH_2NMe_2$)(Me_2NCH_2Ph)] (Binol-$SiAr_3$ = 3,3′-bis-(trisarylsilyl)-2,2′-dihydroxy-1,1′-binapthyl; Ar = 3,5-xylyl),[56] (b); [(^{Ph2}Box)-LaR_2] (Box = 2,2′-bis(2-oxazoline)methylenyl)[60] and (c); (S)-[Y{NOBIN--TPS/TPS}(o-$C_6H_4CH_2NMe_2$)] (R = R′ = ^{t}Bu).[61]

As previously mentioned, for trivalent rare earth catalyzed alkene hydroamination, catalytic activity typically increases in parallel with metal ionic radius. For example, in cyclization reactions with $H_2C{=}CHCH_2CMe_2CH_2NH_2$, the activity of [$Cp^*_2Ln(CH(SiMe_3)_2)$], [($Me_2Si(C_5Me_4)_2$)$Nd(CH(SiMe_3)_2)$] ((d) in Figure 1.7) and [(L)$Ln(C_6H_4(CH_2NMe_2)$-o)] ((c) in Figure 1.7; R = $SiPh_3$, R′ = Me) increased in the order (a) Lu < Sm < La,[53,54] (b) Lu < Sm < Nd,[62]

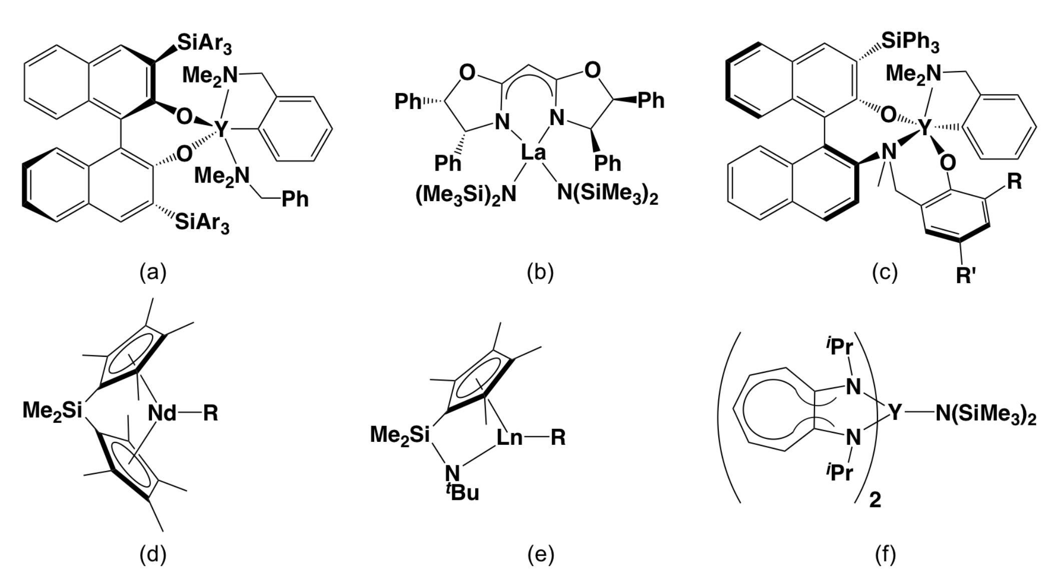

Figure 1.7: Literature Examples of Rare Earth Metal Complexes that Catalyze Intramolecular Hydroamination (a–f) and Intermolecular Hydroamination (a, c, and d).

and (c) Sc < Lu < Y,[61] respectively. Similarly, with *E*-PhHC=CHCH$_2$CPh$_2$-CH$_2$NH$_2$ as the substrate, the activity of [{(Ind)(CH$_2$)$_2$N(*o*-C$_6$H$_{10}$)NMe$_2$}Ln-(N(SiMe$_3$)$_2$)] (Ind = 1-indenyl) increased in the order Sc < Lu < Y < Sm,[63] and for H$_2$C=CHCH$_2$CPh$_2$CH$_2$NH$_2$ cyclization at 60 °C, [{OC$_6$H$_3$(*o*-^{t}Bu)-(*o*-CH=NAr)}$_2$Ln(CH$_2$SiMe$_2$Ph)] (Ar = C$_6$H$_3$^{i}Pr$_2$-2,6) was inactive for Sc, but active for Y.[58,64] By contrast, for alkyne hydroamination, this trend is reversed, and higher activity is commonly observed for smaller rare earth ions. As an example, the activity of [Cp*$_2$Ln(CH(SiMe$_3$)$_2$)] for HC≡C(CH$_2$)$_3$NH$_2$ cyclization increased in the order La < Nd < Sm < Lu.[65] However, these general trends are not always followed: for H$_2$C=CHCH$_2$CMe$_2$CH$_2$NH$_2$ cyclization, the activity of [Ln(N(SiMe$_3$)$_2$)$_3$] grafted onto partially hydroxylated periodic mesoporous silica increased in the order Nd < La < Y.[66] Additionally, for intermolecular hydroamination of $Ph(CH_2)_2CH{=}CH_2$ with benzylamine, yttrium and lutetium $[(L)Ln(C_6H_4(CH_2NMe_2)\text{-}o)]$ ((c) in Figure 1.7, R = R′ = ^{t}Bu) catalysts showed comparable activity,[61] while the lanthanum analogue was nearly inactive.[67–76]

1.3.3 Intramolecular Hydroamination with Group 4 Transition Metal Catalysts

The typical mechanism for alkene hydroamination using neutral group 4 transition metal catalysts is described in Scheme 1.5. The first step forms a metal imido species through protonolysis followed by α-hydrogen abstraction from the newly created amido ligand by the remaining alkyl anion. The next step is a [2+2] cycloaddition of the metal-imido bond with the alkene, which is then followed by protonolysis and α-hydrogen abstraction, regenerating the catalyst and releasing the heterocyclic product.[42,43,77–79]

Catalysts based on neutral group 4 compounds were initially reported to catalyze intra- and inter-molecular hydroamination reactions with alkynes and allenes.[80,81] More recently, neutral group 4 compounds were found to catalyze intramolecular hydroamination reactions with primary aminoalkenes.[42,43,82] Some catalysts that were reported to cyclize 1-amino-2,2-diphenyl-4-pentene include $[Zr(dpm)(NMe_2)_2]_2$ (dpm = 5,5-dimethyldipyrrolylmethane) (2.5 mol %, 100 °C with 100% conversion after 1 h),[83] $Ti(NMe_2)_4$ (5 mol %, 110 °C with 92% conversion after 24 h),[78] $Zr(NMe_2)_4$ (5 mol %, 100 °C with 92% conversion after 1 h)[83] and $[(NPS)Zr(NMe_2)_2]$ (NPS = bis(thiophosphinic-amidate)-), the latter of which catalyzed 1-amino-2,2-dimethyl-4-pentene cyclization

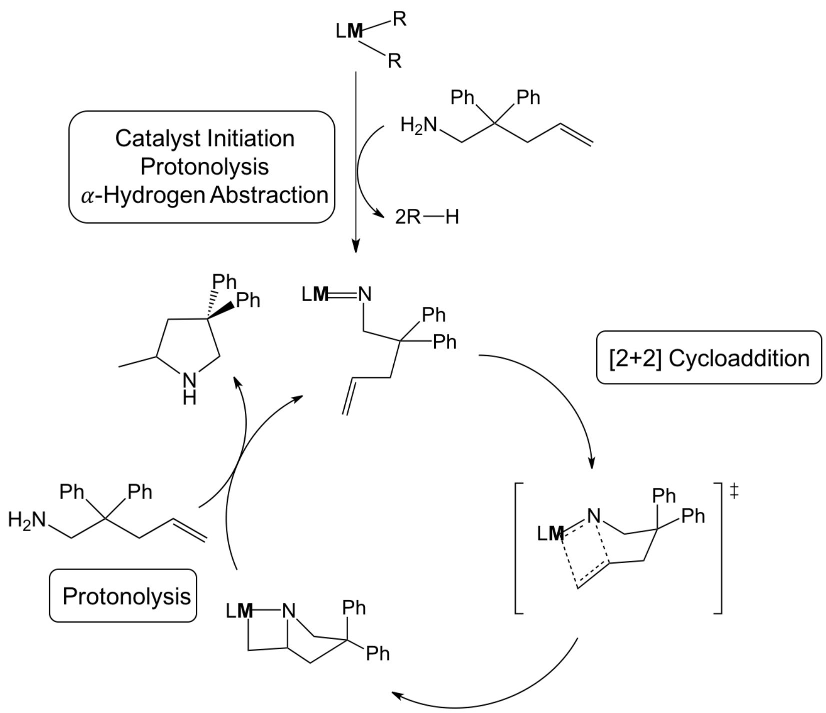

Scheme 1.5: General Mechanism for Group 4 Metal Intramolecular Hydroamination Catalysis, (M = Group 4 Metal).

(10 mol %, 150 °C with 98% conversion after 2.5 h).[79] Cationic group 4 metal compounds have also been reported to catalyze hydroamination reactions with secondary aminoalkenes, and the mechanism is believed to be similar to that of rare earth metal catalysts, involving 1,2-insertion reactions of group 4 amido species rather than cycloaddition reactions of imido compounds.[42,80,84]

1.3.4 Intermolecular Hydroamination

Intermolecular hydraomination involves the reaction between two substrates: an amine-containing compound and an unsaturated carbon compound. This reaction typically follows the same mechanisms as intramolecular hydroamination. However, it is significantly more difficult as coordination of the weakly-coordinating alkene to the catalyst is less favorable since the alkene is not tethered to the amine (as in intramolecular hydroamination). Therefore, this reaction often requires a large excess of the alkene to promote the required coordination, leading to the hydroamination product.[42,85]

There are only a handful of electropositive metal complexes that show high catalytic activity for intermolecular hydroamination.[42,43,49,51] Generally, these catalysts are either lanthanocene-, half-sandwich- or binaphtholate-based in the case of rare earth catalysts, and titanocene-/zirconocene-, half-sandwich- or bis(indenyl)-based for group 4 catalysts.[42,43,81]

The first group 4 compound to catalyze intermolecular hydroamination with alkynes was a bis(amido)zirconocene complex ($Cp_2Zr(NHAr)_2$, Ar = 2,6-$Me_2C_6H_3$) reported in the early 1990's by Bergman *et al.*, which was able to catalyze the hydroamination of diphenylacetylene with 2,6-dimethylaniline.[43,86] A monocyclopentadienyl amido-imido titanium complex, [Cp(py)(2,6-Me_2C_6-H_3NH)Ti=N(2,6-$Me_2C_6H_3$)], reported by Bergman *et al.* in 2001 was more reactive, able to catalyze the hydroamination of diphenylacetylene with 2,6-dimethylaniline at a decreased temperature and with a higher yield compared to the initially reported zirconocene complex.[43,87] The bis(indenyl) titanium complex (Ind_2TiMe_2) has been described as one of the most general catalysts for hydroamination, as it is able to catalyze a wide range of substrates.[42,43,88,89] Group 4 based catalysts have also been successful for the intermolecular hydroamination of allenes, however further discussion of these substrates is beyond the scope of this thesis.[42,43,80,81]

Intermolecular hydroamination of activated olefins such as vinyl arenes, 1,3-dienes and strained bicyclic alkenes with rare earth catalysts have been reported,[42,90] however, reactions with unactivated alkenes have gained recent interest. For example, the triphenylsilyl-substituted binaphtholate yttrium complex reported by Hultzsch *et al.* (Figure 1.7, (a); Ar = Ph) was able to catalyze the hydroamination reaction of benzylamine with 1-heptene at 150 °C; 5 mol % catalyst resulted in a 90 % yield after 36 h.[90] The related yttrium complex, also reported by Hultzsch *et al.* (Figure 1.7, (c); R = R′ = ^{t}Bu), was also able to catalyze benzylamine with 1-heptene at 150 °C; 5 mol % catalyst resulted in 85 % yield after 96 h.[61] One of the most active rare earth intermolecular catalysts is [$Me_2Si(C_5Me_4)_2Nd(CH(SiMe_3)_2)$] (Figure 1.7, (d)), which is reported to catalyze the reaction of *n*-propylamine with 1-pentene at 60 °C; 20 mol % catalyst resulted in a 90 % yield after 11 h.[42,85,91]

1.4 Introduction to Polymerization

A polymer is defined as a large molecule made up of many repeating units (termed monomers). Different kinds of polyolefins such as polyethylene, polypropylene and other polymers based on α-olefins, are synthesized on massive industrial scales (nearly 70 billion kg per annum) and consequently the study and optimization of α-olefin polymerization is of great interest.[92] In the 1930's the industrial process involved a high-pressure radical polymerization that resulted in a highly-branched material with limited applications.[93] In the 1950's, heterogeneous Ziegler-Natta based catalysts were reported and yielded linear chain polymers that have substantially more applicability, and a Nobel

Prize was awarded for this work in 1963.[94,95] While the Ziegler-Natta type catalysts provided a substantial advancement in this field, one of the drawbacks with Ziegler-Natta catalysts is the broad molecular weight distribution, which was solved through the use of single-site molecular catalysts (*vide infra*, Section 1.4.3).

One of the main characteristics of single site homogeneous catalysts is an organic ligand that remains coordinated to the active metal center. This supporting ligand can have a substantial effect on catalyst activity and thermal stability, and also plays a key role in determining polymer characteristics such as molecular weight, molecular weight distribution and stereochemistry.[96] Polymer characteristics such as density, number average molecular weight (M_n) and weight average molecular weight (M_w) are very important as they allow for the direct comparison of polymers synthesized by different catalysts. Low density polyethylene occurs when the polymer has a substantial number of branched chains, while high density polyethylene has linear, largely unbranched chains. The number average molecular weight (M_n) is defined as the weight of the polymer chain of an average length, while the weight average molecular weight (M_w) is the weight of the polymer chain of an average mass. The polydispersity index (PDi) is also a very useful value, as it is the measure of the distribution of the molecular weight and it can be calculated by dividing M_w by M_n.[97] The study of single site catalysts has advanced the field of polymer chemistry through the development of catalysts that can control the molecular weight and molecular weight distribution of the polymer.[96] Additionally, these investigations have allowed for detailed analyses of the structural and mechanistic attributes of these active catalysts, thus facilitating the future evolution of improved catalysts.

1.4.1 Introduction to Ethylene Polymerization by Rare Earth and Group 4 Transition Metal Catalysts

The basic mechanism for ethylene polymerization, termed the Cossee-Arlman mechanism, is shown in Scheme 1.6.[98,99] The first step is coordination of the alkene to a vacant site on the metal center, which then undergoes 1,2-insertion. This creates a new vacant site on the metal that can coordinate to a new alkene and the cycle repeats numerous times (termed propagation) until chain termination occurs. Chain termination can occur through various avenues such as β-Hydrogen Transfer and β-Hydrogen Elimination (Scheme 1.8), with β-Hydrogen Transfer usually being the most common route to chain termination.[100] An improvement on the Cossee-Arlman mechanism was published in 1983 by Brookhart and Green and includes an α-agostic interaction, which helps to stabilize the metal center and thereby facilitate the 1,2-insertion. The so called Brookhart-Green mechanism is shown in Scheme 1.7.[101]

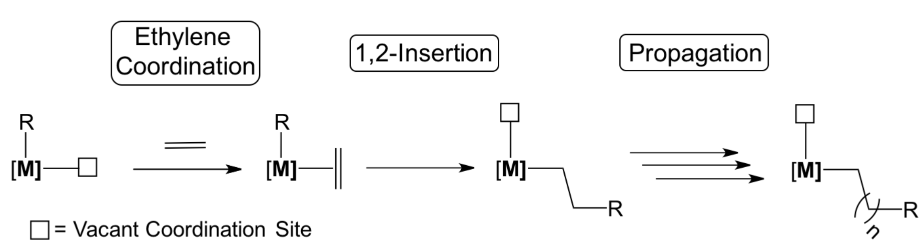

Scheme 1.6: The Cossee-Arlman Mechanism.

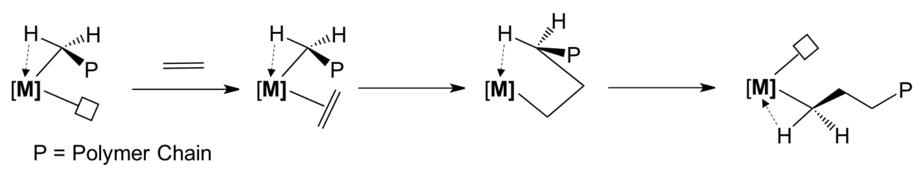

Scheme 1.7: The Brookhart-Green Mechanism.

In general, ethylene polymerization catalysts are cationic as they are highly reactive due to the increased electrophilicity and the decreased coordination number (compared to the neutral species), which are ideal features to promote chain propagation. There are several ways to generate these cationic species including reactions with methylaluminoxane (MAO), Lewis acidic boranes such as tris(pentaflurophenyl)borane ($B(C_6F_5)_3$) and borate salts such as trityl tetrakis(pentafluorophenyl)borate ($[CPh_3][B(C_6F_5)_4]$) and dimethylanilinium tetrakis(pentafluorophenyl)borate ($[HNMe_2Ph][B(C_6F_5)_4]$).

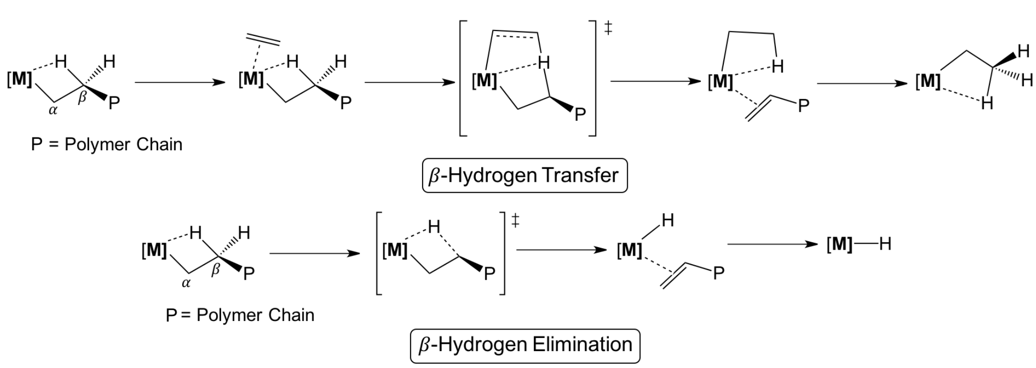

Scheme 1.8: The β-Hydrogen Transfer and β-Hydrogen Elimination Mechanisms for Polymerization Chain Termination.

1.4.2 Routes to Cationic Alkyl Complexes

Methylaluminoxane (MAO) is derived from the partial hydrolysis of $AlMe_3$ and has a non-uniform structure with the general formula $[MeAl(\mu\text{-}O)]_n$. It is a highly reactive co-catalyst in combination with group 4 metallocene complexes as it has been shown to generate highly active catalysts. One of the most active systems reported in the literature is that of Cp_2ZrCl_2/MAO, where the MAO acts as a methylating agent, a Lewis acid for abstraction of an alkyl group, and after alkyl abstraction, a component of the weakly-coordinating counter-ion paired with the zirconium cation, as shown in Scheme 1.9. Some of the drawbacks with utilizing MAO are that it needs to be present in a massive excess (∼1000 fold), the structure is not precisely known, and cations formed using MAO are not readily crystallized.[5,102] This hinders the ability of researchers to study, understand, and improve upon the catalytically active species, leading to the desire for development of alternative co-catalysts that will allow for the isolation and characterization of said active species. To this end, other Lewis acids were investigated and it was found that organoboranes (e.g. $B(C_6F_5)_3$) and stabilized carbocations (e.g. $[CPh_3][B(C_6F_5)_4]$) in combination with polyalkyl metallocenes produced highly active catalysts for olefin polymerization via alkyl abstraction.[103] The advantage of these systems is that the catalytic species can be isolated, and studied, and the supporting ligands can be rationally manipulated.

Tris(pentaflurophenyl)borane ($B(C_6F_5)_3$) is one of the most common activators, and in combination with a metal alkyl complex, it can abstract an alkyl anion, forming a coordinatively-unsaturated cationic metal center paired

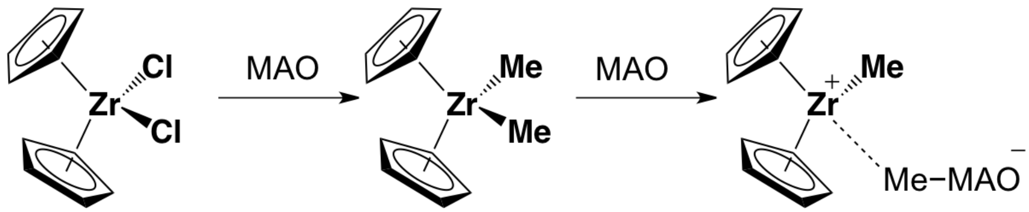

Scheme 1.9: Activation of $[Cp_2ZrCl_2]$ by Methylaluminoxane (MAO).

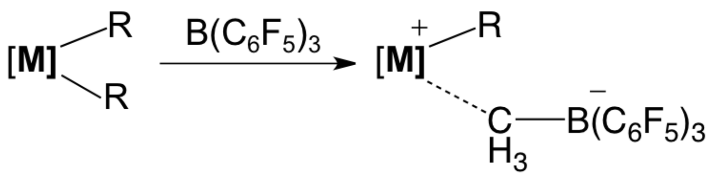

Scheme 1.10: Metal Alkyl Abstraction with Tris(pentaflurophenyl)borane (B-$(C_6F_5)_3$).

with a weakly-coordinating $[RB(C_6F_5)_3]^-$ anion, which can facilitate ethylene and α-olefin polymerization. This active species can be considered to involve a competition between the metal and the borane for coordination to the alkyl anion, typically resulting in an elongated M–C bond, in which the alkyl group is strongly associated to the borane (Scheme 1.10).[102,103] This cation–anion pairing is strong enough to stabilize the complex, leading to an increased catalyst lifetime (relative to alkyl cations paired with a less coordinating $[B(C_6F_5)_4]^-$ anion; *vide infra*) and allowing for characterization via X-ray crystallography, while weak enough to allow for α-olefin coordination.[102]

By contrast, trityl tetrakis(pentafluorophenyl)borate ($[CPh_3][B(C_6F_5)_4]$) will react with a polyalkyl metal complex to abstract and eliminate an alkyl group as the neutral byproduct R–CPh_3 (R = alkyl), as shown in Scheme 1.11.

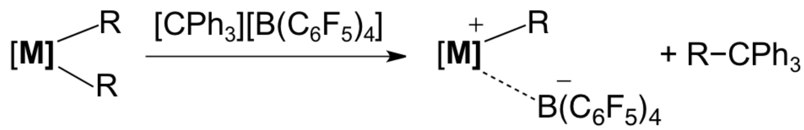

Scheme 1.11: Metal Alkyl Abstraction with Trityl Tetrakis(pentafluorophenyl)borate ($[CPh_3][B(C_6F_5)_4]$).

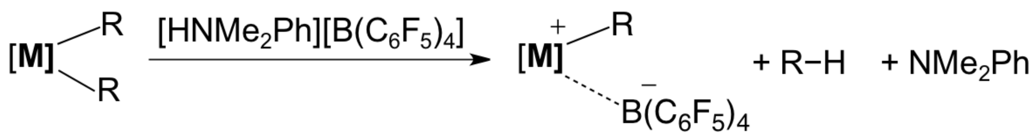

Scheme 1.12: Metal Alkyl Abstraction with Dimethylanilinium Tetrakis(pentafluorophenyl)borate ($[HNMe_2Ph][B(C_6F_5)_4]$).

Dimethylanilinium tetrakis(pentafluorophenyl)borate ($[HNMe_2Ph][B(C_6F_5)_4]$) will also produce a cationic metal center with the non-coordinating $[B(C_6F_5)_4]^-$ anion. However, this activator differs from trityl tetrakis(pentafluorophenyl)borate, in that it is a source of a single proton and will react with a polyalkyl metal complex to eliminate R–H and produce dimethylaniline as a byproduct (Scheme 1.12). Typically, the dimethylaniline does not coordinate to the metal, however, there are examples in which this does occur and the most common coordination mode is via the amine.[104–111] For example, reaction of $[CpZr(NP^tBu_3)Me_2]$ with $[HNMe_2Ph][B(C_6F_5)_4]$ yielded the monoalkyl cationic complex with coordination of NMe_2Ph via the amine.[107] By contrast, reaction of $[(ArNC(CH_3)CHC(CH_3)NAr)Y(CH_2SiMe_2Ph)_2]$ with $[HNMe_2Ph][B(C_6F_5)_4]$ yielded a monoalkyl cationic complex with η^6-arene coordination of the dimethylaniline to the metal center.[105] In both cases, utilizing

$[CPh_3][B(C_6F_5)_4]$ or $[HNMe_2Ph][B(C_6F_5)_4]$, the cationic metal center typically interacts weakly with the non-coordinating $[B(C_6F_5)_4]^-$ anion through long F···M contacts.[102,112] The absence of a more coordinating $[RB(C_6F_5)_3]^-$ anion (*vide supra*), generally causes complexes activated with a borate salt to suffer from poor thermal stability, decreased solubility in hydrocarbons, and low crystallizability.[102] However, in spite of these shortcomings, borate salt activated complexes have been proven to be highly active catalysts for α-olefin polymerization.[102,113]

1.4.3 Introduction to Single Site Rare Earth and Group 4 Metal Catalysts

Since the development of various methods for the generation of active catalyst species (*vide supra*), there has been a flurry of research into homogeneous single site catalysts. The majority of early research focused on group 4 metallocene and half-metallocene complexes, while more recently the focus has shifted to the development of non-metallocene based catalysts.[114,115] The focus of Sections 1.4.4 and 1.4.5 will be on non-metallocene catalysts based on group 4 and rare earth metals with particular attention to those with diamido based ligands that have been reported to polymerize α-olefins, especially ethylene.

1.4.4 Single Site Group 4 Transition Metal Catalysts

Although group 4 transition metal metallocene complexes have generally yielded the highest activities for olefin polymerization, interest in exploring alternative ligands has dominated recent research. The ability to specifically tune the supporting ligands architecture has led to the opportunity to study the ligands effects on activity, number average molecular weight (M_n), weight average molecular weight (M_w) and tacticity.[114,115] As stated above, the focus of this section will be on group 4 transition metal complexes with diamido based ligands that have been reported to polymerize α-olefins, particularly ethylene.

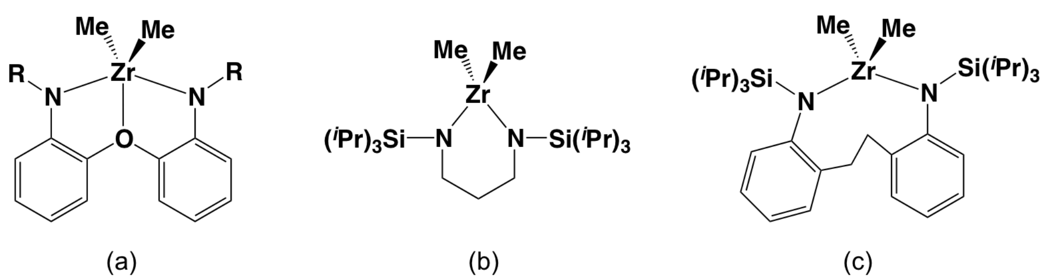

Figure 1.8: Literature Examples of Zirconium Dialkyl Complexes, that after Suitable Activation, Catalyzed the Polymerization of Ethylene, (R = $C(CD_3)_2CH_3$).

The zirconium dimethyl complexes, shown in Figure 1.8, were reported to polymerize ethylene (1 atm) after suitable activation with either $B(C_6F_5)_3$ or $[CPh_3][B(C_6F_5)_4]$. Complex (a); $[(\kappa^3\text{-}^{tBu}NON)ZrMe][MeB(C_6F_5)_3]$ (NON = $[((t\text{-Bu-}d_6)N\text{-}o\text{-}C_6H_4)_2O]$),[29] and (b); $[(\kappa^2\text{-}NN')ZrMe_2]$ (NN′ = $CH_2(CH_2NSi^iPr_3)_2$)[116] were reported to polymerize ethylene at 24 °C and under 1 atm of ethylene with activities of ∼100 kg/(mol·atm·h) (2 min) and 317 kg/(mol·atm·h) (1 h) respectively, while (c); $[LZrMe_2]$ (L = 2,2′-ethylenebis-

(N,N′-triisopropylsilyl)-anilinido)[117] was reported to polymerize ethylene (1 atm) at 0 °C with an activity of 178 kg/(mol·atm·h) after 5 minutes. The zirconium dialkyl complexes of general formula [(L)ZrR$_2$] reported by Schrock *et al.* (Figure 1.9), (L = (a); cis-2,5-(Ar′NCH$_2$)$_2$(C$_4$H$_6$O),[28] (b); [(ArNCH$_2$CH$_2$)$_2$O],[118] (c); [((*t*-Bu-*d*$_6$)N-*o*-C$_6$H$_4$)$_2$O][27], (d); [(^{i}PrN-*o*-C$_6$H$_4$)$_2$O] and (e); [(C$_6$H$_{11}$N-*o*-C$_6$H$_4$)$_2$O][119]) when activated with a borane activator were reported to polymerize 1-hexene.

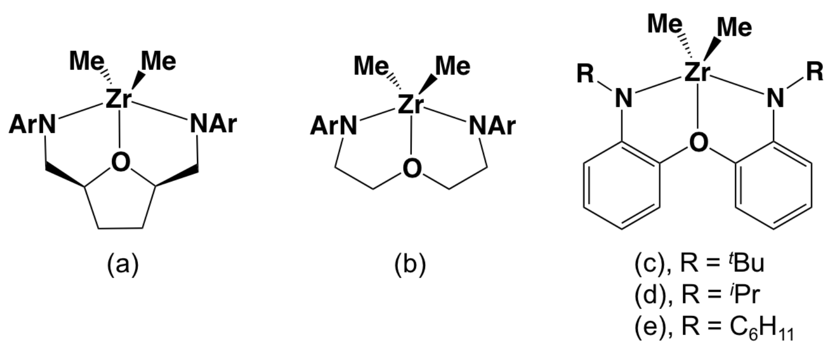

Figure 1.9: Literature Examples of Zirconium Dialkyl Complexes, that after Suitable Activation, Catalyzed the Polymerization of 1-hexene.

1.4.5 Single Site Rare Earth Metal Catalysts

Polymerization catalysts based on rare earth metal complexes have gained recent interest due to their capability of achieving certain catalytic abilities that are not typically observed with transition metal catalysts. For example, rare earth metal catalysts have been shown to yield polyethylene with high levels of α-olefin incorporation, as well as co-polymerizations of ethylene with styrene, cyclic olefins and dienes.[12,120–124] A disadvantage of rare earth metal complexes is their general low thermal stability, which can hinder the ability to operate at the high temperatures required to ensure that the polymer product (in solution polymerization) is a liquid, rather than a solid.

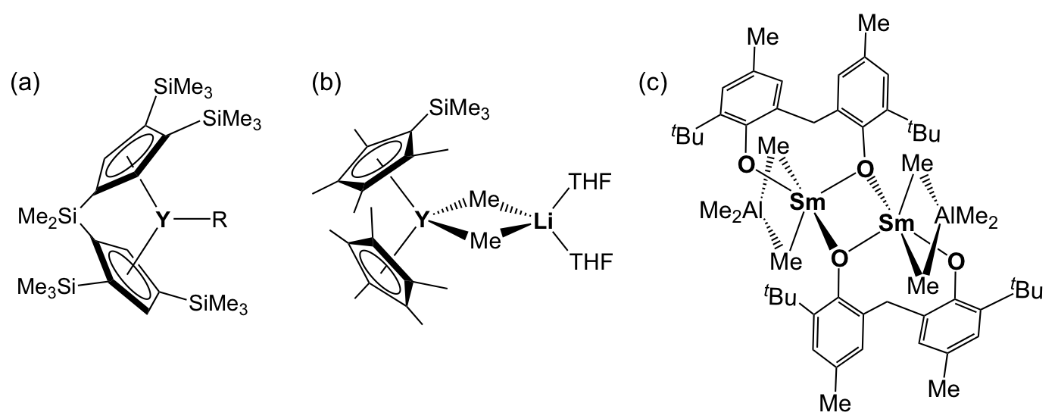

Figure 1.10: Highly active Single Component Rare Earth Catalysts for Ethylene Polymerization (R = $CH(SiMe_3)_2$).

Although rare, there are literature examples in which neutral (single component) rare earth complexes have been reported to polymerize α-olefins.[124] Examples include the samarium tetramethylaluminate complex [Sm-μ-{6,-6′-methylene-bis(2-*tert*-butyl-4-methylphenol)}{μ-Me_2AlMe_2}]$_2$, reported by Gambarotta *et al.*,[125] the yttrocene complex [Me_2Si{2,4-$(Me_3Si)_2C_5H_2$}{3,4--$(Me_3Si)_2C_5H_2$}$Y(CH(SiMe_3)_2)$],[126] and [(η^5-$C_5Me_4SiMe_3$)(η^5-C_5H_5)Y(μ-Me)-$_2$Li(THF)$_2$],[127] which were all reported to polymerize ethylene at room temperature under 1 atm of ethylene (Figure 1.10). By contrast, the neutral yttrium monoalkyl complex [(L)Y($CH(SiMe_3)_2$)(THF)] with the [((*t*-Bu-d_6)N-*o*-C_6-H_4)$_2$O] ligand was unreactive towards ethylene, likely due to the coordinated THF, which has been shown to hinder reactivity.[30]

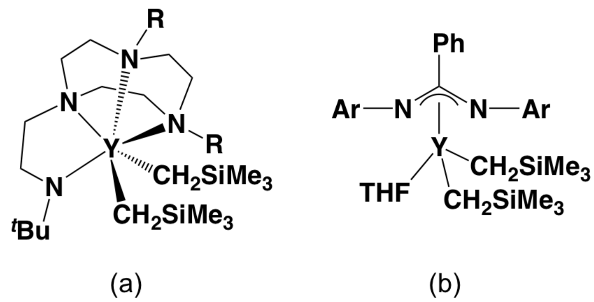

Figure 1.11: Literature Examples of Yttrium Complexes, that after Suitable Activation, Catalyzed the Polymerization of Ethylene, (R = Me, ^{i}Pr; Ar = 2,6-diisopropylphenyl).

As with group 4, the majority of research with rare earth metal polymerization catalysts has been focused on metallocene and half-metallocene complexes. Some examples of rare earth metal olefin polymerization catalysts include, [{Y(η-$C_5H_4SiMe_3$)$_2$Me}$_2$] reported by Ballard *et al.*,[128] [Cp^*_2LuMe]-reported by Watson *et al.*,[129,130] [{Cp^*_2MH}$_2$] (M = La, Nd, Lu) reported by Marks *et al.*[131] as well as others,[115,120,121,124,132,133] however, detailed discussions on these catalyst types are beyond the scope of this thesis. The development of non-cyclopentadienyl based catalysts have increased during the past two decades with some reported activities being at least 1000 kg/(mol·atm·h), including [{*N*,*N′*-R_2-tacn-*N″*-$(CH_2)_2N^tBu$}$Y(CH_2SiMe_3)_2$] (R = Me, ^{i}Pr; tacn = triazacyclononane) when activated with [$PhNMe_2H$][$B(C_6F_5)_4$] (Figure 1.11, (a)),[134] [$(PhC(NAr)_2)Y(CH_2SiMe_3)_2(THF)$] when activated with [$PhNMe_2H$]-[$B(C_6F_5)_4$] (Figure 1.11, (b)),[135] and [$Y(CH_2SiMe_3)_3(THF)_2$] when activated with [$PhNMe_2H$][$B(C_6F_5)_4$] in the presence of [$Al(CH_2SiMe_3)_3$].[136]

1.5 Thesis Goals

Early organolanthanide chemistry was dominated by the use of cyclopentadienyl (Cp) and Cp-derivatives as ligands.[137,138] However, as described in the previous sections, the use of non-Cp ligands has greatly increased and remains an area of interest due to their vast potential for selective modification with respect to electronic and steric tunability. Previously in the Emslie group, the XA_2 ligand was used to synthesize a variety of thorium[19–22] and uranium[23,24] compounds including a neutral thorium dialkyl complex that was shown to polymerize ethylene.[139] Following on from this work, it was of interest to explore both the effects of varying the ligand donor atoms, and the potential for alkene/alkyne hydroamination and ethylene/α-olefin polymerization by neutral and cationic rare earth and group 4 transition metal complexes. Therefore, the objectives of this Ph.D. research were (1) to synthesize an analogue of the XA_2 ligand in which the amido donors are replaced with phosphido donors (XP_2) and to explore the chemistry of this ligand in combination with actinide (Th, U), rare earth and group 4 transition metals (Chapter 3); and (2) to synthesize the directly analogous XN_2 ligand and explore the rare earth (Chapters 2 and 4) and group 4 transition metal (Chapter 5) chemistry of XN_2, including the potential activity for intra- and inter-molecular hydroamination and ethylene/α-olefin polymerization. Herein is presented the progress made towards accomplishing these goals.

Chapter 2

Yttrium and Aluminum Complexes of a Rigid Bis-Anilido NON-Donor Ligand; Synthesis and Hydroamination Catalysis

Adapted with permission from: Motolko, K. S. A.; Emslie, D. J. H.; Jenkins, H. A. *Organometallics* **2017**, *36*, 1601-1608. Copyright 2017 American Chemical Society.

2.1 Introduction

Group 3 transition metal and *f*-element complexes are among the most active catalysts for intramolecular alkene hydroamination. By contrast, intermolecular hydroamination of unactivated alkenes remains particularly challenging and only a handful of electropositive metal complexes show high catalytic activity, as discussed in Chapter 1, Section 1.3.4.[42,43,49,51] The majority of hydroamination catalysts are neutral, whereas most olefin polymerization catalysts are cationic,[115,120,124] capitalizing on lower coordination numbers and more electrophilic metal centers. Nevertheless, a small number of highly active neutral (single component) rare earth alkyl ethylene polymerization catalysts have been reported (*vide supra*, Section 1.4.3).[124–127]

For both alkene/alkyne hydroamination and olefin polymerization, catalytic activity is highly sensitive to the steric and electronic properties of the supporting ligand(s). For example, the rate of 1-amino-2,2-dimethyl-4-pentene cyclization by [(L)Lu(CH(SiMe$_3$)$_2$)] catalysts increased substantially as the ligand set, L, was varied from two C$_5$Me$_5$ (Cp*) anions to Me$_2$Si(C$_5$Me$_4$)$_2$ to Me$_2$Si(C$_5$Me$_5$)(N^{t}Bu).[140] Furthermore, the supporting ligand set plays a critical role in defining the temperature range within which a catalyst can operate.

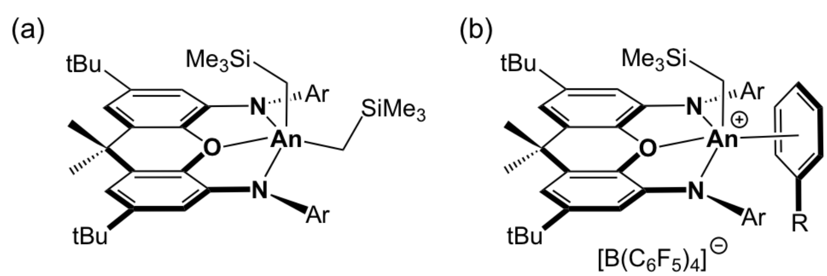

Figure 2.1: Actinide(IV) Alkyl Complexes of the XA$_2$ Pincer Ligand: (a) Neutral [(XA$_2$)An(CH$_2$SiMe$_3$)$_2$]; (b) Cationic [(XA$_2$)An(CH$_2$SiMe$_3$)(η^n-arene)][B(C$_6$F$_5$)$_4$] (An = Th, U; Ar = 2,6-diisopropylphenyl; R = H, Me, F).

Previous research in the Emslie group explored the potential for the highly-rigid, dianionic pincer ligand, 4,5-bis(2,6-diisopropylanilido)-2,7-di-*tert*-butyl-9,9-dimethylxanthene (XA$_2$) to provide access to actinide(IV) alkyl complexes with high thermal stability and reactivity. This led to the synthesis and isolation of neutral $[(XA_2)An(CH_2R)_2]$ (An = Th, R = $SiMe_3$ and Ph;[19] An = U,[24] R = $SiMe_3$ and CMe_3) complexes, which decomposed only slowly at 80 °C (R = $SiMe_3$). Furthermore, reactions of $[(XA_2)Th(CH_2R)_2]$ (R = $SiMe_3$ or Ph) with $[CPh_3][B(C_6F_5)_4]$ afforded the first examples of non-cyclopentadienyl thorium alkyl cations, $[(XA_2)Th(CH_2SiMe_3)(\eta^n\text{-arene})][B(C_6F_5)_4]$ (arene = benzene or toluene; Figure 2.1) and $[(XA_2)Th(CH_2Ph)(\eta^n\text{-toluene})][B(C_6F_5)_4]$.[20,21] However, in toluene and benzene, these thorium alkyl cations were inactive for ethylene (1 atm) polymerization, likely due to an inability of ethylene to compete with the arene solvents for coordination to thorium.

Following on from this research, the Emslie group became interested in determining whether 4,5-bis(anilido)xanthene ligands (i.e. XA_2 and related rigid pincer ligand dianions) could provide access to thermally robust monoalkyl complexes of trivalent rare earth elements, and whether these neutral complexes would exhibit appreciable activity for olefin polymerization or alkene-/alkyne hydroamination; alkyl complexes with high thermal stability are of particular interest for intermolecular hydroamination since this challenging transformation typically requires extended reaction times at elevated temperature.

Described herein is the synthesis of thermally robust yttrium monoalkyl and tetramethylaluminate complexes of a 4,5-bis(anilido)xanthene pincer ligand (XN_2) that is closely related to XA_2, isolation of a base-free aluminum methyl analogue, and both intra- and inter-molecular hydroamination using the yttrium trimethylsilylmethyl complex.

2.2 The XN_2 Ligand Synthesis

The synthesis of the XN_2 ligand begins with the synthesis of 2,4,6-triiso-propylaniline ($TrippNH_2$) (Scheme 2.1) and 4,5-dibromo-2,7-di-*tert*-butyl-9,9--dimethylxanthene (XBr_2) (Scheme 2.2). Following the literature procedures, $TrippNH_2$ was synthesized in two steps beginning with the reaction of 1,3,5--triisopropylbenzene with nitric acid to form 1-nitro-2,4,6-triisopropylbenzene ($TrippNO_2$).[141–143] This reaction was performed on a 95 g scale and cleanly yielded $TrippNO_2$ in a 78 % yield. The subsequent reaction with hydrazine hydrate was routinely performed on an 8 g scale, and $TrippNH_2$ was isolated in a 66 % yield, was dried over calcium hydride and distilled prior to the reaction with XBr_2.[141–143]

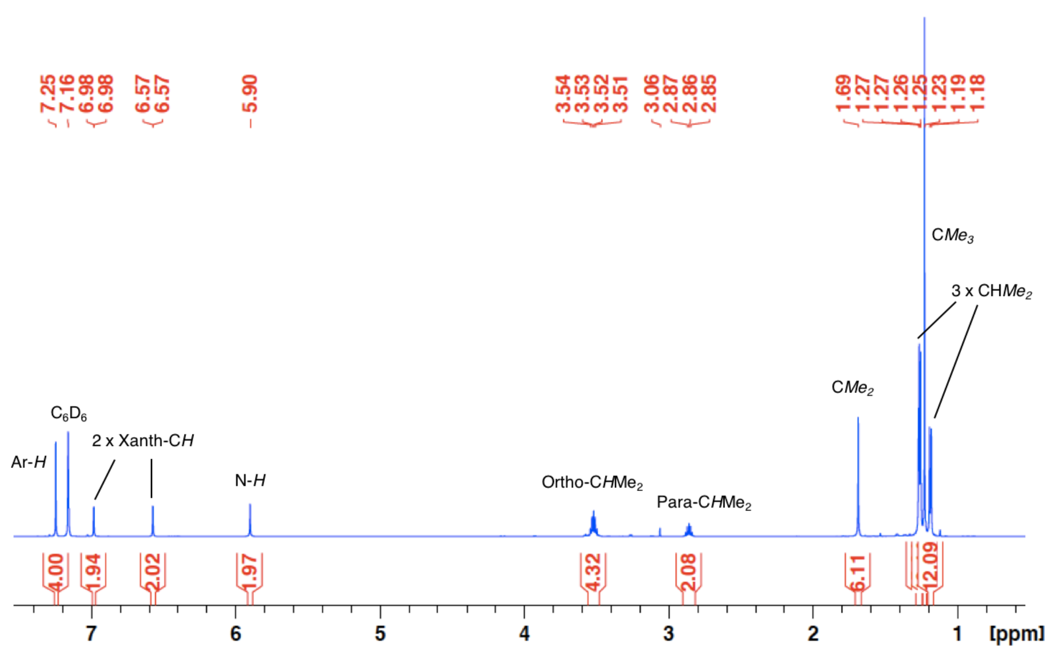

Figure 2.2: The ^1H NMR Spectrum of H_2XN_2 (**1**) (600 MHz, C_6D_6).

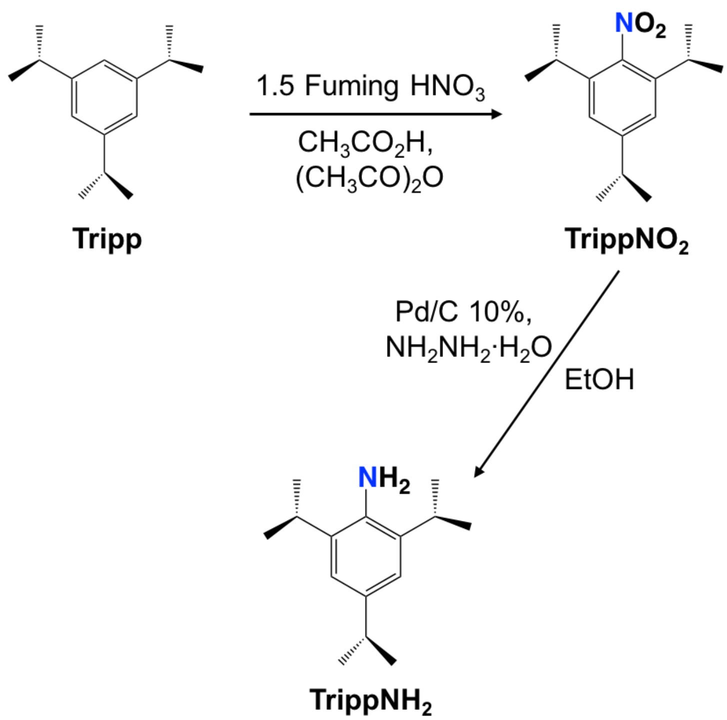

Scheme 2.1: The Synthesis of 2,4,6-Triisopropylaniline (**TrippNH$_2$**) from 1,3,5-Triisopropylbenzene (**Tripp**).

4,5-Dibromo-2,7-di-*tert*-butyl-9,9-dimethylxanthene (XBr_2) was synthesized following literature procedures in three steps from commercially-available xanthone (Scheme 2.2).[144] The reaction of xanthone with $AlMe_3$ was performed on a 50 g scale and 9,9-dimethylxanthene was isolated in 90 % yield. The subsequent Friedel-Crafts alkylation was performed on a 48 g scale and yielded 2,7-di-*tert*-butyl-9,9-dimethylxanthene in 54 % yield. The bromination reaction was routinely performed on a 10 g scale and formed XBr_2 in 55 % yield after purification via recrystalization (Scheme 2.2).

Hartwig-Buchwald coupling of 4,5-dibromo-2,7-di-*tert*-butyl-9,9-dimethylxanthene (XBr_2) with two equivalents of 2,4,6-triisopropylaniline afforded the

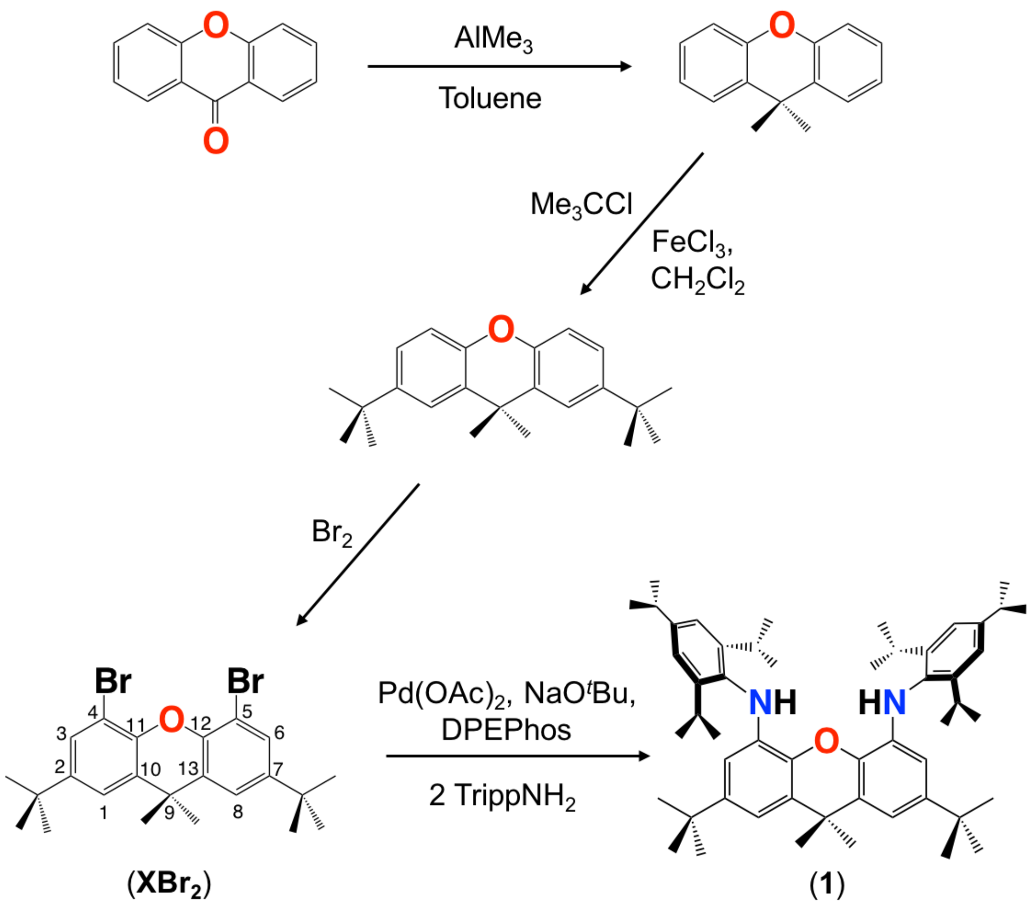

Scheme 2.2: The Synthesis of H_2XN_2 (**1**).

pro-lingand 4,5-bis(2,4,6-triisopropylanilino)-2,7-di-*tert*-butyl-9,9-dimethylxanthene (H_2XN_2, **1**) in a 52 % isolated yield (Scheme 2.2, Figure 2.2).

Stirring H_2XN_2 with excess KH in DME at 24 °C produced the dipotassium salt of the 4,5-bis(2,4,6-triisopropylanilido)-2,7-di-*tert*-butyl-9,9-dimethylxanthene ligand, $[K_2(XN_2)(DME)_x]$ (**2**; $x = 2$-2.5), as a beige solid in 80 % isolated yield (Scheme 2.3).

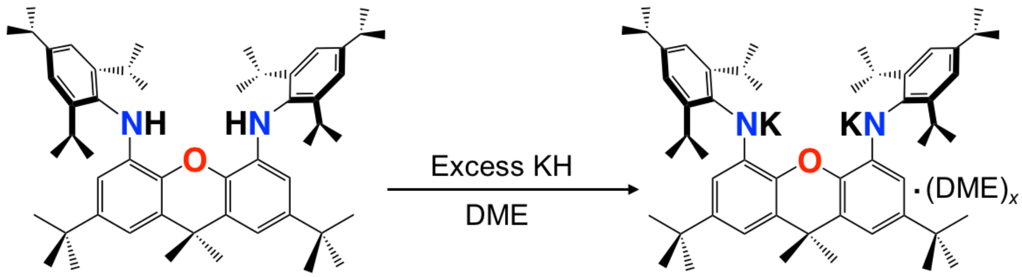

(1)

(2)
x = 2-2.5

Scheme 2.3: The Synthesis of $[K_2(XN_2)(DME)_x]$ (**2**).

2.3 Yttrium and Aluminum Alkyl Complexes Bearing the XN_2 Ligand

The salt metathesis reaction of $[K_2(XN_2)(DME)_2]$ (**2**) with $[YI_3(THF)_{3.5}]$-produced $[(XN_2)YI(THF)]$, but in numerous attempts the reaction was always contaminated by a small amount (10–20 %) of pro-ligand. It is suspected that the source of the pro-ligand is $[YI_3(THF)_{3.5}]$, which may not be completely dry and therefore converts some of the potassium salt back to the pro-ligand. However, even after attempted drying of YI_3 by stirring for 24 h in neat Me_3Si-I, followed by the synthesis of $[YI_3(THF)_{3.5}]$, the subsequent reaction with $[K_2$-$(XN_2)(DME)_2]$ (**2**) still resulted in pro-ligand being observed (10 % relative to the product). Due to the very high solubility of $[(XN_2)YI(THF)]$ and H_2XN_2, separation proved to be futile and isolation of pure $[(XN_2)YI(THF)]$ was not achieved nor pursued further.

As an alternative to salt metathesis for ligand attachment, alkane elimination was pursued; the reaction of H_2XN_2 with $[Y(CH_2SiMe_2R)_3(THF)_2]$ (R

= Me or Ph),[18,145] followed by crystallization from $O(SiMe_3)_2$, afforded the monoalkyl yttrium complexes, $[(XN_2)Y(CH_2SiMe_3)(THF)]\cdot(O(SiMe_3)_2)_x$ (**3**, x = 1-1.5, 52 % yield) and $[(XN_2)Y(CH_2SiMe_2Ph)(THF)]\cdot(O(SiMe_3)_2)$ (**4**, 49 % yield) respectively (Scheme 2.4). Both **3** and **4** were only ~50 % decomposed after 12 h at 100 °C, demonstrating appreciable thermal stability.

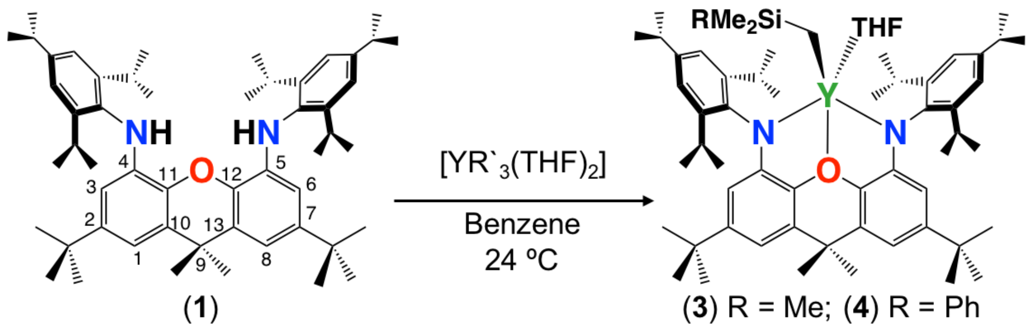

Scheme 2.4: The Synthesis of Yttrium Complexes **3** (R = Me) and **4** (R = Ph) from $[YR'_3(THF)_2]$ ($R' = CH_2SiMe_2R$).

The ^{1}H NMR spectra of **3** and **4** (Figures 2.3 and 2.4) are consistent with the expected C_s-symmetric structures, as evidenced by two Ar-H, two ortho-CHMe$_2$, and two CMe_2 peaks, and in both compounds the yttrium-CH_2 signal was observed as a low frequency doublet (–0.22 and –0.07 ppm, respectively); the $^2J_{1H,89Y}$ coupling is 3.5 Hz, which is slightly above the usual range of 1.8 to 2.8 Hz.[12,30,57,146,147]

X-ray quality crystals of $[(XN_2)Y(CH_2SiMe_3)(THF)]\cdot O(SiMe_3)_2$ (**3**·O(Si-Me$_3$)$_2$) were obtained by cooling a concentrated $O(SiMe_3)_2$ solution to –30 °C (Figure 2.5, Table 2.1). Yttrium is 5-coordinate with the three anionic donors and THF arranged in an approximate tetrahedron around the metal center.

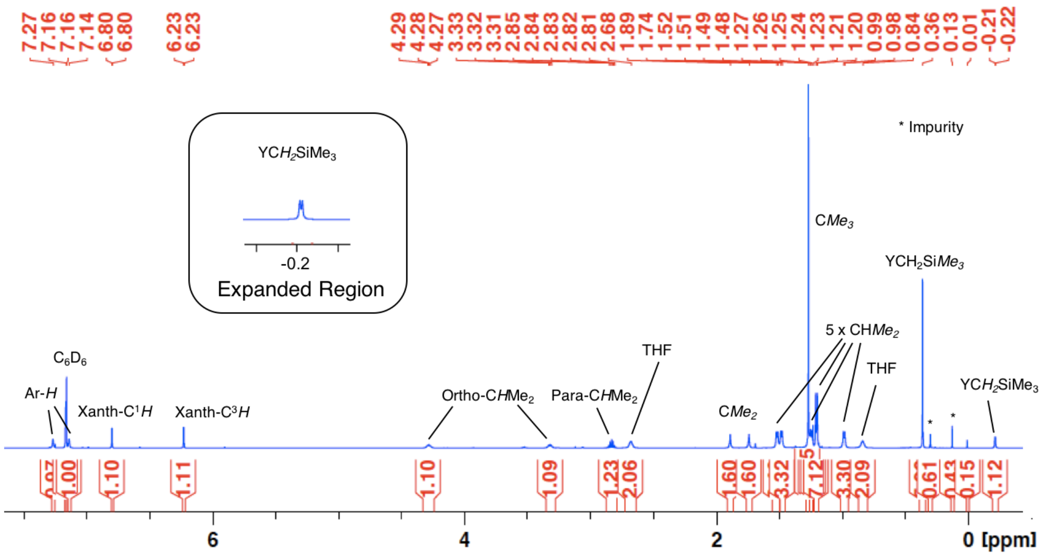

Figure 2.3: The ^{1}H NMR Spectrum of Complex **3** (600 MHz, C_6D_6).

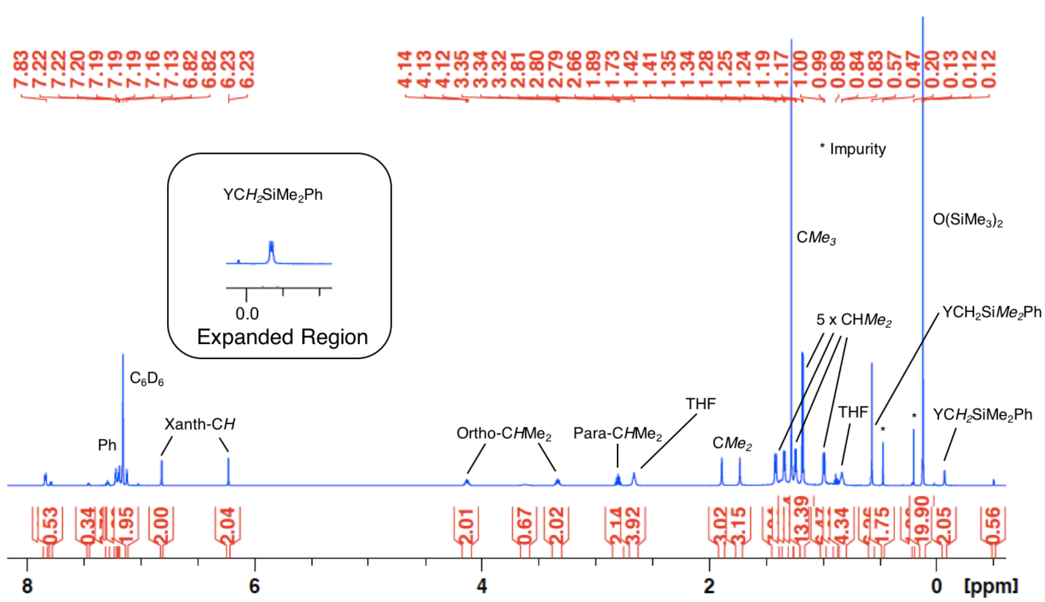

Figure 2.4: The ^{1}H NMR Spectrum of Complex **4** (600 MHz, C_6D_6).

The smallest angle in this distorted tetrahedron is the O(2)–Y–C(54) angle of 97°, and the largest is the N(1)–Y–N(2) angle of 129°, while the others are

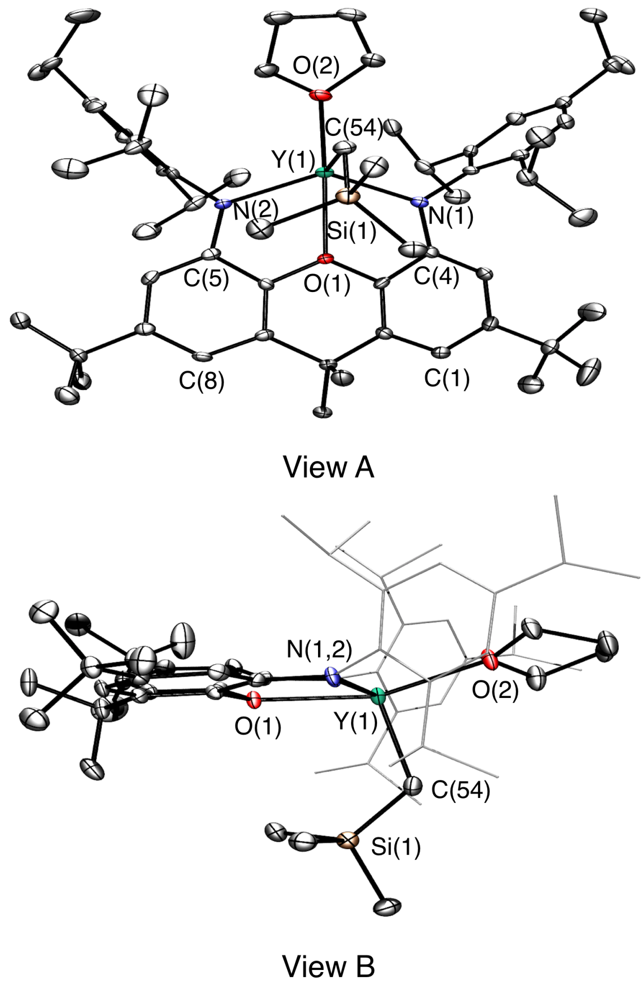

Figure 2.5: Two views of the X-ray crystal structure for compound **3**·O-$(SiMe_3)_2$. Ellipsoids are set to 50 %. Hydrogen atoms and lattice solvent are omitted, and in view B the 2,4,6-triisopropylphenyl groups are depicted in wire-frame format for clarity. Selected bond lengths [Å] and angles [°]: Y–N(1) 2.252(3), Y–N(2) 2.252(3), Y–C(54) 2.364(3), Y–O(1) 2.347(2), Y–O(2) 2.312(2), N(1)–Y–N(2) 128.88(9), N(1)–Y–C(54) 105.9(1), N(2)–Y–C(54) 109.9(1), O(1)–Y–C(54) 103.98(9), O(2)–Y–C(54) 97.4(1), O(2)–Y–N(2) 106.62(8), O(2)–Y–N(1) 103.60(9), Y–C(54)–Si(1) 121.3(2).

between 104 and 110°. The central oxygen of the xanthene backbone is then coordinated on the N(1)/N(2)/C(54) face of the tetrahedron, closest to the nitrogen donors, with 68-69° N(1)–Y–O(1) and N(2)–Y–O(1) angles. Yttrium lies 0.74 Å out of the plane of the XN_2 ligand donor atoms, leading to a 50° angle between the NON plane and the NYN plane. The xanthene backbone of the XN_2 ligand is slightly bent, with a 25° angle away from planarity, based on the relative orientation of the two aryl rings of the ligand backbone. Additionally, in order to accommodate yttrium within the coordination pocket of the ligand, the nitrogen donors of the ligand are bent towards the metal, as illustrated by C(1)···C(8), C(4)···C(5) and N(1)···N(2) distances of 4.98 Å, 4.56 Å and 4.06 Å respectively.

The Y–N distances of 2.252(3) Å in **3** are within the expected range compared to those in related yttrium alkyl compounds, including [(O{C_6H_4(N^{t}Bu)-*o*}$_2$)Y(CH($SiMe_3$)$_2$)(THF)] (2.294(9) and 2.286(10) Å);[30] [{(*R*)-$C_{20}H_{12}$($NSiMe_3$)$_2$}Y(CH_2SiMe_3)(THF)$_2$] (2.254(3) and 2.278(3) Å);[146] and [(ArN(CH_2)$_3$NAr)Y(CH_2Ph)(THF)$_2$] (Ar = $C_6H_3{}^i Pr_2$-2,6; 2.215(4) and 2.191(3) Å).[148] Additionally, the Y–O_{THF} and Y–O(1) distances (2.312(2) Å and 2.347(2) Å, respectively) are unremarkable, and similar to those in [(O{C_6H_4(N^{t}Bu)-*o*}$_2$)Y(CH($SiMe_3$)$_2$)(THF)] (Y–O_{THF} = 2.356(8) Å, Y–O_{OAr2} = 2.337(8) Å).[30] The Y–C(54) distance is 2.364(3) Å, which falls at the lower end of the range typically observed for 5-coordinate yttrium alkyl compounds such as [(O{C_6H_4(N^{t}Bu)-*o*}$_2$)Y(CH($SiMe_3$)$_2$)(THF)] (2.422(11) Å);[30] [{(*R*)-$C_{20}H_{12}$($NSiMe_3$)$_2$}Y(CH_2SiMe_3)(THF)$_2$] (2.434(4) Å);[146] [{(*Z*)-ArNC(Me)=C(Me)NAr}Y(CH_2SiMe_3)(THF)$_2$] (Ar = $C_6H_3{}^i Pr_2$; 2.399(2) Å);[147] and [{ArNCMeCHCMeN(CH_2)$_2$N^{t}Bu}Y(CH_2SiMe_3)(THF)] (2.377(3) Å).[149]

The neutral monoalkyl complex $[(XN_2)Y(CH_2SiMe_3)(THF)]\cdot(O(SiMe_3)_2)_x$ (**3**; x = 1-1.5) was tested for ethylene polymerization catalysis at 20 °C and 80 °C for 1 h (toluene, 1 atm of ethylene), but showed near-zero activity. The potential for **3** to polymerize 1-octene was also evaluated, with and without the addition of $Al(octyl)_3$ (20 equiv.) to act as a scavenger for residual moisture or reactive impurities, and again no polymer formation was observed. However, a ^{1}H NMR spectrum of **3** in the presence of $Al(octyl)_3$ or $AlMe_3$ revealed the formation of a new yttrium complex, and $[(XN_2)Y\{(\mu\text{-}Me)_2AlMe_2\}(THF)]\cdot O(SiMe_3)_2$ (**5**$\cdot O(SiMe_3)_2$) was isolated from the reaction of **3** with excess $AlMe_3$ (Scheme 2.5), followed by crystallization from $O(SiMe_3)_2$. Compound **5** is C_s symmetric featuring a doublet at –0.56 ppm ($^2J_{1H,89Y}$ = 3.8 Hz) for the twelve Al*Me₄* protons in the ^{1}H NMR spectrum, indicative of rapidly exchanging terminal and bridging methyl groups at room temperature (Figure 2.6). Similar behavior has previously been reported by Anwander *et al.* for $[\{HC(NAr)_2\}Y(AlMe_4)_2]$,[150] $[\{N(NC_6H_4Ar\text{-}o)_2\}Y(AlMe_4)_2]$ (Ar = $C_6H_3{}^iPr_2$-2,6),[151] $[(BDPP)Y(AlMe_4)]$ (BDPP = 2,6-bis(2,6-diisopropylanilidomethyl)-pyridine),[32] and $[\{(AlMe_4)Y(\mu\text{-}N(C_6H_2{}^tBu_3\text{-}2,4,6))\}_2]$[152] with $^2J_{1H,89Y}$ couplings between 2.3 Hz and 3.0 Hz.

Small crystals of $[(XN_2)Y\{(\mu\text{-}Me)_2AlMe_2\}(THF)]\cdot(O(SiMe_3)_2$ (**5**$\cdot O(SiMe_3)_2$, 20 % yield) were obtained by cooling a concentrated $O(SiMe_3)_2$ solution to –30 °C. However, even after multiple attempts, only very small crystals were obtained, leading to a high R factor (12 %) and a structure that is only suitable to establish connectivity (Figure 2.7, Table 2.1). In the solid state, **5** adopts a distorted octahedral geometry at yttrium with one methyl group of

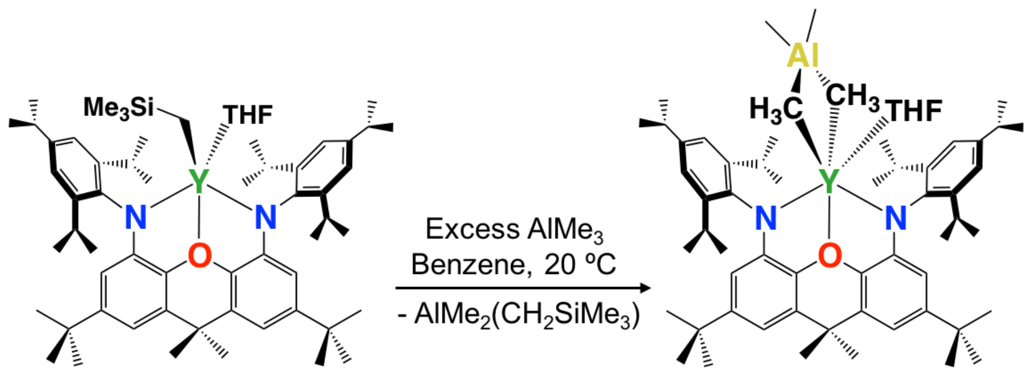

(**3**) (**5**)

Scheme 2.5: Reaction of Yttrium Alkyl Complex **3** with Excess $AlMe_3$ To Form $[(XN_2)Y\{(\mu\text{-}Me)_2AlMe_2\}(THF)]\cdot O(SiMe_3)_2$ ($\mathbf{5}\cdot O(SiMe_3)_2$).

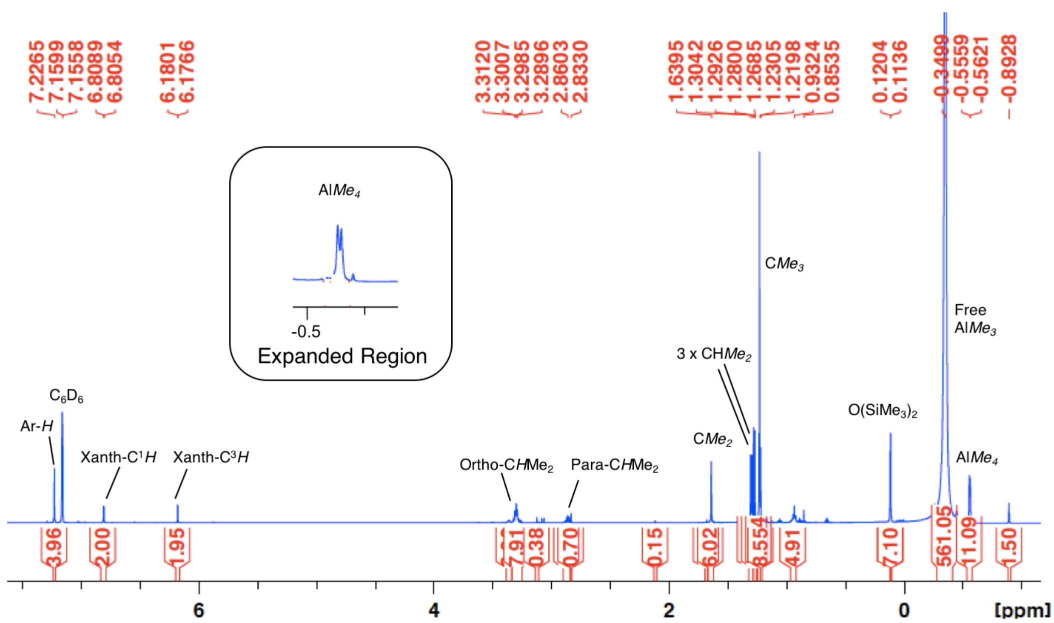

Figure 2.6: The ^1H NMR Spectrum of Complex **5** (600 MHz, C_6D_6).

the $AlMe_4$ anion located in the plane of the NON-donors of the XN_2 ligand, resulting in a more planar XN_2 ligand backbone relative to 5-coordinate **3**.

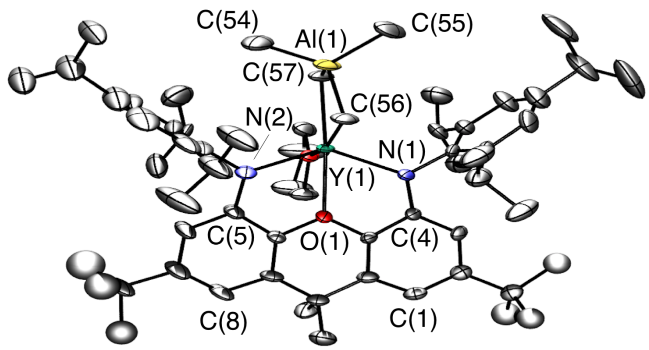

View A

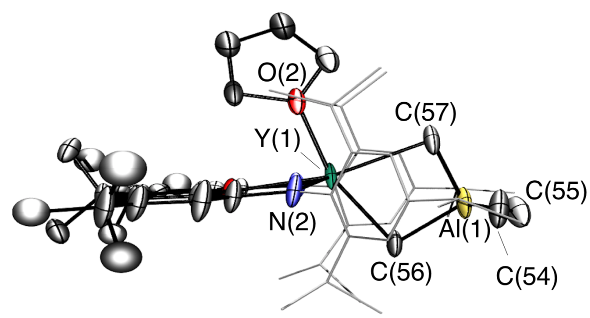

View B

Figure 2.7: Two views of the X-ray crystal structure for compound **5**·$O(SiMe_3)_2$. Ellipsoids are set to 50 %. Hydrogen atoms and lattice solvent are omitted for clarity. The *tert*-butyl groups are rotationally disordered over two positions and only one is shown for clarity. In view B the 2,4,6-triisopropylphenyl groups are depicted in wire-frame format for clarity.

A range of rare earth tetramethylaluminate complexes have previously been prepared by reaction of a metal alkyl or amido complex with a trialkylalane. However, in some cases these reactions resulted in multidentate ligand transfer from the rare earth metal to aluminum, as illustrated in Scheme 2.6.[153–155] Furthermore, ligand transfer to aluminum has been observed in the reac-

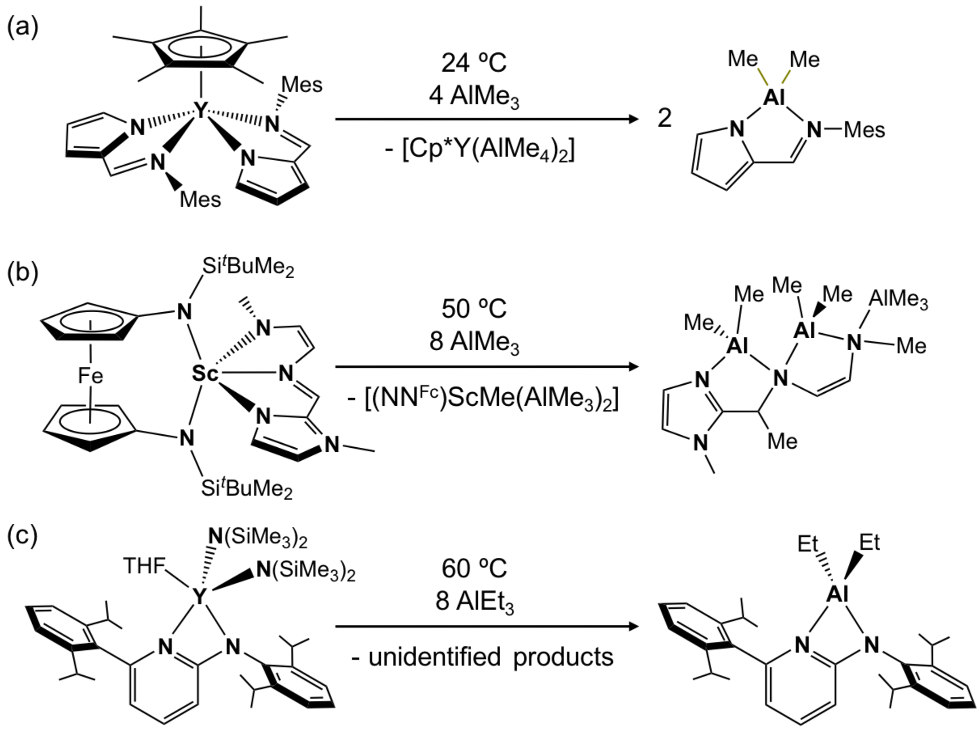

Scheme 2.6: Literature Reactions Involving Multidentate Ligand Transfer from a Rare Earth Element to Aluminum.

tions of several protio-ligands or alkali metal ligand salts with $[Ln(AlMe_4)_3]$ reagents.[32,151,156,157] However, XN_2 ligand transfer to Al was not observed in the reaction to generate **5**, and compound **5** proved to be quite thermally robust, showing no sign of decomposition after heating at 80 °C in benzene for 24 h in the presence of excess $AlMe_3$. This lack of ligand transfer to aluminum is not due to an inability of the XN_2 ligand to accommodate aluminum, since $[(XN_2)AlMe]\cdot O(SiMe_3)_2$ (**6**$\cdot O(SiMe_3)_2$) was successfully synthesized from the reaction between H_2XN_2 and $AlMe_3$ at 85 °C in 54 % yield (Scheme 2.7, Figure 2.8).

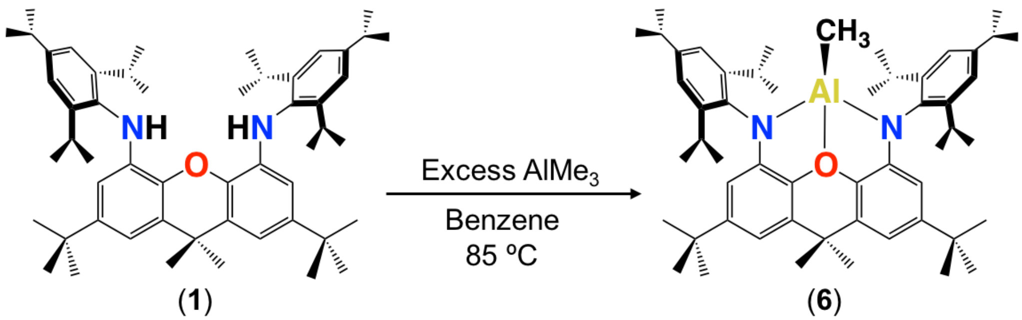

Scheme 2.7: The Synthesis of Aluminum Complex **6**.

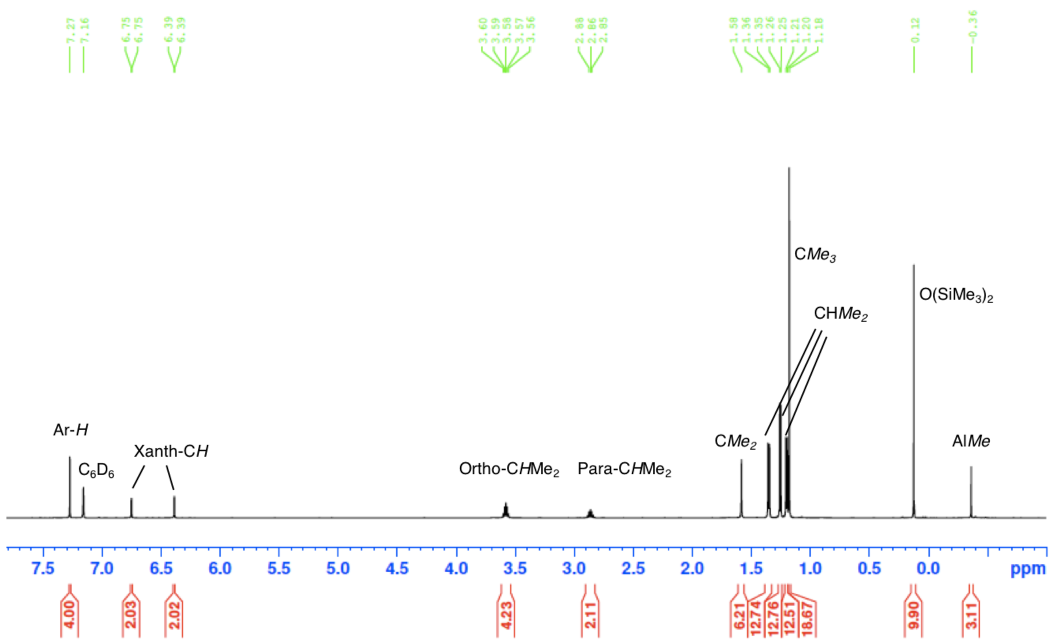

Figure 2.8: The ^{1}H NMR Spectrum of Complex **6** (600 MHz, C_6D_6).

X-ray quality crystals of $[(XN_2)AlMe]\cdot(O(SiMe_3)_2)_{0.5}$ (**6**$\cdot(O(SiMe_3)_2)_{0.5}$) were obtained by cooling a concentrated $O(SiMe_3)_2$ solution to –30 °C (Figure 2.9, Table 2.1). Aluminum is 4-coordinate with a significantly distorted trigonal planar arrangement of the three anionic donors; the sum of the N(1)–

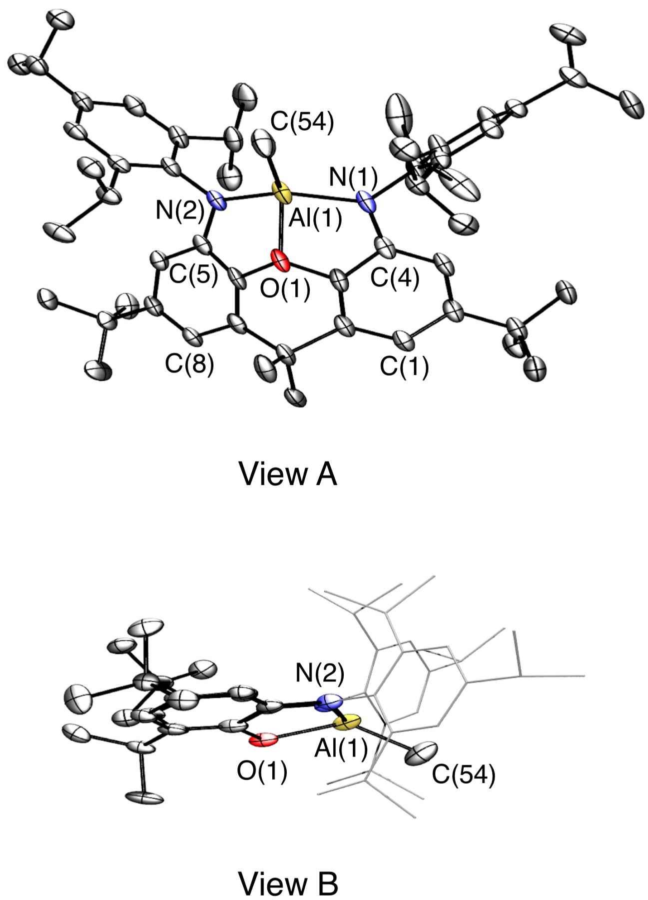

Figure 2.9: Two views of the X-ray crystal structure for compound **6**·(O(SiMe$_3$)$_2$)$_{0.5}$. Ellipsoids are set to 50 %. Hydrogen atoms and lattice solvent are omitted for clarity. In view B the 2,4,6-triisopropylphenyl groups are depicted in wire-frame format for clarity. Selected bond lengths [Å] and angles [°]: Al–N(1) 1.858(2), Al–N(2) 1.871(2), Al–C(54) 1.942(2), Al–O(1) 1.973(2), N(1)–Al–N(2) 134.26(7), N(1)–Al–C(54) 110.77(9), N(2)–Al–C(54) 110.27(9), O(1)–Al–C(54) 134.80(9), O(1)–Al–N(1) 82.57(7), O(1)–Al–N(2) 82.73(7).

Al(1)–C(54), N(2)–Al(1)–C(54) and N(1)–Al(1)–N(2) angles is 355°, and C(54) is located 0.84 Å out of the N(1)/Al/N(2) plane. The neutral oxygen donor coordinates to aluminum with an obtuse O(1)–Al(1)–C(54) angle of 135°, but the Al(1)–O(1) distance of 1.973(2) Å is unremarkable. For example, it is only slightly longer than that in [{O(C_6H_4(NCy)-*o*)$_2$}AlMe] (1.937(2) Å), in which the more flexible NON-donor accommodates a more acute O–Al–C angle of 117.0(1)°,[158] and it is identical within error to the Al–O distance in [{($Me_3Si)_3C$}$AlMe_2$(THF)] (1.969(2) Å).[159]

Structure	**3**·O($SiMe_3$)$_2$	**5**·O($SiMe_3$)$_2$	**6**·(O($SiMe_3$)$_2$)$_{0.5}$
Formula	$C_{67}H_{111}N_2O_3Si_3Y_1$	$C_{67}H_{113}Al_1N_2O_3Si_2Y_1$	$C_{114}H_{172}Al_2N_4O_3Si_2$
Formula wt	1165.75	1166.66	1756.69
T (K)	100(2)	100(2)	100(2)
Cryst. Syst.	Monoclinic	Monoclinic	Monoclinic
Space Group	P 21/c	P 21/c	I2/a
a (Å)	24.029(2)	21.812(3)	19.330(2)
b (Å)	14.7584(12)	12.0055(19)	29.736(2)
c (Å)	20.3216(17)	27.328(4)	20.4953(14)
α [°]	90	90	90
β [°]	106.291(2)	101.616(4)	108.901(2)
γ [°]	90	90	90
Volume [Å^3]	6917.3(10)	7009.9(19)	11145.7(16)
Z	4	4	4
Density (calcd; Mg/m^3)	1.119	1.105	1.047
μ (mm^{-1})	0.937	0.920	0.096
F(000)	2528	2532	3848
Crystal Size (mm^3)	0.277×0.138×0.047	0.272×0.142×0.110	0.583×0.345×0.074
θ Range for Collection [°]	1.730–25.419	1.521–24.760	1.860–26.407
No. of Refns. Collected	64960	61948	47064
No. of Indep. Refns.	12729	11965	11425
Completeness to θ Max (%)	100.0	99.5	100.0
Absorption Correction	Multi-Scan	Numerical	Numerical
Max and Min Transmission	1.000,0.8609	1.000,0.7679	24.389,2.226
GOF on F^2	1.001	1.041	1.036
Final R_1 [$I > 2\sigma(I)$]	R1 = 0.0533 wR2 = 0.1049	R1 = 0.1233 wR2 = 0.2467	R1 = 0.0522 wR2 = 0.1249
R indices (all data)	R1 = 0.1060 wR2 = 0.1221	R1 = 0.1998 wR2 = 0.2819	R1 = 0.0842 wR2 = 0.1427

Table 2.1: Crystallographic Data Collection and Refinement Parameters for Complexes **3**, **5** and **6**.

In the solid state, the xanthene backbone of the XN_2 ligand in **6** is significantly bent, with a 47° angle between the two aryl rings of the backbone, as compared to the 25° angle observed for **3**. Aluminum lies 0.72 Å above the NON plane of the XN_2 ligand donors, leading to an 88° angle between the NON plane and the NAlN plane. Once again, this angle is significantly larger than the angle observed for **3** (50°). Furthermore, the amido donors of the XN_2 ligand are strongly bent towards aluminum, as illustrated by C(1)···C(8), C(4)···C(5) and N(1)···N(2) distances of 4.86 Å, 4.20 Å and 3.44 Å respectively. These structural features enable the XN_2 ligand to accommodate Al–N bonds in **6** that are almost 0.4 Å shorter than the Y–N bonds in **3** (1.858(2) Å and 1.871(2) Å for **6** vs 2.252(3) Å for **3**). The Al–N distances in **6** are similar to those in 4-coordinate [{$O(C_6H_4(NCy)$-*o*$)_2$}AlMe] (1.837(2) and 1.854(2) Å)[158] and longer than those in 3-coordinate [{$ArN(CH_2)_3NAr$}AlMe] (Ar = C_6H_3-$^i Pr_2$-2,6; 1.760(3) and 1.766(3) Å).[160] This same trend is followed for the Al–C bonds, which are 1.942(2) Å in **6**, and 1.947(3) Å[158] and 1.915(4) Å,[160] respectively, for the aforementioned 4- and 3-coordinate literature complexes.

The synthetic accessibility of both **3** and **6** demonstrates the ability of the XN_2 ligand to accommodate both small and large metal ions, although this does not detract from the ability of 4,5-bis(anilido)xanthene dianions to function as rigid meridionally-coordinating pincer ligands upon coordination to large rare earth and actinide elements.

2.4 [(XN$_2$)Y(CH$_2$SiMe$_3$)(THF)] Intramolecular and Intermolecular Hydroamination Catalysis

[(XN$_2$)Y(CH$_2$SiMe$_3$)(THF)·(O(SiMe$_3$)$_2$)$_x$ (**3**; x = 1-1.5) was investigated as a catalyst for both intra- and inter-molecular hydroamination with a variety of reagents, the results of which are summarized in Tables 2.2 and 2.3.

Entry	Reagent	Product	Mol %	Time	Temp. (°C)	Product Formation[a]	N_t (h^{-1})[b]
1	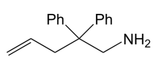	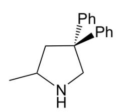	0.2	< 20 min	24	> 99 %	≥ 1500
2	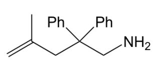	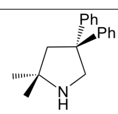	1	1.5 h	24	> 99 %	∼67
3	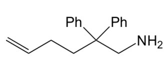	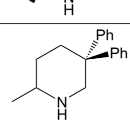	10	< 10 min	24	> 99 %	≥60
4	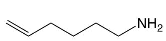	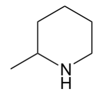	10	34 h ≤45 min	24 60	> 99 % > 99 %	∼0.3 ≥13

Table 2.2: Intramolecular Hydroamination Reactivity with **3**.
*Reactions performed in C$_6$D$_6$; [a] Conversion of Reactant to Product Determined by NMR Spectroscopy; [b] Turnover Frequency.

Complex **3** catalyzed intramolecular hydroamination of aminoalkenes in deuterated benzene at 24 °C, leading to >99 % product formation in all cases, confirmed by ^{1}H NMR spectroscopy (Table 2.2). The reaction with 1-amino--2,2-diphenyl-4-pentene (entry 1) was complete within 10 minutes with 1 mol % catalyst loading, and within 20 minutes with 0.2 mol % catalyst. By contrast, the reactions with 1-amino-2,2-diphenyl-4-methyl-4-pentene (entry 2) and 1-amino-2,2-diphenyl-5-hexene (entry 3) required a longer reaction time or higher catalyst loading, respectively, for >99 % conversion. The lower reactivity of these substrates is a consequence of increased alkene steric hindrance (entry 2 compared to 1) and less favorable 6- versus 5-membered ring formation (entry 3 compared to 1). The room temperature activity of **3** for 1-amino-2,2-diphenyl-4-pentene hydroamination (turnover frequency, $N_t \geq 1500\ h^{-1}$) is comparable to that of the most active rare earth catalysts, including Hultzsch's yttrium catalysts (a) and (c) in Figure 1.7 (Ar = $C_6H_3Me_2$-3,5; R = R′ = ^{t}Bu),[56,61] and other group 3 and *f*-element catalysts reported by Marks *et al*; [(^{Ph2}Box)LaR_2] (Box = 2,2′-bis(2-oxazoline)methylenyl),[60] [(CGC)AnR_2]- (CGC = $Me_2Si(C_5Me_4)(N^tBu)$),[161] and Schafer *et al.*; [(AI)YR_2(THF)] (AI = *o*-C_6H_4(NAr)(CH=NAr), Ar = $C_6H_3{}^iPr_2$-2,6).[58]

In comparison to 1-amino-2,2-diphenyl-5-hexene (Table 2.2, entry 3), cyclization of 1-amino-5-hexene (entry 4) required 10 mol % catalyst and an extended (34 h) reaction time for >99 % conversion, due to the absence of cyclization-promoting geminal phenyl groups (the Thorpe-Ingold effect, *vide supra*, Section 1.3.1).[45,46] The ability of **3** to catalyze this reaction at room temperature is unusual, and at 60 °C the reaction was complete after 45 minutes, corresponding to a turnover frequency of 13 h^{-1}. For comparison, -[$Cp^*{}_2La(CH(SiMe_3)_2)$][54] and [(CGC)Th(NMe_2)$_2$],[161] reported by Marks *et al.*, catalyzed 1-amino-5-hexene cyclization with turnover frequencies of 5 h^{-1} and 0.2 h^{-1} at 60 °C, respectively, and the yttrium binol catalyst reported by Hultzsch *et al.* ((a) in Figure 1.7; Ar = $C_6H_3Me_2$-3,5) achieved a turnover frequency of 1.6 h^{-1} at 80 °C.[164]

Entry	Amine	Alkene or Alkyne[a]	Product	Time	Temp. (°C)	Product Formation[b],[c]	% Markovnikov Product[c]	N_t (h^{-1})[d]
1	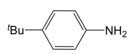	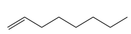	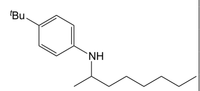	72 h	110	23 %	97	0.03
2	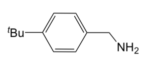		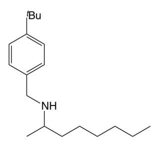	24 h	110	95 %	>99[e]	0.40
3	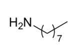		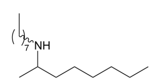	24 h	110	>99 %	96	0.42
4	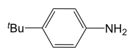		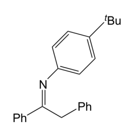	24 h	110	97 %[f]	N/A	0.40
5	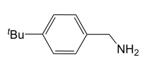		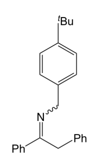	24 h	110	80 %[f]	N/A	0.33
6	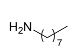		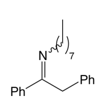	24 h	110	>99 %[f]	N/A	0.42

Table 2.3: Intermolecular Hydroamination Reactivity with **3**.
*Reactions performed in d_8-Toluene with 10 mol % catalyst loading; [a] Alkene/Alkyne present in 20 fold excess relative to the amine; [b] Conversion Determined by Product : Unreacted Amine ratio; [c] Determined by GC-MS; [d] Turnover Frequency; [e] Selectivity Determined by ^{1}H NMR Spectroscopy; [f] in entry 4 the product is formed as a single isomer, whereas in entries 5 and 6 the products are formed as 1:0.4 and 1:0.35 mixtures of the E and Z isomers (based on literature assignments for similar compounds),[162,163] respectively.

Intermolecular hydroamination is significantly more challenging compared to intramolecular hydroamination, and a limited number of rare earth catalysts are known.[43,61,165,166] At a catalyst loading of 10 mol %, compound **3** catalyzed intermolecular hydroamination reactions utilizing 4-*tert*-butyl-aniline, 4-*tert*-butylbenzylamine and *n*-octylamine in combination with 1-octene and diphenylacetylene (Table 2.3). The reactions were performed in toluene at 110 °C with a 20-fold excess of the alkene or alkyne substrate, and in all reactions with 1-octene the Markovnikov product was formed with high selectivity. Reactions with *n*-octylamine gave the highest conversion after 24 h, yielding >99 % product with both 1-octene and diphenylacetylene (entries 3 and 6). Even with a shorter reaction time, the reaction of 1-octene with 4-*tert*-butylbenzylamine (entry 2), afforded a higher conversion to the hydroamination product than the reaction with 4-*tert*-butyl-aniline (entry 1), consistent with the reduced steric hindrance and unimpeded basicity of the former amine. By contrast, the turnover frequency for the analogous reactions with diphenylacetylene shows little variation between the three amine substrates (entries 4-6).

2.5 Summary

In summary, a rigid NON-donor pincer ligand, XN_2, has been employed for the synthesis of two thermally robust yttrium alkyl complexes (**3** and **4**), a yttrium tetramethylaluminate complex (**5**) and an aluminum methyl complex (**6**). The ability of XN_2 to accommodate both yttrium and aluminum demonstrates the versatility of the ligand for coordination to metal ions with very different radii. The neutral yttrium alkyl complex, **3**, was tested as a polymerization catalyst for both ethylene and 1-octene with little success. However, **3** was found to be highly active for both intra- and inter-molecular hydroamination with a variety of substrates. The ability of **3** to catalyze room temperature intramolecular hydroamination of more challenging substrates, such as 1-amino-5-hexene, and intermolecular hydroamination of unactivated alkenes, positions **3** as one of the most active and general rare earth hydroamination catalysts reported thus far.

Chapter 3

Potassium and Yttrium Complexes of a Rigid Bis-Phosphido POP-Donor Ligand

Adapted with permission from: Motolko, K. S. A.; Emslie, D. J. H.; Jenkins, H. A.; Britten, J. F. *Eur. J. Inorg. Chem.* **2017**, 2920-2927.

3.1 Introduction

Ancillary ligands play a critical role in defining the thermal stability and reactivity of metal complexes, and the Emslie group has previously explored the use of rigid 4,5-bis(anilido)xanthene ligands in actinide and lanthanide chemistry. For example, the XA_2 (4,5-bis(2,6-diisopropylanilido)-2,7-di-*tert*-butyl-9,9-dimethylxanthene) pincer ligand was employed for the synthesis of thorium(IV), uranium(IV) and uranium(III) chloro complexes,[19,23] as well as dialkyl complexes of tetravalent thorium[19,20] and uranium[24] (Figure 3.1), thorium(IV) monoalkyl cations, and a thorium(IV) dication.[20,21] Furthermore, we recently reported the synthesis of a Y derivative of the XN_2 (4,5-bis(2,-4,6-triisopropylanilido)-2,7-di*tert*-butyl-9,9-dimethylxanthene) ligand, including monoalkyl derivatives (Figure 3.1), which are highly active catalysts for alkene and alkyne hydroamination.[167,168]

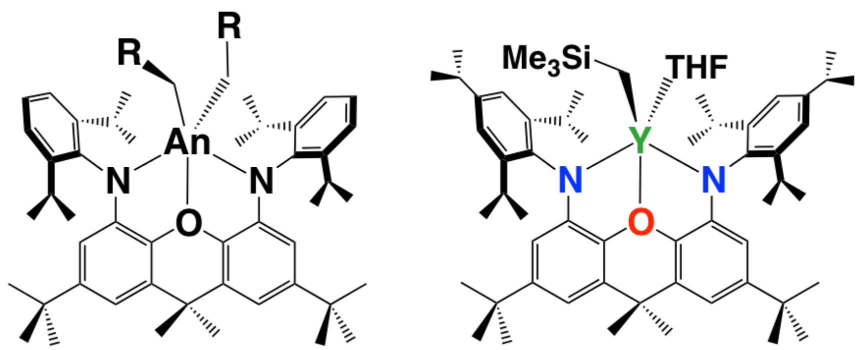

An = Th, U

(3)

Figure 3.1: Neutral 4,5-Bis(anilido)xanthene Alkyl Complexes of Thorium(IV), Uranium(IV) and Yttrium(III) (R = $SiMe_3$ or Ph).

In combination with large rare earth and actinide elements, the xanthene-backbone XA_2 and XN_2 ligands present a rigid meridionally-coordinating pincer array that is capable of stabilizing highly reactive organometallic derivatives. Additionally, the rigidity of the ligand framework provides an opportunity to introduce softer donor atoms into the coordination sphere of rare earth or actinide elements, and the Emslie group has previously prepared uranium(III) and (IV) complexes of a thioxanthene analogue of the XA_2 ligand, TXA_2.[23] As an extension of this concept, we became interested in probing the rare earth coordination behavior of a 4,5-bis(arylphosphido)xanthene analogue of XN_2.

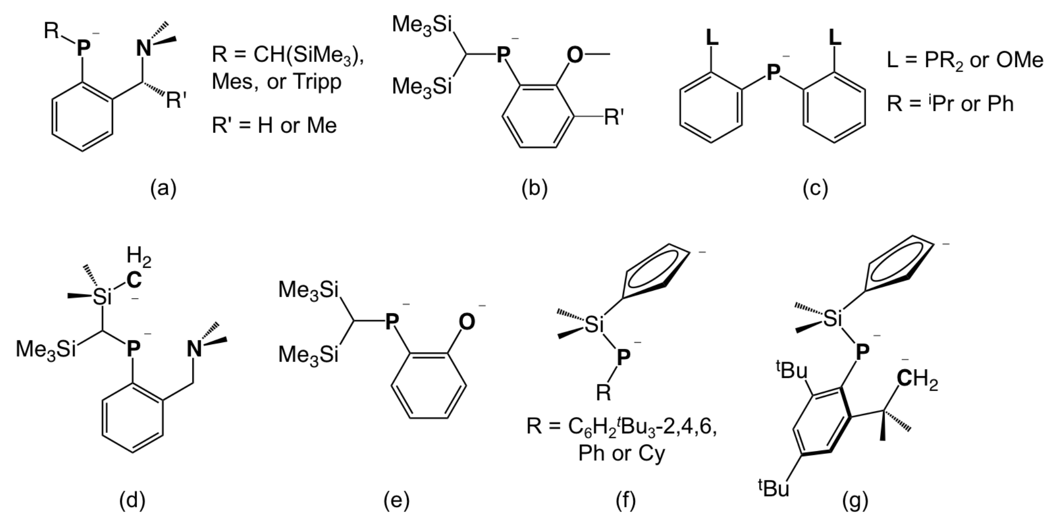

Figure 3.2: Multidentate Phosphido Ligands Employed in Rare Earth Chemistry.

In comparison to amido ligands, phosphido ligands are far less explored in group 3 and *f*-element chemistry,[169] especially multidentate ligands containing phosphido donors. Ligands of this type that have been employed in rare earth chemistry are illustrated in Figure 3.2. The PN-, PO-, PPP-, OPO- and Cp/P-donor ligands (a),[170–173] (b),[170,174] (c) ($L = PR_2$),[175] (c) ($L = OMe$),[176] and (f)[177,178] were assembled prior to metal coordination. By contrast, (d)[173,179] and (g)[178] resulted from cyclometallation, and dianionic (e)[174] formed from monoanionic (b) ($R' = H$) via metal-mediated transfer of a methyl group from oxygen to the phosphorus donor of a second equivalent of ligand (b).

Described herein is the synthesis of a direct phosphorus analogue of the H_2XN_2 pro-ligand, H_2XP_2, and potassium complexes of the XP_2 dianion, including the first example of a potassium phosphido compound with a K_4P_4 cubic cage structure. The synthesis and structural characterization of an yttrium iodo XP_2 complex is also described, allowing comparison of the binding preferences of XP_2 and XN_2 in the coordination sphere of yttrium.

3.2 Synthesis of the XP_2 Ligand and the Di- and Tetra-metallic Potassium Salts

The synthesis of the XP_2 ligand required the synthesis of 2,4,6-triisopropylphenyldichlorophosphine ($TrippPCl_2$) (Scheme 3.1) and 4,5-dibromo-2,7-di-*tert*-butyl-9,9-dimethylxanthene (XBr_2) (*vide supra*, Section 2.2, Scheme 2.2). $TrippPCl_2$ was synthesized following literature procedures, starting with the bromination reaction of commercially-available 1,3,5-triisopropylbenzene (Tripp) on a 50 g scale to form 1-bromo-2,4,6-triisopropylbenzene (TrippBr) in 68 % yield.[180,181] Route A, involving lithiation of TrippBr followed by reaction with PCl_3, was initially utilized for the synthesis of $TrippPCl_2$. However, this reaction produced multiple products (the expected product, $TrippPCl_2$, as well as TrippPClBr and $TrippPBr_2$) and was low yielding (12 %). These products proved inseparable due to the similarities in solubility, and use of this mixture in the subsequent step of the synthesis resulted in low yields (15 %). The desired $TrippPCl_2$ precursor was therefore synthesized via Route B in Scheme 3.1, involving the synthesis of 2,4,6-triisopropylphenylmagnesium bromide from TrippBr and magnesium, and subsequent reaction with PCl_3. This reaction afforded $TrippPCl_2$ in 34 % yield after recrystalization (Scheme 3.1),[180,181] and Route B was chosen for all subsequent syntheses of $TrippPCl_2$ as it not only yields pure product, but it can be carried out on a large scale (reactions were routinely performed on a 10 g scale).

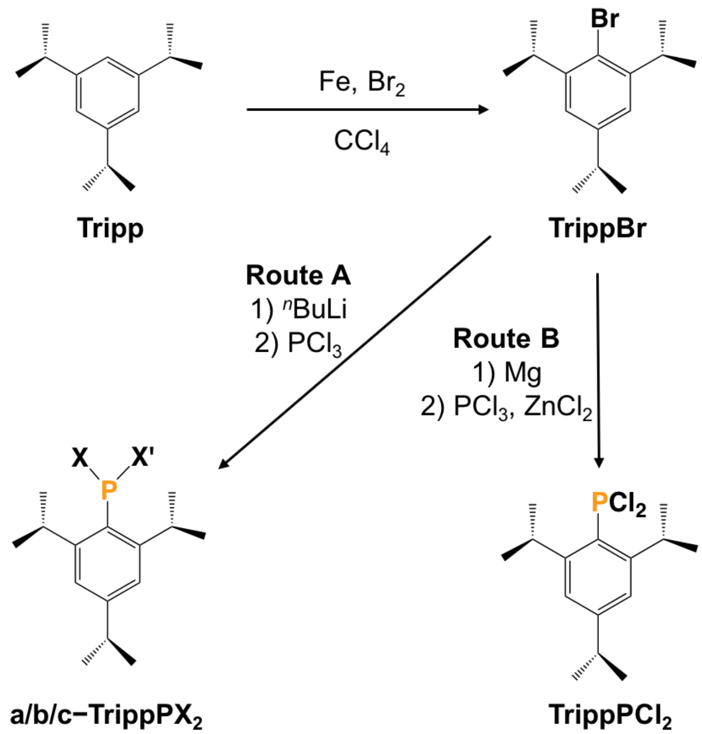

Scheme 3.1: The Synthesis of 2,4,6-Triisopropylphenyldichlorophosphine (**TrippPCl**$_2$) from 1,3,5-Triisopropylbenzene (**Tripp**). a-TrippX_2: X = X′ = Cl, b-TrippX_2: X = Cl, X′ = Br, c-TrippX_2: X = X′ = Br.

Reaction of 4,5-dibromo-2,7-di-*tert*-butyl-9,9-dimethylxanthene (XBr_2) with 2 equivalents of ^{n}BuLi in THF, followed by the addition of 2 equivalents of 2,4,6-triisopropylphenyldichlorophosphine ($TrippPCl_2$) afforded a 73 % yield of 4,5-bis(2,4,6-triisopropylphenylchlorophosphino)-2,7-di-*tert*-butyl-9,9-dimethylxanthene (XP_2Cl_2, **7**) as an approximate 1:1 ratio of diastereomers (Scheme 3.2; diastereomers were not identified as *rac* or *meso* due to overlapping C*Me$_2$* signals in the ^{1}H and ^{13}C NMR spectra of the C_s-symmetric *meso* isomer). Samples enriched in each diastereomer could be obtained by washing the isolated solid with a small volume of hexanes; the solid residue contained > 95 % of one diastereomer, while the liquor contained > 60 % of the other diastereomer.

Pure or enriched samples of the diastereomers of XP_2Cl_2 (**7**) were used to simplify NMR characterization. However, separation of diastereomers was not required prior to reaction with $LiAlH_4$ to form 4,5-bis(2,4,6-triisopropylphenylphosphino)-2,7-di-*tert*-butyl-9,9-dimethylxanthene ($H_2XP_2{\cdot}nLiCl$; **8**, n = 1–1.5), which was isolated in 87 % yield as an approximate 1:1 mixture of diastereomers, containing 1–1.5 equivalents of occluded LiCl based on elemental analysis (Scheme 3.2). The ^1H and ^{31}P NMR spectra of H_2XP_2 (**8**) revealed $^1J_{1H,31P}$ couplings of 225 Hz and 229 Hz for the P-H signals of the two diastereomers (Figure 3.3). These coupling constants are similar to those in Ph_2PH (218 Hz),[182] as well as related PCP-,[41] PNP-[39] and POP-donor[40] pro-ligands (211-227 Hz).

Stirring H_2XP_2 (**8**) with excess KH in DME at 24 °C for 72 h produced the dipotassium salt of the 4,5-bis(2,4,6-triisopropylphenylphosphido)-2,7-di-*tert*-butyl-9,9-dimethylxanthene dianion, $[K_2XP_2(DME)_{2.5}]$ (**9**) as an orange solid in 80 % isolated yield (Scheme 3.2). The ^{31}P NMR spectrum of $[K_2XP_2(DME)_{2.5}]$ (**9**) comprises of a single peak at –83.7 ppm, consistent with the removal of chirality at phosphorus upon deprotonation, and the ^1H NMR spectrum is indicative of C_{2v} symmetry. Crystals of $[K_2XP_2(DME)_4]$ were grown by cooling a concentrated DME solution to –30 °C (Figure 3.4, Table 3.1) and reveal a P_2K_2 rhombus shaped core, with 78–82° angles between the P(1)/C(4)/C(5)/P(2) and P(1)/K/P(2) planes. Two DME molecules are

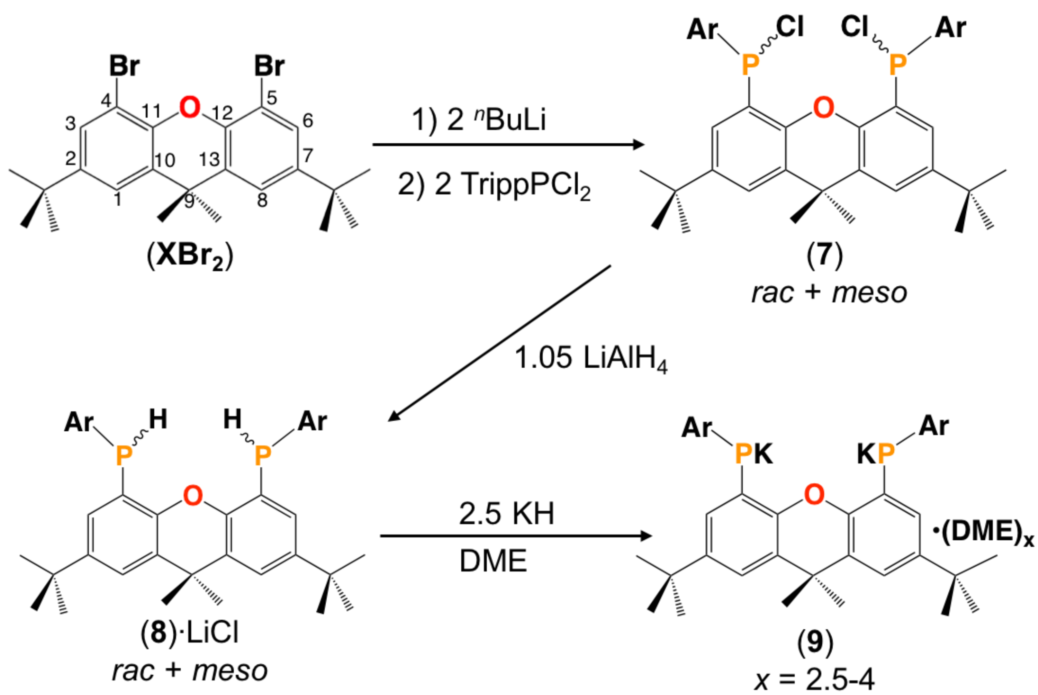

Scheme 3.2: The Synthesis of Complexes **7**, **8** and **9**. Ar = 2,4,6-triisopropyl-phenyl.

coordinated to each potassium atom and the ligand backbone is essentially planar with a 1° angle between the planes of the two aryl rings in the backbone.

Related phosphido complexes include polymeric $[(K_2(POP))_\infty]$ (POP = 4,5-bis(*tert*-butylphosphido)-9,9-dimethylxanthene) featuring K···P and K···C_{aryl} contacts between adjacent K_2(POP) units,[40], $[((PNP)K_2(THF)_3)_2]$-(PNP = 2,6-bis(2-(phenylphosphido)phenyl)-pyridine) with a ladder-like K_4P_4 core,[39] and polymeric $[((RPhP)K(pmdeta))_2]$ (R = $CH(SiMe_3)_2$; pmdeta = N,N,N′,N″,N″-pentamethyldiethylenetriamine) with rhombus-shaped K_2P_2 cores.[183] The K–O_{xant} distances of 2.868(3) Å and 2.958(2) Å in **9** are similar

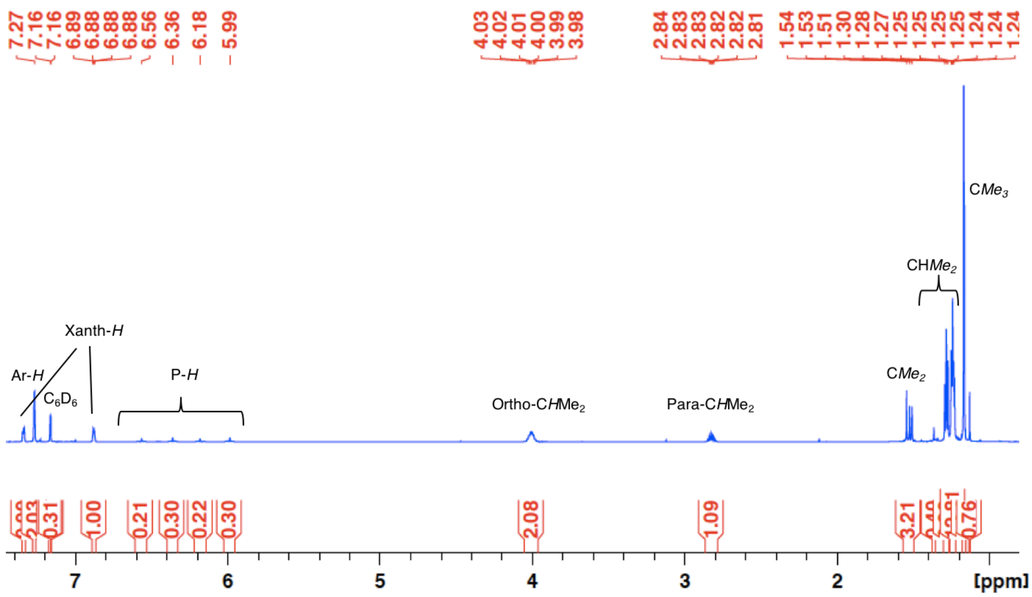

Figure 3.3: The ^{1}H NMR Spectrum of Compound **8** (600 MHz, C_6D_6).

to those in K_2(POP) (2.869(2) Å),[40] and the K–P distances in **9** (3.3945(15) Å, 3.3202(13) Å, 3.3322(13) Å and 3.2769(14) Å) fall within the range reported for the aforementioned literature compounds (3.128(1)–3.538(1) Å).[39,40,183] However, the C–P–C angles of 97.8(2)° and 100.6(2)° are acute, more so than the compounds cited above (102.7(1)–107.5(1)°), presumably to minimize unfavorable steric interactions between *ortho*-isopropyl groups and the two DME ligands on each potassium center.

Interestingly, stirring $[K_2XP_2(DME)_{2.5}]$ (**9**) in THF at 24 °C for 5 h, followed by removal of the solvent *in vacuo* and recrystallization from hexanes, afforded $[K_4(XP_2)_2(THF)_4]$ (**10**) as orange crystals in 22 % yield. The ^{1}H NMR spectrum of **10** contains a single complement of peaks for a top-bottom-symmetric XP_2 ligand (distinct from those of compound **9**), and the ^{31}P NMR

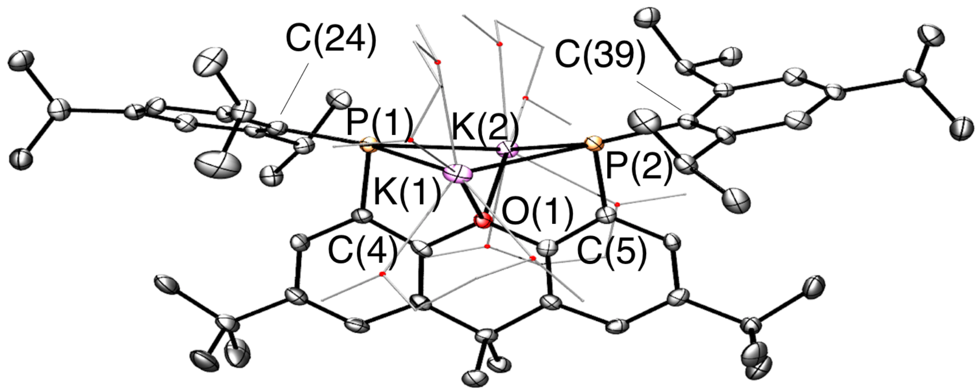

Figure 3.4: The X-ray crystal structure for compound **9**. Ellipsoids are set to 50 %. The *tert*-butyl groups are rotationally disordered over multiple positions, and in each case only one is shown for clarity. Hydrogen atoms are omitted, and the coordinating DME molecules are depicted in wire-frame format for clarity. Selected bond lengths [Å] and angles [°]: P(1)–K(1) 3.3945(15), P(1)–K(2) 3.3202(13), P(2)–K(1) 3.3322(13), P(2)–K(2) 3.2769(14), K(1)–O(1) 2.868(3), K(2)–O(1) 2.958(2), P(1)–K(1)–P(2) 80.12(3), K(1)–P(2)–K(2) 98.06(3), P(2)–K(2)–P(1) 82.03(3), K(2)–P(1)–K(1) 96.00(3). C(4)–P(1)–C(24) 97.81(16), C(5)–P(2)–C(39) 100.62(16), K(1)–O(1)–K(2) 117.83(8), C(4)–P(1)–K(1) 84.2(1), C(4)–P(1)–K(2) 88.9(1), C(5)–P(2)–K(1) 85.5(1), C(5)–P(2)–K(2) 87.4(1), C(24)–P(1)–K(1) 134.1(1), C(24)–P(1)–K(2) 129.8(1), C(39)–P(2)–K(1) 130.2(1), C(39)–P(2)–K(2) 131.3(1).

spectrum features only a single peak, which is slightly shifted compared to that of **9** (–85.14 ppm for **10** and –83.73 ppm for **9**). This reaction is reversible, since stirring **10** in DME at 24 °C regenerated compound **9** (Scheme 3.3).

The solid state structure of **10** consists of two $K_2(XP_2)$ units linked to form a K_4P_4 cube, with K–P–K and P–K–P angles of 80–90° and 89–101°, respectively (Figure 3.5, Table 3.1). The K–P distances in the square faces bridged by the xanthene backbone lie in a narrow range (3.201(3)–3.249(3) Å), and are shorter than the K–P bonds in **9**. By contrast, the K–P distances

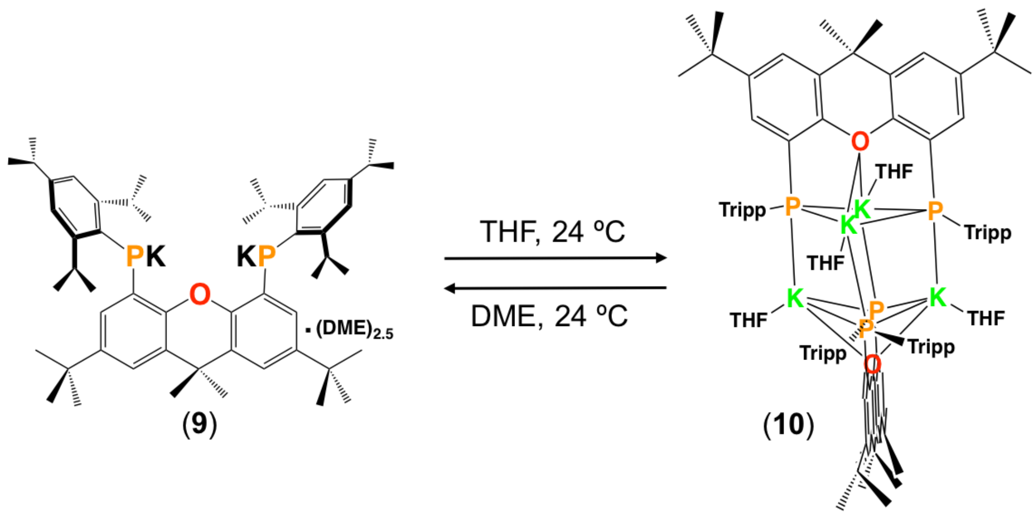

Scheme 3.3: The Reversible Conversion of Dimetallic **9** into Tetrametallic **10**.

linking these two faces are longer, at 3.328(3) Å, 3.335(3) Å, 3.540(3) Å, and 3.568(3) Å; the two shorter K–P bonds are augmented by interactions between potassium and the *ipso*- and *ortho*-carbon atoms of an aryl group on phosphorus (K–C = 3.32(1)-3.40(1) Å; (f) in Figure 3.6), whereas the longer K–P bonds are not bridged by comparable K-C_{aryl} interactions (K–C > 3.8 Å). Nevertheless, a similar range of K–P distances was reported for polymeric [$(K_2(POP))_\infty$] (3.220(1)–3.518(1) Å)[40] and tetrametallic [((PNP)$K_2(THF)_3$)-$_2$] (3.228(1)–3.538(1) Å).[39]

The K–O_{THF} distances of 2.667(5)-2.712(6) Å lie within the typical range.[39,184,185] By contrast, the K–O_{xant} distances are significantly longer; at 3.033(6)–3.141(6) Å, these bonds are longer than the K–O_{xant} bonds in [K_2-(XAT)(alkane)] (XAT = 4,5-bis(2,6-dimesitylanilido)-2,7-di-*tert*-butyl-9,9-di-

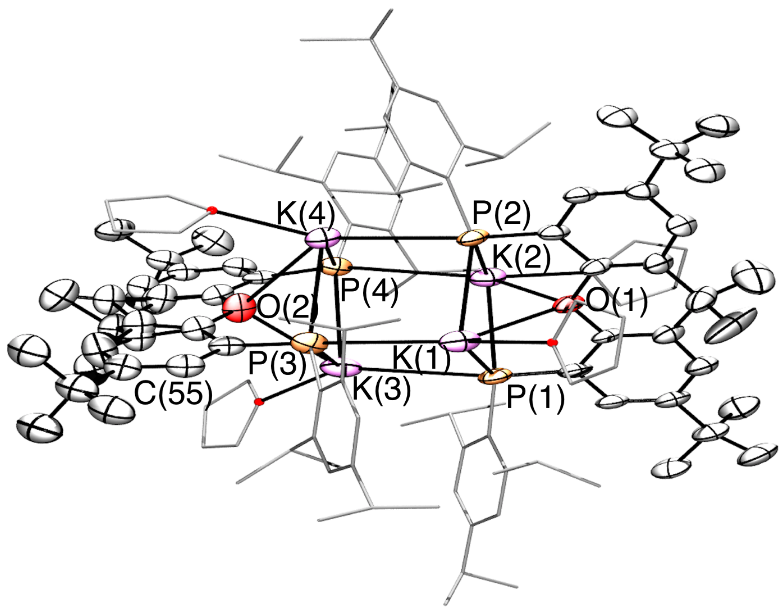

Figure 3.5: The X-ray crystal structure for compound **10**. Ellipsoids are set to 50 %. Hydrogen atoms are omitted, and the 2,4,6-triisopropylphenyl groups and coordinated THF molecules are depicted in wire-frame format. Interactions between K(1) and the aryl ring on P(3), and K(4) and the aryl ring on P(2) are not shown for clarity. The *tert*-butyl groups are rotationally disordered over multiple positions, and in each case only one is shown for clarity. Selected bond lengths [Å] and angles [°]: P(1)–K(1) 3.203(3), P(1)–K(2) 3.201(3), P(2)–K(1) 3.218(3), P(2)–K(2) 3.232(3), K(1)–O(1) 3.141(6), K(2)–O(1) 3.049(5), K(1)–P(3) 3.328(3), P(1)–K(3) 3.568(3), K(2)–P(4) 3.540(3), P(2)–K(4) 3.335(3), P(3)–K(3) 3.249(3), P(3)–K(4) 3.221(3), P(4)–K(3) 3.217(3), P(4)–K(4) 3.215(2), K(3)–O(2) 3.033(6), K(4)–O(2) 3.127(5), K(2)–P(1)–K(3) 79.56(6), P(1)–K(3)–P(4) 99.71(7), K(3)–P(4)–K(2) 79.77(6), P(4)–K(2)–P(1) 100.62(7), P(1)–K(1)–P(3) 95.66(7), K(1)–P(3)–K(3) 88.38(8), P(3)–K(3)–P(1) 90.37(7), K(3)–P(1)–K(1) 85.06(7).

methylxanthene, (2.534(3)-2.619(2) Å)),[25] K_2(POP) (2.869(2) Å),[40] and **9** (2.868(3)–2.958(2) Å).

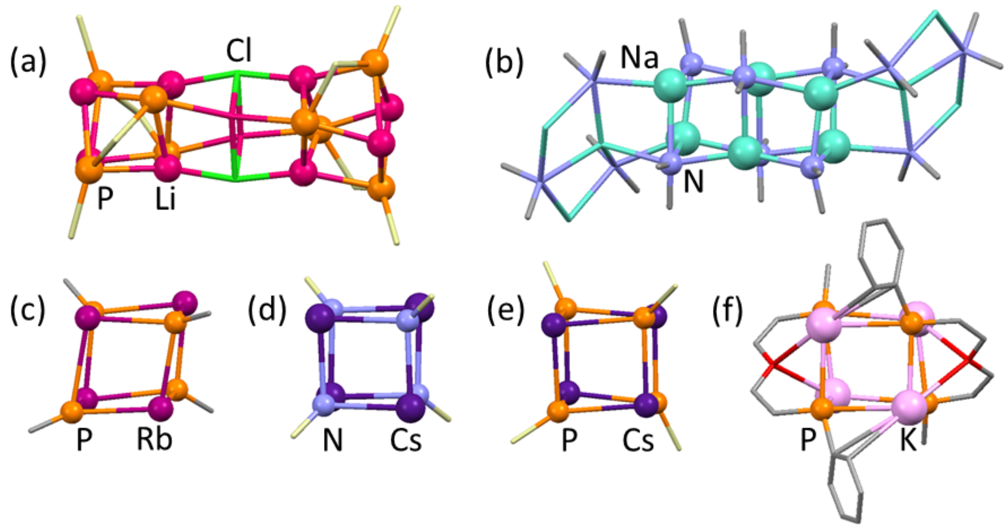

Figure 3.6: The central cores of (a) $[(Li_4(PH\text{-}Si^tBuAr\text{-}PSiPh_3)_2)_2(Li_2Cl_2)]$, (b) $[(Na_6(NMe_2)_6)((Na(tmeda))_3(NMe_2)_3)_2]$, (c) $[(Rb(PH(Dmp)))_4]{\cdot}C_7H_8$ (Dmp = 2,6-dimesitylphenyl), (d) $[Cs_4(NH(SiMe_3))_4]$, (e) $[(Cs(\eta^6\text{-Toluene}))_4(P(H)\text{-}Si^tBu_3)_4]$, and (f) compound **10**. M_4Pn_4 cores are shown in ball-and-stick format, while key surrounding atoms (not including H atoms) are shown as capped sticks.

While a significant number of $Li_4(NR_2)_4$ cubic cage structures have been described,[186–195] only a handful of cubic $M_4(PnR_2)_4$ cage structures incorporating heavier alkali metal and/or pnictogen elements have been reported. In fact, structurally characterized examples are limited to $[(Li_4(PH\text{-}Si^tBuAr\text{-}P\text{-}SiPh_3)_2)_2(Li_2Cl_2)]$ featuring two Li_4P_4 cubes bridged by a Li_2Cl_2 unit ((a) in Figure 3.6);[196] $[(Na_4(NMe_2)_4)((Na(tmeda))_3(NMe_2)_3)_2]$ presenting a central Na_4N_4 cube linked via opposite faces to Na_3N_3 ladder structures; related [-$(Na_6(NMe_2)_6)((Na(tmeda))_3(NMe_2)_3)_2]$ with a Na_6N_6 core composed of two face-sharing cubes ((b) in Figure 3.6); $[(Rb(PH(Dmp)))_4]{\cdot}C_7H_8$ (Dmp = 2,6--dimesitylphenyl) with a Rb_4P_4 core ((c) in Figure 3.6);[197] $[Cs_4(NH(SiMe_3)$-$)_4]$ with a Cs_4N_4 core ((d) in Figure 3.6);[198] and $[(Cs(\eta^6\text{-Toluene}))_4(P(H)Si$-

${}^{t}Bu_3)_4$] with a Cs_4P_4 core ((e) in Figure 3.6).[199] Compound **10** is therefore the first structurally characterized phosphido complex featuring a cubic K_4P_4 core.

3.3 Yttrium Complexes Bearing the XP_2 Ligand

Reaction of [$K_2XP_2(DME)_{2.5}$] (**9**) with [$YI_3(THF)_{3.5}$] in THF produced a mixture of products (consistently >10 peaks in the ^{31}P NMR spectrum) including [$(XP_2)YI(THF)_2$] (**11**) and tris(2,4,6-triisopropylphenylphosphinidene) (P_3Tripp_3); the latter compound was identified by comparison of the NMR spectra with an independently prepared sample,[200,201] in addition to X-ray crystallography (Figure 3.9, Table 3.1). The structure is closely analogous to those of $(PMes)_3$[202] and $(PAnt)_2(PAr)$;[203] Mes = mesityl, Ant = 9-anthracenyl; Ar = $C_6H_2(o\text{-}CH(SiMe_3)_2)_2(p\text{-}C(SiMe_3)_3)$). Crude **11** was isolated as the major product after washing with a small volume of hexanes, and pure **11** was isolated as an orange powder through a second washing with a small volume of either $O(SiMe_3)_2$ or hexanes in an 18 % overall yield (Scheme 3.4). X-ray quality crystals were obtained by cooling a concentrated hexanes solution of **11** to –30 °C (Figure 3.8, Table 3.1). It is of note that the unexpected byproducts formed in the synthesis of **11** do not arise from thermal decomposition over the duration of the reaction, given that the ^{31}P NMR signal for **11** increased in intensity as the reaction progressed and did not decrease once the reaction reached completion.

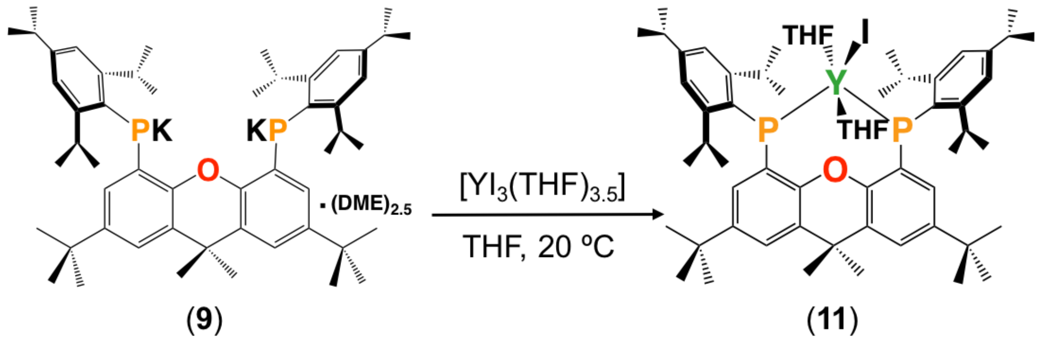

Scheme 3.4: The Synthesis of the Yttrium Complex **11**.

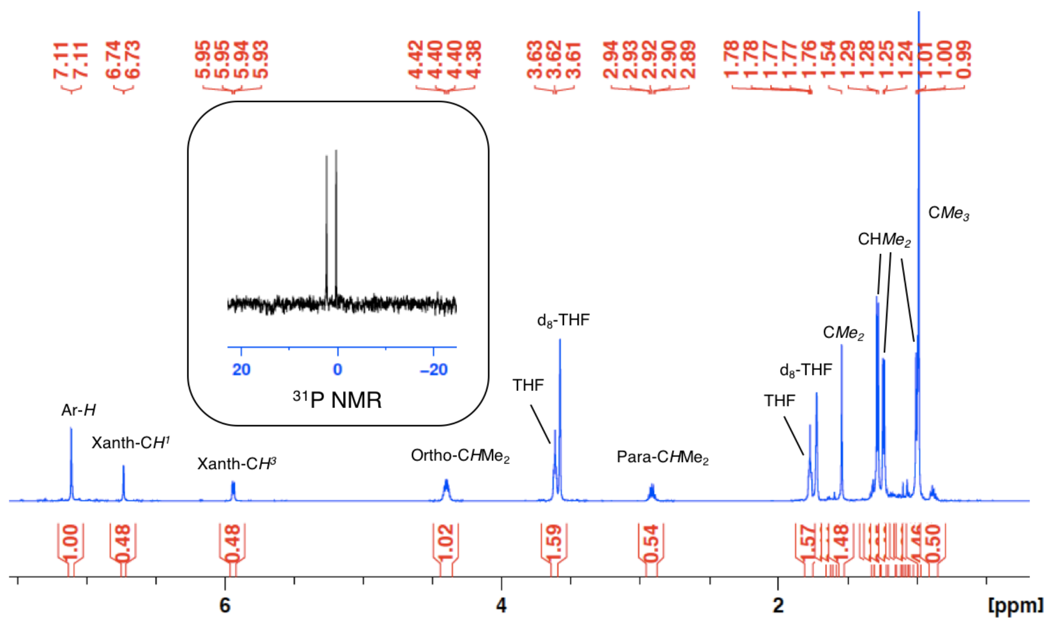

Figure 3.7: The ^{1}H NMR and ^{31}P NMR Spectra of Complex **11** (600 and 81 MHz respectively, d$_8$-THF).

The X-ray crystal structure of **11** (Figure 3.8) revealed that the xanthene backbone of the XP_2 ligand is planar, and the geometry at yttrium is approximately face-capped trigonal bipyramidal with the anionic donors in equatorial positions and the THF ligands in axial positions. Yttrium lies

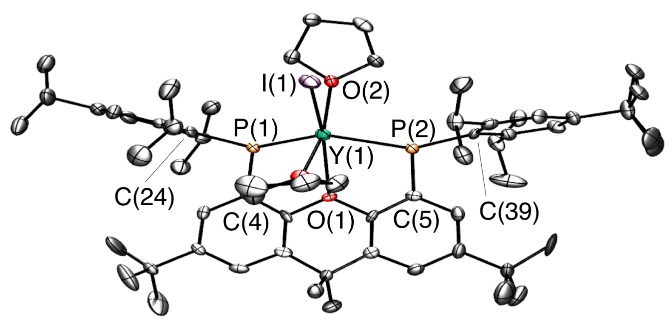

View A

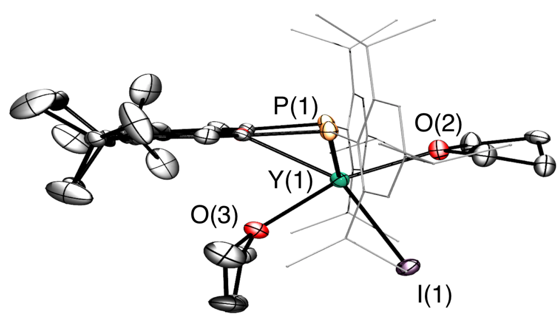

View B

Figure 3.8: Two views of the X-ray crystal structure for compound **11**. Ellipsoids are set to 50 %. Hydrogen atoms are omitted. The *tert*-butyl groups are rotationally disordered over multiple positions, and in each case only one is shown for clarity. In view B, the 2,4,6-triisopropylphenyl groups are depicted in wire-frame format for clarity. Selected bond lengths [Å] and angles [°]: Y–P(1) 2.715(2), Y–P(2) 2.762(2), Y–I 2.9639(10), Y–O(2) 2.322(5), Y–O(3) 2.336(5), Y–O(1) 2.508(4), P(1)–Y–P(2) 110.87(7), P(1)–Y–I 122.43(5), P(2)–Y–I 121.79(5), O(2)–Y–O(3) 162.0(2), O(2)–Y–I 81.6(1), O(3)–Y–I 81.9(1), O(1)–Y–O(2) 126.6(2), O(1)–Y–O(3) 70.3(2), O(1)–Y–P(1) 68.6(1), O(1)–Y–P(2) 67.4(1).

1.55 Å out of the P(1)/C(4)/C(5)/P(2) plane, leading to an 85° angle between the P(1)/C(4)/C(5)/P(2) plane and the PYP plane. By comparison,

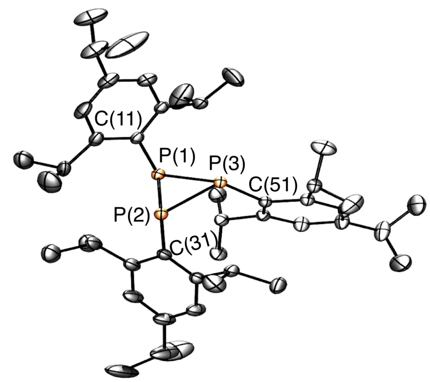

View A

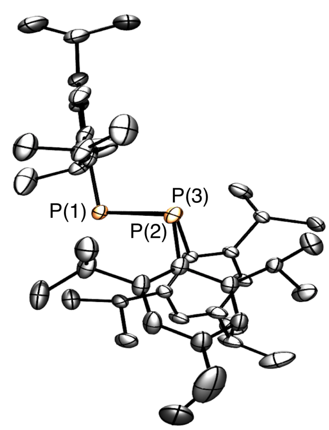

View B

Figure 3.9: Two views of the X-ray crystal structure for tris(2,4,6-triisopropylphenylphosphinidene) (P_3Tripp_3). Ellipsoids are set to 50 %. Hydrogen atoms are omitted for clarity. Selected bond lengths [Å] and angles [°]: P(1)–P(2) 2.2367(6), P(1)–P(3) 2.2060(6), P(2)–P(3) 2.2151(6), P(1)–C(11) 1.8635(17), P(2)–C(31) 1.8522(18), P(3)–C(51) 1.8492(16), P(1)–P(2)–P(3) 59.408(19), P(1)–P(3)–P(2) 60.78(2), P(2)–P(1)–P(3) 59.809(19), C(11)–P(1)–P(2) 101.01(5), C(11)–P(1)–P(3) 96.76(5), C(31)–P(2)–P(1) 107.69(6), C(31)–P(2)–P(3) 112.08(6), C(51)–P(3)–P(1) 115.24(5), C(51)–P(3)–P(2) 116.53(5).

yttrium lies 0.50 Å out of the N(1)/C(4)/C(5)/N(2) plane of the related XN_2 ligand in [$(XN_2)Y(CH_2SiMe_3)THF$] (**3**, Figure 2.5, Section 2.3), with a 31°

angle between the N(1)/C(4)/C(5)/N(2) plane and the NYN plane.[167] The P(1)–Y–P(2), P(1)–Y–I, and P(2)–Y–I angles in the equatorial plane of **11** are 110.87(7)°, 122.43(5)° and 121.79(5)°, respectively, with an I–Y–(P(1)P(2) centroid) angle of 159.5°. The O(2)–Y–O(3) angle is 162.0(2)°, and the O(2)–Y–I and O(3)–Y–I angles are 81.6(1)° and 81.9(1)°, respectively. The O(1) donor of the xanthene backbone caps the center of the P(1)/P(2)/O(3) face with O(1)–Y–P and O(1)–Y–O(3) angles in the narrow range of 67.4(1)° to 70.3(2)°.

The Y–P distances in **11** are 2.715(2) Å and 2.762(2) Å, falling near the middle of the spectrum observed for the terminal phosphido ligands in $[(Y(P(SiMe_3)_2)_2(\mu\text{-}P(SiMe_3)_2))_2]$ (2.660(2)-2.693(2) Å),[204] $[Y(P(SiMe_3)Ar)\text{-}I_2(THF)_3]$ (Ar = 2,6-$C_6H_3{}^iPr_2$) (2.699(2) Å),[205] $[(Cp^{TMS2})_2Y(PHR)(THF)\text{-}]$ (Cp^{TMS2} = 1,3-$C_5H_3(SiMe_3)_2$; R = Si^tBu_3) (2.770(1) Å),[204] $[((Me_4C_5\text{-}Si\text{-}Me_2\text{-}PAr)Y(THF)(\mu\text{-}H))_2]$ (Ar = 2,4,6-$C_6H_2{}^tBu_3$; 2.724(1) Å), $[(Me_4C_5\text{-}Si\text{-}Me_2\text{-}P\text{-}C_6H_2(2,4\text{-}{}^tBu)_2(6\text{-}CMe_2CH_2))Y(THF)_2]$ (2.789(2) Å), $[(Me_4C_5\text{-}SiMe_2\text{-}\text{-}PPh)Y(THF)(\mu\text{-}H)_2(\mu\text{-}PhP\text{-}SiMe_2\text{-}C_5Me_4)Y(THF)_2]$ (2.826(2) Å),[178] and -$[(\kappa^3\text{-}Tp^*)(Cp)Y(PPh_2)(THF)]$ (Tp* = tris(3,5-dimethylpyrazolyl)-hydroborate) (2.845(2) Å).[206]

The Y–I distance of 2.964(1) Å in **11** is also within the range previously reported for yttrium iodo compounds. For example, the Y–I distances are 2.9287(3) Å and 2.9464(3) Å in $[HC\{C(CH_3)NAr\}_2YI_2(THF)]$,[207] 2.947(1)–2.979(1) Å in $[Y(P(SiMe_3)Ar)I_2(THF)_3]$ (Ar = 2,6-$C_6H_3{}^iPr_2$),[205] and 3.0161-(8) Å in $[YI(N(SiMe_3)_2)_2(CH_2PPh_3)]$.[208] The Y–$O_{THF}$ distances of 2.322(5) Å and 2.336(5) Å are typical,[207,209] whereas the Y–O(1) distance of 2.508(4) Å is substantially elongated, reflecting the poor donor ability of a diarylether ligand, combined with steric constraints imposed by the rigidity of the XP_2 pincer ligand framework.

Between 25 °C and –90 °C, the solution ^{1}H NMR spectra for **11** in d_8-THF are indicative of apparent C_{2v} symmetry, consistent with rapid migration of the $YI(THF)_2$ unit from one side of the plane of the ligand backbone to the other. Compound **11** gave rise to a ^{31}P NMR signal at 1.28 ppm with a $^1J_{31P,89Y}$ coupling of 162 Hz (Figure 3.7). This coupling is slightly larger compared to that observed for the terminal yttrium phosphido complexes $[Y(P(SiMe_3)\text{-}Ar)I_2(THF)_3]$ (Ar = 2,6-$C_6H_3{}^iPr_2$; 157 Hz),[205] $[(Cp^{TMS2})_2Y(PHR)(THF)]$-($Cp^{TMS2}$ = 1,3-$C_5H_3(SiMe_3)_2$; R = Si^tBu_3; 144 Hz),[204] (144 Hz) and $[(Y\text{-}(P(SiMe_3)_2)_2(\mu\text{-}P(SiMe_3)_2))_2]$ (122 Hz),[210] and significantly larger than those reported for the aforementioned intact and cyclometallated Me_4C_5-$SiMe_2$-PAr complexes (53–84 Hz).[178]

In an attempt to isolate an XP_2 yttrium monoalkyl complex, two routes were employed; alkane elimination and salt metathesis. The alkane elimination reaction between $[Y(CH_2SiMe_3)_3(THF)_2]$ and H_2XP_2 (**8**; C_6D_6 solvent, 20 °C) yielded only unreacted **8**, and the products of $[Y(CH_2SiMe_3)_3(THF)_2]$ thermal decomposition. The salt metathesis reaction between **11** and $NaCH_2SiMe_3$ (1 or 2 equivalents in THF) afforded a major product believed to be $Na[\text{-}(XP_2)Y(CH_2SiMe_3)_2(THF)_x]$ by ^{1}H NMR spectroscopy. Integration of the peaks corresponding to the alkyl protons in the ^{1}H NMR spectrum consistently indicated that two alkyl groups are bound to the metal instead of the expected one. However, this reaction was not clean and the product was highly soluble,

Structure	**9**	**10**	**11**	P_3Tripp_3
Formula	$C_{69}H_{113}K_2O_9P_2$	$C_{122}H_{180}K_4O_6P_4$	$C_{61}H_{90}I_1O_3P_2Y_1$	$C_{45}H_{69}P_3$
Formula wt	1226.73	2022.93	1149.07	702.91
T (K)	100(2)	100(2)	100(2)	173(2)
Cryst. Syst.	Triclinic	Triclinic	Monoclinic	Triclinic
Space Group	P–1	P–1	P 21/n	P–1
a (Å)	13.192(3)	18.376(5)	19.575(3)	11.4722(9)
b (Å)	16.631(4)	18.413(4)	16.647(2)	13.1828(10)
c (Å)	19.121(4)	18.504(5)	19.831(3)	14.5358(12)
α [°]	96.640(4)	94.225(6)	90	93.0650(10)
β [°]	109.379(3)	94.683(6)	112.577(2)	98.1550(10)
γ [°]	108.641(4)	90.304(6)	90	95.9790(10)
Volume [Å^3]	3632.4(13)	6223(3)	5967.1(14)	2159.1(3)
Z	2	2	4	2
Density (calcd; Mg/m^3)	1.122	1.080	1.279	1.081
μ (mm^{-1})	0.224	0.243	1.589	0.166
F(000)	1334	2192	2408	768
Crystal Size (mm^3)	0.482×0.200×0.142	0.245×0.198×0.17	0.222×0.199×0.096	0.330×0.172×0.082
θ Range for Collection [°]	1.764–25.537	1.503–23.223	1.663–26.476	1.557–27.563
No. of Refns. Collected	34919	54343	13463	40631
No. of Indep. Refns.	13101	17744	13463	9948
Completeness to θ Max (%)	97.6	99.8	99.8	100.0
Absorption Correction	Numerical	Multi-Scan	Multi-Scan	Numerical
Max and Min Transmission	1.000,0.7953	0.7451,0.4302	0.7454,0.5658	1.000,0.9620
GOF on F^2	1.110	1.023	1.006	1.035
Final R_1 [$I > 2\sigma(I)$]	R1 = 0.0787 wR2 = 0.1472	R1 = 0.0767 wR2 = 0.2050	R1 = 0.0793 wR2 = 0.1404	R1 = 0.0462 wR2 = 0.1208
R indices (all data)	R1 = 0.1153 wR2 = 0.1614	R1 = 0.1327 wR2 = 0.2591	R1 = 0.1838 wR2 = 0.1794	R1 = 0.0654 wR2 = 0.1317

Table 3.1: Crystallographic Data Collection and Refinement Parameters for P_3Tripp_3 and Complexes **9**, **10** and **11**.

and consequently it could not be isolated in pure form, despite numerous purification attempts.

Multiple avenues were pursued in an effort to continue the work with the XP_2 ligand, all of which proved unsuccessful. The isolation of thorium and uranium chloride complexes via salt metathesis reactions between [K_2XP_2-(DME)$_{2.5}$] (**9**) and the respective metal chloride precursors resulted in a mixture of products and pure material was not isolated. Attempts to isolate group

4 transition metal (Ti, Zr, Hf) complexes via (1) alkane elimination between titanium and zirconium tetra-neopentyl precursors with H_2XP_2 (**8**) led only to unreacted pro-ligand and $[M(CH_2CMe_3)_4]$ thermal decomposition products, (2) salt metathesis between zirconium and hafnium tetra-chloride precursors with $[K_2XP_2(DME)_{2.5}]$ (**9**) led to multiple unidentified products and (3) amine elimination between tetrakis(dimethylamido)zirconium with H_2XP_2 (**8**), which yielded no reaction after several weeks at 110 °C. Additionally, the isolation of an aluminum complex was attempted by alkane elimination between trimethylaluminum and H_2XP_2 (**8**), which yielded no reaction even at elevated temperatures (110 °C).

3.4 Summary

The rigid POP pincer ligand, H_2XP_2 (**8**) has been successfully synthesized in two steps from 4,5-dibromo-2,7-di-*tert*-butyl-9,9-dimethylxanthene (XBr_2). Double deprotonation with excess KH yielded $[K_2XP_2(DME)_x]$ (**9**, $x = 2.5$-4) with a rhombus-shaped K_2P_2 core, or $[K_4(XP_2)_2(THF)_4]$ (**10**) featuring the first cubic K_4P_4 cage structure, depending on purification conditions. Reaction of **9** with $[YI_3(THF)_{3.5}]$ afforded $[(XP_2)YI(THF)_2]$ (**11**) in which Y is displaced 1.55 Å out of the P(1)/C(4)/C(5)/P(2) plane of the XP_2 ligand, contrasting the coordination behavior of yttrium to XN_2, the amido-analogue of the XP_2 dianion. However, the reaction to form **11** is low yielding due to the formation of multiple products including the tris(2,4,6-triisopropylphenylphosphinidene) cyclic trimer, P_3Tripp_3, indicative of poor ligand stability in the presence of strong Lewis acids.

Chapter 4

Lutetium and Lanthanum Complexes of a Rigid Bis-Anilido NON-Donor Ligand; Synthesis and Hydroamination Catalysis

Adapted with permission from: Motolko, K. S. A.; Emslie, D. J. H.; Britten, J. F. *RSC Advances* **2017**, *7*, 27938-27945.

4.1 Introduction

Chapter 2 (Sections 2.3 and 2.4) described the synthesis and hydroamination activity of [(XN_2)Y(CH_2SiMe_3)(THF)] (**3**).[167] In this chapter the chemistry of the XN_2 ligand is expanded to investigate smaller and larger rare earth metals (the ionic radii of Sc (III), Lu(III), Y(III) and La(III) are 0.745 Å, 0.861 Å, 0.900 Å and 1.032 Å respectively).[6] These complexes were targeted in order to probe the effectiveness of the rigid XN_2 pincer ligand to support robust alkyl derivatives of smaller and larger rare earth elements, and to assess the activity of the complexes for intra- and inter-molecular hydroamination.

4.2 Lutetium and Lanthanum Complexes Bearing the XN_2 Ligand

As the rare earth metal with the smallest ionic radius, scandium(III) was chosen for initial investigation. However, the alkane elimination reaction between H_2XN_2 and $[Sc(CH_2SiMe_3)_3(THF)_2]$ in benzene at 24 °C was unsuccessful, resulting only in unreacted pro-ligand and $[Sc(CH_2SiMe_3)_3(THF)_2]$-thermal decomposition products. Our efforts therefore shifted to the second smallest rare earth metal, lutetium.

In contrast to the aforementioned reaction with $[Sc(CH_2SiMe_3)_3(THF)_2]$, the alkane elimination reaction between H_2XN_2 and $[Lu(CH_2SiMe_3)_3(THF)_2]$ yielded $[(XN_2)Lu(CH_2SiMe_3)(THF)]\cdot(O(SiMe_3)_2)_{1.5}$ (**12**$\cdot(O(SiMe_3)_2)_{1.5}$) in 59 % yield, as a pale yellow powder after recrystallization from $O(SiMe_3)_2$ (Scheme 4.1). The ^1H NMR spectrum of **12**$\cdot(O(SiMe_3)_2)_{1.5}$ is largely analogous to that of $[XN_2Y(CH_2SiMe_3)(THF)]\cdot(O(SiMe_3)_2)$ (**3**$\cdot O(SiMe_3)_2$), which was previously discussed (*vide supra*, Section 2.3), and is indicative of C_s symmetry in solution, with two Ar-H, ortho-CHMe$_2$ and CMe_2 peaks (Figure 4.1). Compound **12**$\cdot(O(SiMe_3)_2)_{1.5}$ was found to be fairly thermally stable, being only 25 % decomposed after 24 h at 90 °C.

Crystals of **12**$\cdot(C_6H_6)_{0.5}$ (lattice solvent is residual benzene from the synthesis) were grown by cooling a concentrated $O(SiMe_3)_2$ solution to –30 °C (Figure 4.2, Table 4.1). In the solid state, the XN_2 backbone is slightly bent

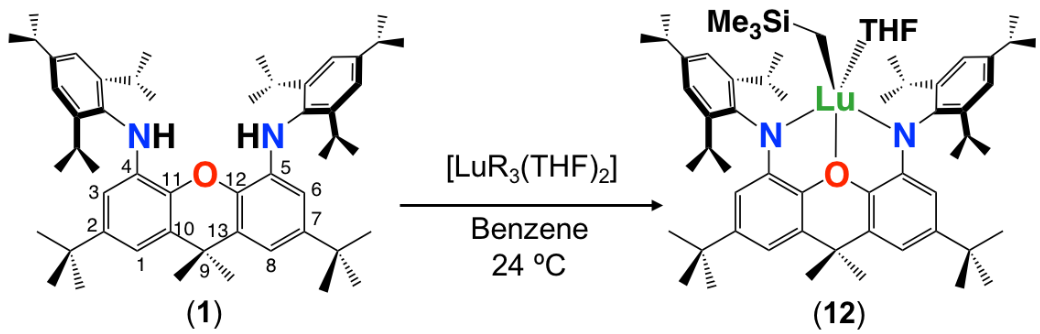

Scheme 4.1: The Synthesis of the Lutetium Complex **12** (R = CH_2SiMe_3).

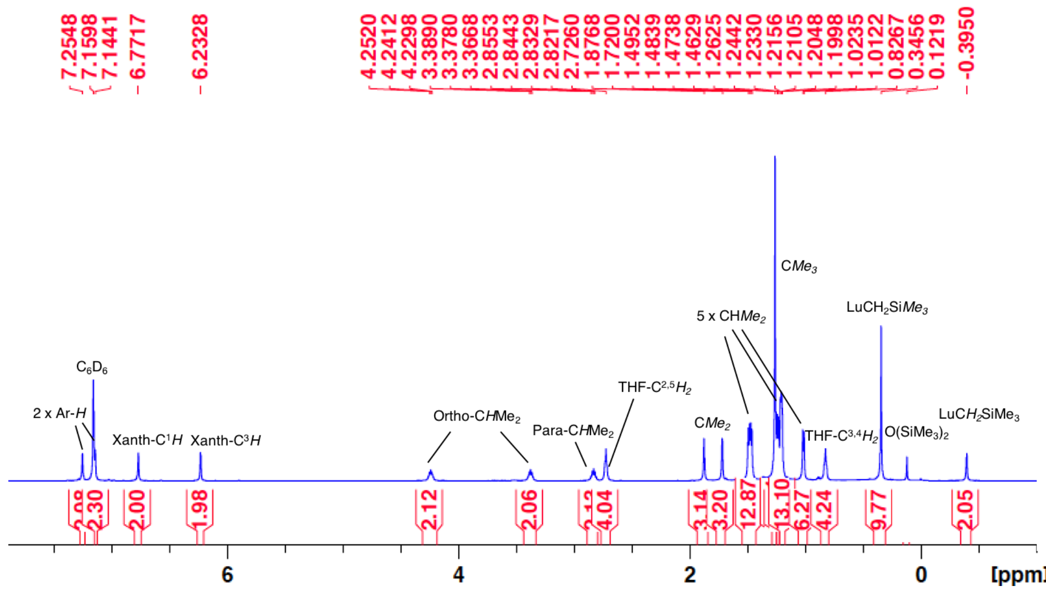

Figure 4.1: The ^{1}H NMR Spectrum of Complex **12** (600 MHz, C_6D_6).

with a 26° angle away from planarity, based on the orientation of the two aryl rings of the xanthene backbone. This orientation is mirrored in [$(XN_2)Y(CH_2$-$SiMe_3)(THF)$] (**3**), which displayed a backbone angle of 25° and a very similar geometry at the rare earth metal.[167] Lutetium is 5-coordinate with the three anionic donors and coordinated THF arranged in an approximate tetrahedron around the metal center. The largest angle in this approximate tetrahedron is the N(1)–Lu–N(2) angle of 130°, and the smallest is the O(2)–Lu–C(54) angle of 97°, while the other angles are between 102° and 110°. The oxygen donor of the xanthene backbone is coordinated on the N(1)/N(2)/C(54) face of the tetrahedron closest to the nitrogen donors. Lutetium lies 0.74 Å out of the plane of the XN_2 ligand donor atoms, leading to a 53° angle between the NON and the NLuN planes. The neutral oxygen donor on the xanthene backbone is located 0.5 Å out of the N(1)/C(4)/C(5)/N(2) plane in order to coordinate to lutetium, with N–Lu–O(1) angles of 69 and 70°. Additionally, the nitrogen donors on the XN_2 ligand are bent towards lutetium, illustrated by the C(1)···C(8), C(4)···C(5) and N(1)···N(2) distances of 5.02 Å, 4.57 Å and 4.04 Å respectively, which are comparable with those in **3** (4.98 Å, 4.56 Å and 4.06 Å; *vide supra*, Section 2.3).[167]

The Lu–N distances of 2.221(2) Å and 2.228(2) Å are slightly shorter than those in [$(XN_2)Y(CH_2SiMe_3)(THF)$] (**3**; 2.252(3) Å),[167] consistent with the smaller ionic radius of Lu^{III} compared to Y^{III} (0.861 Å vs 0.900 Å).[6] Additionally, the Lu–N distances in **12** fall within the range reported for related compounds such as, [{(2-ArN=CMe)(6-ArNCMe$_2$)C_5H_3N}Lu$(CH_2SiMe_3)_2$] (Ar = $C_6H_3{}^iPr_2$-2,6; 2.188(4) Å)[211] and [{1,8-$(Pz^{iPr})_2$Cz}Lu$(CH_2SiMe_3)_2$] (Pz^{iPr} = 1-(3-isopropyl)pyrazolyl; Cz = 3,6-dimethylcarbazole; 2.231(3) Å).[212] The Lu–C(54) distance of 2.326(2) Å is shorter compared to that in [$(XN_2)Y(CH_2SiMe_3)(THF)$] (**3**; 2.364(3) Å), also in keeping with the relative sizes of yttrium and lutetium (*vide supra*). Additionally, this distance falls within the range of Lu–C distances reported in the literature. For example, the Lu–C distances in the aforementioned alkyl complexes range from 2.329(6) Å to 2.374(3) Å,[211,212]

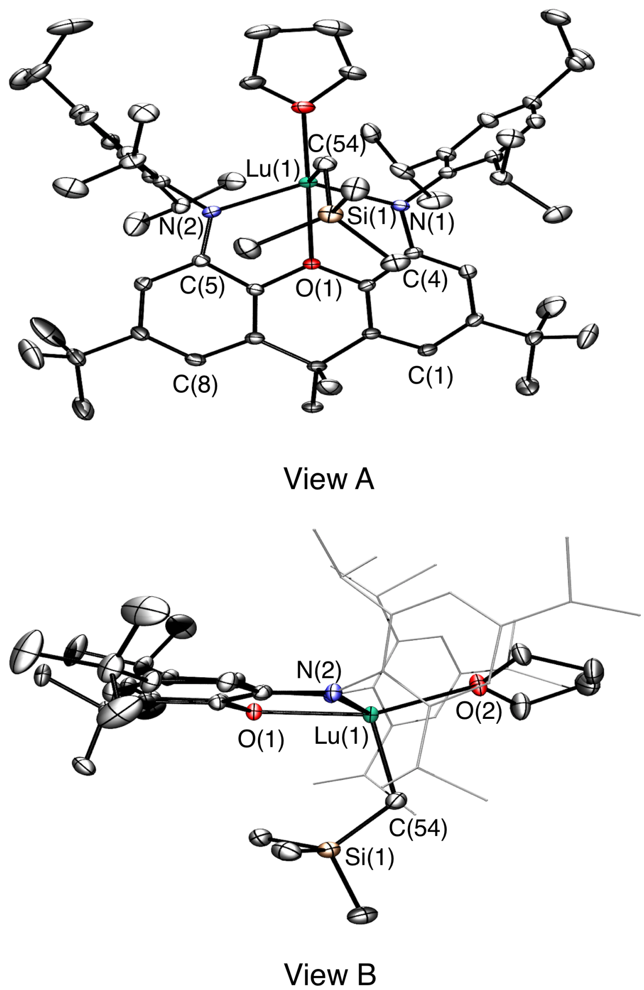

Figure 4.2: Two views of the X-ray crystal structure for compound **12**·$(C_6H_6)_{0.5}$. Ellipsoids are set to 50 %. Hydrogen atoms and lattice solvent are omitted. The *tert*-butyl groups are rotationally disordered over two positions, and only one is shown for clarity. In view B the 2,4,6-triisopropylphenyl groups are depicted in wire-frame format. Selected bond lengths [Å] and angles [°]: Lu–N(1) 2.221(2), Lu–N(2) 2.228(2), Lu–C(54) 2.326(2), Lu–O(1) 2.299(1), Lu–O(2) 2.264(1), N(1)–Lu–N(2) 130.41(6), N(1)–Lu–C(54) 106.09(7), N(2)–Lu–C(54) 110.41(7), O(1)–Lu–C(54) 104.38(6), O(2)–Lu–C(54) 97.56(7), O(2)–Lu–N(2) 105.39(6), O(2)–Lu–N(1) 101.76(6).

and Lu–C in [{(2-NAr)(6-Xyl)C_5H_3N}$_2$Lu(CH_2SiMe_3)(THF)] (Ar = $C_6H_3{}^iPr_2$-2,6; Xyl = *o*-xylyl) is 2.323(14) Å.[213]

In order to further explore the effectiveness of the XN_2 ligand for rare earth coordination, and the impact of metal ionic radius on hydroamination activity, the synthesis of lanthanum XN_2 complexes was undertaken. As the lanthanum trialkyl compound, [La(CH_2SiMe_3)$_3$(THF)$_x$] is not readily accessible,[214] salt metathesis was employed for ligand attachment in the place of alkane elimination. [K_2(XN_2)(DME)$_2$] (**2**) was reacted with [$LaCl_3$(THF)$_3$] in THF at 24 °C, and after recrystallization from O($SiMe_3$)$_2$, [{(XN_2)LaCl(THF)}$_x$]·(O-($SiMe_3$)$_2$)$_{0.25x}$ (**13**·(O($SiMe_3$)$_2$)$_{0.25x}$; x = 1 or 2) was obtained in 51 % yield as an off-white solid (Scheme 4.2).

Attempts to synthesize a lanthanum monoalkyl complex were undertaken via reactions of trimethylsilylmethyl lithium and methyl lithium with [{(XN_2)-LaCl(THF)}$_x$]·(O($SiMe_3$)$_2$)$_{0.25x}$ (**13**·(O($SiMe_3$)$_2$)$_{0.25x}$; x = 1 or 2). NMR-scale reactions were performed in d_8-THF at 24 °C and all resulted in the formation of a dialkyl-'ate' complex, based on the integrations of the respective alkyl peaks, regardless of whether one equivalent (per La) or an excess of the alkali metal-alkyl reagent was added. The reaction utilizing trimethylsilylmethyl lithium was pursued further, as it provides a direct comparison with the lutetium and yttrium trimethylsilylmethyl complexes of the XN_2 ligand. [{(XN_2)LaCl(THF)}$_x$]·(O($SiMe_3$)$_2$)$_{0.25x}$ (**13**·(O($SiMe_3$)$_2$)$_{0.25x}$; x = 1 or 2) reacted with 2 equivalents of trimethylsilylmethyl lithium in THF at 24 °C, and after removal of the salts by centrifugation in toluene and layering with hexanes at –30 °C, [Li(THF)$_x$][(XN_2)La(CH_2SiMe_3)$_2$]·Toluene·LiCl (**14**·Toluene·LiCl;

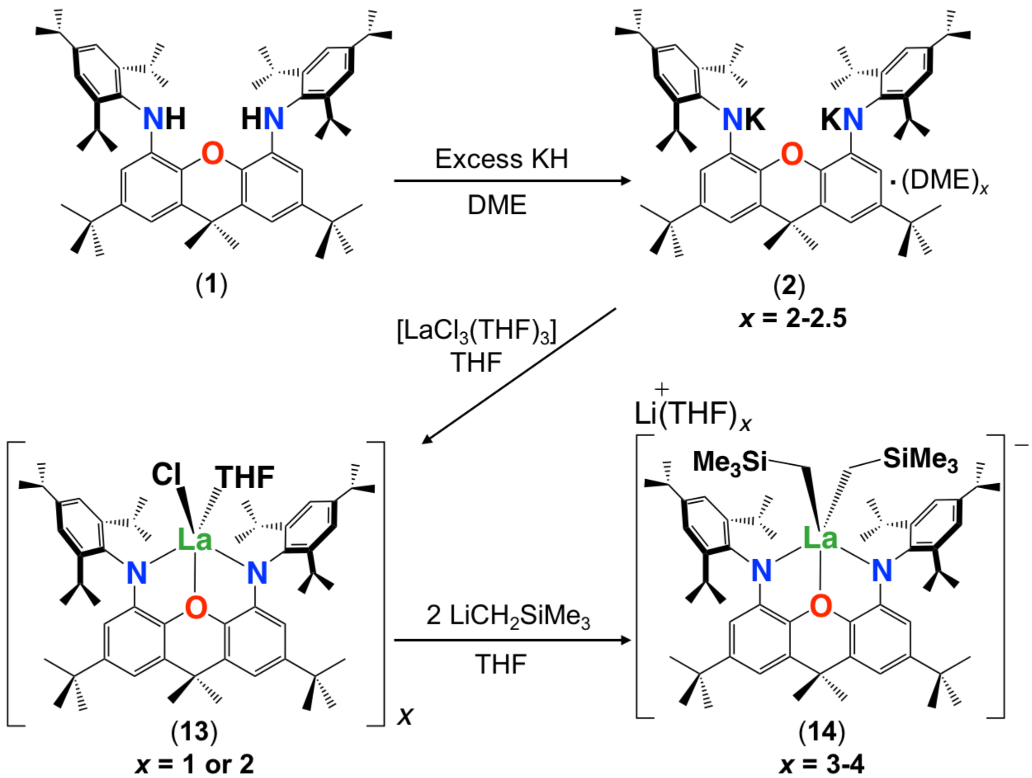

Scheme 4.2: The Synthesis of Lanthanum Complexes **13** and **14**.

x = 3) was isolated as a pale yellow solid in 55 % yield (Scheme 4.2). Compound **14** is sparingly soluble in benzene and other non-polar solvents such as hexanes and pentane, so all characterization was carried out in d_8-THF. The ^{1}H NMR spectrum of **14** (Figure 4.3) revealed the expected signals for the XN_2 ligand backbone and only one set of signals for the two alkyl groups (a singlet with an integration of 18 for $LaCH_2Si\mathit{Me_3}$ and a singlet with an integration of 4 for $LaC\mathit{H_2}SiMe_3$). Upon cooling a d_8-THF solution of **14**, de-coalescence was observed at –80 °C. However, the sample could not be cooled further due to instrumental constraints, and separate environments for LaCH$_2$SiMe_3 and LaCH_2SiMe$_3$ protons were not observed. Crystals of -[Li(THF)$_4$][(XN$_2$)La(CH$_2$SiMe$_3$)$_2$]·THF were grown from a concentrated THF solution of **14**·Toluene·LiCl ($x = 3$), layered with pentane and cooled to –30 °C (Figure 4.4, Table 4.1).

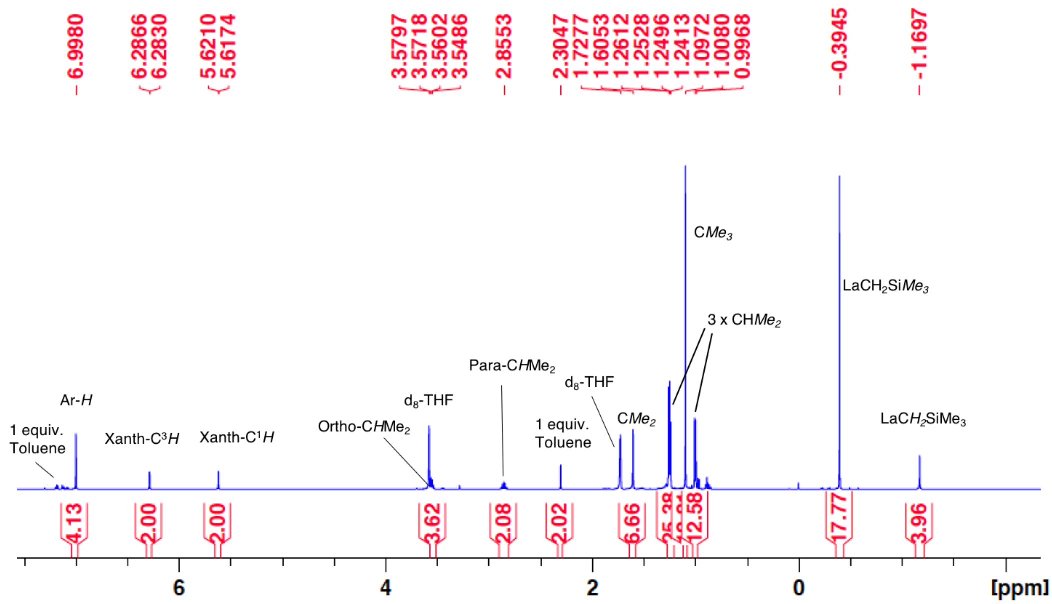

Figure 4.3: The ^{1}H NMR Spectrum of Complex **14** (600 MHz, d$_8$-THF).

In the solid state, lanthanum is 5-coordinate with the two amido donors and two alkyl groups arranged in a distorted tetrahedron around the metal center. The largest angle in this approximate tetrahedron is the N(1)–La–N(2) angle of 118°, and the smallest is the C(54)–La–C(58) angle of 100°, while the other angles are between 101° and 106°. Lanthanum lies 0.96 Å out of the plane of the XN$_2$ ligand donor atoms, leading to a 50° angle between the NON and NLaN planes. The XN$_2$ backbone is bent with a 35° angle away from planarity, based on the orientation of the two aryl rings of the xanthene backbone. The neutral oxygen donor of the xanthene backbone is located 0.64 Å out of the

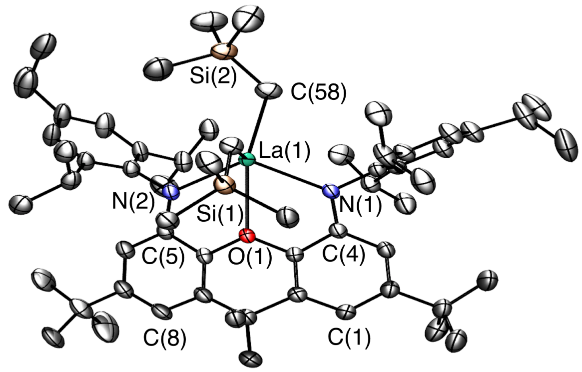

View A

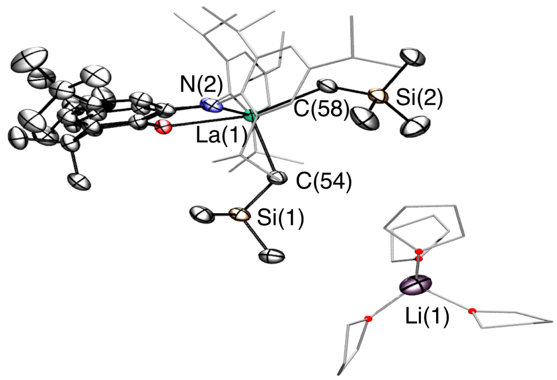

View B

Figure 4.4: Two views of the X-ray crystal structure for compound **14**·THF (x = 4). Ellipsoids are set to 50 %. Hydrogen atoms and lattice solvent are omitted. The *tert*-butyl groups are rotationally disordered over two positions, and only one is shown for clarity. In view A the $[Li(THF)_4]^+$ cation is omitted for clarity. In view B the 2,4,6-triisopropylphenyl groups and the THF molecules are depicted in wire-frame format. Selected bond lengths [Å] and angles [°]: La–N(1) 2.462(5), La–N(2) 2.445(5), La–C(54) 2.573(7), La–C(58) 2.613(7), La–O(1) 2.643(4), N(1)–La–N(2) 118.22(17), N(1)–La–C(54) 108.9(2), N(1)–La–C(58) 100.9(2), N(2)–La–C(54) 106.3(2), N(2)–La–C(58) 120.7(2), O(1)–La–C(54) 97.63(18), O(1)–La–C(58) 159.7(2), C(54)–La–C(58) 100.0(2), N(1)–La–O(1) 63.59(15), N(2)–La–O(1) 62.72(15).

N(1)/C(4)/C(5)/N(2) plane in order to coordinate to lanthanum, resulting in N–La–O(1) angles of 63-64°. In addition, it is of note that the nitrogen donors on the ligand are not bent towards lanthanum to the extent that they are in **12**, illustrated by the C(1)···C(8), C(4)···C(5) and N(1)···N(2) distances in **14** of 4.90 Å, 4.57 Å and 4.21 Å respectively, compared to 5.02 Å, 4.57 Å and 4.04 Å in **12**.

The La–N distances of 2.462(5) Å and 2.445(5) Å are substantially lengthened relative to those in [$(XN_2)Y(CH_2SiMe_3)(THF)$] (**3**; 2.252(3) Å)[167] and [$(XN_2)Lu(CH_2SiMe_3)(THF)]\cdot(O(SiMe_3)_2)_{1.5}$ (**12**; 2.221(2) Å and 2.228(2) Å), which is consistent with the large ionic radius of lanthanum compared to yttrium and lutetium, combined with increased steric hindrance and an overall negative charge in **14**, resulting in a less electrophilic metal center. For analogous reasons, the La–C(54) and La–C(58) distances of 2.573(7) Å and 2.613(7) Å are also substantially elongated compared to those in [$(XN_2)Y$-$(CH_2SiMe_3)(THF)$] (**3**; 2.364(3) Å)[167] and **12** (2.326(2) Å). However, both the La–N and La–C distances in **14** are significantly shorter than those previously reported for [{(*R*)-Binap$(NCyp)_2$}La{(μ-Me)$_2$Li(THF)}{(μ-Me)Li(THF)}$_2$]-(Binap = 2,2′-disubstituted-1,1′-binaphthyl; Cyp = cyclopentyl; La–N = 2.626(7)–2.677(8) Å; La–C = 2.704(8)–2.832(11) Å).[76,215]

Reaction of $[Li(THF)_3][(XN_2)La(CH_2SiMe_3)_2]$·Toluene·LiCl (**14**·Toluene·-LiCl) with $[\{(XN_2)LaCl(THF)\}_x]\cdot(O(SiMe_3)_2)_{0.25x}$ (**13**·$(O(SiMe_3)_2)_{0.25x}$; $x = 1$ or 2) did not result in the isolation of the neutral XN_2 lanthanum alkyl; at 24 °C no reaction was observed and heating to 70 °C resulted only in thermal decomposition of $[Li(THF)_3][(XN_2)La(CH_2SiMe_3)_2]$·Toluene·LiCl (**14**·Toluene·LiCl).

Structure	**12**·$(C_6H_6)_{0.5}$	**14**·$(THF)_5$
Formula	$C_{256}H_{384}Lu_4N_8O_8Si_4$	$C_{81}H_{136}La_1Li_1N_2O_6Si_2$
Formula wt	4513.93	1435.94
T (K)	100(2)	100(2)
Cryst. Syst.	Monoclinic	Monoclinic
Space Group	P 21/c	P 21/n
a (Å)	22.6630(5)	16.931(2)
b (Å)	14.5298(3)	23.782(3)
c (Å)	20.3925(4)	21.090(3)
α [°]	90	90
β [°]	113.6878(11)	98.980(3)
γ [°]	90	90
Volume [Å^3]	6149.3(2)	8388(2)
Z	1	4
Density (calcd; Mg/m^3)	1.219	1.137
μ (mm^{-1})	1.666	0.585
$F(000)$	2380	3088
Crystal Size (mm^3)	0.4×0.2×0.07	0.3×0.25×0.1
θ Range for Collection [°]	2.593–30.508	1.299–26.460
No. of Refns. Collected	207822	120442
No. of Indep. Refns.	18762	17160
Completeness to θ Max (%)	99.9	99.6
Absorption Correction	Multi-Scan	Multi-Scan
Max and Min Transmission	0.7464,0.6309	0.7454,0.6493
GOF on F^2	1.071	1.108
Final R_1 $[I > 2\sigma(I)]$	R1 = 0.0286 wR2 = 0.0652	R1 = 0.0840 wR2 = 0.2367
R indices (all data)	R1 = 0.0405 wR2 = 0.0704	R1 = 0.1057 wR2 = 0.2570

Table 4.1: Crystallographic Data Collection and Refinement Parameters for Complexes **12** and **14**.

4.3 Intramolecular and Intermolecular Hydroamination Catalysis

$[(XN_2)Lu(CH_2SiMe_3)(THF)]\cdot(O(SiMe_3)_2)_{1.5}$ (**12**$\cdot(O(SiMe_3)_2)_{1.5}$) was tested as an ethylene polymerization catalyst at 24 °C and 80 °C (toluene, 1 atm ethylene, 1 h) but exhibited negligible activity. Compound **12**$\cdot(O(SiMe_3)_2)_{1.5}$ was also investigated as a catalyst for both intra- and inter-molecular hydroamination with a variety of reagents and the results are summarized in Tables 4.2 and 4.3. Compound **12**$\cdot(O(SiMe_3)_2)_{1.5}$ catalyzed intramolecular hydroamination of a range of substrates in benzene at 24 °C, proceeding to >99 % completion in all cases (confirmed by ^{1}H NMR spectroscopy). The time required to reach >99 % completion was slightly increased compared to reactions catalyzed by the yttrium complex, $[(XN_2)Y(CH_2SiMe_3)(THF)]\cdot(O(SiMe_3)_2)$-(**3**$\cdot O(SiMe_3)_2$), which is consistent with the majority of previous reports (*vide supra*), in which hydroamination activity increases with increasing rare earth metal size.[6,42] This is particularly evident in entries 2 and 4 in Table 4.2, as $[(XN_2)Y(CH_2SiMe_3)(THF)]\cdot(O(SiMe_3)_2)$ (**3**$\cdot O(SiMe_3)_2$) achieved >99 % conversion after 1.5 h and 34 h (*vide supra*; Section 2.4, Table 2.2),[167] whereas **12**$\cdot(O(SiMe_3)_2)_{1.5}$ required 2.75 h and 48 h, respectively. Nevertheless, the ability of **12**$\cdot(O(SiMe_3)_2)_{1.5}$ and **3**$\cdot O(SiMe_3)_2$ to catalyze these more challenging intramolecular hydroamination reactions at room temperature stands these catalysts apart from most others.[167]

Compound **12**$\cdot(O(SiMe_3)_2)_{1.5}$ also catalyzed intermolecular hydroamination with 4-*tert*-butylaniline, 4-*tert*-butylbenzylamine and octylamine in combination with 1-octene and diphenylacetylene, and in all reactions with 1-

Entry	Reagent	Product	Mol %	Time	Temp. (°C)	Product Formation[a]	N_t (h^{-1})[b]
1	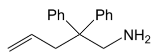	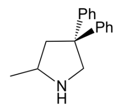	1	< 10 min	24	> 99 %	≥ 600
2	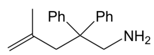	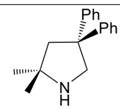	1	2.75 h	24	> 99 %	~36
3	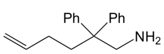	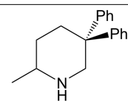	10	< 20 min	24	> 99 %	≥30
4	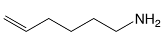	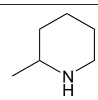	10	48 h	24	> 99 %	~0.2

Table 4.2: Intramolecular Hydroamination Reactivity with **12**.
*Reactions performed in C_6D_6; [a] Conversion of Reactant to Product Determined by NMR Spectroscopy; [b] Turnover Frequency.

octene, the Markovnikov product was formed selectively. These reactions were performed in toluene at 110 °C and the degree of conversion was determined by GC-MS (Table 4.3). Over a 24 h time period, the reaction of 1-octene with octylamine (entry 3) resulted in a turnover frequency (N_t) of 0.41 h^{-1}, which is greater than that obtained for the reaction with 4-*tert*-butylbenzylamine (entry 2, 0.35 h^{-1}), which in turn is significantly greater than that obtained for the reaction with 4-*tert*-butylaniline (entry 1, 0.04 h^{-1}). These results are consistent with increased donor ability and reduced steric bulk of the former amines. The same trend was previously observed for $[(XN_2)Y(CH_2SiMe_3)(THF)]\cdot(O(SiMe_3)_2)$ ($\mathbf{3}\cdot O(SiMe_3)_2$),[167] and the ability of $\mathbf{12}\cdot(O(SiMe_3)_2)_{1.5}$ to catalyze intermolecular hydroamination of 1-octene (an unactivated alkene) places it in a select group of catalysts with this capability (*vide supra*). The intermolecular hydroamination activity of $\mathbf{12}\cdot(O(SiMe_3)_2)_{1.5}$ closely mirrors that of the yttrium analogue, although for entries 2 and 5 in Table 4.3, compound

Entry	Amine	Alkene or Alkyne[a]	Product	Time	Temp. (°C)	Product Formation[b],[c]	% Markovnikov Product[c]	N_t (h^{-1})[d]
1	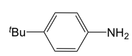	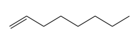	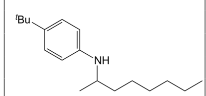	24 h	110	11 %	97	0.04
2	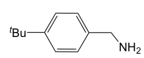		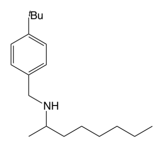	24 h	110	83 %	>99	0.35
3	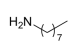		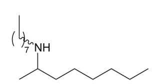	24 h	110	98 %	>99	0.41
4	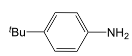		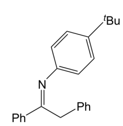	24 h	110	>99 %[e]	N/A	0.42
5	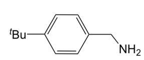		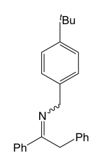	24 h	110	>99 %[e]	N/A	0.42
6	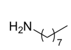		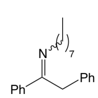	24 h	110	>99 %[e]	N/A	0.42

Table 4.3: Intermolecular Hydroamination Reactivity with **12**.
*Reactions performed in d_8-Toluene with 10 mol % catalyst loading; [a] Alkene/Alkyne present in 20 fold excess relative to the amine; [b] Conversion Determined by Product : Unreacted Amine ratio; [c] Determined by GC-MS; [d] Turnover Frequency; [e] in entry 4 the product is formed as a single isomer, whereas in entries 5 and 6 the products are formed as 1:0.35 and 1:0.24 mixtures of the E and Z isomers (based on literature assignments for similar compounds),[162,163] respectively.

12·$(O(SiMe_3)_2)_{1.5}$ afforded lower and higher activities, respectively ($N_t = 0.35$ vs 0.40 and 0.42 vs 0.33). The intermolecular reactions with the largest conversions after 24 h at 110 °C (10 mol % catalyst) were those utilizing diphenylacetylene (entries 4, 5 and 6), as the amounts of unreacted 4-*tert*-butylaniline, 4-*tert*-butylbenzylamine and octylamine were below the detection limit of the GC instrument. Furthermore, the conversions with 4-*tert*-butylaniline and 4-*tert*-butylbenzylamine are increased compared to those obtained with $[(XN_2)Y(CH_2SiMe_3)(THF)]\cdot(O(SiMe_3)_2)$ (**3**·$O(SiMe_3)_2$; 97 % and 80 % respectively), while the conversion with octylamine was >99 % for both catalysts (*vide supra*; Section 2.4, Table 2.3).[167]

Rare earth alkyl-'ate' complexes have been reported to catalyze intramolecular hydroamination as well as intermolecular hydroamintion. A few examples include; $[\{(R)\text{-Binap}(NCyp)_2\}La\{(\mu\text{-Me})_2Li(THF)\}\{(\mu\text{-Me})Li(THF)\}_2]$-, which catalyzed asymmetric intramolecular hydroamination of amino-1,3-dienes,[76] $[Li(THF)_4][\{(R)\text{-Binap}(NCyp)_2\}Y(CH_2SiMe_3)_2]$ (Binap = 2,2′-disubstituted-1,1′-binaphthyl; Cyp = cyclopentyl), which catalyzed intramolecular hydroamination of secondary aminoalkenes;[216] $[Li(THF)_4][(ArNC(Me){=}C(Me)NAr)Y(CH_2SiMe_3)_2]$ (Ar = $C_6H_3{}^iPr_2$-2,6), which catalyzed the intermolecular hydroamination reaction of styrene and pyrrolidine;[217] and $[\{(R)\text{-Binap}(NCyp)_2\}Y\{(\mu\text{-Me})_2Li(THF)_2\}\{(\mu\text{-Me})Li(THF)\}]$ (Binap = 2,2′-disubstituted-1,1′-binaphthyl; Cyp = cyclopentyl), which catalyzed 1-amino-2,2-diphenyl-4-pentene cyclization, requiring 1.9 h at 25 °C with 6 mol % catalyst loading to reach 100 % conversion.[215] $[Li(THF)_x][(XN_2)La(CH_2SiMe_3)_2]\cdot(\text{Toluene})$ (**14**·Toluene·LiCl, $x = 3$) was tested as a catalyst for intramolecular hydroamination with 1-amino-2,2-diphenyl-4-pentene in d_8-THF at 24 °C.

However, the time required to reach >99 % completion (45 h) was significantly increased compared to that required for $[(XN_2)Y(CH_2SiMe_3)(THF)]\cdot(O(SiMe_3)_2)$ ($\mathbf{3}\cdot O(SiMe_3)_2$) and $[(XN_2)Lu(CH_2SiMe_3)(THF)]\cdot(O(SiMe_3)_2)_{1.5}$ ($\mathbf{12}\cdot(O(SiMe_3)_2)_{1.5}$)) (<10 min) under analogous conditions in benzene (or in THF for the yttrium complex). Due to the low activity of **14** with one of the most readily-cyclized intramolecular hydroamination substrates, further testing with more challenging substrates and intermolecular hydroamination was not pursued.

4.4 Summary

The rigid NON-donor pincer ligand, XN_2, has been successfully employed for the synthesis of a lutetium monoalkyl complex (**12**), a lanthanum chloride complex (**13**) and an anionic lanthanum dialkyl complex (**14**). Complex **14** was tested as a catalyst for intramolecular hydroamination, but showed low activity. By contrast, the neutral lutetium alkyl complex, **12**, is highly active for both intra- and inter-molecular hydroamination with a variety of substrates. For intramolecular alkene hydroamination, the time required to reach >99 % completion was slightly increased compared to the previously reported yttrium analogue. By contrast, the intermolecular hydroamination reaction between 4-*tert*-butylbenzylamine and diphenylacetylene afforded a higher turnover number than the yttrium analogue.

Chapter 5

Zirconium Complexes of a Rigid, Dianionic NON-Donor Pincer Ligand: Alkyl Cations and Olefin Polymerization

5.1 Introduction

In combination with a suitable supporting ligand set and weakly-coordinating counter-anion, group 4 transition metal alkyl cations can achieve high ethylene polymerization activities, in some cases well in excess of 1000 kg/(mol·atm·h). Highly effective catalysts include metallocenes, *ansa*-metallocenes and constrained geometry catalysts such as [Cp^*_2ZrMe][A], [{$Me_2Si(\eta^5$-9-fluorenyl)-(η^5-C_5H_4)}ZrMe][A], and [{$Me_2Si(\eta^5$-$C_5Me_4)(\kappa^1$-N^tBu)}MMe][A] (M = Ti or

Zr), as well as non-cyclopentadienyl (post-metallocene) complexes, for example $[(R_3PN)_2TiMe][A]$, $[(\kappa^2\text{-}CH_2(CH_2NAr)_2)TiMe][A]$ and $[(\kappa^2\text{-}OC_6H_2R_2(o\text{-}CH{=}NR))_2ZrMe][A]$, where A is a weakly-coordinating anion such as $MeB(C_6F_5)_3$ or $B(C_6F_5)_4$.[96,102,114,115,218–220]

Cationic alkyl complexes are often generated *in situ*. However, their isolation and characterization can provide valuable insight into the nature of accessible species in solution. Alkyl cations may be categorized as Contact Ion Pairs (CIPs), such as $[Cp^*_2ZrMe][MeB(C_6F_5)_3]$ in which the anion interacts directly with the cation, and Solvent-Separated Ion Pairs (SSIPs), such as $[Cp^*_2ZrMe(THF)][MeB(C_6F_5)_3]$ in which the cation is coordinated by a molecule of solvent and the anion is not present in the primary coordination sphere of the metal.[102] SSIPs in which the metal is coordinated by a donor solvent (eg. THF, OEt_2 or DME) typically exhibit low or zero polymerization activity, since solvent coordination diminishes the electrophilicity of the metal center and increases coordination number, electron count and steric hindrance, reducing the potential for both ethylene coordination and 1,2-insertion. Such SSIPs have been studied in some detail. By contrast, isolated early transition metal and *f*-element SSIPs incorporating arene solvents are rare (Figure 5.1),[21,221–224] despite the fact that initial polymerization testing is frequently carried out in arene solvents.[225]

The impact of arene-coordination on ethylene polymerization activity is also highly variable. For example, McConville *et al.* proposed arene-coordinated $[(CH_2(CH_2NAr)_2)TiR(\eta^6\text{-toluene})]^+$ (Ar = *o*-xylyl or $C_6H_3{}^iPr_2$-2,6) cations to explain greatly reduced polymerization activities in the presence of

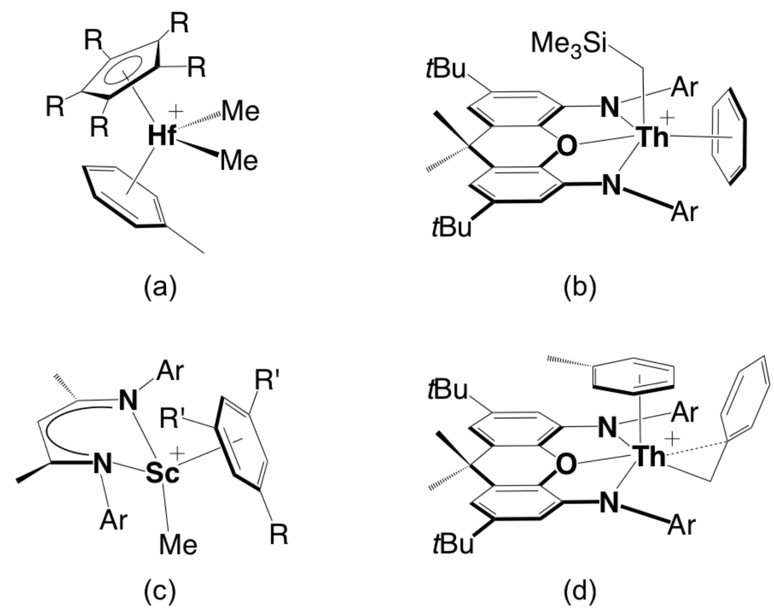

Figure 5.1: Crystallographically-characterized early transition metal and *f*-element arene-solvent-separated ion pairs (Ar = $C_6H_3{}^iPr_2$-2,6). The hafnium complexes were reported by Bochmann (C_5R_5 = 1,3-$C_5H_3(SiMe_3)_2$)[223] and Baird (C_5R_5 = C_5Me_5),[224] and the scandium (R = Me or Br and R′ = H, or R = R′ = Me)[221,222] and thorium[21] complexes were reported by Piers and Emslie, respectively.

small amounts of toluene.[226,227] By contrast, toluene in [(^{t}BuNSiMe$_2$(η^5,η^1-C$_5$Me$_3$CH$_2$))Ti(toluene)][B(C$_6$F$_5$)$_4$] is only weakly bound, and this compound is highly active for ethylene (1 atm) polymerization in toluene.[228] Piers *et al.* also reported the synthesis of [(κ^2-nacnac^{Me2})ScMe(η^6-C$_6$R$_6$)][B(C$_6$F$_5$)$_4$] (nacnac^{Me2} = HC(CMeNAr)$_2$; Ar = $C_6H_3{}^iPr_2$-2,6; C$_6$R$_6$ = bromobenzene, benzene, toluene, *p*-xylene or mesitylene) scandium cations, and while [(κ^2-nacnac^{Me2})ScMe(η^6-C$_6$H$_3$Me$_3$-1,3,5)][B(C$_6$F$_5$)$_4$] is an active ethylene polymerization catalyst in bromobenzene, it shows negligible activity in more-donating toluene.[221,222] The Emslie group also isolated the arene-coordinated thorium cations $[(\kappa^3\text{-XA}_2)\text{Th}(\text{CH}_2\text{SiMe}_3)(\eta^n\text{-arene})][\text{B}(\text{C}_6\text{F}_5)_4]$ (arene = benzene, n = 6; arene = toluene, n = 3) and $[(\kappa^3\text{-XA}_2)\text{Th}(\eta^2\text{-CH}_2\text{Ph})(\eta^6\text{-toluene})][\text{B}(\text{C}_6\text{F}_5)_4]$, which are inactive for ethylene (1 atm) polymerization in benzene and toluene solution.[21] Other d^0 arene-solvent-coordinated alkyl cations are: - $[\text{Cp}''\text{MR}_2(\eta^6\text{-toluene})][\text{RB}(\text{C}_6\text{F}_5)_3]$ (M = Zr, R = Me; M = Hf, R = Me or Et; Cp″ = 1,3-$\text{C}_5\text{H}_3(\text{SiMe}_3)_2$) in which the arene is tightly coordinated,[223] and $[\text{Cp*MMe}_2(\eta^6\text{-C}_6\text{R}_6)][\text{MeB}(\text{C}_6\text{F}_5)_3]$ (M = Ti, C_6R_6 = toluene or mesitylene; M = Zr, C_6R_6 = benzene, toluene, *p*-xylene, *m*-xylene, mesitylene, styrene; M = Hf, C_6R_6 = toluene, *p*-xylene, *m*-xylene, mesitylene, styrene, anisole) in which the arene is particularly labile for M = Ti.[224,229,230]

The complexes discussed above highlight a greater tendency towards arene solvent coordination in more sterically-open cationic alkyl species, especially mono-cyclopentadienyl complexes, and complexes of certain non-cyclopentadienyl ligand systems. The Emslie group has previously reported a range of actinide and rare earth alkyl complexes supported by 4,5-bis(anilido)xanthene pincer ligands, including complexes of Th,[19–21] U,[24] Y (Chapter 2),[167] Lu and La (Chapter 4).[168] Described herein is the attachment of the rigid, dianionic 4,5-bis(anilido)xanthene pincer ligand (XN_2) to zirconium by amine elimination, conversion of the resulting bis(dimethylamido) complex to a dimethyl complex, and subsequent reactions with $\text{B}(\text{C}_6\text{F}_5)_3$ and $[\text{CPh}_3][\text{B}(\text{C}_6\text{F}_5)_4]$ to afford a contact ion pair and an arene-solvent-separated ion pair, respectively. The X-ray structures and ethylene polymerization activity of both alkyl cations is discussed.

5.2 Zirconium Complexes Bearing the XN_2 Ligand

Multiple avenues were explored in attempt to isolate group 4 transition metal complexes with the XN_2 ligand including; (1) alkane elimination utilizing titanium and zirconium tetra-neopentyl reagents, which led only to unreacted pro-ligand and $[M(CH_2CMe_3)_4]$ thermal decomposition products; (2) salt metathesis utilizing the XN_2 dipotassium salt in combination with titanium, zirconium and hafnium tetra-chlorides, zirconium and hafnium tetrachloride THF adducts and even zirconium tetra-iodide, all of which failed to react (Scheme 5.1). By contrast, the reaction of H_2XN_2 with excess tetrakis-(dimethylamido)zirconium (110 °C, 14 days) was successful, yielding $[(XN_2)Zr(NMe_2)_2]\cdot(O(SiMe_3)_2)_{0.5}$ (**15**$\cdot(O(SiMe_3)_2)_{0.5}$) in 73 % yield after recrystallization from $O(SiMe_3)_2$ (Scheme 5.2).

Compound **15**$\cdot(O(SiMe_3)_2)_{0.5}$ exhibits substantial thermal stability, as no decomposition was observed after heating a d_8-toluene solution at 115 °C for one week. In addition, it is of note that the dimethylamido groups are equivalent in the ^{1}H NMR spectrum at 24 °C (Figure 5.2). However, upon cooling, de-coalescence was observed, resulting in two different Zr-NMe_2, Ar-H, ortho-CHMe$_2$ and CMe_2 environments at –70 °C (Figure 5.3). The low-temperature ^{1}H NMR spectrum is indicative of C_s symmetry, presumably with one NMe_2 group located approximately in the plane of the ligand, and one in an apical site.

X-ray quality crystals of **15** were grown from a concentrated $O(SiMe_3)_2$ solution cooled to –30 °C (Figure 5.4, Table 5.1), and the solid state structure

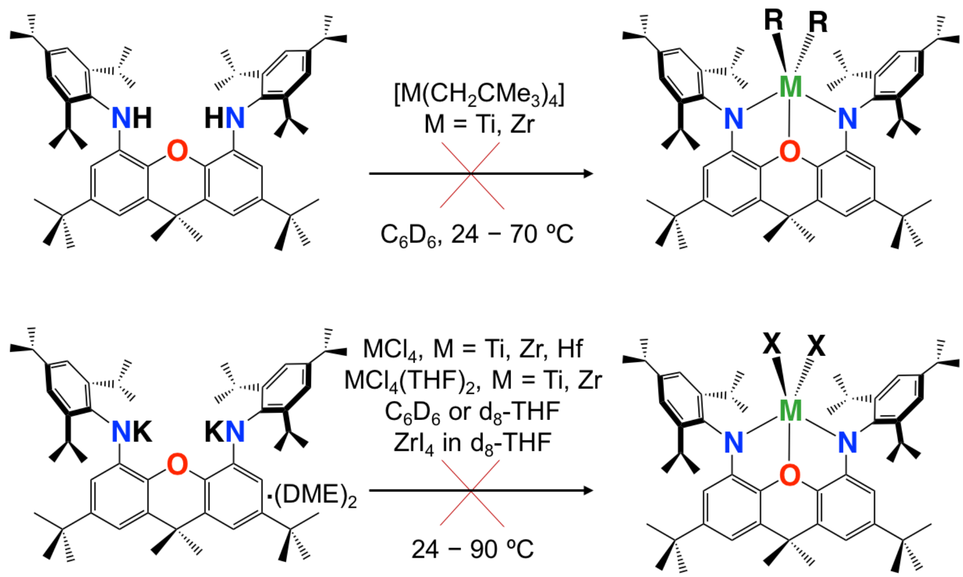

Scheme 5.1: The Unsuccessful Avenues Explored in an Attempt to Isolate XN_2 Group 4 Transition Metal Complexes. ($R = CH_2CMe_3$, X = Cl/I).

confirmed that zirconium is 5-coordinate with a distorted square pyramid geometry, in which the XN_2 ligand donors and one dimethylamido group (N(3)) occupy basal positions, while the second dimethylamido group (N(4)) occupies the axial position. This arrangement of the monodentate ligands mirrors that in structurally-related $[(XN_2)Ln(CH_2SiMe_3)(THF)]$ (Ln = Lu (**12**) and Y (**3**); *vide supra*, Sections 4.2 and 2.3 respectively),[167,168] $[Li(THF)_4][(XN_2)La(CH_2SiMe_3)_2]$ (**14**; *vide supra*, Section 4.2)[168] and $[(XA_2)An(CH_2SiMe_3)_2]$ (An = Th and U; XA_2 = 4,5-bis(2,6-diisopropyl-anilino)-2,7-di-*tert*-butyl-9,9-dimethylxanthene),[19,24] and is favored so as to allow the *N*-aryl groups to rotate away from the apical dimethylamido ligand in order to minimize unfavorable steric interactions. Consequently, the distance between the isopropyl *C*HMe$_2$

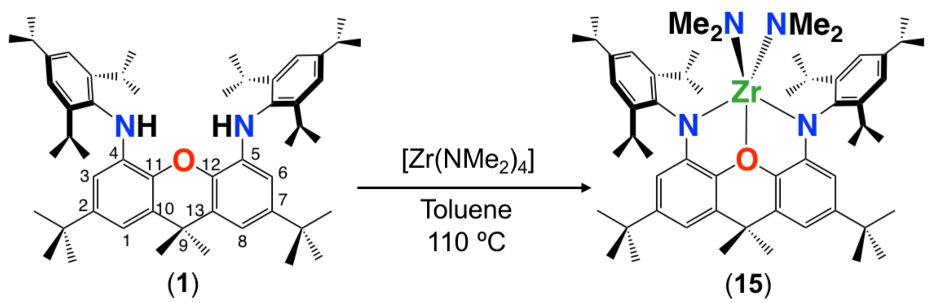

Scheme 5.2: The Synthesis of the Zirconium Complex **15**.

carbon atoms flanking the top of the square pyramid in **15** (C(33)···C(45) = 7.46 Å) is significantly greater than that below the base of the square pyramid (C(30)···C(48) = 5.03 Å). The square pyramidal coordination geometry of **15** also mirrors that of closely related $[(L^{Cy})Ti(NMe_2)_2]$ (L^{Cy} = 4,5-dicyclohexyl-2,7-di-*tert*-butyl-9,9-dimethylxanthene), prepared via a salt metathesis reaction between $Li_2(L^{Cy})$ and $[TiCl_2(NMe_2)_2]$.[231]

The angles in **15** between N(4) and the equatorial atoms range from 99–107°. The smallest angles in the square plane are the N(1)–Zr–O(1) and N(2)–Zr–O(1) angles of 68.2(2)° and 67.9(1)°, whereas the N(1)–Zr–N(3) and N(2)–Zr–N(3) angles are 103.4(2)° and 108.5(2)° respectively, causing the sum of the angles in the square plane to be 348°. The XN_2 ligand is slightly bent with a 16° angle away from planarity, based on the orientation of the two aryl rings of the xanthene backbone. Zirconium lies 0.50 Å out of the N(1)/C(4)/C(5)/N(2) plane, leading to a 32° angle between the N(1)/C(4)/C(5)/N(2) and the N(1)/Zr/N(2) planes. The neutral oxygen donor on the xanthene backbone is located 0.38 Å out of the N(1)/C(4)/C(5)/N(2) plane in order to coordinate to zirconium.

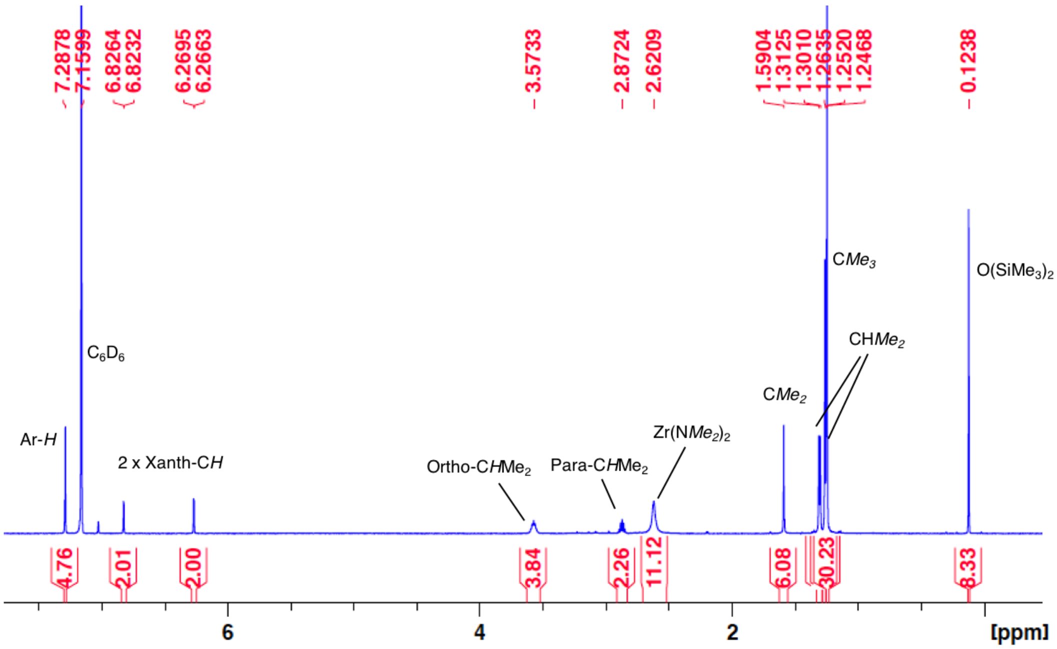

Figure 5.2: The ^{1}H NMR Spectrum of Complex **15** (600 MHz, C_6D_6).

The Zr–N(3) and Zr–N(4) distances of 2.035(5) Å and 2.031(5) Å are in the expected range compared to related zirconium complexes containing dimethylamido ligands such as [(κ^3-NPN)Zr(NMe_2)$_2$] (NPN = PhP(C_4H_nE(*o*-NAr))$_2$; E = S, n = 2, Ar = mesityl; E = CH_2, n = 4, Ar = *o*-xylyl; 2.0191(10)–2.0670(10) Å),[38,232] [(κ^3-NPN′)Zr(NMe_2)$_2$] (NPN′ = PhP(C_6H_4(*o*-CH_2NAr)-)$_2$, Ar = *m*-xylyl; 2.0606(16) Å and 2.0510(16) Å),[233] [(κ^3-NNN)Zr(NMe_2)$_2$]-(NNN = 2,6-NC_5H_3(C_6H_4(*o*-NMes))$_2$; 2.0264(10) Å and 2.028(10) Å),[33] [(κ^2-NN)Zr(NMe_2)$_2$] (NN = (C_6H_3(*o*-Me)(*o*-NAr))$_2$, Ar = C_6H_3(*m*-^{t}Bu)$_2$; 2.015(5)–2.050(3) Å),[234] and others.[235,236] The Zr–NMe_2 distances in **15** are, however, shorter compared to Zr–N distances reported for complexes containing Zr–NPh_2 ligands (2.143(2)–2.170(3) Å).[237–240]

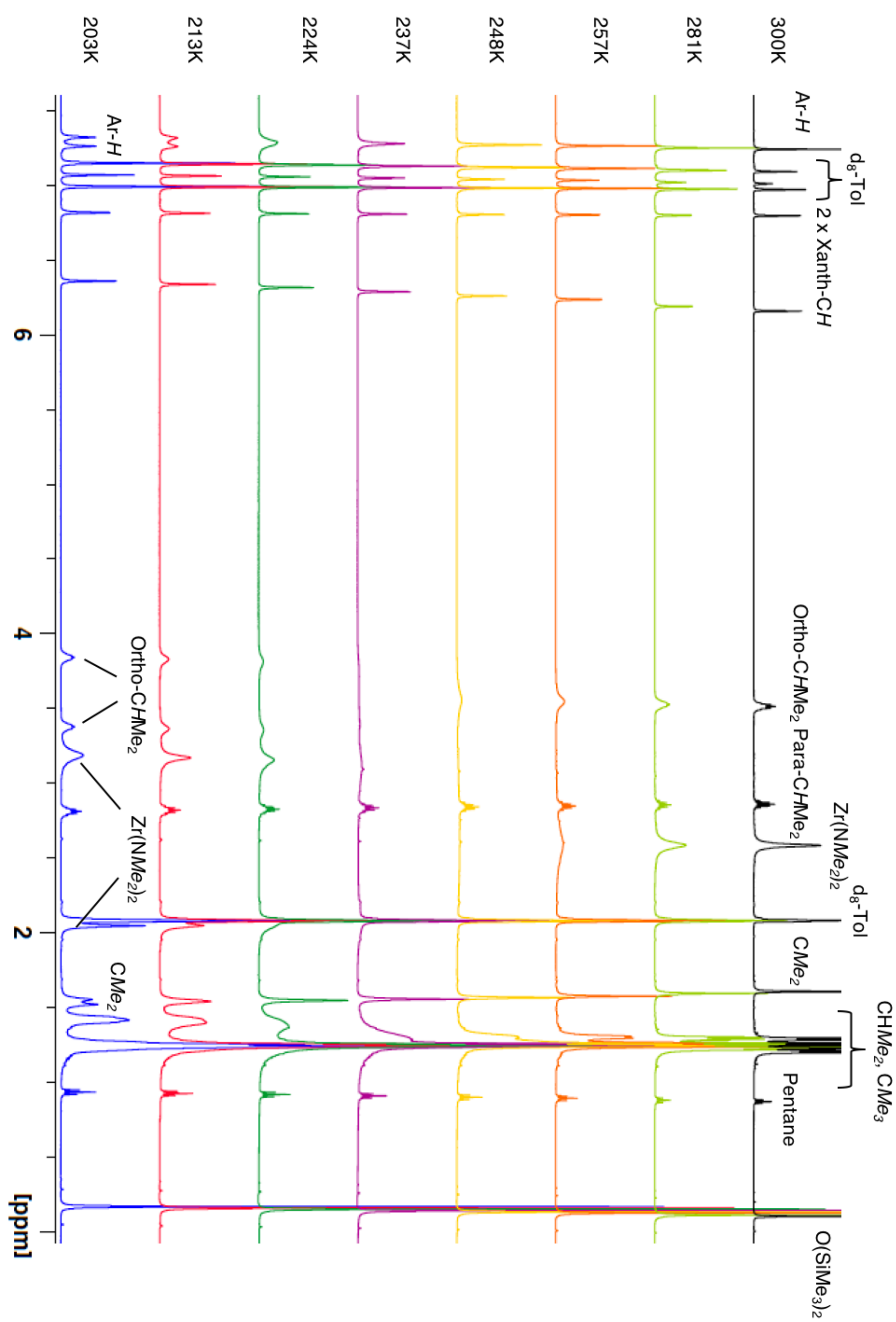

Figure 5.3: Variable Temperature ^{1}H NMR Spectra of **15** (500 MHz, d_8-Tol).

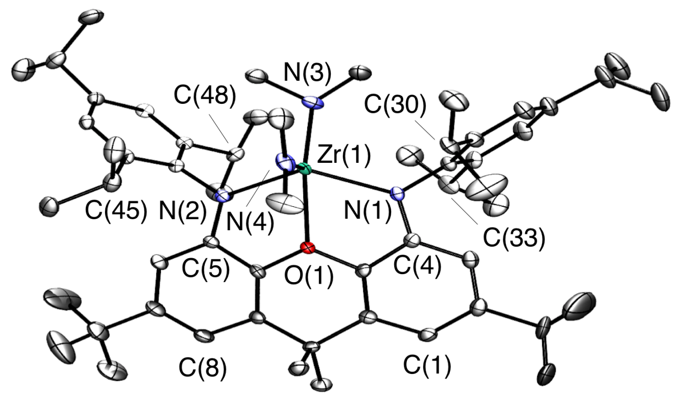

View A

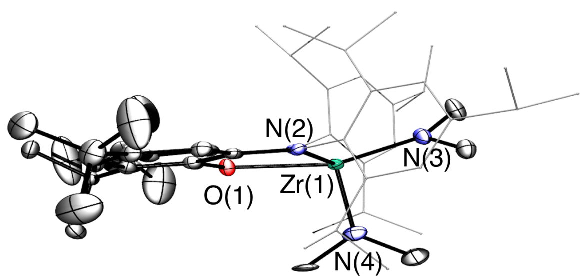

View B

Figure 5.4: Two views of the X-ray crystal structure for compound **15**. The whole molecule is disordered over two positions, and only the major position (92 %) is shown. Ellipsoids are set to 50 %. Hydrogen atoms are omitted. In view B the 2,4,6-triisopropylphenyl groups are depicted in wire-frame format for clarity. Selected bond lengths [Å] and angles [°]: Zr–N(1) 2.167(4), Zr–N(2) 2.196(4), Zr–N(3) 2.034(5), Zr–N(4) 2.031(5), Zr–O(1) 2.324(4), N(1)–Zr–N(2) 129.19(16), O(1)–Zr–N(3) 159.02(17), O(1)–Zr–N(4) 99.43(18), N(3)–Zr–N(4) 101.3(2), N(1)–Zr–N(4) 104.58(18), N(2)–Zr–N(4) 106.59(17), N(1)–Zr–O(1) 68.18(15), N(2)–Zr–O(1) 67.90(14), N(1)–Zr–N(3) 103.38(18), N(2)–Zr–N(3) 108.52(18).

By comparison, the Zr–N(1) and Zr–N(2) distances of 2.167(4) Å and 2.19-6(4) Å are elongated compared to those for the more electron-donating and less sterically-hindered dimethylamido groups in **15**. However, they are in the typical range for diarylamido ligands; 2.102(5)–2.232(2) Å in the aforementioned zirconium complexes.

In order to investigate the potential for ethylene polymerization, a dialkyl zirconium complex was desired, and in an effort to achieve this, two routes were employed (Scheme 5.3). Route A involved the reaction of $[(XN_2)Zr(NMe_2)_2]\cdot(O(SiMe_3)_2)_{0.5}$ ($\mathbf{15}\cdot(O(SiMe_3)_2)_{0.5}$) with excess trimethylaluminum in benzene (24 °C, 7 days), and afforded $[(XN_2)ZrMe_2]$ (**16**) as a yellow powder in 62 % yield.

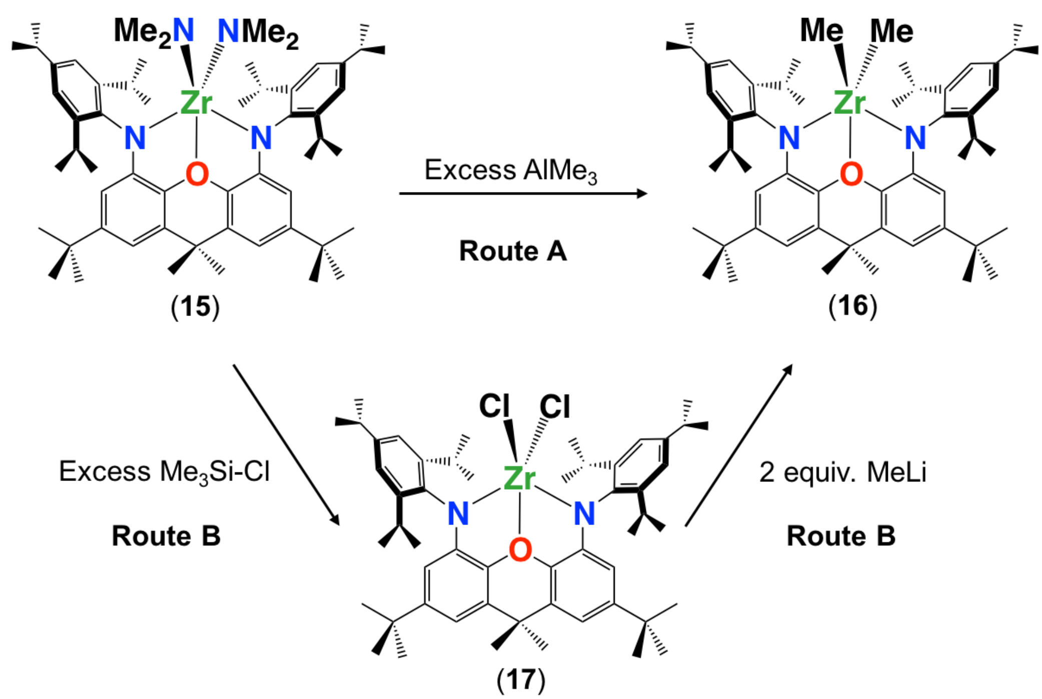

Scheme 5.3: The Synthesis of Zirconium Complexes **16** and **17**.

Alternatively, compound **16** could be prepared in two steps via Route B (Scheme 5.3). Firstly, [(XN_2)$ZrCl_2$] (**17**) was isolated in 64 % yield through the reaction of [(XN_2)Zr(NMe_2)$_2$]·(O($SiMe_3$)$_2$)$_{0.5}$ (**15**·(O($SiMe_3$)$_2$)$_{0.5}$) with excess trimethylsilyl-chloride in benzene at 24 °C. This reaction required two weeks to reach completion proceeding via [(XN_2)Zr(NMe_2)Cl], which is the major product after four days of reaction. This is observed in the *in situ* ^{1}H NMR spectrum (Figure 5.5). The Zr(NMe_2)Cl peak (middle spectrum) is visible at 2.2 ppm, which is not observed in the final product (bottom spectrum), and the Me_2N-$SiMe_3$ by-product is apparent in both the intermediate and final *in situ* spectra, but can easily be removed *in vacuo* and is not present in the pure material (Figure 5.6). Compound **17** was subsequently reacted with excess methyl lithium in C_6D_6 and the ^{1}H NMR spectrum revealed a clean reaction to form [(XN_2)$ZrMe_2$] (**16**). Route A was chosen as the preferred route for the isolation of **16** on a preparative scale as it is more direct.

The difference in the thermal stability of **16** compared to [(XN_2)Zr(NMe_2)-$_2$]·(O($SiMe_3$)$_2$)$_{0.5}$ (**15**·(O($SiMe_3$)$_2$)$_{0.5}$) is significant, as a d_8-toluene solution of **16** was approximately 15 % decomposed after 1 h at 115 °C, and completely decomposed after 18 h, resulting in a mixture of unidentified products. The ^{1}H NMR spectrum of [(XN_2)$ZrMe_2$] (**16**) between 24 °C and –70 °C revealed a single peak (Figure 5.7; 0.7 ppm at 24 °C in C_6D_6) corresponding to the two methyl substituents on zirconium, suggesting either approximate trigonal bipyramidal geometry at zirconium, or a square pyramidal geometry with rapid exchange of the methyl groups in apical and basal positions (*vide intra*).

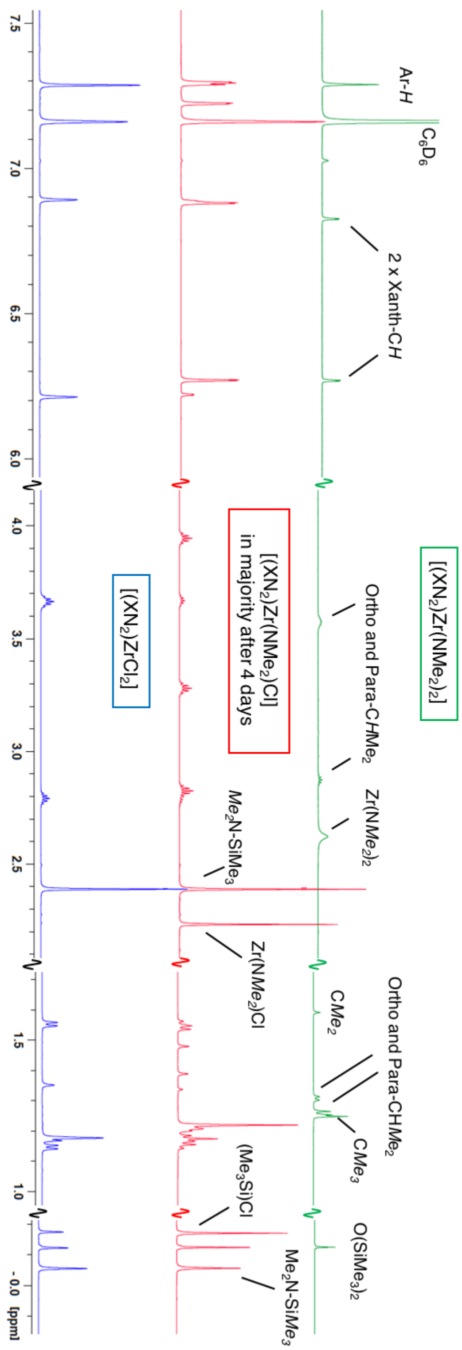

Figure 5.5: *In Situ* ^{1}H NMR Spectra of the Reaction Between $[(XN_2)Zr(NMe_2)_2]\cdot(O(SiMe_3)_2)_{0.5}$ (**15**) and Me_3SiCl to Form $[(XN_2)ZrCl_2]$ (**17**).

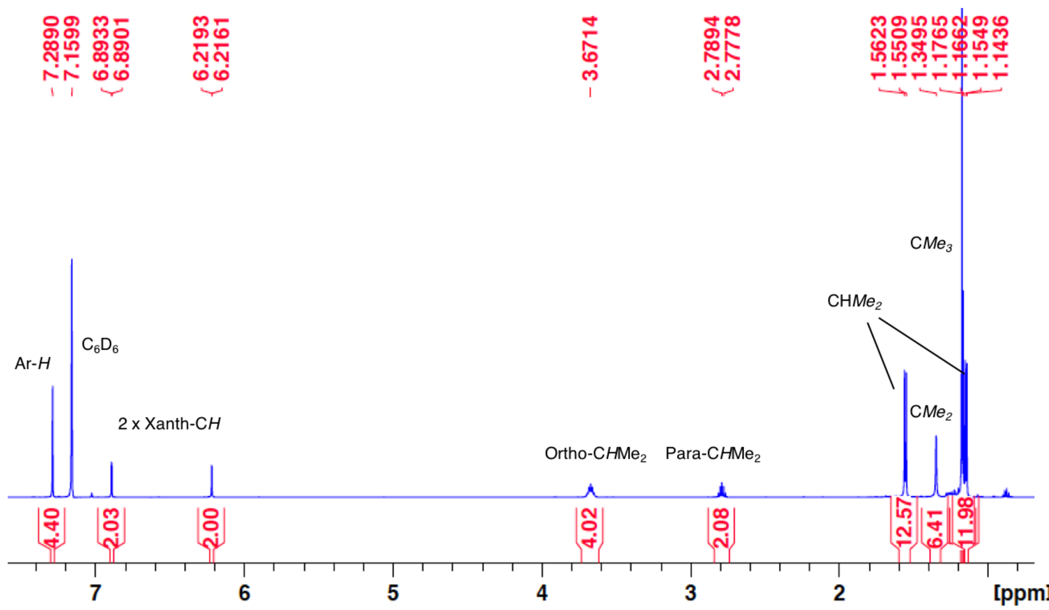

Figure 5.6: The [1]H NMR Spectrum of Complex **17** (600 MHz, C_6D_6).

Crystals of **16** were grown from a concentrated pentane solution cooled to –30 °C (Figure 5.9, Table 5.1) and in contrast to the structure of **15**·(O-$(SiMe_3)_2)_{0.5}$, compound **16** adopts a distorted trigonal bipyramidal geometry with the amido donors of the XN_2 ligand in the axial positions and the oxygen and two methyl groups occupying the equatorial positions. This coordination geometry is likely preferred due to the reduced steric requirements of methyl compared to dimethylamido ligands. The N(1)–Zr–N(1′) angle is 137.23(7)° due to constraints imposed by ligand rigidity, while the sum of the O–Zr–C(28), O–Zr–C(28′) and C(28)–Zr–C(28′) angles is 360° due to a C_2-axis running through the Zr–O(1) bond. The XN_2 ligand is essentially planar with a 2° angle away from planarity, based on the orientation of the two aryl rings of the xanthene backbone, and zirconium lies in the plane of the XN_2 ligand donor atoms. The C_2 axis through the Zr–O(1) bond also leads to identical

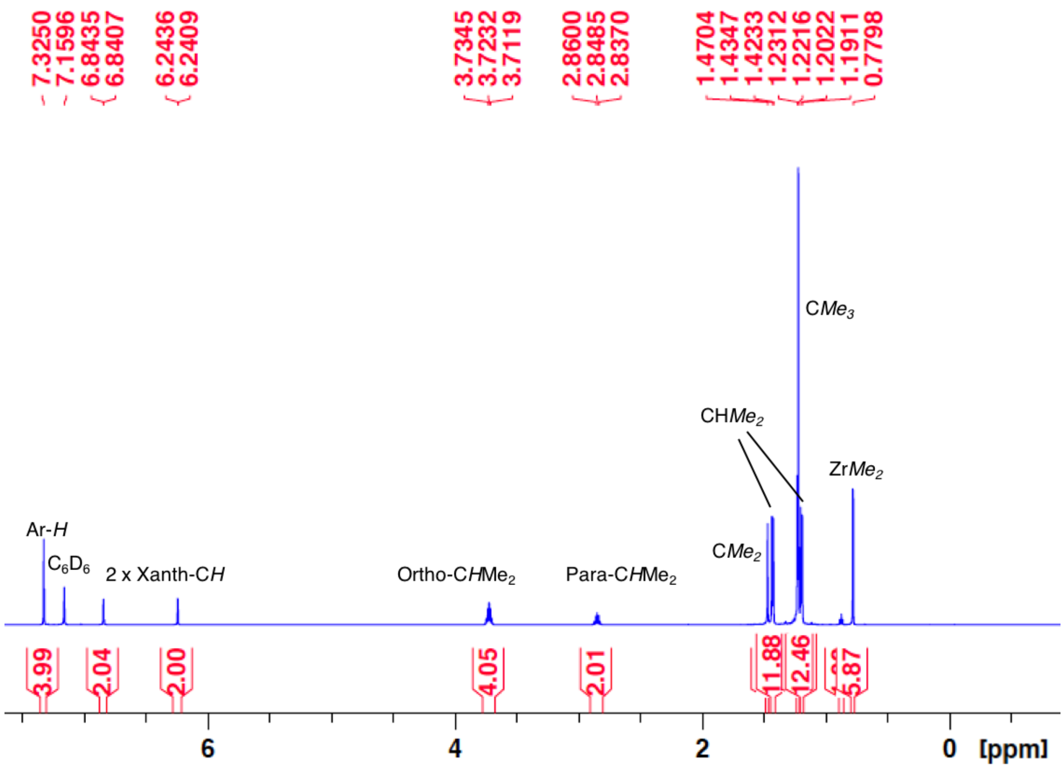

Figure 5.7: The ^{1}H NMR Spectrum of Complex **16** (600 MHz, C_6D_6).

distances between the *C*HMe$_2$ carbon atoms on either side of the plane of the ligand backbone (C(19)···C(22) = 6.32 Å).

It is noteworthy that in the solid state structure of **16**, the XN_2 ligand is meridionally (*mer*) coordinated rather than facially (*fac*) coordinated (Scheme 5.8). By contrast, the related complex [(κ^3-^{tBu}NON)ZrMe$_2$] (^{tBu}NON = O(C$_6$H$_4$(N^{t}Bu-*o*))$_2$) is described as having a twisted *fac* coordination mode in which the two ligand amido donors and one methyl group are in the equatorial positions, while the other methyl group and the oxygen donor are in axial positions.[27] This highlights a unique feature of the XN_2 ligand and its designed architecture as it exclusively binds in a meridional fashion.

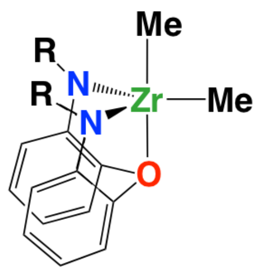

[(NON)ZrMe$_2$]
(*fac*)

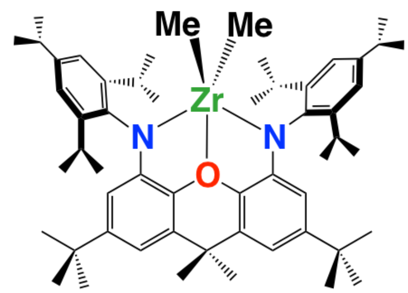

(**16**)
(*mer*)

Figure 5.8: The *fac* Coordination Mode of the ^{tBu}NON Ligand in [(κ^3-^{tBu}-NON)ZrMe$_2$],[27] and the *mer* Coordination Mode of the XN$_2$ Ligand in Zirconium Complex **16** (R = ^{t}Bu).

The Zr–C distances of 2.226(2) Å are comparable with those in complexes such as [(κ^3-^{tBu}NON)ZrMe$_2$] (^{tBu}NON = O(C$_6$H$_4$(N^{t}Bu-*o*))$_2$, 2.235(5) Å and 2.280(5) Å)[27], [(κ^3-N$_2$NMe)ZrMe$_2$] (N$_2$NMe = [(MesNCH$_2$CH$_2$)$_2$NMe]; Mes = mesityl, 2.240(7) Å and 2.265(7) Å),[241] and other dimethyl zirconium complexes with bisamido supporting ligands (2.233(6)–2.294(5) Å).[15,28,35,119,242,243] The Zr–N distances of 2.135(1) Å are shorter than the corresponding distances in **15**, perhaps due to reduced steric hindrance. However, they are longer than those in the aforementioned literature compounds (2.087(4)–2.096(4) Å), likely due to the large binding pocket of the XN$_2$ ligand enforced by the rigidity of the xanthene backbone.

Reaction of [(XN$_2$)ZrMe$_2$] (**16**) with one equivalent of B(C$_6$F$_5$)$_3$ in C$_6$D$_6$ resulted in complete conversion to [(XN$_2$)ZrMe][MeB(C$_6$F$_5$)$_3$] (**18**), accompanied by an immediate solution color change from pale yellow to bright, golden yellow (Scheme 5.4). The alkyl zirconium cation [(XN$_2$)ZrMe][MeB(C$_6$F$_5$)$_3$] (**18**)

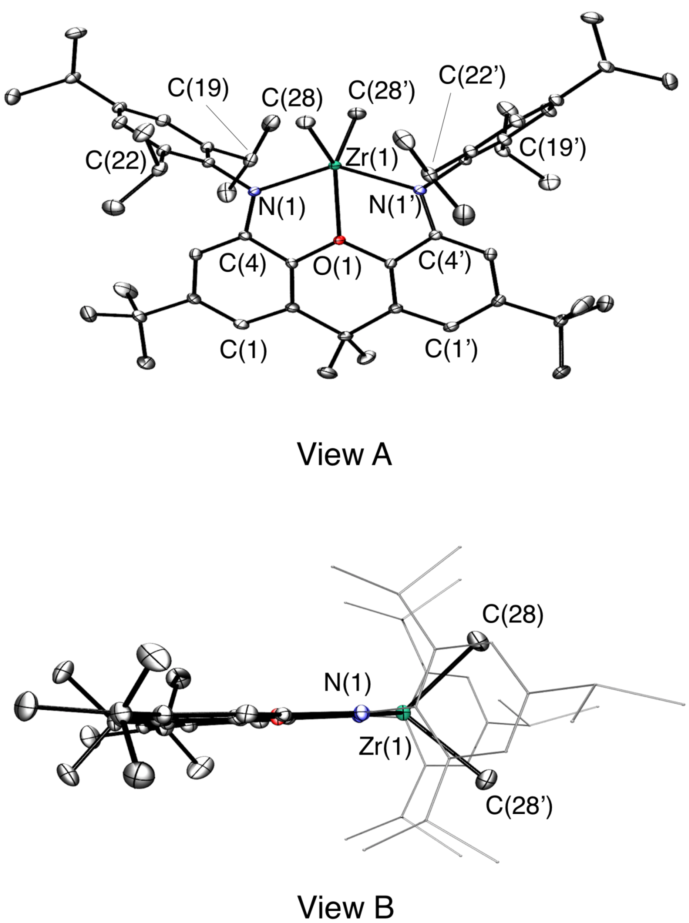

Figure 5.9: Two views of the X-ray crystal structure for compound **16**. Ellipsoids are set to 50 %. Hydrogen atoms are omitted. In view B the 2,4,6-triisopropylphenyl groups are depicted in wire-frame format for clarity. Selected bond lengths [Å] and angles [°]: Zr–N(1) 2.135(1), Zr–C(28) 2.226(2), Zr–O(1) 2.2882(14), N(1)–Zr–N(1′) 137.23(7), N(1)–Zr–O(1) 68.62(4), O(1)–Zr–C(28) 130.49(6), N(1)–Zr–C(28) 104.61(7), C(28)–Zr–C(28′) 99.03(11).

was isolated as bright yellow crystals in 77 % yield from a concentrated toluene solution layered with pentane and cooled to –30 °C. The ^{1}H NMR spectrum revealed top-bottom asymmetry with two different Ar-*H*, ortho-C*H*Me$_2$, C*Me$_2$* and four different ortho-CH*Me$_2$* environments (Figure 5.10). The Zr-*Me* reso-

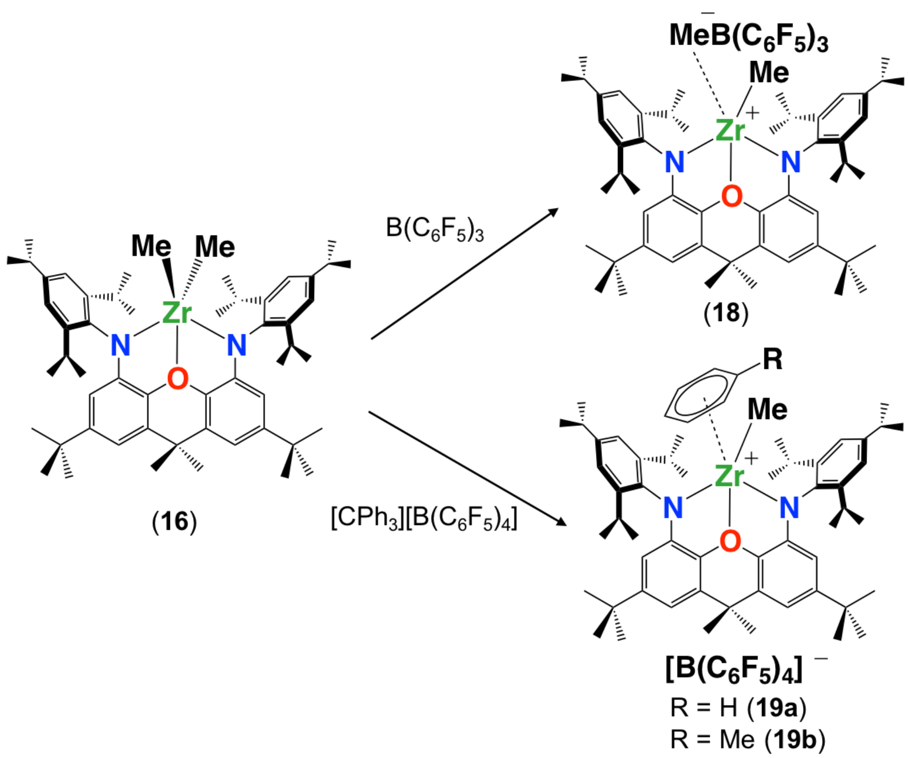

Scheme 5.4: The Synthesis of Zirconium Complexes **18** and **19**.

nances in the ^{1}H and ^{13}C NMR spectra of **18** (1.87 and 55.56 ppm, respectively) are shifted to higher frequency relative to those of neutral [(XN$_2$)Zr*Me$_2$*] (**16**) (0.78, 50.02 ppm, respectively). The B-*Me* signals were observed at 1.80 ppm and 35.20 ppm in the ^{1}H and ^{13}C NMR spectra respectively, and the large value of $\Delta\delta(m,p\text{-F})$ (the difference between the *meta*- and *para*-C_6F_5 chemical shifts in the ^{19}F NMR) (3.59 ppm) is indicative of a contact ion pair, in which the methyl group of the anion interacts significantly with the cation.[116,244] At 24 °C, benzene solutions of **18** are stable for 24 h but decomposition becomes increasingly noticeable over a period of 7 days (leading to a mixture of unidentified products). Heating a benzene solution of [(XN$_2$)ZrMe][MeB(C$_6$F$_5$)$_3$] (**18**) at 60 °C for one hour resulted in 20 % thermal decomposition, and after 18 h complex **18** was fully decomposed, resulting in multiple unidentified products.

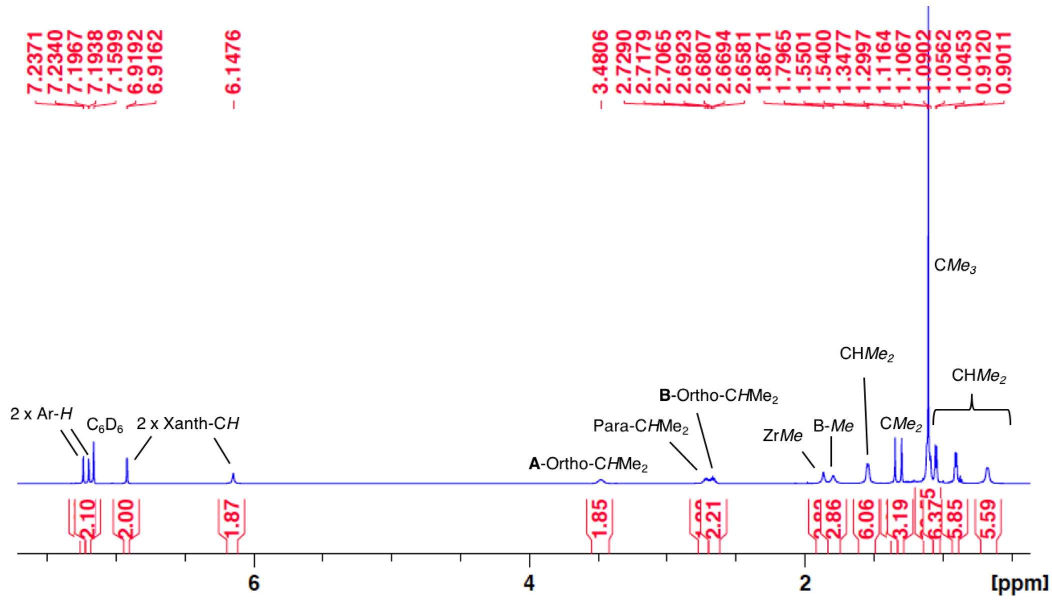

Figure 5.10: The *In Situ* ^{1}H NMR Spectrum of the Reaction Between Complex **16** and $B(C_6F_5)_3$ to Form Complex **18** (600 MHz, C_6D_6).

In the solid state structure of **18** (Figure 5.11, Table 5.1), zirconium adopts a distorted square pyramidal geometry with the two amido donors, the central oxygen of the ligand backbone, and the methylborate anion (coordinated via C(55)) occupying the square plane, while the remaining methyl ligand (C(54)) caps the pyramid. The smallest angles in this distorted square pyramid are the N–Zr–O angles of 69.18(5)° and 69.01(5)°, and the largest is the N(2)–Zr–C(55) angle of 110.97(6)°, while the other angles are between 93° and 105°. The XN_2 ligand is slightly bent with a 16° angle away from planarity, based on the orientation of the two aryl rings of the xanthene backbone. Zirconium lies 0.32 Å out of the N(1)/C(4)/C(5)/N(2) plane, leading to a 22° angle between the N(1)/C(4)/C(5)/N(2) and the N(1)/Zr/N(2) planes. The neutral oxygen donor of the XN_2 ligand is situated 0.36 Å out of the N(1)/C(4)/C(5)/N(2) plane to coordinate to zirconium, and the C(33)···C(45) and C(30)···C(48) distances are 7.61 Å and 4.82 Å, respectively.

A range of zirconium alkyl cations paired with a $MeB(C_6F_5)_3^-$ anion (CIPs) have been reported, with Zr–C_{Me}, Zr–C_{MeBAr3} and Me–B distances in the ranges 2.20–2.29 Å, 2.49–2.67 Å and 1.64–1.69 Å, respectively.[27,29,245–255] The crystal structure of **18** is most closely related to [(^{tBu}NON)ZrMe][Me-B($C_6F_5)_3$] (^{tBu}NON = O(C_6H_4(N^{t}Bu-*o*))$_2$), which features a more flexible dianionic ^{tBu}NON-donor.[27,29] However, as with complex **16** (*vide supra*), a major difference is that the rigid XN_2 ligand in **18** is coordinated meridonally, whereas the ^{tBu}NON-donor ligand in [(^{tBu}NON)ZrMe][MeB($C_6F_5)_3$] is facially coordinated; the angle between the N(1)–Zr–O and N(2)–Zr–O planes is 161° in **18** compared to 121° in the ^{tBu}NON complex. The Zr–N distances of 2.093(2) Å in **18** are shortened relative to those in [(XN_2)ZrMe_2] (**16**; 2.135(1) Å) consistent with increased Lewis acidity at zirconium, and are equal within error to those in [(^{tBu}NON)ZrMe][MeB($C_6F_5)_3$] (2.05(1) Å and 2.07(1) Å).[14,27,29]

The Zr–C(54) distance in **18** is 2.207(2) Å, which is only marginally shorter than the Zr–Me distance in neutral [(XN_2)ZrMe_2] (**16**; 2.226(2) Å) and is very similar to that in cationic [(^{tBu}NON)ZrMe][MeB($C_6F_5)_3$] (2.200(13) Å).[14,27,29] The Zr–C(55) distance to the methylborate anion is 2.560(2) Å, which is lengthened by 0.35 Å compared to to Zr–C(54), and is significantly longer than the Zr–C_{MeBAr3} distance in [(^{tBu}NON)ZrMe][MeB($C_6F_5)_3$] (2.487(12) Å), likely

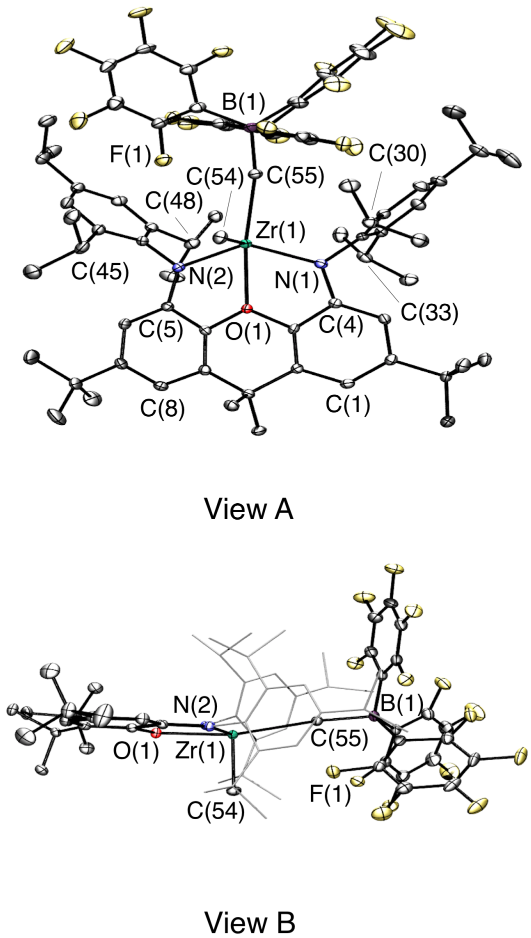

Figure 5.11: Two views of the X-ray crystal structure for compound **18**·-Toluene. Ellipsoids are set to 50 %. Hydrogen atoms and lattice solvent are omitted. In view B the 2,4,6-triisopropylphenyl groups are depicted in wire-frame format for clarity. Selected bond lengths [Å] and angles [°]: Zr–N(1) 2.093(2), Zr–N(2) 2.093(2), Zr–C(54) 2.207(2), Zr–C(55) 2.560(2), B(1)–C(55) 1.691(3), Zr–O(1) 2.254(1), N(1)–Zr–N(2) 134.32(5), N(1)–Zr–C(54) 100.42(6), N(1)–Zr–C(55) 105.00(6), N(2)–Zr–C(54) 99.03(7), N(2)–Zr–C(55) 110.97(6), O(1)–Zr–C(54) 92.59(6), O(1)–Zr–C(55) 165.58(5), C(54)–Zr–C(55) 101.54(7), O(1)–Zr–N(1) 69.18(5), O(1)–Zr–N(2) 69.01(5).

due to increased steric hindrance in the XN_2 compound. However, the Zr–C(55) distance does fall around the middle of the range previously observed for contact ion pairs involving a methyl zirconium cation and a $MeB(C_6F_5)_3^-$ anion (*vide supra*). The B–C(55) distance of 1.691(3) Å is equal within error to that in $[(^{tBu}NON)ZrMe][MeB(C_6F_5)_3]$ (1.69(2) Å).[14,27,29]

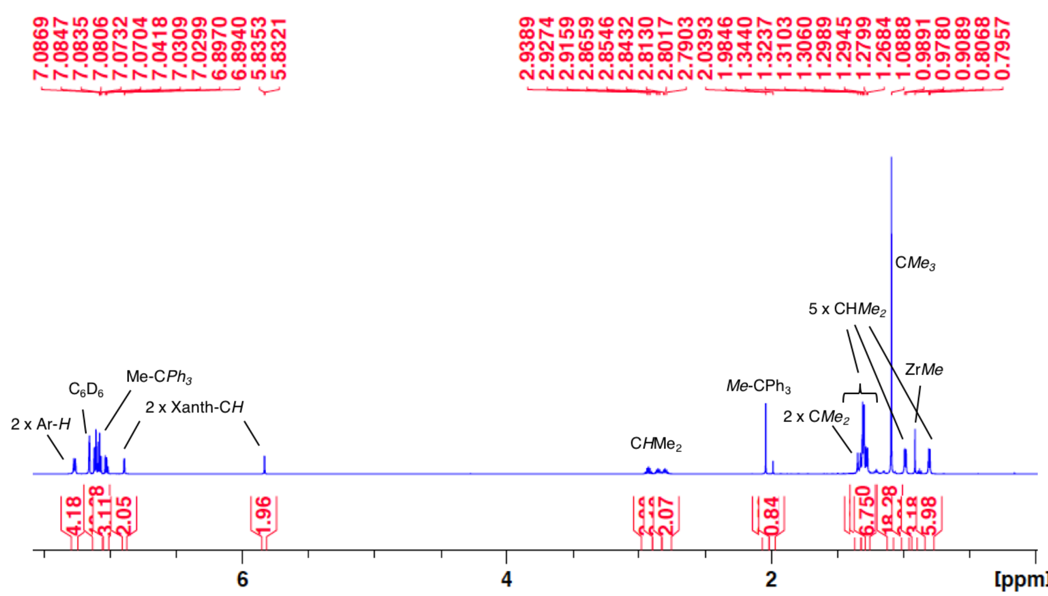

Figure 5.12: The *In Situ* ^{1}H NMR Spectrum of the Reaction Between Complex **16** and $[CPh_3][B(C_6F_5)_4]$ to Form Complex **19a** (600 MHz, C_6D_6).

Neutral $[(XN_2)ZrMe_2]$ (**16**) was also treated with one equivalent of $[CPh_3][B(C_6F_5)_4]$ in C_6D_6 or d_8-toluene, resulting in complete conversion to $[(XN_2)ZrMe(arene)][B(C_6F_5)_4]$ (arene = η^6-benzene **19a** or η^6-toluene **19b**), accompanied by an immediate solution color change from pale yellow to bright red-amber (Scheme 5.4). The ^{1}H NMR spectra of $[(XN_2)ZrMe(\eta^6\text{-arene})]$-$[B(C_6F_5)_4]$ (arene = C_6D_6 **19a**; Figure 5.12, and arene = d_8-toluene **19b**) contains two different Ar-*H*, ortho-C*H*Me$_2$ and C*Me$_2$* signals and four ortho-CH*Me$_2$* environments, indicative of C_s symmetry, and cation formation is supported by a shift of the Zr–*Me* ^{1}H NMR resonance to higher frequency: from 0.78 ppm in neutral **16** in C_6D_6 to 0.91 ppm in **19a**.

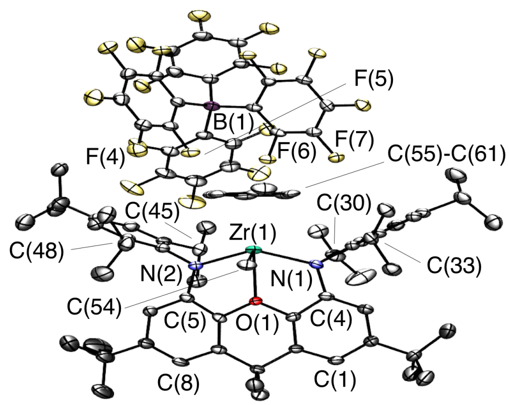

View A

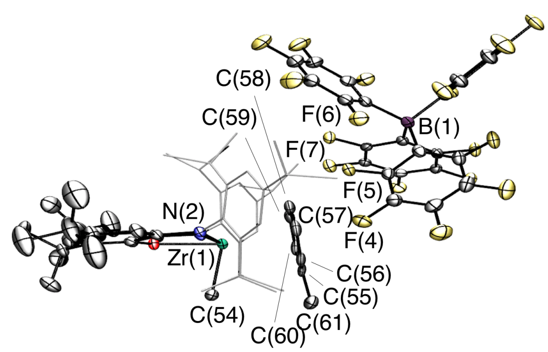

View B

Figure 5.13: Two views of the X-ray crystal structure for compound **19b**·(Toluene)$_{0.62}$·(Pentane)$_{1.38}$. Ellipsoids are set to 50 %. Hydrogen atoms and lattice solvent are omitted. In view B the 2,4,6-triisopropylphenyl groups are depicted in wire-frame format for clarity. Selected bond lengths [Å] and angles [°]: Zr–N(1) 2.142(4), Zr–N(2) 2.138(4), Zr–C(54) 2.239(5), Zr–C(55,Tol) 2.841(5), Zr–C(56,Tol) 2.789(5), Zr–C(57,Tol) 2.766(5), Zr–C(58,Tol) 2.706(5), Zr–C(59,Tol) 2.696(5), Zr–C(60,Tol) 2.746(5), Zr–O(1) 2.220(3), N(1)–Zr–N(2) 132.28(15), N(1)–Zr–C(54) 99.47(18), N(2)–Zr–C(54) 99.34(17), O(1)–Zr–C(54) 81.01(15), O(1)–Zr–N(1) 70.07(12), O(1)–Zr–N(2) 70.18(13).

Crystals of **19b**·(Toluene)$_{0.62}$·(Pentane)$_{1.38}$ were isolated from a concentrated solution of toluene layered with pentane and cooled to –30 °C (Figure 5.13, Table 5.1). Compound **19b** is an arene-solvent-separated ion pair with a toluene molecule π-coordinated to zirconium. The $B(C_6F_5)_4^-$ anion is also located in fairly close proximity to the toluene ligand, with relatively short distances between two fluorine atoms of each of two C_6F_5 rings and the *meta* and *para* carbon atoms of toluene (C(57)–F(4) = 3.114 Å, C(57)–F(5) 3.103 Å, C(58)–F(5) 3.052 Å, C(58)–F(6) 3.358 Å, C(59)–F(7) 3.131 Å).

The three anionic donors, O(1), and the centroid of aromatic ring of toluene can be considered to form either a distorted square pyramid with C(54) in the apical site, or an edge-capped tetrahedron with O(1) capping the N(1)–N(2) edge. The N–Zr–C(54) angles are 99.3(2)° and 99.5(2)°, the N(1)–Zr–N(2) angle of 132.3(2)°, and the E–Zr–Cent (E = N(1), N(2) or C(54); Cent = the C_6H_5Me ring centroid) angles are between 105° and 109°. Additionally, the N–Zr–O angles are 70.1(1)° and 70.2(1)°; the C(54)–Zr–O(1) angle is 81.0(2)°, and the O–Zr–Cent angle is 174°. The XN_2 ligand backbone is slightly bent with a 19° angle between the xanthene aryl rings.

Zirconium lies 0.52 Å out of the N(1)/C(4)/C(5)/N(2) plane, leading to a 37° angle between the N(1)/C(4)/C(5)/N(2) plane and the N(1)/Zr/N(2) plane. This distance and angle are significantly larger than those in **18** (0.32 Å and 22°), indicative of increased steric hindrance in **19b** compared to **18** as a result of toluene rather methylborate coordination. The difference in the distances between the isopropyl *C*HMe$_2$ carbon atoms on either side of the plane of the xanthene backbone is also larger in **19b** than in **18**; 7.61 Å and

4.82 Å (in **19b**, C(33)···C(48) = 7.79 Å and C(30)···C(45) = 4.54 Å). However, the neutral oxygen donor of the XN_2 ligand is situated 0.36 Å out of the N(1)/C(4)/C(5)/N(2) plane in both **18** and **19b**.

Structure	**15**	**16**	**18**·Toluene	**19b**·(Toluene)$_{0.62}$·(Pentane)$_{1.38}$
Formula	$C_{57}H_{86}N_4O_1Zr_1$	$C_{55}H_{80}N_2O_1Zr_1$	$C_{80}H_{88}B_1F_{15}N_2O_1Zr_1$	$C_{96.24}H_{106.54}B_1F_{20}N_2O_1Zr_1$
Formula wt	934.51	876.43	1480.55	1789.21
T (K)	100(2)	100(2)	100(2)	100(2)
Cryst. Syst.	Monoclinic	Tetragonal	Triclinic	Triclinic
Space Group	P 21/n	P –4 21 c	P–1	P–1
a (Å)	18.071(3)	13.5266(7)	14.4159(4)	13.4504(19)
b (Å)	10.5237(16)	13.5266(7)	16.4758(4)	18.762(3)
c (Å)	28.755(4)	27.6280(14)	17.9749(5)	19.166(3)
α [°]	90	90	96.3120(10)	103.688(2)
β [°]	97.660(3)	90	112.4310(10)	98.459(2)
γ [°]	90	90	107.6460(10)	99.073(2)
Volume [Å^3]	5419.6(14)	5055.1(6)	3635.14(17)	4554.0(11)
Z	4	4	2	2
Density (calcd; Mg/m^3)	1.145	1.152	1.353	1.305
μ (mm^{-1})	0.243	0.255	0.236	0.209
F(000)	2016	1888	1540	1862
Crystal Size (mm^3)	0.418×0.237×0.04	0.43×0.4×0.35	0.36×0.24×0.12	0.5×0.15×0.05
θ Range for Collection [°]	1.260–26.506	1.474–33.208	2.255–30.445	2.654–25.423
No. of Refns. Collected	85443	180242	143719	79852
No. of Indep. Refns.	11155	9700	21954	16724
Completeness to θ Max (%)	99.9	99.9	99.9	99.4
Absorption Correction	Analytical	Multi-Scan	Multi-Scan	Multi-Scan
Max and Min Transmission	1.0000,0.7487	0.7465,0.7046	0.7461,0.7075	0.7452,0.5906
GOF on F^2	1.259	1.052	1.025	1.000
Final R_1 [$I > 2\sigma(I)$]	R1 = 0.0964 wR2 = 0.1979	R1 = 0.0316 wR2 = 0.0736	R1 = 0.0456 wR2 = 0.0937	R1 = 0.0775 wR2 = 0.1734
R indices (all data)	R1 = 0.1161 wR2 = 0.2058	R1 = 0.0410 wR2 = 0.0774	R1 = 0.0782 wR2 = 0.1060	R1 = 0.1397 wR2 = 0.1998

Table 5.1: Crystallographic Data Collection and Refinement Parameters for Complexes **15**, **16**, **18** and **19**.

The Zr–C(54) (2.239(5) Å) and Zr–N (2.142(4) Å and 2.138(4) Å) distances in **19b** are slightly longer than those in cationic **18** (Zr–C(54): 2.207(2) Å, Zr–N: 2.093(2) Å and 2.093(2) Å) and neutral **16** (Zr–C(54): 2.226(2) Å, Zr–N: 2.135(1) Å and 2.135(1) Å), perhaps as a consequence of increased steric hindrance. However, the Zr–O distance in cation **19b** is marginally shorter than that in **18** (2.220(3) vs 2.254(1) Å), and the Zr–C_{alkyl}, Zr–N and Zr–O distances in **19b** are otherwise unremarkable. The Zr–C_{arene} distances range from 2.706(5) Å (*para* position) to 2.696(5)–2.789(5) Å (*ortho* and *meta*) and 2.841(5) Å (*ipso*), all of which are well within the sum of the van der Waals radii (3.9–4.3 Å),[256–259] consistent with approximate η^6-coordination (Zr–C_{arene} (ave.) = 2.76 Å).

Compound **19b** is the first crystallographically-characterized example of an arene-solvent-coordinated zirconium alkyl cation. The M–C_{arene} distances in **19b** are longer, on average, than those in [(C_5R_5)HfMe_2(η^6-toluene)] (C_5-R_5 = $C_5H_3(SiMe_3)_2$-1,3 and C_5Me_5; Figure 5.1) which range from 2.62 to 2.81 Å (Zr–C_{arene} (ave.) = 2.69 Å). The structure of **19b** is also similar to that of [(XA_2)Th(CH_2SiMe_3)(η^6-C_6H_6)] (Figure 5.1), although the M–C_{arene} distances in the thorium complex range from 3.21 to 3.31 Å,[21] indicative of a significantly weaker metal-arene interaction, given that the difference in the ionic radii of thorium(IV) and zirconium(IV) is 0.22 Å.[6]

After removal of supernatant from crystals of **19b**, the solid is stable for very short periods of time under argon. However, after 10 minutes under argon in the glovebox or after exposure to vacuum, ^{1}H NMR spectroscopy showed extensive decomposition to unidentified products. Presumably, coordinated toluene in **19b** readily dissociates, and in the absence of other stabilizing donor ligands, decomposition ensues. By contrast, in solution in d_8-toluene, complex **19b** is thermally stable at 24 °C, and minimal decomposition was observed after 18 h at 60 °C. However, 50 % decomposition was evident after 18 h at 80 °C, and decomposition was complete after 48 h at this temperature

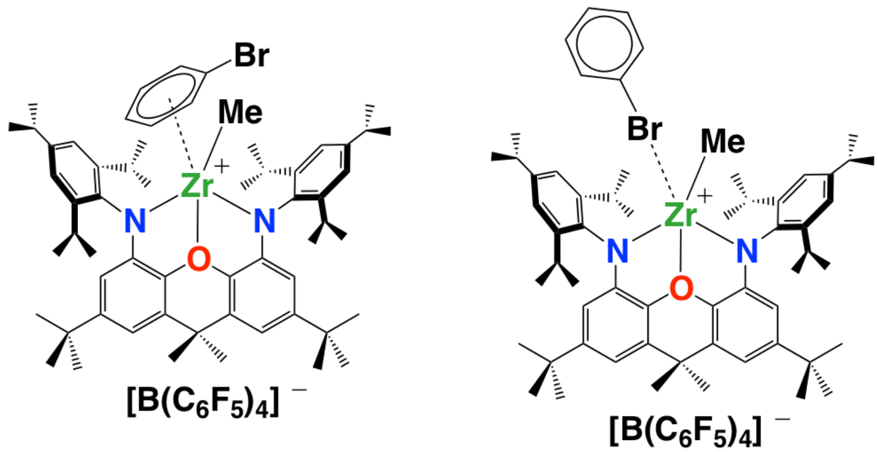

Figure 5.14: Plausible Structures for Isomers A and B of $[(XN_2)ZrMe(bromobenzene)][B(C_6F_5)_4]$ (**19c**).

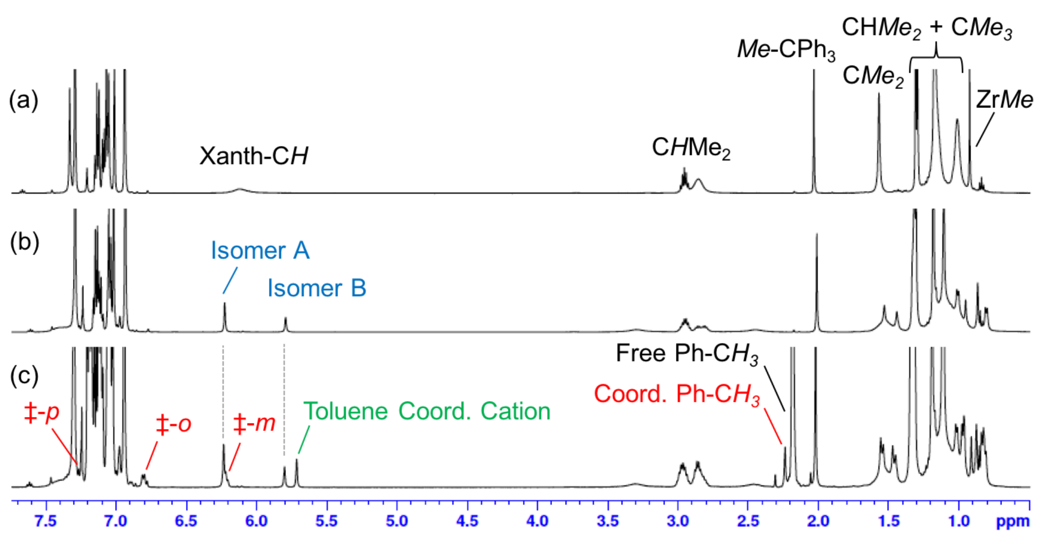

Figure 5.15: ^{1}H NMR spectra of $[(XN_2)ZrMe(arene)][B(C_6F_5)_4]$ (**19**; arene = C_6D_5Br or η^6-C_6H_5Me) generated *in situ* via the reaction of $[(XN_2)ZrMe_2]$ (**16**) with one equivalent of $[CPh_3][B(C_6F_5)_4]$ in d_5-bromobenzene, (a) at 25 °C, (b) at –25 °C, and (c) at –25 °C after addition of 10 equivalents of toluene. ‡ = C_6H_5Me peaks of coordinated toluene. Isomers A and B are isomers of $[(XN_2)ZrMe(C_6D_5Br)][B(C_6F_5)_4]$.

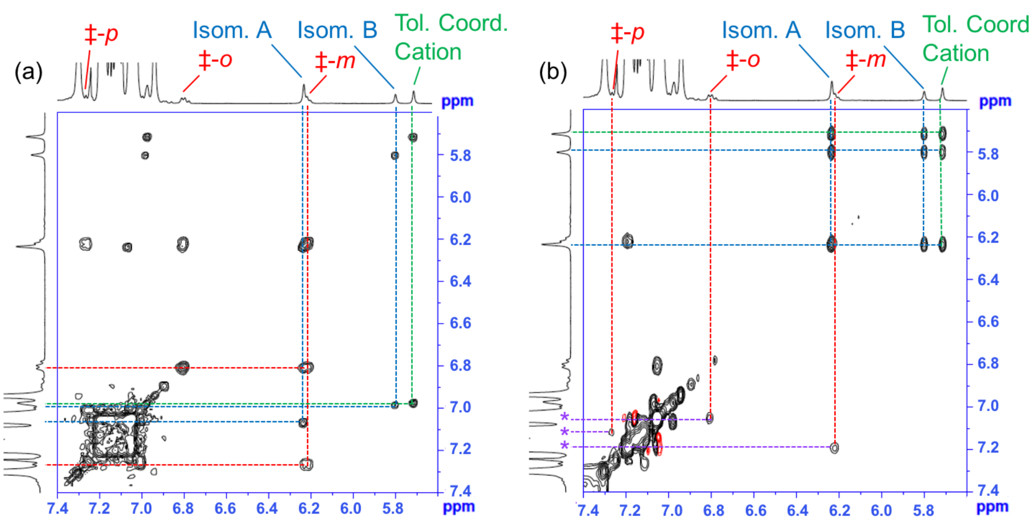

Figure 5.16: Selected regions of the –25 °C 2D-COSY (a) and 2D-EXSY (b) NMR spectra of $[(XN_2)ZrMe(arene)][B(C_6F_5)_4]$ (**19**; arene = C_6D_5Br and η^6--C_6H_5Me) generated *in situ* in d_5-bromobenzene, followed by addition of 10 equivalents of toluene. * = C_6H_5Me peaks of free toluene. ‡ = C_6H_5Me peaks of coordinated toluene. Isomers A and B are isomers of $[(XN_2)ZrMe(C_6D_5$-$Br)][B(C_6F_5)_4]$.

(resulting in a mixture of unidentified products). The solution stability of **19b** contrasts that of **18**, which was fully decomposed after 18 h at 60 °C (*vide supra*), suggesting that toluene coordination in **19b** contributes significantly to the stability of the complex.

The bromobenzene-coordinated cation, $[(XN_2)ZrMe(arene)][B(C_6F_5)_4]$ (**19-c**; arene = C_6D_5Br) was also generated via the 1:1 reaction of **16** with $[CPh_3]$-$[B(C_6F_5)_4]$ in C_6D_5Br, and the resulting cation, $[(XN_2)ZrMe(C_6D_5Br)][B$-$(C_6F_5)_4]$ (**19c**) exists as a 1:0.53 mixture of isomers in solution. These isomers do not appear to involve $B(C_6F_5)_4$ anion coordination, since addition of 2 equivalents of $[NBu_4][B(C_6F_5)_4]$ did not change the ratio of the two isomers, nor did it give rise to a new set of ^{19}F NMR signals or significantly alter the

^{19}F NMR chemical shifts for the $B(C_6F_5)_4$ anion. Therefore, the two isomers of **19c** are likely a $\kappa^1 Br$-coordinated and a π-coordinated isomer (isomers A and B; Figure 5.14).[260–264]

At room temperature, the two isomers are in rapid exchange, but at –25°C, a distinct set of xanthene-C*H* peaks is observed for each isomer ((a) and (b) in Figure 5.15). Addition of 6 equivalents of toluene to a solution of **19c** in C_6-D_5Br afforded a ^{1}H NMR spectrum (–25°C) with a new set of signals for toluene-coordinated **19b** in addition those for **19c** (both isomers) in a 0.26:1 ratio, which increased to 0.44:1 upon introduction of 4 further equivalents of toluene ((c) in Figure 5.15). A 2D-EXSY NMR spectrum ((b) in Figure 5.16) at –25°C showed that **19b** and both isomers of **19c** are in equilibrium. Furthermore, signals for coordinated toluene are observed at 7.26, 6.80, 6.21 and 2.23 ppm (C*H*-*p*, C*H*-*o*, C*H*-*m* and CH_3, respectively), with COSY peaks between the *meta* resonance and the *ortho* and *para* resonances, and EXSY correlations between all four coordinated toluene signals and free toluene ((a) and (b) in Figure 5.16).

The behavior of **19b** in C_6D_5Br contrasts that of the thorium analogue, $[(XA_2)Th(CH_2SiMe_3)(\eta^6\text{-toluene})]$, which exhibits sharp peaks due to free (6 equivalents) and coordinated toluene (6.92, 6.67, 5.91, 2.02 ppm for the C*H*-*p*, C*H*-*o*, C*H*-*m* and CH_3 signals, respectively) in the room temperature ^{1}H NMR spectrum, and is not in equilibrium with a noticeable amount of a bromobenzene-coordinated cation.[21] The greater lability of toluene in **19b** is surprising given that the average M–C_{arene} distances in the solid state structure of **19b** are significantly shorter than those in the thorium cation, even after taking into account differences in metal ionic radii.

5.3 Hydroamination and Ethylene Polymerization Catalysis Using $[(XN_2)ZrMe(arene)][B(C_6F_5)_4]$ and $[(XN_2)ZrMe][MeB(C_6F_5)_3]$

Cations $[(XN_2)ZrMe(\eta^6\text{-}C_6D_6)][B(C_6F_5)_4]$ (**19a**) and $[(XN_2)ZrMe][MeB(C_6F_5)_3]$ (**18**) (generated *in situ*) were tested as catalysts for intramolecular hydroamination utilizing 1-amino-2,2-diphenyl-4-pentene with 10 mol % catalyst loading at 24 °C in C_6D_6 and resulted in very slow conversion to the product (55 % and 95 % complete for **18** and **19a** respectively after 17 days). Due to the low activity of **18** and **19a** for cyclization of 1-amino-2,2-diphenyl-4-pentene, which is considered to be one of the most readily cyclized substrates for intramolecular hydroamination, further testing was not pursued. Neutral **16** was also tested as a catalyst for intramolecular hydroamination utilizing 1-amino-2,2-diphenyl-4-pentene under the same conditions (10 mol %, 24 °C in C_6D_6) and resulted in negligible conversion after 2 weeks. However, heating **16** in combination with 1-amino-2,2-diphenyl-4-pentene (10 mol %, 110 °C in d_8-toluene) resulted in 10 % conversion after 24 h, and >99 % after 7 days.

Both $[(XN_2)ZrMe][MeB(C_6F_5)_3]$ (**18**) and $[(XN_2)ZrMe(\eta^6\text{-toluene})][B(C_6F_5)_4]$ (**19b**) are active for ethylene polymerization catalysis at 24 °C and 80 °C (approximately 1.2 mM in toluene, 1 atm ethylene), and catalytic results are summarized in Table 5.2. Compound **18** showed a moderate activity of 23.5 kg/(mol·atm·h) after 30 min at 24 °C, while **19b** achieved high activities of 273 kg/(mol·atm·h) after 30 min and 883 kg/(mol·atm·h) after 5 min at 24 °C. At 80 °C (after 30 min), the activity of $[(XN_2)ZrMe][MeB(C_6F_5)_3]$ (**18**) increased to 118 kg/(mol·atm·h) whereas that of $[(XN_2)ZrMe(\eta^6\text{-toluene})][B(C_6F_5)_4]$ (**19b**) decreased to 113 kg/(mol·atm·h), despite the fact that **19** was found to be more thermally stable than **18** (*vide supra*).

The decreased activity of **19b** after 30 min compared to 5 min at 24 °C is likely due to ensnarement of the catalyst in precipitated polyethylene, given that the catalyst maintains some activity at 80 °C. Nevertheless, the decreased activity of **19b** at 80 °C compared to 24 °C is presumably an indication of significant catalyst decomposition at 80 °C, highlighting the important role of the anion in stabilizing the cationic species involved in catalysis. The apparent discrepancy in the relative thermal stabilities of **18** and **19b** alone, versus in the presence of ethylene at 80 °C can be attributed to differences in the solution species present under these conditions, including ethylene-coordinated and β--hydrogen-containing alkyl cations under polymerization conditions.

Polyethylene samples generated by **18** or **19b** in toluene have fairly high polystyrene equivalent weight-average molecular weights (M_w = 70,800–88,100 g/mol) with a relatively high polydispersity (M_w/M_n) of 3.94 for cation **18** (80 °C) and 4.65–4.67 for cation **19b** (24 °C and 80 °C). By contrast, cation **19c** generated in bromobenzene (24 °C, 2 min) yielded a lower molecular weight polymer (52,200 g/mol) with a somewhat narrower polydispersity (3.30), compared to the closely analogous reaction in toluene (Table 5.2). Polyethylene generated by **18** at 24 °C had the highest DSC peak melting temperature (T_m = 125.8 °C vs 121.0-124.6 °C for all other samples), and was insufficiently

Entry	Activator	Temp. (°C)	Time (min)	Yield (g)	Activity (kg/(mol·atm·h))	M_w (g/mol)[a]	M_w/M_n[a]	T_m (°C)[b]
1	$B(C_6F_5)_3$	24	30	0.067	23.5	–[d]	–[d]	125.8
2	$B(C_6F_5)_3$	80	30	0.338	118	70 800	3.94	121.0
3	$[CPh_3]^+[B(C_6F_5)_4]^-$	24	30	0.778	273	78 300	4.66	124.6
4	$[CPh_3]^+[B(C_6F_5)_4]^-$	24	5	0.418	883	88 100	4.65	123.0
5	$[CPh_3]^+[B(C_6F_5)_4]^-$	80	30	0.332	113	81 900	4.67	123.2
6[c]	$[CPh_3]^+[B(C_6F_5)_4]^-$	24	2	0.057	300	52 200	3.30	124.4

Table 5.2: Ethylene Polymerization of **18** and **19**. The catalyst is generated *in situ* (1.2 mM in toluene, 1 atm ethylene) [a] GPC is relative to polystyrene standards, and M_w and M_w/M_n values are averages from two duplicate GPC runs, [b] Peak melting temperature, T_m determined by DSC analysis (2nd heating run), [c] *in situ* catalyst generation and polymerization was carried out in bromobenzene, [d] The sample was insoluble in 1,2,4-trichlorobenzene at 140 °C and therefore was not amenable to analysis by GPC.

soluble in 1,2,4-trichlorobenzene at 140 °C for GPC, suggestive of a higher molecular weight polymer. However, all of the observed T_m values are lower than those typically observed for polyethylene with similar M_w values, perhaps indicative of appreciable chain branching.

The ethylene polymerization activity of **19b** and **19c** compares well with that of other non-cyclopentadienyl zirconium catalysts. For example, (a) [-(κ^3-^{tBu}NON)ZrMe][MeB(C_6F_5)$_3$] afforded an activity of ~100 kg/(mol·atm·h) under 1-2 atm ethylene (22 °C, 2 min),[29] (b) [(κ^2-NN′)ZrMe$_2$] (NN′ = CH$_2$(C-H$_2$NSi^{i}Pr$_3$)$_2$) achieved an activity of 1.5 kg/(mol·atm·h) after activation with B(C_6F_5)$_3$ and 317 kg/(mol·atm·h) after activation with [CPh$_3$][B(C_6F_5)$_4$] at 24 °C (1 atm of ethylene, 1 h),[116] and (c) [(κ^3-NN″)ZrMe$_2$]/ B(C_6F_5)$_3$ (NN″ =

$(CH_2(o\text{-}C_6H_4)NSi^iPr_3)_2$) yielded an activity of 178 kg/(mol·atm·h) after 5 min at 0 °C under 1 atm of ethylene, affording a M_w value of 165 kg/mol and a PDi (M_w/M_n) of 1.96.[117] By contrast, $[(\kappa^3\text{-NNN}')ZrMe_2]$ (NNN′ = $NC_5H_3(o\text{-CH-ArNAr}')(o\text{-X})$; X = 2-pyrrolyl or 2-indolyl; Ar = $C_6H_4{}^iPr\text{-}2$; Ar′ = $C_6H_3{}^iPr_2\text{-}2,6$) achieved no more than trace activity under 1 atm of ethylene at 25 °C after activation with $B(C_6F_5)_3$ or $[CPh_3][B(C_6F_5)_4]$.[16] Nonetheless, substantially higher activities have been reported for some homogeneous zirconium catalyst systems, such as $[(\kappa^3\text{-Tp}^{Ms*})ZrCl_3]$/MAO ($Tp^{Ms*}$ = HB(3-mesitylpyrazolyl)-$_2$(5-mesitylpyrazolyl))[265] and $[(\kappa^2\text{-L})_2ZrCl_2]$/MAO (L = salicylaldiminate = OC_6H_2(2-CH=NCy)(4-Me)(6-CMe_2Ph)).[220]

5.4 Summary

Attempts to coordinate the XN_2 ligand to zirconium via salt metathesis or alkane elimination were unsuccessful. However, coordination of the XN_2 ligand to zirconium was achieved through the reaction of H_2XN_2 with $[Zr(NMe_2)_4]$ to form $[(XN_2)Zr(NMe_2)_2]\cdot(O(SiMe_3)_2)_{0.5}$ (**15**$\cdot(O(SiMe_3)_2)_{0.5}$). This complex facilitated the synthesis of $[(XN_2)ZrCl_2]$ (**17**), $[(XN_2)ZrMe_2]$ (**16**), $[(XN_2)ZrMe][MeB(C_6F_5)_3]$ (**18**), and $[(XN_2)ZrMe(arene)][B(C_6F_5)_4]$ (arene = η^6-benzene (**19a**), η^6-toluene (**19b**), and bromobenzene (**19c**)). Compound **18** is a contact ion pair whereas **19b** is a rare example of an arene-solvent--separated ion pair, and both highlight the ability of rigid 4,5-bis(anilido)xanthene ligands such as XN_2 to stabilize highly-reactive organometallic species. Cationic **18** and **19a** are only mildly active for intramolecular hydroamination. By contrast, **18** and **19b** are moderately to highly active for ethylene polymerization at 24 °C or 80 °C under 1 atm, yielding polymers with weight-average molecular weights of 52,200–88,100 g/mol with polydispersities of 3.30–4.67 across all samples. The highest observed activity was for **19b** with an activity of 883 kg/(mol·atm·h) after 5 min under 1 atm of ethylene at 24 °C.

Future work in this area could continue through the investigation of the XN_2 ligand with titanium and hafnium, and comparison of the physical and catalytic properties with the zirconium counterparts. $[(XN_2)Hf(NMe_2)_2]\cdot(O(SiMe_3)_2)_{0.5}$ (**20**$\cdot(O(SiMe_3)_2)_{0.5}$) has been successfully synthesized in 40 % yield through the reaction of H_2XN_2 and $[Hf(NMe_2)_4]$ (*vide infra*, Section 6.1). Future research can involve subsequent reactions to form a dialkyl complex, followed by reactions with $B(C_6F_5)_3$ and $[CPh_3][B(C_6F_5)_4]$ to form cationic complexes, and testing of their catalytic activity for ethylene polymerization and alkene/alkyne hydroamination.

Chapter 6

Future Directions and Conclusions

6.1 Future Directions of the XN_2 Ligand and Group 4 Transition Metals

The work described in this thesis highlights the ability and versatility of the XN_2 ligand to coordinate a range of elements, including rare earth metals and zirconium. Future work with the XN_2 ligand can continue to focus on the group 4 transition metals through investigations with titanium and hafnium, and comparing the physical and catalytic properties with the zirconium counterparts from Chapter 5. This section includes the results obtained thus far directed towards that goal.

6.1.1 Zirconium

In an effort to continue investigations with the XN_2 ligand and zirconium, preliminary reactions to form another zirconium dialkyl complex, a bis(trimethylsilylmethyl) complex, were performed with the goal of comparing the physical and catalytic properties of this pre-catalyst to those of the dimethyl analogue. This is of interest since altering the alkyl groups can have a profound effect on the thermal stability of the resulting complex. This is demonstrated by the comparison of three thorium dialkyl complexes previously reported by the Emslie group. The dianionic BDPP ligand (BDPP = 2,6-bis(2,6-diisopropylanilidomethyl)pyridine) was utilized for the synthesis of a thorium bis-*n*-butyl complex ([(BDPP)Th(^{n}Bu)$_2$]),[22] a thorium dimethyl complex (-[(BDPP)ThMe$_2$]),[22] and a thorium bis-trimethylsilylmethyl complex ([(BDPP)Th(CH$_2$SiMe$_3$)$_2$]),[19] which displayed vastly different thermal stabilities. The [(BDPP)Th(^{n}Bu)$_2$] and [(BDPP)Th(CH$_2$SiMe$_3$)$_2$] complexes showed high thermal stability, with no decomposition observed after several days at 60 °C and 90 °C respectively, while [(BDPP)ThMe$_2$] was fully decomposed within two hours at room temperature.[19,22]

[(XN$_2$)ZrCl$_2$] (**17**) was reacted with two equivalents of trimethylsilylmethyl lithium in benzene at 24 °C, and after removal of the salts by centrifugation in toluene, and recrystallization from pentane at –30 °C, [(XN$_2$)Zr(CH$_2$SiMe$_3$)$_2$] was isolated as a pale yellow solid. However, even after multiple attempts a pure sample could not be isolated. The ^{1}H NMR spectrum indicates that [(XN$_2$)Zr(CH$_2$SiMe$_3$)$_2$] has C_s symmetry in solution at 24 °C, with two Ar-*H*, ortho-C*H*Me$_2$, ZrC*H*$_2$SiMe$_3$ and ZrCH$_2$Si*Me*$_3$ peaks. However, upon heating coalescence was observed (Figure 6.1). Crystals suitable for X-ray crystallography were not obtained.

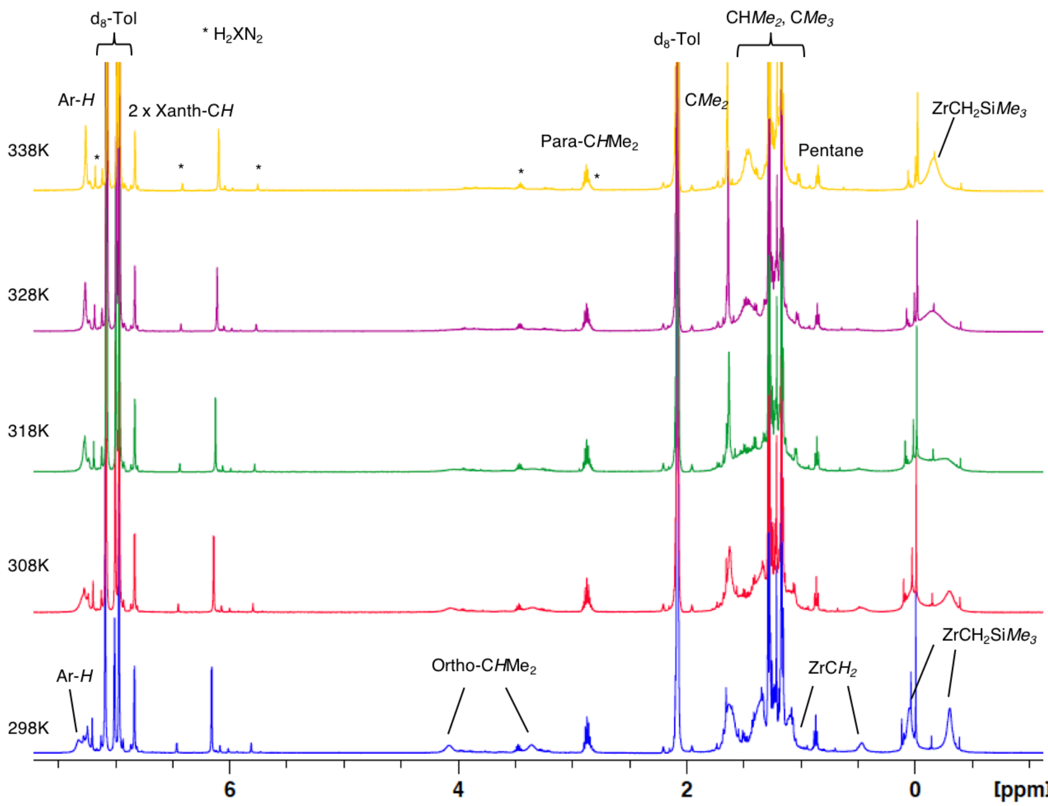

Figure 6.1: Variable Temperature ^{1}H NMR Spectra of [$(XN_2)Zr(CH_2SiMe_3)$-$_2$] (500 MHz, d_8-Tol).

6.1.2 Hafnium and Titanium

As discussed previously, further investigations of the XN_2 ligand with titanium and hafnium would be of interest, particularly to investigate the effect of different group 4 transition metals on the activity of α-olefin and ethylene polymerization catalysis. It has been reported that analogous complexes can have substantially different polymerization activities when the transition metal is altered. For example, [$(Cp)TiCl_2(NPR_3)$] and [$(Cp)TiMe_2(NPR_3)$-] type complexes have been reported to be active for ethylene polymerization (1 atm ethylene, 24 °C) with activities ranging from 16–881 kg/(mol·atm·h) and 225–1807 kg/(mol·atm·h) after activation by MAO and $[CPh_3][B(C_6F_5)_4]$, respectively.[266] By contrast, the analogous zirconium complexes were reported to polymerize ethylene (1 atm ethylene, 24 °C) with activities ranging from near-zero to 43 kg/(mol·atm·h).[267] The reverse is true for zirconium and titanium dichloride complexes based on various salicylbenzoxazole ligands, which were tested for ethylene polymerization catalysis (1 atm ethylene, 30 °C) after activation with MAO. It was found that the titanium complexes yielded only trace amounts of polyethylene, while the zirconium analogues yielded activities of up to 1000 kg/(mol·atm·h).[268]

To begin this work the $[(XN_2)Hf(NMe_2)_2]\cdot(O(SiMe_3)_2)_{0.5}$ (**20**$\cdot(O(SiMe_3)_2)_{0.5}$) complex has been successfully synthesized in 40 % yield, through the reaction of H_2XN_2 and $[Hf(NMe_2)_4]$ (Scheme 6.1). The ^1H and ^{13}C NMR spectra are largely analogous to those of $[(XN_2)Zr(NMe_2)_2]\cdot(O(SiMe_3)_2)_{0.5}$ (**15**$\cdot(O(SiMe_3)_2)_{0.5}$). The dimethylamido groups in the ^1H NMR spectrum of **20**$\cdot(O(SiMe_3)_2)_{0.5}$ are equivalent at 24 °C (2.69 ppm) however, upon cooling, de-coalescence was observed, resulting in two different Hf-N*Me₂*, Ar-*H*, ortho-C*H*Me₂ and C*Me₂* environments observed at –70 °C (Figure 6.2). The thermal stability is also comparable to **15**$\cdot(O(SiMe_3)_2)_{0.5}$, as a d_8-toluene solution of **20**$\cdot(O(SiMe_3)_2)_{0.5}$ was heated at 115 °C for 7 days and no decomposition was observed.

Crystals of **20** were grown from a concentrated $O(SiMe_3)_2$ solution cooled to –30 °C. Multiple crystals were submitted for X-ray crystallography analysis. However, each contained at least 10 % whole-molecule disorder, leading to a high R factor (10 %), preventing an accurate analysis of the structure apart

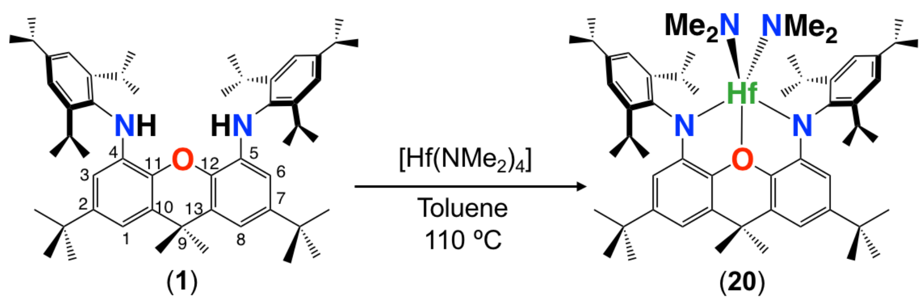

Scheme 6.1: The Synthesis of the Hafnium Complex **20**.

Structure **20**·$(O(SiMe_3)_2)$				
Formula	$C_{120}H_{190}Hf_2N_8O_3Si_2$		Density (calcd; Mg/m^3)	1.199
Formula wt	2205.95		μ (mm^{-1})	1.766
T (K)	296(2)		$F(000)$	2324
Cryst. Syst.	Triclinic		Crystal Size (mm^3)	0.3×0.22×0.06
Space Group	P–1		θ Range for Collection [°]	1.052–28.421
a (Å)	15.7970(8)		No. of Refns. Collected	208071
b (Å)	20.1072(10)		No. of Indep. Refns.	30336
c (Å)	21.2014(10)		Completeness to θ Max (%)	99.6
α [°]	68.448(2)		Absorption Correction	Multi-Scan
β [°]	77.491(2)		Max and Min Transmission	0.9394,0.6612
γ [°]	83.668(3)		GOF on F^2	1.261
Volume [Å^3]	6111.3(5)		Final R_1 $[I > 2\sigma(I)]$	R1 = 0.1032 wR2 = 0.2345
Z	2		R indices (all data)	R1 = 0.1126 wR2 = 0.2384

Table 6.1: Crystallographic Data Collection and Refinement Parameters for Complex **20**·$O(SiMe_3)_2$.

from establishing connectivity (Figure 6.3). In the solid state, **20** is described as a distorted square pyramid at hafnium with the XN_2 ligand donors and one dimethylamido group occupying the equatorial positions while the second dimethylamido group occupies the axial site. This geometry is mirrored in **15**.

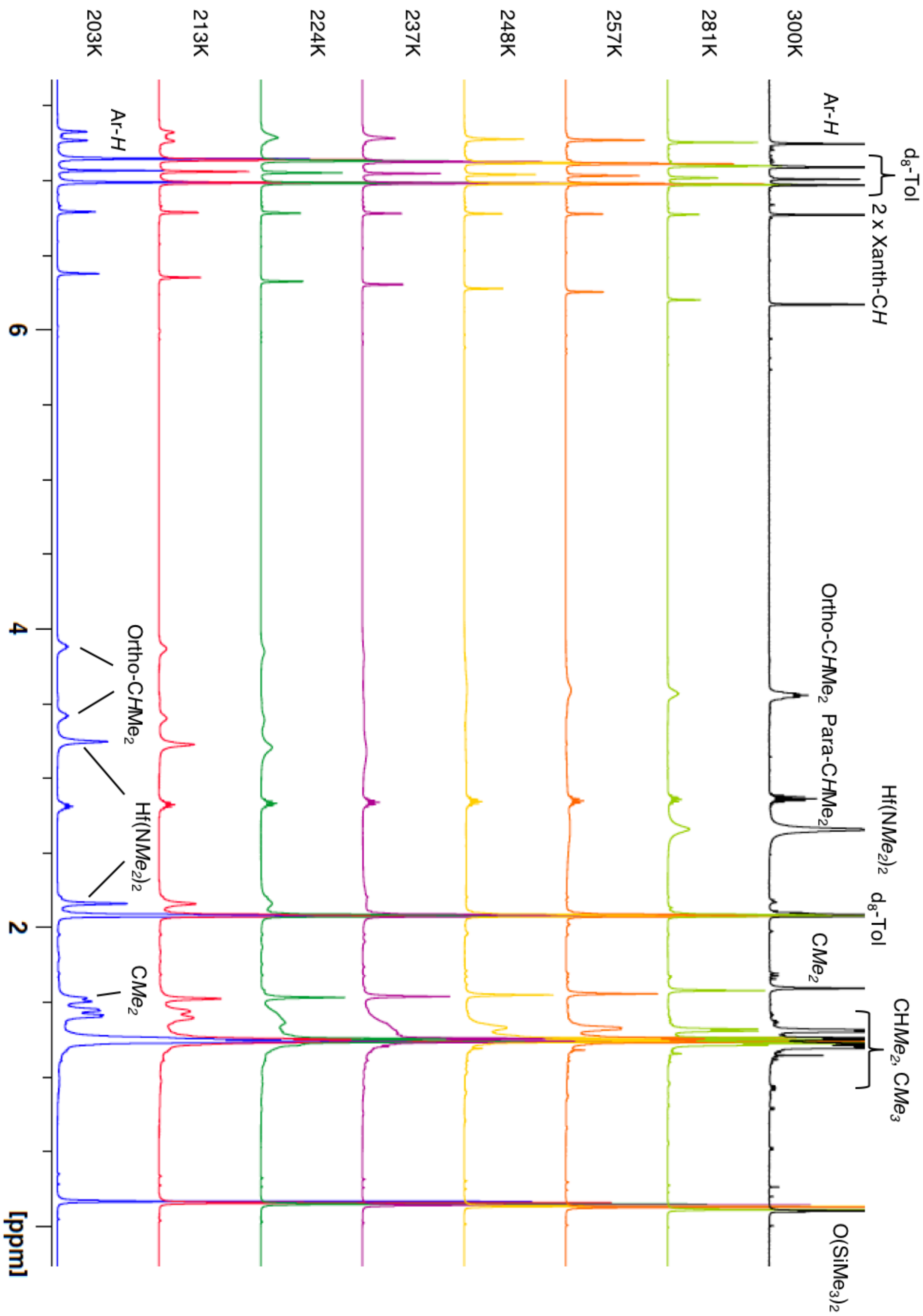

Figure 6.2: Variable Temperature [1]H NMR Spectra of **20** (500 MHz, d_8-Tol).

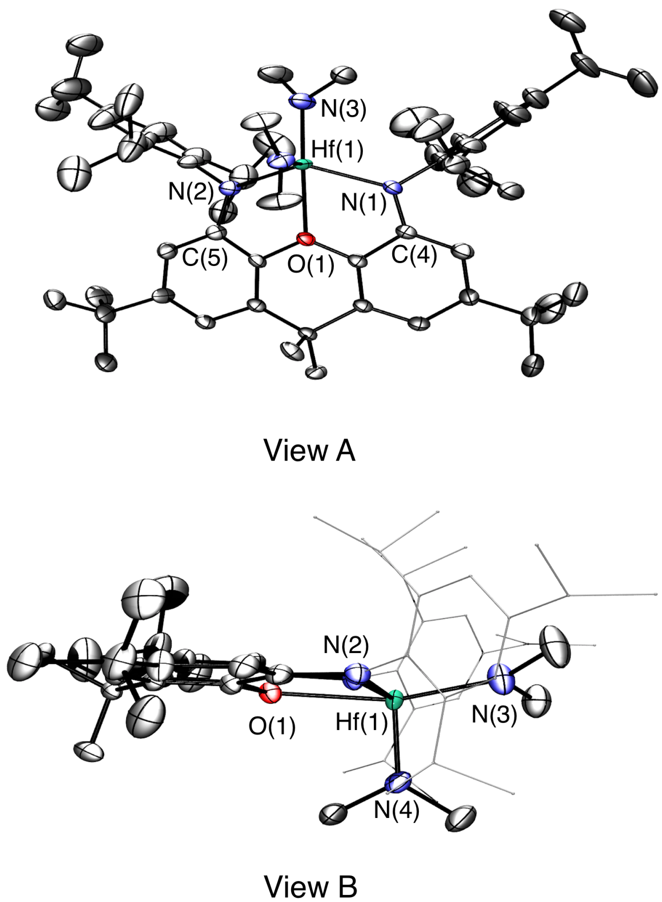

Figure 6.3: Two views of the X-ray crystal structure for compound **20**. Two molecules were found in the asymmetric unit and only one is shown for clarity. The whole molecule is disordered over two positions, and only the major position (89 %) is shown. Ellipsoids are set to 50 %. Hydrogen atoms and lattice solvent are omitted for clarity. In view B the 2,4,6-triisopropylphenyl groups are depicted in wire-frame format for clarity.

Through the successful isolation of $[(XN_2)Hf(NMe_2)_2]\cdot(O(SiMe_3)_2)_{0.5}$ (**20**$\cdot$-$(O(SiMe_3)_2)_{0.5}$), forthcoming research can be accessed by subsequent reactions to form an XN_2 hafnium dialkyl complex, followed by the synthesis of cationic complexes, and testing of catalytic activity in olefin and ethylene polymerization and hydroamination.

6.2 Summary and Conclusions

In conclusion, this thesis describes the synthesis of two rigid dianionic pincer-type ligands; the XN_2 ligand containing bisamido donors and the XP_2 ligand with bisphosphido donors. It also describes the preparation of rare earth and group 4 transition metal complexes including the exploration of catalytic activity for alkene/alkyne hydroamination and ethylene polymerization. Furthermore, the ability of XN_2 to accommodate aluminum, rare earth (Lu, Y and La) and group 4 (Zr, Hf) transition metals demonstrates the versatility of this ligand architecture for coordination to metal ions with very different ionic radii. Future work in this area could focus on expanding the utility of the XN_2 ligand with other metals, such as titanium and hafnium, as well as modification of the ligand backbone and flanking amido groups to maximize the thermal stability and polymerization activities of cationic group 4 alkyl species.

Chapter 7

Experimental Methods

7.1 General Details

7.1.1 Laboratory Equipment and Apparatus

An argon-filled MBraun UNIlab glove box equipped with a –30 °C freezer was employed for the manipulation and storage of all air-sensitive compounds, and reactions were performed on a double manifold high vacuum line using standard techniques.[269] Residual oxygen and moisture was removed from the argon stream by passage through an Oxisorb-W scrubber from Matheson Gas Products. A Fisher Scientific Ultrasonic FS-30 bath was used to sonicate reaction mixtures where indicated. A VWR Clinical 200 Large Capacity Centrifuge (with 28° fixed-angle rotors that hold 12 × 15 mL or 6 × 50 mL tubes) in combination with 15 mL Kimble Chase glass centrifuge tubes was used when required (inside the glovebox). Commonly utilized specialty glassware includes the swivel frit assembly, J-Young NMR tubes, and thick walled flasks equipped with Teflon stopcocks.

7.1.2 Solvents

Diethyl ether (Et_2O), tetrahydrofuran (THF), toluene, benzene and hexanes were initially dried and distilled at atmospheric pressure from Na/Ph_2CO. Hexamethyldisiloxane ($O(SiMe_3)_2$) was dried and distilled at atmospheric pressure from Na. Unless otherwise noted, all protio solvents were stored over an appropriate drying agent (pentane, hexanes, hexamethyldisiloxane ($O(TMS)_2$ / $O(SiMe_3)_2$) = Na/Ph_2CO/tetra-glyme; Et_2O, 1,2-dimethoxyethane (DME), THF, toluene, benzene = Na/Ph_2CO) and introduced to reactions via vacuum transfer with condensation at –78 °C. The deuterated solvents (ACP Chemicals) C_6D_6, THF-d_8 and toluene-d_8 were dried over Na/Ph_2CO.

7.1.3 Starting Materials

The 2,4,6-triisopropylaniline,[141–143] 4,5-dibromo-2,7-di-*tert*-butyl-9,9-dimethylxanthene,[144] $[Y(CH_2SiMe_3)_3(THF)_2]$,[18] $[Y(CH_2SiMe_2Ph)_3(THF)_2]$,[18,145] - $[Lu(CH_2SiMe_3)_3(THF)_2]$,[18] 2,4,6-triisopropylphenyldichlorophosphine,[180,181] $NaCH_2SiMe_3$[270] and the commercially unavailable intramolecular hydroamination reagents[271] were prepared according to literature procedures. 1-Amino--5-hexene was purchased from GFS Chemicals, dried over CaH_2 and distilled prior to use. 1,3,5-Triisopropylbenzene, xanthone, KH (30 wt % in mineral oil), $LiCH_2SiMe_3$ (1.0 M in pentane), MeLi (1.6 M in Et_2O), *n*BuLi (1.6 M in hexanes), Br_2, YI_3, NaH, NaO^tBu, $Pd(OAc)_2$, DPEPhos, [bis{2-(diphenylphosphino)phenyl}ether], diphenylacetylene, $LiAlH_4$, $MgSO_4$ and $(Me_3Si)Cl$ were purchased from Sigma-Aldrich. Solid $LiCH_2SiMe_3$ and MeLi were obtained by removal of solvent *in vacuo*, and solid KH was obtained by filtration and washing with hexanes. YCl_3, $LuCl_3$, $LaCl_3$, $[Zr(NMe_2)_4]$, $[Hf(NMe_2)_4]$, $AlMe_3$ and trityltetrakis(pentafluorophenyl)borate were purchased from Strem Chemicals. $[YCl_3(THF)_{3.5}]$, $[YI_3(THF)_{3.5}]$, $[LuCl_3(THF)_3]$ and $[LaCl_3(THF)_3]$ were obtained by refluxing the anhydrous metal trihalide in THF for 24 h followed by removal of the solvent *in vacuo*. $[Zr(NMe_2)_4]$ and $[Hf(NMe_2)_4]$ were sublimed prior to use. 4-*tert*-Butyl-aniline, 4-*tert*-butylbenzylamine, *n*-octylamine and 1-octene were purchased from Sigma-Aldrich, dried over molecular sieves and distilled prior to use. C_6F_5Br (used for the synthesis of $B(C_6F_5)_3$) was purchased from Oakwood Chemicals and distilled from molecular sieves prior to use. $B(C_6F_5)_3$ was prepared from C_6F_5MgBr and $BF_3{\cdot}Et_2O$ according to the literature procedure.[272] $[NBu_4][B(C_6F_5)_4]$ was prepared from $K[B(C_6F_5)_4]$ and $[NBu_4]Br$ according to the literature procedure.[23] Argon (99.999 % purity) and ethylene (99.999 % purity) were purchased from Praxair.

7.1.4 Instrumentation and Analysis

Combustion elemental analyses were performed on a Thermo EA1112 CHNS/O analyzer by Dr. Steve Kornic and Ms. Megan Fair at McMaster University and by Midwest Microlab, LLC, Indianapolis, IN, USA. NMR spectroscopy (^1H, $^{13}C\{^1H\}$, $^{31}P\{^1H\}$, ^{19}F, DEPT-Q, COSY, HSQC, HMBC) was performed on Bruker AV-200, DRX-500 and AV-600 spectrometers. All ^1H NMR and ^{13}C NMR spectra were referenced relative to $SiMe_4$ through a resonance of the employed deuterated solvent or protio impurity of the solvent; C_6D_6 (7.16 ppm), d_8-Tol (2.08, 6.97, 7.01, 7.09 ppm), d_8-THF (1.72, 3.58 ppm) for ^{1}H NMR; and C_6D_6 (128.0 ppm), d_8-Tol (20.43, 125.13, 127.96, 128.87, 137.48 ppm), d_8-THF (25.31, 67.21 ppm) for ^{13}C NMR. ^{31}P{^{1}H} NMR spectra were referenced using an external standard of 85 % H_3PO_4 in D_2O (0.0 ppm). ^{19}F NMR spectra were referenced using an external standard of $CFCl_3$ (0.0 ppm). In each case for ^{31}P and ^{19}F NMR, the NMR spectra of the test compound was obtained first, after which the reference standard was run unlocked at the same field. Herein, numbered proton and carbon atoms refer to the positions of the xanthene backbone, as shown in Scheme 2.2 for XN_2 and Scheme 3.2 for XP_2. Inequivalent ortho isopropyl protons are labeled A and B, while inequivalent aryl ring protons and inequivalent methyl protons are labeled $'$ and $''$, so that the corresponding carbon resonances can be identified.

X-ray crystallographic analyses were performed on suitable crystals coated in Paratone oil and mounted on a SMART APEX II diffractometer with a 3 kW sealed tube Mo generator in the McMaster Analytical X-Ray (MAX) Diffraction Facility by Dr. Hilary Jenkins and Dr. James Britten who were responsible for, crystal mounting, data acquisition, refinement and structure solution for all single crystal X-ray diffraction experiments.

GC-MS analyses were performed by Dr. Kirk Green and Dr. Fan Fei using an Agilent 6890N gas chromatograph (Santa Clara, CA, USA), equipped with a DB-17ht column (30 m $\times$ 0.25 mm i.d. $\times$ 0.15 μm film, J & W Scientific) and a retention gap (deactivated fused silica, 5 m $\times$ 0.53 mm i.d.), and coupled to an Agilent 5973 MSD single-quadrupole mass spectrometer. One microliter of sample was injected using Agilent 7683 autosampler in splitless mode. The injector temperature was 230 °C and carrier gas (helium) flow was 0.7 mL/min.

The transfer line was 280 °C and the MS source temperature was 230 °C. The column temperature started at 50 °C and was raised to 300 °C at 8 °C/min. It was then held at 300 °C for 15 min to give a total run time of 46.25 min. Full scan mass spectra between m/z 50 and 800 were acquired after five minute solvent delay.

All DSC data were recorded on a TA DSC Q20 instrument between 40 °C and 160-180 °C using a heating and cooling rate 10 °C per minute; peak melting temperatures were obtained from the second of two heating runs. All GPC data were recorded on an Agilent PL220 high temperature instrument equipped with differential refractive index (DRI) and viscometry (VS) detectors at the University of Warwick, Coventry, UK by Dr. D. W. Lester and Dr. I. Hancox. The system was equipped with 2 × PLgel Mixed D columns (300 × 7.5 mm) and a PLgel 5 μm guard column. Samples were dissolved in TCB (trichlorobenzene) and left to solubilise for 12 hours on an Agilent PL SP260VS at 140 °C and all data was calibrated against polystyrene. The mobile phase was TCB stabilised with 250 ppm BHT and run at a flow rate of 1 mL/min at 160 °C.

7.2 Synthetic Procedures and Characterization Pertaining to the Work of Chapter 2

H_2XN_2 (1)

4,5-Dibromo-2,7-di-*tert*-butyl-9,9-dimethylxanthene (5.0 g, 10.41 mmol), NaO^{t}Bu (2.8 g, 29.14 mmol), $Pd(OAc)_2$ (86.48 mg, 0.38 mmol) and DPEPhos (307.0 mg, 0.57 mmol) were dissolved in toluene (100 mL) followed by the addition of 2,4,6-triisopropylaniline (4.56 g, 20.8 mmol) via syringe. The reaction mixture was heated to 100 °C for 5 days over which time a color change to chocolate brown was observed. The reaction mixture was then quenched with water, extracted into toluene (3 × 50 mL), dried over $MgSO_4$, filtered and concentrated to approximately 10 mL. Recrystalization from hot ethanol yielded H_2XN_2 as an off-white solid (4.76 g, 60 %). To remove excess moisture the solid was stirred at room temperature with NaH (452 mg, 18.84 mmol) in toluene (35 mL) for 24 h followed by filtration and concentration of the mother liquor yielded an off-white solid, which was then dissolved in hexanes (20 mL), centrifuged and the solvent was removed *in vacuo* to yield H_2XN_2 as an off-white solid (4.08 g, 52 % from starting materials).

^{1}H NMR (C_6D_6, 600 MHz): δ 7.25 (s, 4H, Ar-*H*), 6.98 (d, 2H, $^4J_{H,H}$ 2.16 Hz, Xanth-C*H*^{1}), 6.57 (d, 2H, $^4J_{H,H}$ 2.14 Hz, Xanth-C*H*^{3}), 5.90 (s, 2H, N*H*), 3.52 (sept, 4H, $^3J_{H,H}$ 6.8 Hz, ortho-C*H*Me$_2$), 2.86 (sept, 2H, $^3J_{H,H}$ 6.8 Hz, para-C*H*Me$_2$), 1.69 (s, 6H, C*Me$_2$*), 1.264 (d, 12H, $^3J_{H,H}$ 6.8 Hz, ortho-CH*Me$_2$*), 1.260 (d, 12H, $^3J_{H,H}$ 6.8 Hz, para-CH*Me$_2$*), 1.23 (s, 18H, C*Me$_3$*), 1.188 (d, 12H, $^3J_{H,H}$ 6.8 Hz, ortho-CH*Me$_2$*)

^{13}C NMR (C_6D_6, 126 MHz): δ 148.12 (para-*C*CHMe$_2$), 147.78 (Ar-C_{ipso}), 146.14 (Xanth-C^2), 136.56 (Xanth-C^{11}), 133.62 (ortho-*C*CHMe$_2$), 129.27 (Xanth-C^{10}), 122.15 (Ar-*C*H), 111.68 (Xanth-C^1H), 107.82 (Xanth-C^3H), 35.07 (Xanth-C^9Me$_2$), 34.81 (*C*Me$_3$), 34.78 (para-*C*HMe$_2$), 32.96 (C*Me$_2$*), 31.71 (C*Me$_3$*), 28.89 (ortho-*C*HMe$_2$), 24.82 (ortho-CH*Me$_2$*), 24.41 (para-CH*Me$_2$*), 23.64 (ortho-CH*Me$_2$*) Anal. Calcd. For $C_{53}H_{76}N_2O$: C, 84.06; H, 10.12; N, 3.69 %. Found: C 83.88; H, 10.45; N, 3.28 %.

$[K_2(XN_2)(DME)_x]$ (x = 2-2.5) (2)

H_2XN_2 (0.50 g, 0.66 mmol) and KH (0.106 g, 2.64 mmol) were stirred in DME (40 mL) at 24 °C for 72 h, yielding a cloudy off-white solution, which was filtered and the solvent was removed *in vacuo*. The resulting off-white solid was dissolved in hexanes (10 mL), centrifuged, and the solvent was removed *in vacuo* yielding $[K_2(XN_2)(DME)_x]$ (x = 2-2.5) as a beige solid (0.535 g, 80 %). Multiple syntheses of K_2XN_2 revealed that either 2 or 2.5 equivalents of DME were present in the sample. The NMR characterization and elemental analysis is reported for a sample which contained 2.5 equivalents of DME.

^{1}H NMR (C_6D_6, 600 MHz): δ 7.24 (s, 4H, Ar-H), 6.50, 6.16 (d, 2 × 2H, $^4J_{H,H}$ 2.12 Hz, Xanth-CH^1 and Xanth-CH^3), 3.28 (s, 10H, 2.5 equiv. DME-CH_2), 3.10 (sept, 4H, $^3J_{H,H}$ 6.91 Hz, ortho-CHMe$_2$), 3.08 (s, 15H, 2.5 equiv. DME-CH_3), 2.97 (sept, 2H, $^3J_{H,H}$ 6.86 Hz, para-CHMe$_2$), 1.93 (s, 6H, CMe_2), 1.40 (d, 12H, $^3J_{H,H}$ 6.78 Hz, ortho-CHMe_2), 1.37 (s, 18H, CMe_3), 1.35 (d, 12H, $^3J_{H,H}$ 6.86 Hz, para-CHMe_2), 1.06 (d, 12H, $^3J_{H,H}$ 7.05 Hz, ortho-CHMe_2)

^{13}C NMR (C_6D_6, 126 MHz): δ 151.32 (Ar-C_{ipso}), 146.76 (Xanth-C^2), 142.26 (ortho-CCHMe$_2$), 139.34 (para-CCHMe$_2$), 137.38 (Xanth-C^{11}), 130.91 (Xanth-C^{10}), 121.36 (Ar-CH), 107.97, 100.19 (Xanth-C^1H and Xanth-C^3H), 72.07 (DME-CH$_2$), 58.63 (DME-CH$_3$), 35.65 (Xanth-C^9Me$_2$), 34.97 (CMe$_3$), 34.64 (para-CHMe$_2$), 32.28 (CMe_3), 31.71 (CMe_2), 28.02 (ortho-CHMe$_2$), 25.25 (ortho-CHMe_2), 24.98 (para-CHMe_2), 24.38 (ortho-CHMe_2) Anal. Calcd. For $[K_2(XN_2)(DME)_{2.5}]$, $C_{63}H_{99}N_2O_6K_2$: C, 71.47; H, 9.42; N, 2.64 %. Found: C, 71.25; H, 9.39; N, 2.56 %.

$[(XN_2)Y(CH_2SiMe_3)(THF)]\cdot(O(SiMe_3)_2)$ ($3\cdot O(SiMe_3)_2$)

H_2XN_2 (0.150 g, 0.198 mmol) was dissolved in 5 mL of benzene and added to $[Y(CH_2SiMe_3)_3(THF)_2]$ (0.107 g, 0.217 mmol) which was then stirred at 24 °C in the glove box for 24 h. The solvent was removed *in vacuo* and the yellow solid was recrystalized from $O(SiMe_3)_2$ at –30 °C yielding a yellow solid (0.120 g, 52 %).

^{1}H NMR (C_6D_6, 600 MHz): δ 7.27 (s, 2H, Ar-H'), 7.14 (s, 2H, Ar-H''), 6.80 (d, 2H, $^4J_{H,H}$ 2.06 Hz, Xanth-CH^1), 6.23 (d, 2H, $^4J_{H,H}$ 2.05 Hz, Xanth-CH^3), 4.28 (sept, 2H, $^3J_{H,H}$ 6.64 Hz, **A**-ortho-CHMe$_2$), 3.32 (sept, 2H, $^3J_{H,H}$ 6.64 Hz, **B**-ortho-CHMe$_2$), 2.83 (sept, 2H, $^3J_{H,H}$ 6.87 Hz, para-CHMe$_2$), 2.68 (s, 4H, 1 equiv. THF-C^{2,5}H_2), 1.89 (s, 3H, CMe_2'), 1.74 (s, 3H, CMe_2''), 1.50 (d, 6H, $^3J_{H,H}$ 6.70 Hz, **A**-ortho-CHMe_2'), 1.49 (d, 6H, $^3J_{H,H}$ 6.70 Hz, **A**-ortho-CHMe_2''), 1.27 (s, 18H, CMe_3), 1.12 (d, 6H, $^3J_{H,H}$ 6.70 Hz, **B**-ortho-CHMe_2'), 1.21 (d, 12H, $^3J_{H,H}$ 6.93 Hz, para-CHMe_2), 0.99 (d, 6H, $^3J_{H,H}$ 6.70 Hz, **B**-ortho-CHMe_2''), 0.84 (s, 4H, 1 equiv. THF-C^{3,4}H_2), 0.36 (s, 9H, YCH$_2$SiMe_3), -0.22 (d, 2H, $^2J_{Y,H}$ 3.55 Hz, YCH_2SiMe$_3$)

^{13}C NMR (C_6D_6, 126 MHz): δ 147.66 (Xanth-C^2), 147.21 (**A**-ortho-CC-HMe$_2$), 146.33 (**B**-ortho-CCHMe$_2$), 145.34 (para-CCHMe$_2$), 141.33 (Xanth-C^{11}), 140.83 (Ar-C_{ipso}), 130.49 (Xanth-C^{10}), 122.23 (Ar-CH$'$), 121.90 (Ar-CH$''$), 108.68 (Xanth-C^3H), 106.52 (Xanth-C^1H), 70.27 (THF-$C^{2,5}$H$_2$), 35.57 (Xanth-C^9Me$_2$), 35.41 (CMe_2'), 35.03 (CMe$_3$), 34.52 (para-CHMe$_2$), 34.02 (d, $^1J_{Y,C}$ 51.12 Hz, YCH$_2$SiMe$_3$), 31.91 (CMe_3), 28.38 (**B**-ortho-CHMe$_2$), 27.90 (**A**-ortho-CHMe$_2$), 27.17 (**A**-ortho-CHMe_2''), 26.06 (**B**-ortho-CHMe_2''), 25.36 (**B**-ortho-CHMe_2'), 25.14 (CMe_2''), 24.90 (THF-$C^{3,4}$H$_2$), 24.60 (**A**-ortho-CHMe_2'), 24.49 (para-CHMe_2), 4.09 (YCH$_2$SiMe_3) Anal. Calcd. For

$C_{67}H_{111}N_2O_3Y_1Si_3$: C, 69.02; H, 9.59; N, 2.40 %. Found: C, 68.61; H, 9.40; N, 2.82 %.

$[(XN_2)Y(CH_2SiMe_2Ph)(THF)]\cdot(O(SiMe_3)_2)$ ($4\cdot O(SiMe_3)_2$)

H_2XN_2 (0.100 g, 0.132 mmol) was dissolved in 7 mL of benzene and added to $[Y(CH_2SiMe_2Ph)_3(THF)_2]$ (0.098 g, 0.145 mmol) which was then stirred at 24 °C in the glove box for 14 days. The solvent was removed *in vacuo* and the dark yellow solid was recrystalized from $O(SiMe_3)_2$ at –30 °C yielding a yellow/brown solid (0.079 g, 49 %).

^{1}H NMR (C_6D_6, 600 MHz): δ 7.84 (m, 2H, $YCH_2SiMe_2\mathit{Ph}$), 7.22 (d, 2H, $^4J_{H,H}$ 1.68 Hz, Ar-H'), 7.20 (m, 3H, $YCH_2SiMe_2\mathit{Ph}$), 7.13 (d, 2H, $^4J_{H,H}$ 1.68 Hz, Ar-H''), 6.82 (d, 2H, $^4J_{H,H}$ 2.03 Hz, Xanth-CH^3), 6.23 (d, 2H, $^4J_{H,H}$ 2.03 Hz, Xanth-CH^1), 4.13 (sept, 2H, $^3J_{H,H}$ 6.75 Hz, **A**-ortho-CHMe$_2$), 3.34 (sept, 2H, $^3J_{H,H}$ 6.75 Hz, **B**-ortho-CHMe$_2$), 2.80 (sept, 2H, $^3J_{H,H}$ 6.86 Hz, para-CHMe$_2$), 2.66 (s, 4H, 1 equiv. THF-C$^{2,5}H_2$), 1.89 (s, 3H, CMe_2'), 1.73 (s, 3H, CMe_2''), 1.41 (d, 6H, $^3J_{H,H}$ 6.75 Hz, **A**-ortho-CHMe_2'), 1.34 (d, 6H, $^3J_{H,H}$ 6.75 Hz, **A**-ortho-CHMe_2''), 1.28 (s, 18H, CMe_3), 1.24 (d, 6H, $^3J_{H,H}$ 6.75 Hz, **B**-ortho-CHMe_2'), 1.18 (d, 12H, $^3J_{H,H}$ 6.75 Hz, para-CHMe_2), 1.00 (d, 6H, $^3J_{H,H}$ 6.75 Hz, **B**-ortho-CHMe_2''), 0.84 (s, 4H, 1 equiv. THF-C$^{3,4}H_2$), 0.57 (s, 6H, YCH$_2$SiMe_2Ph), -0.07 (d, 2H, $^2J_{Y,H}$ 3.56 Hz, YCH_2SiMe$_2$Ph)

^{13}C NMR (C_6D_6, 126 MHz): δ 147.79 (Xanth-C^2), 147.66 (**A**-ortho-CCH-Me$_2$), 147.20 (YCH$_2$SiMe$_2$$Ph_{ipso}$), 146.19 (**B**-ortho-$C$CHMe$_2$), 145.40 (para-$C$CHMe$_2$), 141.23 (Xanth-$C^{11}$), 140.66 (Ar-$C_{ipso}$), 133.89 (YCH$_2$SiMe$_2$$Ph$), 130.46 (Xanth-$C^{10}$), 127.50 (YCH$_2$SiMe$_2$$Ph$), 122.28 (Ar-$C$H′), 121.87 (Ar-$C$H″), 108.77 (Xanth-$C^1$H), 106.72 (Xanth-$C^3$H), 70.37 (THF-$C^{2,5}H_2$), 35.59

(C*Me₂′*), 35.06 (Xanth-C^9Me$_2$), 34.87 (*C*Me$_3$), 34.50 (para-*C*HMe$_2$), 31.92 (C*Me$_3$*), 30.25 (Y*C*H$_2$SiMe$_2$Ph), 28.42 (**B**-ortho-*C*HMe$_2$), 27.92 (**A**-ortho-*C*HMe$_2$), 27.19 (**A**-ortho-CH*Me$_2$″*), 26.06 (**B**-ortho-CH*Me$_2$″*), 25.41 (**B**-ortho-CH*Me$_2$′*), 25.20 (C*Me$_2$″*), 24.91 (THF-$C^{3,5}$H$_2$), 24.57 (**A**-ortho-CH*Me$_2$′*), 24.49 (para-CH*Me$_2$*), 2.39 (YCH$_2$Si*Me$_2$*Ph) Anal. Calcd. For $C_{72}H_{113}N_2O_3Y_1Si_3$: C, 70.43; H, 9.27; N, 2.28 %. Found: C 70.28; H, 8.99; N, 2.29 %.

[(XN$_2$)Y{(μ-Me)$_2$AlMe$_2$}(THF)]·(O(SiMe$_3$)$_2$) (5·O(SiMe$_3$)$_2$)

[(XN$_2$)Y(CH$_2$SiMe$_3$)(THF)] (0.04 g, 0.034 mmol) was dissolved in 8 mL of benzene and added to an excess of AlMe$_3$ (0.05 g, 0.686 mmol) which was then stirred at 24 °C for 1 h. The solvent was removed *in vacuo* and the yellow solid was recrystalized from O(SiMe$_3$)$_2$ at –30 °C yielding colorless crystals (0.008 g, 20 %).

^{1}H NMR (C$_6$D$_6$, 600 MHz): δ 7.23 (s, 4H, Ar-*H*), 6.81 (d, 2H, $^4J_{\rm H,H}$ 2.05 Hz, Xanth-C*H^1*), 6.18 (d, 2H, $^4J_{\rm H,H}$ 2.08 Hz, Xanth-C*H^3*), 3.30 (sept, 4H, $^3J_{\rm H,H}$ 6.89 Hz, ortho-C*H*Me$_2$), 3.29 (m, 4H, 1 equiv. THF-C^{2,5}*H$_2$*), 2.83 (sept, 2H, $^3J_{\rm H,H}$ 6.89 Hz, para-C*H*Me$_2$), 1.64 (s, 6H, C*Me$_2$*), 1.30 (d, 12H, $^3J_{\rm H,H}$ 6.91 Hz, **A**-ortho-CH*Me$_2$*), 1.28 (d, 12H, $^3J_{\rm H,H}$ 6.91 Hz, para-CH*Me$_2$*), 1.23 (s, 18H, C*Me$_3$*), 1.22 (d, 12H, $^3J_{\rm H,H}$ 6.91 Hz, **B**-ortho-CH*Me$_2$*), 0.93 (m, 4H, 1 equiv. THF-C^{3,4}*H$_2$*), -0.56 (d, 12H, $^2J_{\rm Y,H}$ 3.76 Hz, Al*Me$_4$*)

^{13}C NMR (C$_6$D$_6$, 126 MHz): δ 148.06 (Xanth-*C^2*), 146.84 (para-*C*CHMe$_2$), 146.25 (Xanth-*C^4*), 145.55 (ortho-*C*CHMe$_2$), 140.47 (Xanth-*C^{11}*), 138.05 (Ar-*C$_{ipso}$*), 129.81 (Xanth-*C^{10}*), 122.89 (Ar-*C*H), 109.56 (Xanth-*C^3*H), 108.78 (Xanth-*C^1*H), 70.11 (THF-*C^{2,5}*H$_2$), 35.07 (*C*Me$_3$), 35.04 (Xanth-*C^9*Me$_2$), 34.72 (para-*C*HMe$_2$), 31.79 (C*Me$_3$*), 31.46 (C*Me$_2$*), 29.43 (ortho-*C*HMe$_2$), 27.28 (**B**-

ortho-CHMe_2), 24.83 (THF-$C^{3,4}$H$_2$), 24.39 (para-CHMe_2), 23.67 (**A**-ortho-CHMe_2), 3.22 (AlMe_4) Anal. Calcd. For $C_{67}H_{112}N_2O_3Y_1Al_1Si_2$: C, 69.03; H, 9.68; N, 2.41 %. Found: C, 68.51; H, 9.27; N, 2.53 %.

$[(XN_2)AlCH_3]\cdot(O(SiMe_3)_2)$ (6·$O(SiMe_3)_2$)

H_2XN_2 (0.05 g, 0.066 mmol) was dissolved in 3 mL of benzene and added to $AlMe_3$ (0.007 g, 0.099 mmol) which was then stirred at 85 °C in a sealed Schlenk flask for 6 days. The solvent was removed *in vacuo* and the off-white solid was recrystalized from $O(SiMe_3)_2$ at –30 °C yielding colorless crystals (0.034 g, 54 %).

^{1}H NMR (C_6D_6, 600 MHz): δ 7.27 (s, 4H, Ar-H), 6.75 (d, 2H, $^4J_{H,H}$ 1.95 Hz, Xanth-CH^1), 6.39 (d, 2H, $^4J_{H,H}$ 1.95 Hz, Xanth-CH^3), 3.58 (sept, 4H, $^3J_{H,H}$ 6.85 Hz, ortho-CHMe$_2$), 2.86 (sept, 2H, $^3J_{H,H}$ 6.90 Hz, para-CHMe$_2$), 1.58 (s, 6H, CMe_2), 1.36 (d, 12H, $^3J_{H,H}$ 6.85 Hz, **A**-ortho-CHMe_2), 1.26 (d, 12H, $^3J_{H,H}$ 6.90 Hz, para-CHMe_2), 1.20 (d, 12H, $^3J_{H,H}$ 6.85 Hz, **B**-ortho-CHMe_2), 1.18 (s, 18H, CMe_3), -0.36 (s, 3H, AlMe)

^{13}C NMR (C_6D_6, 126 MHz): δ 149.45 (Xanth-C^2), 146.88 (ortho-CCHMe$_2$), 146.36 (para-CCHMe$_2$), 143.73 (Xanth-C^4), 141.83 (Xanth-C^{11}), 138.38 (Ar-C_{ipso}), 133.82 (Xanth-C^{10}), 122.31 (Ar-CH), 111.42 (Xanth-C^3H), 107.74 (Xanth-C^1H), 37.58 (Xanth-C^9Me$_2$), 35.18 (CMe$_3$), 34.53 (para-CHMe$_2$), 31.72 (CMe_3), 29.20 (ortho-CHMe$_2$), 27.33 (CMe_2), 26.00 (**B**-ortho-CHMe_2), 24.57 (**A**-ortho-CHMe_2), 24.36 (para-CHMe_2), -12.74 (AlMe) Anal. Calcd. For $C_{60}H_{95}N_2O_2Al_1Si_2$: C, 75.10; H, 9.98; N, 2.92 %. Found: C, 75.12; H, 9.78; N, 2.92 %.

General Procedure for Intramolecular Hydroamination

In the glove box, the appropriate amounts of the catalyst and the hydroamination substrate were weighed into separate vials, dissolved in C_6D_6, and placed in a teflon-valved J-Young NMR tube. The reactions were monitored at 24 °C by ^{1}H NMR spectroscopy and the expected products were confirmed by their agreement to reported literature spectra.[271]

General Procedure for Intermolecular Hydroamination

In the glove box, the appropriate amounts of the catalyst, amine, and the alkene/alkyne were weighed into separate vials, dissolved in d_8-Tol, placed in a teflon-valved J-Young NMR tube and then placed into a preheated oil bath at 110 °C. After heating for the designated amount of time, NMR spectra were obtained and the sample was submitted for analysis by GC-MS.

7.3 Synthetic Procedures and Characterization Pertaining to the Work of Chapter 3

XP_2Cl_2 (7)

A 1.6 M solution of ^{n}BuLi in hexanes (12.3 mL, 19.6 mmol) was added to a solution of 4,5-dibromo-2,7-di-*tert*-butyl-9,9-dimethylxanthene (4.72 g, 9.82 mmol) in THF (120 mL) at -78 °C, and the reaction mixture was stirred at -78 °C for 6 h. A solution of 2,4,6-triisopropylphenyldichlorophosphine (6.0 g, 19.6 mmol) in THF (45 mL) was then added, and the reaction mixture and was allowed to warm to room temperature (24 °C) and stirred for 40 h. The solvent was removed *in vacuo* and the resulting yellow solid was dissolved in toluene (75 mL), centrifuged and the mother liquors were decanted and evaporated to dryness. To the resulting yellow tacky solid, hexanes (60 mL) was added followed by sonication and solvent removal *in vacuo* to yield XP_2Cl_2 as an free flowing off-white solid (6.1 g, 73 %). This product is an approximate 1:1 mixture of diastereomers, and was of sufficient purity to proceed to the next step of the ligand synthesis (diastereomers were not identified as *rac* or *meso*, since both diastereomers gave rise to only one C*Me₂* signal in the ^{1}H and ^{13}C NMR spectra, presumably due to overlapping signals in the case of the *Cs*-symmetric *meso* isomer). However, to obtain analytically pure material, the diastereomers (referred to as *A* and *B*) could be separated by sonication in hexanes (4 mL per g of product) followed by centrifugation and separation of the solid from the mother liquors. The solid is > 95 % diastereomer-*A* (isolated in 26 % yield from the crude) while the mother liquors are enriched in the diastereomer-*B* (a 3:1 *B*:*A* ratio is typical).

NMR data for diastereomer A: ^{1}H NMR (C_6D_6, 600 MHz): δ 7.43, 7.15 (s, 2 × 2H, Xanth-CH^1 and Xanth-CH^3), 7.23 (s, 4H, Ar-*H*), 4.25, 4.26 (sept, 2 × 2H, $^3J_{H,H}$ 6.5 Hz, ortho-C*H*Me$_2$), 2.76 (sept, 2H, $^3J_{H,H}$ 7.0 Hz, para-C*H*Me$_2$), 1.45 (s, 6H, CMe_2), 1.30, 1.26 (d, 2 × 12H, $^3J_{H,H}$ 6.5 Hz, ortho-CHMe_2), 1.20, 1.19 (d, 2 × 6H, $^3J_{H,H}$ 7.0 Hz, para-CHMe_2), 1.17 (s, 18H, CMe_3). ^{13}C NMR (C_6D_6, 126 MHz): δ 156.40 (ortho-*C*CHMe$_2$), 152.54 (para-*C*CHMe$_2$), 150.56 (Xanth-C^{11}), 144.97 (Xanth-C^2), 130.64 (d, Ar-C_{ipso}), 129.83 (Xanth-C^{10}), 127.81, 125.85 (Xanth-C^1H and Xanth-C^3H), 122.94 (Ar-*C*H), 34.76 (para-*C*HMe$_2$), 33.42 (CMe_2), 32.31, 32.15 (2 × ortho-*C*HMe$_2$), 31.42 (CMe_3), 26.03, 24.40 (2 × ortho-CHMe_2), 24.02, 23.89 (2 × para-CHMe_2). ^{31}P NMR (C_6D_6, 243 MHz): δ 75.52.

NMR data for diastereomer B: ^{1}H NMR (C_6D_6, 600 MHz): δ 7.55, 7.41 (s, 2 × 2H, Xanth-C*H*^{1} and Xanth-C*H*^{3}), 7.24 (s, 4H, Ar-*H*), 4.31, 4.32 (sept, 2 × 2H, $^3J_{H,H}$ 6.7 Hz, ortho-C*H*Me$_2$), 2.78 (sept, 2H, $^3J_{H,H}$ 6.8 Hz, para-C*H*Me$_2$), 1.36 (s, 6H, C*Me$_2$*), 1.32, 1.27 (d, 2 × 12H, $^3J_{H,H}$ 6.7 Hz, ortho-CH*Me$_2$*), 1.24 (d, 12H, $^3J_{H,H}$ 6.8 Hz, para-CH*Me$_2$*), 1.13 (s, 18H, C*Me$_3$*) ^{13}C NMR (C_6D_6, 126 MHz): δ 156.38 (ortho-*C*CHMe$_2$), 151.25 (Xanth-*C^{11}*), 149.15 (para-*C*CHMe$_2$), 147.46 (Xanth-*C^2*), 131.50 (Xanth-*C^{10}*), 130.62 (Ar-C_{ipso}), 127.83, 124.94 (Xanth-*C^1*H and Xanth-*C^3*H), 122.80 (Ar-*C*H), 34.73 (para-*C*HMe$_2$), 31.83, 31.60 (2 × ortho-*C*HMe$_2$), 31.70 (C*Me$_2$*), 31.49 (C*Me$_3$*), 25.62, 24.99 (2 × ortho-CH*Me$_2$*), 24.46, 24.40 (2 × para-CH*Me$_2$*). ^{31}P NMR (C_6D_6, 243 MHz): δ 76.81. Anal. Calcd. For $C_{53}H_{74}P_2OCl_2$: C, 74.01; H, 8.67 %. Found: C, 73.85; H, 8.95 %.

[H_2XP_2]·nLiCl (n = 1–1.5) (8)

A solution of XP_2Cl_2 (4.0 g, 4.65 mmol) in toluene (60 mL) was added to a solution of $LiAlH_4$ (0.194 g, 5.11 mmol) in diethylether (200 mL) at -78 °C. The reaction mixture was stirred for 2 h before warming to room temperature (24 °C) and stirring for an additional 24 h. The solvent was removed *in vacuo* followed by centrifugation in toluene (45 mL) and evaporation of the mother liquor to dryness to yield a pale yellow solid. Hexanes (35 mL) was added followed by centrifugation and evaporation of the mother liquor. The resulting white solid was heated under vacuum at 60 °C for 2 days to remove all remaining solvent, yielding H_2XP_2 (3.20 g, 87 %).

^{1}H NMR (C_6D_6, 600 MHz): δ 7.34, 6.88 (m, 2 × 4H, Xanth-C*H*^{1} and Xanth-C*H*^{3} *rac* and *meso*), 7.27 (s, 8H, Ar-*H*, *rac* and *meso*), 6.37 (d, 2H,

$^1J_{H,P}$ 229 Hz, P-*H*), 6.17 (d, 2H, $^1J_{H,P}$ 225 Hz, P-*H*), 4.01, 4.00 (2 sept, 2 × 4H, $^3J_{H,H}$ 6.5 Hz, ortho-C*H*Me$_2$ *rac* and *meso*), 2.83, 2.82 (2 sept, 2 × 2H, $^3J_{H,H}$ 7.0 Hz, para-C*H*Me$_2$ *rac* and *meso*), 1.54 (s, 6H, C*Me$_2$* *rac*), 1.53, 1.51 (s, 2 × 3H, C*Me$_2$* *meso*), 1.30, 1.27 (d, 2 × 12H, $^3J_{H,H}$ 6.5 Hz, ortho-CH*Me$_2$*), 1.25-1.23 (m, 48H, ortho- + para-CH*Me$_2$*), 1.17, 1.17 (s, 2 × 18H, C*Me$_3$* *rac* and *meso*).

^{13}C NMR (C_6D_6, 126 MHz): δ 155.43, (ortho-*C*CHMe$_2$), 151.12 (para-*C*CHMe$_2$), 149.71, 149.31 (Xanth-*C^{11}*), 145.98, 145.87 (Xanth-*C^2*), 129.36, 128.94 (Xanth-*C^{10}*), 127.81, 127.68 (Xanth-*C^1*H or Xanth-*C^3*H), 122.02, 121.87, 121.71 (Ar-*C*H + 2 × Xanth-*C^1*H or Xanth-*C^3*H), 35.26, 35.07, 34.67 (2 × Xanth-*C^9*Me$_2$ + *C*Me$_3$), 34.94 (para-*C*HMe$_2$), 33.49, 31.42 (C*Me$_2$* *meso*), 33.39, 33.35, 33.31 (ortho-*C*HMe$_2$), 32.07 (C*Me$_2$* *rac*), 31.63 (C*Me$_3$*), 25.43, 25.38 (ortho-CH*Me$_2$*), 24.45, 24.43, 24.25, 24.19 (ortho-CH*Me$_2$* + para-CH*Me$_2$*). ^{31}P NMR (C_6D_6, 81 MHz): δ -93.07 d, ($^1J_{P,H}$ = 225 Hz), -93.77 d, ($^1J_{P,H}$ = 229 Hz) Anal. Calcd. For $C_{53}H_{76}P_2O$: C, 80.46; H, 9.68 %. Range from duplicate analyses on 4 different batches: C 76.49; H 9.72 % to C 74.78; H 8.70 %. These data correspond to ($C_{53}H_{76}P_2O$)·nLiCl (n = 1-1.5), since anal. calcd. for $C_{53}H_{76}P_2OLiCl$ is C 76.36; H 9.19 %, and anal calcd. for $C_{53}H_{76}P_2OLi_{1.5}Cl_{1.5}$ is C 74.47; H 8.96 %.

[$K_2(XP_2)(DME)_{2.5}$] (9)

Solid KH (0.126 g, 3.16 mmol) was added to a solution of $H_2[XP_2]$·nLiCl (n=1), (1.0 g, 1.20 mmol) in DME (40 mL), and the reaction was stirred at 24 °C for 72 h in the glove box. The orange reaction mixture was filtered, and the filtrate was evaporated to dryness *in vacuo*. Addition of hexanes

(15 mL), centrifugation, and evaporation of the mother liquors to dryness afforded $[K_2(XP_2)(DME)_{2.5}]$ (1.1 g, 80 %) as an orange solid. Crystals of $[K_2(XP_2)(DME)_4]$ were grown by cooling a concentrated DME solution to –30 °C.

^{1}H NMR (C_6D_6, 600 MHz): δ 7.43 (s, 4H, Ar-*H*), 6.78, 6.65 (s, 2H, Xanth-CH^1 and Xanth-CH^3), 4.54 (sept, 4H, $^3J_{H,H}$ 6.5 Hz, ortho-C*H*Me$_2$), 3.06 (sept, 2H, $^3J_{H,H}$ 7.0 Hz, para-C*H*Me$_2$), 2.99 (s, 10H, 2.5 equiv. DME-CH_2), 2.88 (s, 15H, 2.5 equiv. DME-CH_3), 1.86 (s, 6H, CMe_2), 1.52 (d, 12H, $^3J_{H,H}$ 6.5 Hz, ortho-CHMe_2), 1.45 (d, 12H, $^3J_{H,H}$ 7.0 Hz, para-CHMe_2), 1.38 (d, 12H, $^3J_{H,H}$ 6.5 Hz, ortho-CHMe_2), 1.30 (s, 18H, CMe_3).

^{13}C NMR (C_6D_6, 126 MHz): δ 155.16 (ortho-*C*CHMe$_2$), 146.78 (para-*C*CHMe$_2$), 144.70 (Xanth-C^{11}), 144.27 (Xanth-C^2), 141.18 (Ar-C_{ipso}), 126.34 (Xanth-C^{10}), 123.75, 110.69 (Xanth-C^1H and Xanth-C^3H), 120.69 (Ar-*C*H), 71.46 (DME-*C*H$_2$), 58.49 (DME-*C*H$_3$), 35.12 (para-*C*HMe$_2$), 34.61 (Xanth-C^9Me$_2$ and/or *C*Me$_3$), 34.16 (CMe_2), 33.73 (ortho-*C*HMe$_2$), 31.96 (CMe_3), 26.07, 25.00 (2 $\times$ ortho-CHMe_2), 24.72 (para-CHMe_2). ^{31}P NMR (C_6D_6, 81 MHz): δ -83.73. Anal. Calcd. For $C_{63}H_{99}P_2O_6K_2$: C, 69.25; H, 9.13 %. Found: C, 69.69; H, 8.98 %.

$[K_4(XP_2)_2(THF)_4]$ (10)

$[K_2(XP_2)(DME)_{2.5}]$ (95 mg, 0.087 mmol) was dissolved in THF (12 mL) and stirred at 24 °C for 5 h. The solution was evaporated to dryness *in vacuo* and the amber colored solid was recrystalized from hexanes (1.5 mL) to yield $[K_4(XP_2)_2(THF)_4]$ (0.038 g, 21.6 %) as red-orange crystals.

^{1}H NMR (C_6D_6, 600 MHz): δ 7.43 (s, 8H, Ar-*H*), 6.87 (d, 4H, $^4J_{H,H}$ 2.29 Hz, Xanth-CH^1), 6.61 (broad s, 4H, Xanth-CH^3), 4.37 (sept, 8H, $^3J_{H,H}$ 7.01 Hz, ortho-C*H*Me$_2$), 3.55 (m, 16H, 4 equiv. THF-C$^{2,5}H_2$), 3.07 (sept, 4H, $^3J_{H,H}$ 7.01 Hz, para-C*H*Me$_2$), 1.88 (s, 12H, CMe_2), 1.50 (d, 24H, $^3J_{H,H}$ 6.99 Hz, **A**-ortho-CHMe_2), 1.46 (d, 24H, $^3J_{H,H}$ 7.02 Hz, para-CHMe_2), 1.41 (m, 16H, 4 equiv. THF-C$^{3,4}H_2$), 1.34 (d, 24H, $^3J_{H,H}$ 6.99 Hz, **B**-ortho-CHMe_2), 1.33 (s, 36H, CMe_3)

^{13}C NMR (C_6D_6, 126 MHz): δ 154.99 (ortho-*C*CHMe$_2$), 147.06 (para-*C*CHMe$_2$)), 144.57 (Xanth-C^2), 126.98 (Xanth-C^{10}), 124.07 (Xanth-C^3H), 120.80 (Ar-*C*H), 110.75 (Xanth-C^1H), 67.82 (THF-$C^{2,5}$H$_2$), 35.12 (para-*C*H-Me$_2$), 34.83 (Xanth-C^9Me$_2$), 34.66 (*C*Me$_3$), 33.69 (ortho-*C*HMe$_2$), 33.54 (C-Me_2), 31.95 (CMe_3), 25.94 (**B**-ortho-CHMe_2), 25.80 (THF-$C^{3,4}$H$_2$), 25.04 (**A**-ortho-CHMe_2), 24.69 (para-CHMe_2) ^{31}P NMR (C_6D_6, 81 MHz): δ -85.14 Anal. Calcd. For $C_{122}H_{180}O_6P_4K_4$: C, 72.43; H, 8.97 %. Found: C, 72.38; H, 8.75 %.

[(XP$_2$)YI(THF)$_2$] (11)

[$K_2(XP_2)(DME)_{2.5}$] (0.250 g, 0.228 mmol) and [$YI_3(THF)_{3.5}$] (0.166 g, 0.228 mmol) were stirred in THF (25 mL) for 72 h at 24 °C. The bright yellow solution was filtered and the solvent was removed *in vacuo*. The resulting yellow solid was slurried in hexanes (8 mL) before the mixture was centrifuged and the mother liquors were evaporated to dryness to provide impure [(XP$_2$)YI(THF)$_2$] (0.110 g) as an orange solid. 5 mL of O(SiMe$_3$)$_2$ was added to the impure solid followed by centrifugation. The resulting solid was isolated and dried *in vacuo* yielding pure [(XP$_2$)YI(THF)$_2$] (0.048 g, 18 % yield). The remaining mother liquors contain a mixture of products, including

$(PTripp)_3$ and X-ray quality crystals of $(PTripp)_3$ were obtained by cooling a concentrated hexanes solution of this mixture to –30 °C. X-ray quality crystals of **11** were grown by cooling a concentrated hexanes solution of **11** to –30 °C. Solid samples of $[(XP_2)YI(THF)_2]$ were observed to lose THF slowly under dynamic vacuum, and the sample used for NMR spectroscopic characterization contained just 1.5 equiv. of THF.

^{1}H NMR (d_8-THF, 600 MHz): δ 7.11 (s, 4H, Ar-*H*), 6.74 (d, 2H, $^4J_{H,H}$ 2.0 Hz, Xanth-CH^1), 5.94 (dd, 2H, $^4J_{H,H}$ 2.0 Hz, $^3J_{P,H}$ 8.0 Hz, Xanth-CH^3), 4.40 (sept, 4H, $^3J_{H,H}$ 7.0 Hz, ortho-C*H*Me_2), 3.62 (m, 6H, 1.5 equiv. THF-$C^{2,5}H_2$), 2.92 (sept, 2H, $^3J_{H,H}$ 7.0 Hz, para-C*H*Me_2), 1.77 (m, 6H, 1.5 equiv. THF-$C^{3,4}H_2$), 1.54 (s, 6H, CMe_2), 1.28 (d, 12H, $^3J_{H,H}$ 7.0 Hz, para-CHMe_2), 1.24 (d, 12H, $^3J_{H,H}$ 7.0 Hz, **A**-ortho-CHMe_2), 1.01 (d, 12H, $^3J_{H,H}$ 7.0 Hz, **B**-ortho-CHMe_2), 0.99 (s, 18H, CMe_3).

^{13}C NMR (d_8-THF, 126 MHz): δ 155.69 (ortho-*C*CHMe_2), 149.28 (para-*C*CHMe_2)), 144.06 (Xanth-C^2), 136.51 (d, Ar-C_{ipso}), 128.02 (Xanth-C^{10}), 123.94 (Xanth-C^3H), 121.66 (Ar-*C*H), 114.83 (Xanth-C^1H), 35.24 (para-*C*HMe_2), 34.66 (*C*Me_3), 34.53 (ortho-*C*HMe_2), 34.45 (Xanth-$C^9$$Me_2$), 33.11 (C$Me_2$), 31.49 (C$Me_3$), 26.18 (**B**-ortho-CH$Me_2$), 25.66 (**A**-ortho-CH$Me_2$), 24.34 (para-CH-$Me_2$). ^{31}P NMR ($d_8$-THF, 81 MHz): δ 1.28 (d, $^1J_{Y,P}$ = 162 Hz). Anal. Calcd. For $C_{61}H_{90}P_2YIO_3$: C, 63.76; H, 7.89 %. Found: C, 60.56; H, 7.95 %. (This compound is extremely air, moisture and temperature sensitive and it is probable that decomposition occurred during transport prior to elemental analysis).

7.4 Synthetic Procedures and Characterization Pertaining to the Work of Chapter 4

[$(XN_2)Lu(CH_2SiMe_3)(THF)]\cdot(O(SiMe_3)_2)_{1.5}$ (**12**$\cdot(O(SiMe_3)_2)_{1.5}$)

H_2XN_2 (0.10 g, 0.132 mmol) was dissolved in 2 mL of benzene and added to [$Lu(CH_2SiMe_3)_3(THF)_2$] (0.084 g, 0.145 mmol) which was then stirred at 24 °C in the glove box for 4 weeks. The solvent was removed *in vacuo* and the yellow solid was recrystalized from $O(SiMe_3)_2$ at –30 °C yielding 12$\cdot(O(SiMe_3)_2)_{1.5}$ as a light yellow powder (0.096 g, 55 %).

^{1}H NMR (C_6D_6, 600 MHz): δ 7.25 (s, 2H, Ar-H'), 7.14 (s, 2H, Ar-H''), 6.77 (br s, 2H, Xanth-CH^1), 6.23 (br s, 2H, Xanth-CH^3), 4.24 (sept, 2H, $^3J_{H,H}$ 6.73 Hz, **A**-ortho-CHMe$_2$), 3.38 (sept, 2H, $^3J_{H,H}$ 6.78 Hz, **B**-ortho-CHMe$_2$), 2.83 (sept, 2H, $^3J_{H,H}$ 6.74 Hz, para-CHMe$_2$), 2.73 (s, 4H, 1 equiv. THF-C^{2,5}H_2), 1.88 (s, 3H, CMe_2'), 1.72 (s, 3H, CMe_2''), 1.49 (d, 6H, $^3J_{H,H}$ 6.73 Hz, **A**-ortho-CHMe_2'), 1.47 (d, 6H, $^3J_{H,H}$ 6.73 Hz, **A**-ortho-CHMe_2''), 1.26 (s, 18H, CMe_3), 1.24 (d, 6H, $^3J_{H,H}$ 6.78 Hz, **B**-ortho-CHMe_2'), 1.21 (m, 12H, para-CHMe_2), 1.01 (d, 6H, $^3J_{H,H}$ 6.78 Hz, **B**-ortho-CHMe_2''), 0.83 (s, 4H, 1 equiv. THF-C^{3,4}H_2), 0.35 (s, 9H, LuCH$_2$SiMe_3), -0.40 (s, 2H, LuCH_2SiMe$_3$)

^{13}C NMR (C_6D_6, 126 MHz): δ 147.83 (Xanth-C^4), 147.72 (Xanth-C^2) 147.38 (**A**-ortho-CCHMe$_2$), 146.17 (**B**-ortho-CCHMe$_2$), 145.33 (para-CCH-Me$_2$), 141.82 (Ar-C_{ipso}), 141.30 (Xanth-C^{11}), 130.56 (Xanth-C^{10}), 122.20 (Ar-CH$'$), 121.85 (Ar-CH$''$), 109.35 (Xanth-C^3H), 106.47 (Xanth-C^1H), 70.85 (THF-$C^{2,5}$H$_2$), 37.99 (LuCH$_2$SiMe$_3$), 35.57 (Xanth-C^9Me$_2$), 35.25 (CMe_2'), 35.05 (CMe$_3$), 34.50 (para-CHMe$_2$), 31.91 (CMe_3), 28.39 (**B**-ortho-CHMe$_2$), 27.67 (**A**-ortho-CHMe$_2$), 27.12 (**A**-ortho-CHMe_2''), 25.85 (**B**-ortho-CHMe_2''), 25.48

(**B**-ortho-CH*Me2′*), 25.04 (C*Me2″*), 24.85 (THF-$C^{3,4}$H$_2$), 24.62 (**A**-ortho-CH-*Me2′*), 24.51 (para-CH*Me2*), 4.13 (LuCH$_2$Si*Me3*) Anal. Calcd. For $C_{70}H_{120}$-$N_2O_{3.5}Lu_1Si_4$: C, 63.07; H, 9.07; N, 2.10 %. Found: C, 63.03; H, 8.61; N, 2.30 %.

[{(XN$_2$)LaCl(THF)}$_x$]·(O(SiMe$_3$)$_2$)$_{0.25x}$ (x = 1 or 2) (13·(O(Si-Me$_3$)$_2$)$_{0.25x}$)

K$_2$(XN$_2$)(DME)$_2$ (0.53 g, 0.523 mmol) and [LaCl$_3$(THF)$_3$] (0.244 g, 0.528 mmol) were dissolved in 40 mL of THF and stirred at 24 °C for 4 days. The cloudy beige solution was centrifuged and the mother liquor solvent was removed *in vacuo.* The resulting solid was dissolved in toluene (60 mL), followed by centrifugation and removal of the mother liquor solvent *in vacuo* to yield a beige solid. Recrystallization from O(SiMe$_3$)$_2$ at –30 °C yielded [{(XN$_2$)LaCl-(THF)}$_x$]·(O(SiMe$_3$)$_2$)$_{0.25x}$ ($x = 1$ or 2) as an off-white solid (0.28 g, 51 %).

^{1}H NMR (d$_8$-THF, 600 MHz): δ 7.08 (s, 4H, Ar-*H*), 6.57 (br. s, 2H, Xanth-C*H′*), 5.81 (br. s, 2H, Xanth-C*H″*), 3.62 (s, 4H, 1 equiv. THF-C^{2,5}*H2*), 3.15 (sept, 4H, $^3J_{\mathrm{H,H}}$ 6.74 Hz, ortho-C*H*Me$_2$), 2.88 (sept, 2H, $^3J_{\mathrm{H,H}}$ 6.86 Hz, para-C*H*Me$_2$), 1.77 (s, 4H, 1 equiv. THF-C^{3,4}*H2*), 1.72 (s, 6H, C*Me2*), 1.23 (d, 12H, $^3J_{\mathrm{H,H}}$ 6.75 Hz, **A**-ortho-CH*Me2*), 1.21 (d, 12H, $^3J_{\mathrm{H,H}}$ 6.85 Hz, para-CH*Me2*), 1.15 (s, 18H, C*Me3*), 1.01 (d, 12H, $^3J_{\mathrm{H,H}}$ 6.76 Hz, **B**-ortho-CH*Me2*)

^{13}C NMR (d$_8$-THF, 126 MHz): δ 146.81 (Xanth-C^2), 146.17 (ortho-*C*CH-Me$_2$), 145.26 (para-*C*CHMe$_2$), 140.45 (Ar-C_{ipso}), 128.34 (Xanth-C^{10}), 122.57 (Ar-*C*H), 108.43 (Xanth-*C″*H), 107.41 (Xanth-*C′*H), 67.22 (THF-$C^{2,5}$H$_2$), 35.07 (*C*Me$_3$), 34.96 (para-*C*HMe$_2$), 34.85 (Xanth-C^9Me$_2$), 33.05 (C*Me2*), 31.81 (C*Me3*), 29.19 (ortho-*C*HMe$_2$), 25.84 (**B**-ortho-CH*Me2*), 25.25 (THF-$C^{3,4}$H$_2$), 24.52 (para-CH*Me₂*), 24.16 (**A**-ortho-CH*Me₂*)) Anal. Calcd. For $[(XN_2)LaCl(THF)]\cdot(O(SiMe_3)_2)_{0.25}$, $C_{58.5}H_{86.5}N_2O_{2.25}Si_{0.5}La_1Cl_1$: C, 67.41; H, 8.36; N, 2.68 %. Found: C, 66.89; H, 8.83; N, 2.60 %.

$[Li(THF)_x][(XN_2)La(CH_2SiMe_3)_2]$ (14·Toluene·LiCl)

$[\{(XN_2)LaCl(THF)\}_x]\cdot(O(SiMe_3)_2)_{0.25x}$ ($x = 1$ or 2) (0.086 g, 0.082 mmol of La) was dissolved in 4 mL of THF and added to $LiCH_2SiMe_3$ (0.015 g, 0.165 mmol), which was stirred at 24 °C for 5 days. The solvent was removed *in vacuo* and the yellow solid was dissolved in toluene (1 mL), centrifuged and the mother liquor was layered with hexanes and stored at –30 °C. Very small pale yellow crystals of $[Li(THF)_3][(XN_2)La(CH_2SiMe_3)_2]$·Toluene·LiCl were obtained (0.064 g, 55 %). X-ray quality crystals of $[Li(THF)_4][(XN_2)La(CH_2SiMe_3)_2]$·THF were grown from a concentrated THF solution of **14**, layered with pentane and cooled to –30 °C.

^{1}H NMR (d_8-THF, 600 MHz): δ 7.00 (s, 4H, Ar-*H*), 6.28 (d, 2H, $^4J_{H,H}$ 2.16 Hz, Xanth-C*H*^{3}), 5.62 (d, 2H, $^4J_{H,H}$ 2.18 Hz, Xanth-C*H*^{1}), 3.55 (sept, 4H, $^3J_{H,H}$ 6.84 Hz, ortho-C*H*Me₂), 2.86 (sept, 2H, $^3J_{H,H}$ 6.93 Hz, para-C*H*Me₂), 1.61 (s, 6H, C*Me₂*), 1.25 (d, 12H, $^3J_{H,H}$ 6.9 Hz, para-CH*Me₂*), 1.24 (d, 12H, $^3J_{H,H}$ 6.8 Hz, **A**-ortho-CH*Me₂*), 1.10 (s, 18H, C*Me₃*), 1.00 (d, 12H, $^3J_{H,H}$ 6.8 Hz, **B**-ortho-CH*Me₂*), -0.39 (s, 18H, $LaCH_2Si$*Me₃*), -1.17 (br. s, 4H, LaC*H₂*SiMe₃)

^{13}C NMR (d_8-THF, 126 MHz): δ 149.03 (Xanth-*C*^{4}), 146.12 (ortho-*C*CHMe₂), 145.20 (Xanth-*C*^{2}), 143.09 (para-*C*CHMe₂), 142.71 (Ar-C_{ipso}), 142.38 (Xanth-*C*^{11}), 129.52 (Xanth-*C*^{10}), 121.70 (Ar-*C*H), 107.97 (Xanth-*C*^{1}H), 102.90 (Xanth-*C*^{3}H), 48.35 (La*C*H₂SiMe₃), 35.30 (*C*Me₃), 35.07 (para-*C*HMe₂), 34.93

(Xanth-C^9Me$_2$), 32.04 (C*Me$_3$*), 30.56 (C*Me$_2$*), 28.21 (ortho-*C*HMe$_2$), 26.39 (**B**-ortho-CH*Me$_2$*), 25.58 (**A**-ortho-CH*Me$_2$*), 24.71 (para-CH*Me$_2$*), 4.51 (La-CH$_2$Si*Me$_3$*) Anal. Calcd. For [Li(THF)$_3$][(XN$_2$)La(CH$_2$SiMe$_3$)$_2$]·Toluene·LiCl, $C_{80}H_{128}N_2O_4Si_2La_1Li_2Cl_1$: C, 67.36; H, 9.04; N, 2.24 %. Found: C, 66.98; H, 8.63; N, 2.53 %.

7.5 Synthetic Procedures and Characterization Pertaining to the Work of Chapter 5

[(XN$_2$)Zr(NMe$_2$)$_2$]·(O(SiMe$_3$)$_2$)$_{0.5}$ (15·(O(SiMe$_3$)$_2$)$_{0.5}$)

H$_2$XN$_2$ (1.5 g, 1.98 mmol) was dissolved in 14 mL of toluene and added to [Zr(NMe$_2$)$_4$] (1.58 g, 5.94 mmol) which was then stirred at 110 °C in a sealed Schlenk flask for 14 days. The solvent was removed *in vacuo* and the brown solid was heated at 90 °C to remove excess [Zr(NMe$_2$)$_4$] by sublimation. The remaining product was recrystalized from O(SiMe$_3$)$_2$ at –30 °C yielding [(XN$_2$)Zr(NMe$_2$)$_2$]·(O(SiMe$_3$)$_2$)$_{0.5}$ as a brown solid (1.46 g, 73 %).

^{1}H NMR (C$_6$D$_6$, 600 MHz): δ 7.28 (s, 4H, Ar-*H*), 6.82 (d, 2H, $^4J_{H,H}$ 1.96 Hz, Xanth-C*H*^{1}), 6.25 (d, 2H, $^4J_{H,H}$ 1.96 Hz, Xanth-C*H*^{3}), 3.57 (sept, 4H, $^3J_{H,H}$ 6.86 Hz, ortho-C*H*Me$_2$), 2.88 (sept, 2H, $^3J_{H,H}$ 6.86 Hz, para-C*H*Me$_2$), 2.62 (br. s, 12H, Zr(N*Me$_2$*)$_2$), 1.60 (s, 6H, C*Me$_2$*), 1.30 (d, 12H, $^3J_{H,H}$ 6.86 Hz, **A**-ortho-CH*Me$_2$*), 1.26 (d, 12H, $^3J_{H,H}$ 6.86 Hz, para-CH*Me$_2$*), 1.25 (d, 12H, $^3J_{H,H}$ 6.86 Hz, **B**-ortho-CH*Me$_2$*), 1.24 (s, 18H, C*Me$_3$*)

^{13}C NMR (C$_6$D$_6$, 126 MHz): δ 148.13 (Xanth-C^2), 147.17 (Xanth-C^4), 146.36 (para-*C*CHMe$_2$), 146.26 (ortho-*C*CHMe$_2$), 140.86 (Ar-C_{ipso}), 139.66

(Xanth-C^{11}), 130.11 (Xanth-C^{10}), 122.09 (Ar-*C*H), 109.81 (Xanth-C^{3}H), 108.53 (Xanth-C^{1}H), 42.37 (Zr(N*Me₂*)₂), 35.56 (Xanth-C^{9}Me₂), 35.10 (*C*Me₃), 34.57 (para-*C*HMe₂), 31.87 (C*Me₃*), 30.23 (C*Me₂*), 28.55 (ortho-*C*HMe₂), 26.01 (**B**-ortho-CH*Me₂*), 24.79 (**A**-ortho-CH*Me₂*), 24.41 (para-CH*Me₂*) Anal. Calcd. For $[(XN_2)Zr(NMe_2)_2]\cdot(O(SiMe_3)_2)_{0.5}$, $C_{60}H_{95}N_4O_{1.5}Si_1Zr_1$: C, 70.95; H, 9.42; N, 5.51 %. Found: C, 70.99; H, 9.23; N, 5.47 %.

$[(XN_2)ZrMe_2]$ (16)

$[(XN_2)Zr(NMe_2)_2]\cdot(O(SiMe_3)_2)_{0.5}$ (0.095 g, 0.093 mmol) was dissolved in 2 mL of benzene, to which $AlMe_3$ (0.067 g, 0.935 mmol) was added and the solution was stirred at 24 °C in a sealed Schlenk flask for 7 days. The solvent was removed *in vacuo* and the yellow solid was recrystalized from a concentrated pentane solution cooled to –30 °C, yielding yellow crystals of **16** (0.051 g, 62 %).

^{1}H NMR (C_6D_6, 600 MHz): δ 7.33 (s, 4H, Ar-*H*), 6.84 (d, 2H, $^{4}J_{H,H}$ 1.84 Hz, Xanth-CH^{1}), 6.24 (d, 2H, $^{4}J_{H,H}$ 1.87 Hz, Xanth-CH^{3}), 3.72 (sept, 4H, $^{3}J_{H,H}$ 6.72 Hz, ortho-C*H*Me₂), 2.85 (sept, 2H, $^{3}J_{H,H}$ 6.89 Hz, para-C*H*Me₂), 1.47 (s, 6H, C*Me₂*), 1.43 (d, 12H, $^{3}J_{H,H}$ 6.88 Hz, **A**-ortho-CH*Me₂*), 1.23 (d, 12H, $^{3}J_{H,H}$ 6.87 Hz, para-CH*Me₂*), 1.22 (s, 18H, C*Me₃*), 1.20 (d, 12H, $^{3}J_{H,H}$ 6.70 Hz, **B**-ortho-CH*Me₂*), 0.78 (s, 6H, Zr*Me₂*)

^{13}C NMR (C_6D_6, 126 MHz): δ 148.48 (Xanth-C^{2}), 148.02 (para-*C*CHMe₂), 146.88 (ortho-*C*CHMe₂), 145.86 (Xanth-C^{4}), 140.28 (Xanth-C^{11}), 137.01 (Ar-C_{ipso}), 128.94 (Xanth-C^{10}), 122.84 (Ar-*C*H), 110.90 (Xanth-C^{1}H), 109.79 (Xanth-C^{3}H), 50.02 (Zr*Me₂*), 35.10 (*C*Me₃), 35.09 (Xanth-C^{9}Me₂), 34.50 (para-*C*HMe₂), 31.70 (C*Me₃*), 31.42 (C*Me₂*), 29.01 (ortho-*C*HMe₂), 26.86 (**B**-ortho-

CH*Me₂*), 24.68 (**A**-ortho-CH*Me₂*), 24.24 (para-CH*Me₂*) Anal. Calcd. For $C_{55}H_{80}N_2O_1Zr_1$: C, 75.37; H, 9.20; N, 3.19 %. Found: C, 75.03; H, 8.88; N, 3.08 %.

[(XN$_2$)ZrCl$_2$] (17)

[(XN$_2$)Zr(NMe$_2$)$_2$]·(O(SiMe$_3$)$_2$)$_{0.5}$ (0.15 g, 0.147 mmol) was dissolved in 6 mL of benzene, to which Me$_3$SiCl (0.04 g, 0.369 mmol) was added and the solution was stirred at 24 °C in a sealed Schlenk flask for 14 days. The solvent was removed *in vacuo* and the yellow solid was recrystalized from a concentrated pentane solution cooled to –30 °C yielding [(XN$_2$)ZrCl$_2$] as a bright yellow powder (0.086 g, 64 %).

^{1}H NMR (C$_6$D$_6$, 600 MHz): δ 7.29 (s, 4H, Ar-*H*), 6.89 (d, 2H, $^4J_{\mathrm{H,H}}$ 1.96 Hz, Xanth-C*H′*), 6.22 (d, 2H, $^4J_{\mathrm{H,H}}$ 1.96 Hz, Xanth-C*H″*), 3.67 (sept, 4H, $^3J_{\mathrm{H,H}}$ 6.68 Hz, ortho-C*H*Me$_2$), 2.79 (sept, 2H, $^3J_{\mathrm{H,H}}$ 6.86 Hz, para-C*H*Me$_2$), 1.56 (d, 12H, $^3J_{\mathrm{H,H}}$ 6.80 Hz, **A**-ortho-CH*Me₂*), 1.35 (s, 6H, C*Me₂*), 1.18 (s, 18H, C*Me₃*), 1.17 (d, 12H, $^3J_{\mathrm{H,H}}$ 6.86 Hz, para-CH*Me₂*), 1.14 (d, 12H, $^3J_{\mathrm{H,H}}$ 6.72 Hz, **B**-ortho-CH*Me₂*)

^{13}C NMR (C$_6$D$_6$, 126 MHz): δ 149.46 (Xanth-C^2), 149.07 (para-*C*CHMe$_2$), 146.08 (ortho-*C*CHMe$_2$), 136.75 (Ar-C_{ipso}), 130.21 (Xanth-C^{10}), 123.15 (Ar-*C*H), 112.43 (Xanth-*C′*H), 109.77 (Xanth-*C″*H), 35.58 (Xanth-C^9Me$_2$), 35.17 (*C*Me$_3$), 34.43 (para-*C*HMe$_2$), 31.64 (C*Me₃*), 30.09 (C*Me₂*), 29.24 (ortho-*C*HMe$_2$), 26.58 (**B**-ortho-CH*Me₂*), 24.90 (**A**-ortho-CH*Me₂*), 24.11 (para-CH-*Me₂*) Anal. Calcd. For $C_{53}H_{74}N_2O_1Zr_1Cl_2$: C, 69.39; H, 8.13; N, 3.05 %. Found: C, 68.89; H, 8.02; N, 3.44 %.

[(XN$_2$)ZrMe][MeB(C$_6$F$_5$)$_3$] (18)

[$(XN_2)ZrMe_2$] (0.075 g, 0.085 mmol) was dissolved in 1.5 mL of toluene, to which $B(C_6F_5)_3$ (0.044 g, 0.085 mmol) was added and the solution was stirred at 24 °C for 5 min. The toluene solution was then layered with pentane (5 mL) and cooled to –30 °C, which yielded bright yellow crystals of [$(XN_2)ZrMe$][Me-$B(C_6F_5)_3$] (0.091 g, 77 %).

^{1}H NMR (C_6D_6, 600 MHz): δ 7.24 (d, 2H, $^4J_{\mathrm{H,H}}$ 1.8 Hz, Ar-*H′*), 7.20 (d, 2H, $^4J_{\mathrm{H,H}}$ 1.7 Hz, Ar-*H″*), 6.92 (d, 2H, $^4J_{\mathrm{H,H}}$ 1.8 Hz, Xanth-C*H′*), 6.15 (br. s, 2H, Xanth-C*H″*), 3.48 (br. sept, 2H, **A**-ortho-C*H*Me$_2$), 2.71 (sept, 2H, $^3J_{\mathrm{H,H}}$ 6.8 Hz, para-C*H*Me$_2$), 2.67 (sept, 2H, $^3J_{\mathrm{H,H}}$ 6.8 Hz, **B**-ortho-C*H*Me$_2$), 1.87 (br. s, 3H, Zr-*Me*), 1.80 (br. s, 3H, B-*Me*), 1.55 (d, 6H, $^3J_{\mathrm{H,H}}$ 6.1 Hz, **A**-ortho-CH*Me$_2$′*), 1.35 (s, 3H, C*Me$_2$′*), 1.30 (s, 3H, C*Me$_2$″*), 1.11 (s, 18H, C*Me$_3$*), 1.09 (d, 12H, $^3J_{\mathrm{H,H}}$ 6.8 Hz, para-CH*Me$_2$*), 1.06 (d, 6H, $^3J_{\mathrm{H,H}}$ 6.6 Hz, **A**-ortho-CH*Me$_2$″*), 0.91 (d, 6H, $^3J_{\mathrm{H,H}}$ 6.5 Hz, **B**-ortho-CH*Me$_2$′*), 0.68 (br. d, 6H, **B**-ortho-CH*Me$_2$″*)

^{13}C NMR (C_6D_6, 126 MHz): δ 151.45 (Xanth-*C^2*), 150.03 (para-*C*CHMe$_2$), 148.38 (**A**-ortho-*C*CHMe$_2$), 144.60 (**B**-ortho-*C*CHMe$_2$), 141.74 (Xanth-*C^{11}*), 130.96 (Ar-C_{ipso}), 130.15 (Xanth-*C^{10}*), 125.15 (Ar-*C*H′), 123.64 (Ar-*C*H″), 113.86 (Xanth-*C′*H), 110.08 (Xanth-*C″*H), 55.56 (Zr-*Me*), 35.50 (Xanth-*C^9*Me$_2$), 35.34 (*C*Me$_3$), 35.20 (br., B-*Me*), 35.18 (C*Me$_2$″*), 34.28 (para-*C*HMe$_2$), 31.49 (C*Me$_3$*), 30.59 (**B**-ortho-*C*HMe$_2$), 28.64 (**A**-ortho-*C*HMe$_2$), 26.98 (**A**-ortho-CH*Me$_2$″*), 26.40 (**B**-ortho-CH*Me$_2$′*), 24.82 (C*Me$_2$′*), 24.13 (**A**-ortho-CH*Me$_2$′*), 23.51 (para-CH*Me$_2$*), 23.05 (**B**-ortho-CH*Me$_2$″*)

^{19}F NMR (C_6D_6, 188 MHz): δ -129.1 (d, $^3J_{\mathrm{F,F}}$ 21.8 Hz, ortho-C_6F_5, -158.67 (t, $^3J_{\mathrm{F,F}}$ 20.6 Hz, para-C_6F_5), -162.26 (br. t, meta-C_6F_5)

Anal. Calcd. For $C_{73}H_{80}N_2O_1Zr_1B_1F_{15}$: C, 63.15; H, 5.80; N, 2.02 %. Found: C, 63.67; H, 6.00; N, 2.12 %.

[(XN$_2$)ZrMe(arene)][B(C$_6$F$_5$)$_4$] (arene = benzene, toluene or bromobenzene) (19)

[(XN$_2$)ZrMe](η^6-benzene)[B(C$_6$F$_5$)$_4$] (19a)

[(XN$_2$)ZrMe$_2$] (0.075 g, 0.085 mmol) was dissolved in 1.5 mL of C_6D_6, to which [CPh$_3$][B(C$_6$F$_5$)$_4$] (0.080 g, 0.085 mmol) was added and the solution was stirred at 24 °C for 5 min.

^{1}H NMR (C_6D_6, 600 MHz): δ 7.28 (br. s, 2H, Ar-*H′*), 7.27 (br. s, 2H, Ar-*H″*), 6.90 (d, 2H, $^4J_{H,H}$ 1.7 Hz, Xanth-C*H′*), 5.84 (d, 2H, $^4J_{H,H}$ 1.9 Hz, Xanth-C*H″*), 2.93 (sept, 2H, $^3J_{H,H}$ 6.8 Hz, para-C*H*Me$_2$), 2.85 (sept, 2H, $^3J_{H,H}$ 6.9 Hz, **A**-ortho-C*H*Me$_2$), 2.80 (sept, 2H, $^3J_{H,H}$ 6.8 Hz, **B**-ortho-C*H*Me$_2$), 1.34 (s, 3H, C*Me$_2$′*), 1.32 (s, 3H, C*Me$_2$″*), 1.31 (d, 6H, $^3J_{H,H}$ 6.9 Hz, **A**-ortho-CH*Me$_2$′*), 1.30 (d, 12H, $^3J_{H,H}$ 6.9 Hz, para-CH*Me$_2$*), 1.28 (d, 6H, $^3J_{H,H}$ 6.9 Hz, **B**-ortho-CH*Me$_2$′*), 1.09 (s, 18H, C*Me$_3$*), 0.99 (d, 6H, $^3J_{H,H}$ 6.8 Hz, **A**-ortho-CH*Me$_2$″*), 0.91 (s, 3H, Zr-*Me*), 0.81 (d, 6H, $^3J_{H,H}$ 6.8 Hz, **B**-ortho-CH*Me$_2$″*)

^{13}C NMR (C_6D_6, 126 MHz): δ 150.57 (para-*C*CHMe$_2$), 149.30 (Xanth-*C^2*), 145.79 (Ar-*C$_{ipso}$*), 145.12 (**A**-ortho-*C*CHMe$_2$), 142.78 (**B**-ortho-*C*CHMe$_2$), 141.15 (Xanth-*C^{11}*), 130.17 (Xanth-*C^{10}*), 123.61 (Ar-*C*H′), 122.98 (Ar-*C*H″), 114.13 (Xanth-*C′*H), 111.53 (Xanth-*C″*H), 43.53 (Zr-*Me*), 36.36 (C*Me$_2$″*), 35.07 (*C*Me$_3$), 35.01 (Xanth-*C^9*Me$_2$), 34.57 (para-*C*HMe$_2$), 31.29 (C*Me$_3$*), 30.05 (**B**-ortho-*C*HMe$_2$), 28.23 (**A**-ortho-*C*HMe$_2$), 26.53 (**B**-ortho-CH*Me$_2$″*), 26.43 (**A**-ortho-CH*Me$_2$″*), 24.37 (C*Me$_2$′*), 23.98 (para-CH*Me$_2$*), 23.66 (**A**-ortho-CH*Me$_2$′*), 23.32 (**B**-ortho-CH*Me$_2$′*)

^{19}F NMR (C_6D_6, 188 MHz): δ -130.02 (br. d, ortho-C_6F_5), -160.67 (t, $^3J_{F,F}$ 22.2 Hz, para-C_6F_5), -164.46 (br. t, $^3J_{F,F}$ 18.8 Hz, meta-C_6F_5)

[(XN$_2$)ZrMe](η^6-toluene)[B(C$_6$F$_5$)$_4$] (19b)

[(XN_2)$ZrMe_2$] (0.075 g, 0.085 mmol) was dissolved in 1.5 mL of toluene, to which [CPh_3][B(C_6F_5)$_4$] (0.080 g, 0.085 mmol) was added and the solution was stirred at 24 °C for 5 min. The toluene solution was then layered with pentane (5 mL) and cooled to –30 °C, which yielded bright red crystals of [(XN_2)ZrMe](η^6-toluene)[B(C_6F_5)$_4$] (0.118 g, 84 %). Selected NMR data is provided below.

^{1}H NMR (d_8-Tol, 600 MHz, 300K): δ 0.84 (s, 3H, Zr-*Me*). ^{1}H NMR (C_6D_5Br, 500 MHz, 248 K): δ 7.26 (m, 1H, Coord. Toluene C*H-p*), 6.97 (s, 2H, Xanth-C*H″*), 6.80 (d, 2H, $^3J_{H,H}$ 7.21 Hz, Coord. Toluene C*H-o*), 6.21 (m, 2H, Coord. Toluene C*H-m*), 5.71 (s, 2H, Xanth-C*H′*), 2.23 (s, 3H, Coord. Toluene CH_3).

Anal. Calcd. For $C_{85}H_{85}N_2O_1Zr_1B_1F_{20}$: C, 62.53; H, 5.25; N, 1.71 %. Found: C, 59.29; H, 5.10; N, 1.77 %. (Crystals of this compound rapidly decompose to multiple unidentified products when the crystallization supernatant is removed, and consequently, a successful elemental analysis could not be obtained even after multiple attempts).

[(XN$_2$)ZrMe](bromobenzene)[B(C$_6$F$_5$)$_4$] (19c)

[(XN_2)$ZrMe_2$] (0.075 g, 0.085 mmol) was dissolved in 1.5 mL of C_6D_5Br, to which [CPh_3][B(C_6F_5)$_4$] (0.080 g, 0.085 mmol) was added and the solution was stirred at 24 °C for 5 min. Selected NMR data is provided below.

^{1}H NMR (C_6D_5Br, 500 MHz, 300 K): δ 6.13 (br. s, 2H, Xanth-CH'). ^{1}H NMR (C_6D_5Br, 500 MHz, 248 K): δ 7.06 (br. s, 1.3H, Isomer A Xanth-CH''), 6.98 (br. s, 0.7H, Isomer B Xanth-CH''), 6.23 (s, 1.3H, Isomer A Xanth-CH'), 5.80 (s, 0.7H, Isomer B Xanth-CH').

General Procedure for Intramolecular Hydroamination In the glove box, a d_8-Toluene solution of [(XN_2)$ZrMe_2$] (**16**); or a C_6D_6 solution of [(XN_2)-$ZrMe_2$] (5 mg, 0.0057 mmol) with 1 equivalent of either $B(C_6F_5)_3$ or [CPh_3][B-(C_6F_5)$_4$] was prepared and added to the hydroamination substrate (dissolved in C_6D_6 or d_8-Toluene), and placed in a teflon-valved J-Young NMR tube. The reactions were monitored at 24 °C or 110 °C by ^{1}H NMR spectroscopy and the organic products were confirmed by their agreement to reported literature spectra.[271]

General Procedure for Ethylene Polymerization In the glove box 5 mg (0.0057 mmol) of [(XN_2)$ZrMe_2$] was dissolved in approx. 4.75 mL (approx. 1.2 mM) of toluene and 1 equivalent of either $B(C_6F_5)_3$ or [CPh_3][B(C_6-F_5)$_4$] was added and the solution was allowed to react for 5 min at 24 °C. The solution was briefly evacuated before placing the flask under dynamic ethylene (1 atm) and the solution was allowed to react for the designated period of time. In the case of high temperature polymerization, the solution was placed in a preheated oil bath (80 °C) before opening to ethylene. After the specified period of time, the solution was opened to air and acidified methanol (10 % HCl) was added. The polyethylene solid was filtered, washed with methanol and acetone and then dried in a 40 °C oven and weighed to obtain the yield.

[(XN_2)Hf(NMe_2)$_2$]·(O($SiMe_3$)$_2$)$_{0.5}$ (20·(O($SiMe_3$)$_2$)$_{0.5}$)

H_2XN_2 (0.1 g, 0.132 mmol) was dissolved in 3 mL of toluene and added to $[Hf(NMe_2)_4]$ (0.14 g, 0.396 mmol) which was then stirred at 110 °C in a sealed Schlenk flask for 14 days. The solvent was removed *in vacuo* and the brown solid was heated at 90 °C to remove excess $[Hf(NMe_2)_4]$ by sublimation. The remaining product was recrystalized from $O(SiMe_3)_2$ at –30 °C yielding $[(XN_2)Hf(NMe_2)_2]\cdot(O(SiMe_3)_2)_{0.5}$ as a brown solid (0.058 g, 40 %).

^{1}H NMR (C_6D_6, 600 MHz): δ 7.29 (s, 4H, Ar-*H*), 6.80 (d, 2H, $^4J_{H,H}$ 1.93 Hz, Xanth-C*H*^{1}), 6.27 (d, 2H, $^4J_{H,H}$ 1.93 Hz, Xanth-C*H*^{3}), 3.61 (sept, 4H, $^3J_{H,H}$ 6.8 Hz, ortho-C*H*Me$_2$), 2.88 (sept, 2H, $^3J_{H,H}$ 6.8 Hz, para-C*H*Me$_2$), 2.69 (br. s, 12H, Hf(N*Me$_2$*)$_2$), 1.58 (s, 6H, C*Me$_2$*), 1.33 (d, 12H, $^3J_{H,H}$ 6.8 Hz, **A**-ortho-CH*Me$_2$*), 1.26 (d, 12H, $^3J_{H,H}$ 6.8 Hz, para-CH*Me$_2$*), 1.25 (d, 12H, $^3J_{H,H}$ 6.8 Hz, **B**-ortho-CH*Me$_2$*), 1.24 (s, 18H, C*Me$_3$*)

^{13}C NMR (C_6D_6, 126 MHz): δ 148.37 (Xanth-*C^2*), 147.62 (Xanth-*C^4*), 146.39 (para-*C*CHMe$_2$), 146.39 (ortho-*C*CHMe$_2$), 141.08 (Ar-*C$_{ipso}$*), 139.88 (Xanth-*C^{11}*), 130.24 (Xanth-*C^{10}*), 122.07 (Ar-*C*H), 110.67 (Xanth-*C^3*H), 108.55 (Xanth-*C^1*H), 42.14 (Hf(N*Me$_2$*)$_2$), 35.58 (Xanth-*C^9*Me$_2$), 35.13 (*C*Me$_3$), 34.55 (para-*C*HMe$_2$), 31.86 (C*Me$_3$*), 30.16 (C*Me$_2$*), 28.54 (ortho-*C*HMe$_2$), 26.07 (**B**-ortho-CH*Me$_2$*), 24.79 (**A**-ortho-CH*Me$_2$*), 24.42 (para-CH*Me$_2$*)

Anal. Calcd. For $[(XN_2)Hf(NMe_2)_2]\cdot(O(SiMe_3)_2)_{0.5}$, $C_{60}H_{95}N_4O_{1.5}Si_1Hf_1$: C, 65.33; H, 8.68; N, 5.07 %. Found: C, 65.30; H, 8.71; N, 5.05 %.

Bibliography

[1] Voncken, J. *The Rare Earth Elements An Introduction* (Springer International Publishing, Switzerland, **2016**).

[2] Housecroft, C. E.; Sharpe, A. G. *Inorganic Chemistry* (Pearson Education Limited, Essex, England, **2005**), 2nd ed.

[3] MacDonald, M. R.; Bates, J. E.; Ziller, J. W.; Furche, F.; Evans, W. J. *J. Am. Chem. Soc.* **2013**. *135*, 9857.

[4] Thompson, M. E.; Baxter, S. M.; Bulls, A. R.; Burger, B. J.; Nolan, M. C.; Santarsiero, B. D.; Schaefer, W. P.; Bercaw, J. E. *J. Am. Chem. Soc.* **1987**. *109*, 203.

[5] Elschenbroich, C. *Organometallics* (Wiley-VCH, Weinheim, Germany, **2006**), third completely revised and extended ed.

[6] Shannon, R. D. *Acta Cryst.* **1976**. *A32*, 751.

[7] Moulton, C. J.; Shaw, B. L. *J. Chem. Soc., Dalton Trans.* **1976**. 1020.

[8] Hackett, J. *Warfare in the Ancient World* (Sidgwick and Jackson Limited, New York, United States of America, **1989**).

[9] vanKoten, G.; Milstein, D. *Organometallic Pincer Chemistry* (Springer-Verlag Berlin Heidelberg, **2013**).

[10] OReilly, M. E.; Veige, A. S. *Chem. Soc. Rev.* **2014**. *43*, 6325.

[11] Wicker, B. F.; Pink, M.; Mindiola, D. J. *Dalton Trans.* **2011**. *40*, 9020.

[12] Piers, W. E.; Emslie, D. J. H. *Coord. Chem. Rev.* **2002**. *233*, 131.

[13] van Koten, G.; Gebbink, R. K. *Dalton Trans.* **2011**. *40*, 8731.

[14] Graf, D. D.; Schrock, R. R.; Davis, W. M.; Stumpf, R. *Organometallics* **1999**. *18*, 843.

[15] Schrock, R. R.; Schattenmann, F.; Aizenberg, M.; Davis, W. M. *Chem. Commun.* **1998**. 199.

[16] Li, G.; Zuccaccia, C.; Tedesco, C.; DAuria, I.; Macchioni, A.; Pellecchia, C. *Chem. Eur. J.* **2014**. *20*, 232.

[17] Luconi, L.; Klosin, J.; Smith, A. J.; Germain, S.; Schulz, E.; Hannedouche, J.; Giambastiani, G. *Dalton Trans.* **2013**. *42*, 16056.

[18] Estler, F.; Eickerling, G.; Herdtweck, E.; Anwander, R. *Organometallics* **2003**. *22*, 1212.

[19] Cruz, C. A.; Emslie, D. J. H.; Harrington, L. E.; Britten, J. F.; Robertson, C. M. *Organometallics* **2007**. *26*, 692.

[20] Cruz, C. A.; Emslie, D. J. H.; Harrington, L. E.; Britten, J. F. *Organometallics* **2008**. *27*, 15.

[21] Cruz, C. A.; Emslie, D. J. H.; Robertson, C. M.; Harrington, L. E.; Jenkins, H. A.; Britten, J. F. *Organometallics* **2009**. *28*, 1891.

[22] Cruz, C. A.; Emslie, D. J. H.; Jenkins, H. A.; Britten, J. F. *Dalton Trans.* **2010**. *39*, 6626.

[23] Vidjayacoumar, B.; Ilango, S.; Ray, M. J.; Chu, T.; Kolpin, K. B.; Andreychuk, N. R.; Cruz, C. A.; Emslie, D. J. H.; Jenkins, H. A.; Britten, J. F. *Dalton Trans.* **2012**. *41*, 8175.

[24] Andreychuk, N. R.; Ilango, S.; Vidjayacoumar, B.; Emslie, D. J. H.; Jenkins, H. A. *Organometallics* **2013**. *32*, 1466.

[25] Andreychuk, N. R.; Emslie, D. J. H. *Angew. Chem. Int. Ed.* **2013**. *52*, 1696.

[26] Aizenberg, M.; Turculet, L.; Davis, W. M.; Schattenmann, F.; Schrock, R. R. *Organometallics* **1998**. *17*, 4795.

[27] Schrock, R. R.; Baumann, R.; Reid, S. M.; Goodman, J. T.; Stumpf, R.; Davis, W. M. *Organometallics* **1999**. *18*, 3649.

[28] Flores, M. A.; Manzoni, M. R.; Baumann, R.; Davis, W. M.; Schrock, R. R. *Organometallics* **1999**. *18*, 3220.

[29] Baumann, R.; Davis, W. M.; Schrock, R. R. *J. Am. Chem. Soc.* **1997**. *119*, 3830.

[30] Graf, D. D.; Davis, W. M.; Schrock, R. R. *Organometallics* **1998**. *17*, 5820.

[31] Guérin, F.; McConville, D. H.; Vittal, J. J. *Organometallics* **1996**. *15*, 5586.

[32] Zimmermann, M.; Estler, F.; Herdtweck, E.; Törnroos, K. W.; Anwander, R. *Organometallics* **2007**. *26*, 6029.

[33] Tonks, I. A.; Tofan, D.; Weintrob, E. C.; Agapie, T.; Bercaw, J. E. *Organometallics* **2012**. *31*, 1965.

[34] Friedrich, S.; Schubart, M.; Gade, L. H.; Scowen, I. J.; Edwards, A. J.; McPartlin, M. *Chem. Ber. Rec.* **1997**. *130*, 1751.

[35] Mehrkhodavandi, P.; Schrock, R. R.; Peter J. Bonitatebus, J. *Organometallics* **2002**. *21*, 5785.

[36] Mehrkhodavandi, P.; Bonitatebus, P. J.; Schrock, R. R. *J. Am. Chem. Soc.* **2000**. *122*, 7841.

[37] Batke, S.; Kothe, T.; Haas, M.; Wadepohl, H.; Ballmann, J. *Dalton Trans.* **2016**. *45*, 3528.

[38] Ménard, G.; Jong, H.; Fryzuk, M. D. *Organometallics* **2009**. *28*, 5253.

[39] Winston, M. S.; Bercaw, J. E. *Organometallics* **2010**. *29*, 6408.

[40] Turculet, L.; McDonald, R. *Organometallics* **2007**. *26*, 6821.

[41] Ritch, J. S.; Julienne, D.; Rybchinski, S. R.; Brockman, K. S.; Johnson, K. R. D.; Hayes, P. G. *Dalton Trans.* **2014**. *43*, 267.

[42] Müller, T. E.; Hultzsch, K. C.; Yus, M.; Foubelo, F.; Tada, M. *Chem. Rev.* **2008**. *108*, 3795.

[43] Reznichenko, A. L.; Hultzsch, K. C. *Top. Organomet. Chem.* **2011**. *43*, 51.

[44] Rodriguez-Ruiz, V.; Carlino, R.; Bezzenine-Lafollée, S.; Gil, R.; Prim, D.; Schulz, E.; Hannedouche, J. *Dalton Trans.* **2015**. *44*, 12029.

[45] Jung, M. E.; Piizzi, G. *Chem. Rev.* **2005**. *105*, 1735.

[46] Beesley, R. M.; Ingold, C. K.; Thorpe, J. F. *J. Chem. Soc.* **1915**. *107*, 1080.

[47] Baldwin, J. E. *J. Chem. Soc. Chem. Commun.* **1976**. 734.

[48] Crimmin, M. R.; Arrowsmith, M.; Barrett, A. G. M.; Casely, I. J.; Hill, M. S.; Procopiou, P. A. *J. Am. Chem. Soc.* **2009**. *131*, 9670.

[49] Hong, S.; Marks, T. J. *Acc. Chem. Res.* **2004**. *37*, 673.

[50] Reznichenko, A. L.; Nawara-Hultzsch, A. J.; Hultzsch, K. C. *Top. Curr. Chem.* **2014**. *343*, 191.

[51] Trifonov, A. A.; Basalov, I. V.; Kissel, A. A. *Dalton Trans.* **2016**. *45*, 19172.

[52] Stanlake, L. J. E.; Schafer, L. L. *Organometallics* **2009**. *28*, 3990.

[53] Gagné, M. R.; Marks, T. J. *J. Am. Chem. Soc.* **1989**. *111*, 4109.

[54] Gagné, M. R.; Stern, C. L.; Marks, T. J. *J. Am. Chem. Soc.* **1992**. *114*, 275.

[55] Bürgstein, M. R.; Berberich, H.; Roesky, P. W. *Organometallics* **1998**. *17*, 1452.

[56] Gribkov, D. V.; Hultzsch, K. C.; Hampel, F. *J. Am. Chem. Soc.* **2006**. *128*, 3748.

[57] Aillaud, I.; Lyubov, D.; Collin, J.; Guillot, R.; Hannedouche, J.; Schulz, E.; Trifonov, A. *Organometallics* **2008**. *27*, 5929.

[58] Lauterwasser, F.; Hayes, P. G.; Piers, W. E.; Schafer, L. L.; Bräse, S. *Adv. Synth. Catal.* **2011**. *353*, 1384.

[59] Hultzsch, K. C.; Gribkov, D. V.; Hampel, F. *J. Organomet. Chem.* **2005**. *690*, 4441.

[60] Hong, S.; Tian, S.; Metz, M. V.; Marks, T. J. *J. Am. Chem. Soc.* **2003**. *125*, 14768.

[61] Reznichenko, A. L.; Hultzsch, K. C. *Organometallics* **2013**. *32*, 1394.

[62] Tian, S.; Arredondo, V. M.; Stern, C. L.; Marks, T. J. *Organometallics* **1999**. *18*, 2568.

[63] Chai, Z.; Chu, J.; Qi, Y.; Tang, M.; Hou, J.; Yang, G. *RSC Adv.* **2017**. *7*, 1759.

[64] Lauterwasser, F.; Hayes, P. G.; Bräse, S.; Piers, W. E.; Schafer, L. L. *Organometallics* **2004**. *23*, 2234.

[65] Li, Y.; Marks, T. J. *J. Am. Chem. Soc.* **1996**. *118*, 9295.

[66] Roux, E. L.; Liang, Y.; Storz, M. P.; Anwander, R. *J. Am. Chem. Soc.* **2010**. *132*, 16368.

[67] Spallek, T.; Anwander, R. *Dalton Trans.* **2016**. *45*, 16393.

[68] Brunner, T. S.; Benndorf, P.; Gamer, M. T.; Knöfel, N.; Gugau, K.; Roesky, P. W. *Organometallics* **2016**. *35*, 3474.

[69] Otero, A.; Lara-Sánchez, A.; Castro-Osma, J. A.; Márquez-Segovia, I.; Alonso-Moreno, C.; Fernández-Baeza, J.; Sánchez-Barba, L. F.; Rodríguezc, A. M. *New J. Chem.* **2015**. *39*, 7672.

[70] Huynh, K.; Anderson, B. K.; Livinghouse, T. *Tetrahedron Lett.* **2015**. *56*, 3658.

[71] Huynh, K.; Livinghouse, T.; Lovick, H. M. *Synlett* **2014**. *25*, 1721.

[72] Trambitas, A. G.; Melcher, D.; Hartenstein, L.; Roesky, P. W.; Daniliuc, C.; Jones, P. G.; Tamm, M. *Inorg. Chem.* **2012**. *51*, 6753.

[73] Otero, A.; Lara-Sánchez, A.; Nájera, C.; Fernández-Baeza, J.; Márquez-Segovia, I.; Castro-Osma, J. A.; Martínez, J.; Sánchez-Barba, L. F.; Rodríguez, A. M. *Organometallics* **2012**. *31*, 2244.

[74] Benndorf, P.; Jenter, J.; Zielke, L.; Roesky, P. W. *Chem. Commun.* **2011**. *47*, 2574.

[75] Vitanova, D. V.; Hampel, F.; Hultzsch, K. C. *J. Organomet. Chem.* **2011**. *696*, 321.

[76] Aillaud, I.; Olier, C.; Chapurina, Y.; Collin, J.; Schulz, E.; Guillot, R.; Hannedouche, J.; Trifonov, A. *Organometallics* **2011**. *30*, 3378.

[77] Ackermann, L.; Bergman, R. G.; Loy, R. N. *J. Am. Chem. Soc.* **2003**. *125*, 11956.

[78] Bexrud, J. A.; Beard, J. D.; Leitch, D. C.; Schafer, L. L. *Org. Lett.* **2005**. *7*, 1959.

[79] Kim, H.; Lee, P. H.; Livinghouse, T. *Chem. Commun.* **2005**. 5205.

[80] Gribkov, D. V.; Hultzsch, K. C. *Angew. Chem. Int. Ed.* **2004**. *43*, 5542.

[81] Müller, T. E.; Beller, M. *Chem. Rev.* **1998**. *98*, 675.

[82] Zi, G. *J. Organomet. Chem.* **2011**. *696*, 68.

[83] Majumder, S.; Odom, A. L. *Organometallics* **2008**. *27*, 1174.

[84] Knight, P. D.; Munslow, I.; O'Shaughnessy, P. N.; Scott, P. *Chem. Commun.* **2004**. 894.

[85] Li, Y.; Marks, T. J. *Organometallics* **1996**. *15*, 3770.

[86] Walsh, P. J.; Baranger, A. M.; Bergman, R. G. *J. Am. Chem. Soc.* **1992**. *114*, 1708.

[87] Johnson, J. S.; Bergman, R. G. *J. Am. Chem. Soc.* **2001**. *123*, 2923.

[88] Heutling, A.; Pohlki, F.; Doye, S. *Chem. Eur. J.* **2004**. *10*, 3059.

[89] Marcseková, K.; Wegener, B.; Doye, S. *Eur. J. Org. Chem.* **2005**. 4843.

[90] Reznichenko, A. L.; Nguyen, H. N.; Hultzsch, K. C. *Angew. Chem. Int. Ed.* **2010**. *49*, 8984.

[91] Ryu, J.-S.; Li, G. Y.; Marks, T. J. *J. Am. Chem. Soc.* **2003**. *125*, 12584.

[92] Hustad, P. D. *Science* **2009**. *325*, 704.

[93] Fawcett, E. W.; Gibson, R. O.; Perrin, M. W.; Patton, J. G.; Williams, E. G. *B Patent* **1937**. 471590.

[94] Natta, G. J. *J. Am. Chem. Soc.* **1955**. *77*, 1708.

[95] Ziegler, K.; Holzkamp, E.; Breil, H.; Martin, H. *Angew. Chem.* **1955**. *67*, 426.

[96] Coates, G. W. *Chem. Rev.* **2000**. *100*, 1223.

[97] Tadmor, Z.; Gogos, C. G. *Principles of Polymer Processing* (Wiley, United States of America, **1979**).

[98] Cossee, P. *J. Catal.* **1964**. *3*, 80.

[99] Arlman, E. J.; Cossee, P. *J. Catal.* **1964**. *3*, 99.

[100] Margl, P.; Deng, L.; Ziegler, T. *J. Am. Chem. Soc.* **1999**. *121*, 154.

[101] Brookhart, M.; Green, M. L. H. *J. Organomet. Chem.* **1983**. *250*, 395.

[102] Chen, E. Y.; Marks, T. J. *Chem. Rev.* **2000**. *100*, 1391.

[103] Pédeutour, J.; Radhakrishnan, K.; Cramail, H.; Deffieux, A. *Macromol. Rapid Commun.* **2001**. *22*, 1095.

[104] Marinescu, S. C.; Agapie, T.; Day, M. W.; Bercaw, J. E. *Organometallics* **2007**. *26*, 1178.

[105] Kenward, A. L.; Piers, W. E.; Parvez, M. *Organometallics* **2009**. *28*, 3012.

[106] Kenward, A. L.; Ross, J. A.; Piers, W. E.; Parvez, M. *Organometallics* **2009**. *28*, 3625.

[107] Hollink, E.; Wei, P.; Stephan, D. W. *Organometallics* **2004**. *23*, 1562.

[108] Bei, X.; Swenson, D. C.; Jordan, R. F. *Organometallics* **1997**. *16*, 3282.

[109] Horton, A. D.; de With, J. *Organometallics* **1997**. *16*, 5424.

[110] Horton, A. D.; de With, J.; van-der Linden, A. J.; van de Weg, H. *Organometallics* **1996**. *15*, 2672.

[111] Tjaden, E. B.; Swenson, D. C.; Jordan, R. F.; Petersen, J. L. *Organometallics* **1996**. *14*, 371.

[112] Krossing, I.; Raabe, I. *Angew. Chem. Int. Ed.* **2004**. *43*, 2066.

[113] Jia, L.; Yang, X.; Ishihara, A.; Marks, T. J. *Organometallics* **1995**. *14*, 3135.

[114] McKnight, A. L.; Waymouth, R. M. *Chem. Rev.* **1998**. *98*, 2587.

[115] Gibson, V. C.; Spitzmesser, S. K. *Chem. Rev.* **2003**. *103*, 283.

[116] Lee, C. H.; La, Y.-H.; Park, J. W. *Organometallics* **2000**. *19*, 344.

[117] Jeon, Y.-M.; Park, S. J.; Heo, J.; Kim, K. *Organometallics* **1998**. *17*, 3161.

[118] Schrock, R. R.; Schattenmann, F.; Aizenberg, M.; Davis, W. M. *Chem. Commun.* **1998**. 199.

[119] Baumann, R.; Stumpf, R.; Davis, W. M.; Liang, L.-C.; Schrock, R. R. *J. Am. Chem. Soc.* **1999**. *121*, 7822.

[120] Nishiura, M.; Hou, Z. *Nat. Chem.* **2010**. *2*, 257.

[121] Hou, Z.; Wakatsuki, Y. *Coord. Chem. Rev.* **2002**. *231*, 1.

[122] Konkol, M.; Okuda, J. *Coord. Chem. Rev.* **2008**. *252*, 1577.

[123] Zeimentz, P. M.; Arndt, S.; Elvidge, B. R.; Okuda, J. *Chem. Rev.* **2006**. *106*, 2404.

[124] Gromada, J.; Carpentier, J.-F.; Mortreux, A. *Coord. Chem. Rev.* **2004**. *248*, 397.

[125] Korobkov, I.; Gambarotta, S. *Organometallics* **2009**. *28*, 4009.

[126] Ihara, E.; Yoshioka, S.; Furo, M.; Katsura, K.; Yasuda, H.; Mohri, S.; Kanehisa, N.; Kai, Y. *Organometallics* **2001**. *20*, 1752.

[127] Fridrichova, A.; Varga, V.; Pinkas, J.; Lamac, M.; Ruzicka, A.; Horacek, M. *Eur. J. Inorg. Chem.* **2016**. 3713.

[128] Ballard, D. G. H.; Courtis, A.; Holton, J.; McMeeking, J.; Pearce, R. *J. Chem. Soc., Chem. Commun.* **1978**. 994.

[129] Watson, P. L. *J. Am. Chem. Soc.* **1982**. *104*, 337.

[130] Watson, P. L.; Parshall, G. W. *Acc. Chem. Res.* **1985**. *18*, 51.

[131] Jeske, G.; Lauke, H.; Mauermann, H.; Swepston, P. N.; Schumann, H.; Marks, T. J. *J. Am. Chem. Soc.* **1985**. *107*, 8091.

[132] Nakayama, Y.; Yasuda, H. *J. Organomet. Chem.* **2004**. *689*, 4489.

[133] Hou, Z.; Luo, Y.; Li, X. *J. Organomet. Chem.* **2006**. *691*, 3114.

[134] Bambirra, S.; van Leusen, D.; Meetsma, A.; Hessen, B.; Teuben, J. H. *Chem. Commun.* **2001**. 637.

[135] Bambirra, S.; van Leusen, D.; Meetsma, A.; Hessen, B.; Teuben, J. H. *Chem. Commun.* **2003**. 522.

[136] Arndt, S.; Spaniol, T. P.; Okuda, J. *Angew. Chem. Int. Ed.* **2003**. *42*, 5075.

[137] Butenschön, H. *Chem. Rev.* **2000**. *100*, 1527.

[138] Siemeling, U. *Chem. Rev.* **2000**. *100*, 1495.

[139] Cruz, C. A.; Emslie, D. J. H. Rigid Non-Carbocyclic Ancillary Ligands in Organothorium Chemistry (McMaster University, Hamilton, Ontario, **2010**).

[140] Seyam, A. M.; Stubbert, B. D.; Jensen, T. R.; ODonnell, J. J.; Stern, C. L.; Marks, T. J. *Inorg. Chim. Acta* **2004**. *357*, 4029.

[141] Newton, A. *J. Am. Chem. Soc.* **1943**. *65*, 2434.

[142] Liu, J.-Y.; Zheng, Y.; Li, Y.-G.; Pan, L.; Li, Y.-S.; Hu, N.-H. *J. Organomet. Chem.* **2005**. *690*, 1233.

[143] Liu, J.; Li, Y.; Li, Y.; Hu, N. *J. Applied Polymer Sci.* **2008**. *109*, 700.

[144] Nowick, J. S.; Ballester, P.; Ebmeyer, F.; Rebek, J. *J. Am. Chem. Soc.* **1990**. *112*, 8902.

[145] Emslie, D. J. H.; Piers, W. E.; Parvez, M.; McDonald, R. *Organometallics* **2002**. *21*, 4226.

[146] Chapurina, Y.; Guillot, R.; Lyubov, D.; Trifonov, A.; Hannedouche, J.; Schulz, E. *Dalton Trans.* **2013**. *42*, 507.

[147] Kissel, A. A.; Mahrova, T. V.; Lyubov, D. M.; Cherkasov, A. V.; Fukin, G. K.; Trifonov, A. A.; Rosal, I. D.; Maron, L. *Dalton Trans.* **2015**. *44*, 12137.

[148] Avent, A. G.; Cloke, F. G. N.; Elvidge, B. R.; Hitchcock, P. B. *Dalton Trans.* **2004**. 1083.

[149] Lu, E. L.; Gan, W.; Chen, Y. F. *Organometallics* **2009**. *28*, 2318.

[150] Hamidi, S.; Jende, L. N.; Dietrich, H. M.; Maichle-Mössmer, C.; Törnroos, K. W.; Deacon, G. B.; Junk, P. C.; Anwander, R. *Organometallics* **2013**. *32*, 1209.

[151] Litlabo, R.; Lee, H. S.; Niemeyer, M.; Törnroos, K. W.; Anwander, R. *Dalton Trans.* **2010**. *39*, 6815.

[152] Schädle, D.; Schädle, C.; Törnroos, K. W.; Anwander, R. *Organometallics* **2012**. *31*, 5101.

[153] Huang, W.; Carver, C. T.; Diaconescu, P. L. *Inorg. Chem.* **2011**. *50*, 978.

[154] Döring, C.; Kempe, R. *Eur. J. Inorg. Chem.* **2009**. 412.

[155] Kaneko, H.; Dietrich, H. M.; Schädle, C.; Maichle-Mössmer, C.; Tsurugi, H.; Törnroos, K. W.; Mashima, K.; Anwander, R. *Organometallics* **2013**. *32*, 1199.

[156] Zimmermann, M.; Törnroos, K. W.; Anwander, R. *Angew. Chem. Int. Ed.* **2008**. *47*, 775.

[157] Zimmermann, M.; Takats, J.; Kiel, G.; Törnroos, K. W.; Anwander, R. *Chem. Commun.* **2008**. 612.

[158] Hild, F.; Neehaul, N.; Bier, F.; Wirsum, M.; Gourlaouen, C.; Dagorne, S. *Organometallics* **2013**. *32*, 587.

[159] Schnitter, C.; Roesky, H. W.; Albers, T.; Schmidt, H.-G.; Röpken, C.; Parisini, E.; Sheldrick, G. M. *Chem. Eur. J.* **1997**. *3*, 1783.

[160] Chakraborty, D.; Chen, E. Y. *Organometallics* **2002**. *21*, 1438.

[161] Stubbert, B. D.; Marks, T. J. *J. Am. Chem. Soc.* **2007**. *129*, 4253.

[162] Ahlbrecht, H.; Fischer, S. *Tetrahedron* **1970**. *26*, 2837.

[163] Tonks, I. A.; Meier, J. C.; Bercaw, J. E. *Organometallics* **2013**. *32*, 3451.

[164] Gribkov, D. V.; Hultzsch, K. C.; Hampel, F. *J. Am. Chem. Soc.* **2006**. *128*, 3748.

[165] Ryu, J.-S.; Yanwu-Li, G.; Marks, T. J. *J. Am. Chem. Soc.* **2003**. *125*, 12584.

[166] Reznichenko, A. L.; Nguyen, H. N.; Hultzsch, K. C. *Angew. Chem. Int. Ed.* **2010**. *49*, 8984.

[167] Motolko, K. S. A.; Emslie, D. J. H.; Jenkins, H. A. *Organometallics* **2017**. *36*, 1601.

[168] Motolko, K. S. A.; Emslie, D. J. H.; Britten, J. F. *RSC Adv.* **2017**. *7*, 27938.

[169] Li, T.; Kaercher, S.; Roesky, P. W. *Chem. Soc. Rev.* **2014**. *43*, 42.

[170] Izod, K.; O'Shaughnessy, P.; Sheffield, J. M.; Clegg, W.; Liddle, S. T. *Inorg. Chem.* **2000**. *39*, 4741.

[171] Blair, S.; Izod, K.; Clegg, W. *J. Organomet. Chem.* **2003**. *688*, 92.

[172] Izod, K.; Liddle, S. T.; Clegg, W.; Harrington, R. W. *Dalton Trans.* **2006**. 3431.

[173] Izod, K.; Liddle, S. T.; McFarlane, W.; Clegg, W. *Organometallics* **2004**. *23*, 2734.

[174] Clegg, W.; Izod, K.; Liddle, S. T.; O'Shaughnessy, P.; Sheffield, J. M. *Organometallics* **2000**. *19*, 2090.

[175] Mazzeo, M.; Lamberti, M.; D'Auria, I.; Milione, S.; Peters, J. C.; Pellecchia, C. *J. Polym. Sci. Pol. Chem.* **2010**. *48*, 1374.

[176] Aspinall, H. C.; Moore, S. R.; Smith, A. K. *J. Chem. Soc. Dalton Trans.* **1993**. 993.

[177] Tardif, O.; Hou, Z.; Nishiura, M.; Koizumi, T.; Wakatsuki, Y. *Organometallics* **2001**. *20*, 4565.

[178] Tardif, O.; Nishiura, M.; Hou, Z. *Tetrahedron* **2003**. *59*, 10525.

[179] Izod, K.; Liddle, S. T.; Clegg, W. *Chem. Commun.* **2004**. 1748.

[180] Chandrasekhar, V.; Sasikumar, P.; Boomishankar, R.; Anantharaman, G. *Inorg. Chem.* **2006**. *45*, 3344.

[181] Whitesides, G.; Eisenhut, M.; Bunting, W. *J. Am. Chem. Soc.* **1974**. *96*, 5398.

[182] Bianco, V.; Doronzo, S. *Inorg. Synth.* **1976**. *16*, 161.

[183] Izod, K.; Stewart, J.; Clark, E. R.; Clegg, W.; Harrington, R. W. *Inorg. Chem.* **2010**. *49*, 4698.

[184] Carmichael, C. D.; Fryzuk, M. D. *Can. J. Chem.* **2010**. *88*, 667.

[185] Chang, Y.-N.; Liang, L.-C. *Inorg. Chim. Acta* **2007**. *360*, 136.

[186] Hao, J.; Wei, X.; Huang, S.; Guo, J.; Liu, D. *Appl. Organometal. Chem.* **2005**. *19*, 1010.

[187] Brauer, D.; Bürger, H.; Liewald, G. *J. Organomet. Chem.* **1986**. *308*, 119.

[188] Lehn, J. M.; Javed, S.; Hoffman, D. M. *Inorg. Chem.* **2007**. *46*, 993.

[189] Brask, J. K.; Chivers, T.; Schatte, G. *Chem. Commun.* **2000**. 1805.

[190] Corrente, A. M.; Chivers, T. *Inorg. Chem.* **2008**. *47*, 10073.

[191] Gardiner, M. G.; Raston, C. L. *Inorg. Chem.* **1996**. *35*, 4047.

[192] Gellermann, E.; Klingebiel, U.; Pape, T.; Antonia, F. D.; Schneider, T. R.; Schmatz, S. *Z. Anorg. Allg. Chem.* **2001**. *627*, 2581.

[193] Li, J.-F.; Weng, L.-H.; Wei, X.-H.; Liu, D.-S. *J. Chem. Soc., Dalton Trans.* **2002**. 1401.

[194] Danièle, S.; Drost, C.; Gehrhus, B.; Hawkins, S. M.; Hitchcock, P. B.; Lappert, M. F.; Merle, P. G.; Bott, S. G. *J. Chem. Soc., Dalton Trans.* **2001**. 3179.

[195] Chivers, T.; Fedorchuk, C.; Schatte, G.; Brask, J. K. *Can. J. Chem.* **2002**. *80*, 821.

[196] Dries, M.; Huttner, G.; Knopf, N.; Pritzkow, H.; Zsolnai, L. *Angew. Chem. Int. Ed. Engl.* **1995**. *34*, 316.

[197] Rabe, G. W.; Kheradmandan, S.; Yap, G. P. A. *Inorg. Chem.* **1998**. *37*, 6541.

[198] Tesh, K. F.; Jones, B. D.; Hanusa, T. P.; Huffman, J. C. *J. Am. Chem. Soc.* **1992**. *114*, 6590.

[199] Westerhausen, M.; Weinrich, S.; Schmid, B.; Schneiderbauer, S.; Suter, M.; Nöth, H.; Piotrowski, H. *Z. Anorg. Allg. Chem.* **2003**. *629*, 625.

[200] Yoshifuji, M.; Shima, I.; Inamoto, N. *J. Am. Chem. Soc.* **1981**. *103*, 4587.

[201] Smit, C. N.; van der Knaap, T. A.; Bickelhaupt, F. *Tetrahedron Lett.* **1983**. *24*, 2031.

[202] Frenzel, C.; Hey-Hawkins, E. *Phosphorus Sulfur Silicon Relat. Elem.* **1998**. *143*, 1.

[203] Tokitoh, N.; Tsurusaki, A.; Sasamori, T. *Phosphorus Sulfur Silicon Relat. Elem.* **2009**. *184*, 979.

[204] Westerhausen, M.; Schniederbauer, S.; Hartmann, M.; Warchhold, M.; Noth, H. *Z. Anorg. Allg. Chem.* **2002**. *628*, 330.

[205] Lv, Y.; Xu, X.; Chen, Y.; Leng, X.; Borzov, M. V. *Angew. Chem. Int. Ed.* **2011**. *50*, 11227.

[206] Yi, W. Y.; Zhang, J.; Hong, L. C.; Chen, Z. X.; Zhou, X. G. *Organometallics* **2011**. *30*, 5809.

[207] Liddle, S. T.; Arnold, P. L. *Dalton Trans.* **2007**. 3305.

[208] Crimmin, M. R.; White, A. J. P. *Chem. Commun.* **2012**. *48*, 1745.

[209] Krieck, S.; Görls, H.; Westerhausen, M. *Inorg. Chem. Commun.* **2009**. *12*, 409.

[210] Westerhausen, M.; Hartmann, M.; Schwarz, W. *Inorg. Chim. Acta* **1998**. *269*, 91.

[211] Cameron, T. M.; Gordon, J. C.; Michalczyk, R.; Scott, B. L. *Chem. Commun.* **2003**. 2282.

[212] Johnson, K. R. D.; Kamenz, B. L.; Hayes, P. G. *Organometallics* **2014**. *33*, 3005.

[213] Qayyum, S.; Skvortsov, G. G.; Fukin, G. K.; Trifonov, A. A.; Kretschmer, W. P.; Döring, C.; Kempe, R. *Eur. J. Inorg. Chem.* **2010**. 248.

[214] Bambirra, S.; Perazzolo, F.; Boot, S. J.; Sciarone, T. J. J.; Meetsma, A.; Hessen, B. *Organometallics* **2008**. *27*, 704.

[215] Aillaud, I.; Lyubov, D.; Collin, J.; Hannedouche, R. G. J.; Schulz, E.; Trifonov, A. *Organometallics* **2008**. *27*, 5929.

[216] Queffelec, C.; Boeda, F.; Pouilhès, A.; Meddour, A.; Kouklovsky, C.; Hannedouche, J.; Collin, J.; Schulz, E. *ChemCatChem* **2011**. *3*, 122.

[217] Kissel, A. A.; Mahrova, T. V.; Lyubov, D. M.; Cherkasov, A. V.; Fukin, G. K.; Trifonov, A. A.; Rosal, I. D.; Maron, L. *Dalton Trans.* **2015**. *44*, 12137.

[218] Alt, H. G.; Köppl, A. *Chem. Rev.* **2000**. *100*, 1205.

[219] Collins, R. A.; Russell, A. F.; Mountford, P. *Appl. Petrochem. Res.* **2015**. *5*, 153.

[220] Matsui, S.; Mitani, M.; Saito, J.; Tohi, Y.; Makio, H.; Matsukawa, N.; Takagi, Y.; Tsuru, K.; Nitabaru, M.; Nakano, T.; Tanaka, H.; Kashiwa, N.; Fujita, T. *J. Am. Chem. Soc.* **2001**. *123*, 6847.

[221] Hayes, P. G.; Piers, W. E.; Parvez, M. *J. Am. Chem. Soc.* **2003**. *125*, 5622.

[222] Hayes, P. G.; Piers, W. E.; Parvez, M. *Chem. Eur. J.* **2007**. *13*, 2632.

[223] Lancaster, S. J.; Robinson, O. B.; Bochmann, M.; Coles, S. J.; Hursthouse, M. B. *Organometallics* **1995**. *14*, 2456.

[224] Gillis, D. J.; Quyoum, R.; Tudoret, M.-J.; Wang, Q.; Jeremic, D.; Roszak, A. W.; Baird, M. C. *Organometallics* **1996**. *15*, 3600.

[225] Altae, A.; Badshah, A.; Khan, N.; Marwat, S.; Ali, S. *J. Coord. Chem.* **2011**. *64*, 1815.

[226] Scollard, J. D.; McConville, D. H.; Payne, N. C.; Vittal, J. J. *Macromolecules* **1996**. *29*, 5241.

[227] Scollard, J. D.; McConville, D. H. *J. Am. Chem. Soc.* **1996**. *118*, 10008.

[228] Chen, Y.-X.; Marks, T. J. *Organometallics* **1997**. *16*, 3649.

[229] Gillis, D. J.; Tudoret, M.; Baird, M. C. *J. Am. Chem. Soc.* **1993**. *115*, 2543.

[230] Wang, Q.; Quyoum, R.; Gillis, D. J.; Tudoret, M.-J.; Jeremic, D.; Hunter, B. K.; Baird, M. C. *Organometallics* **1996**. *15*, 693.

[231] Porter, R. M.; Danopoulos, A. A. *Polyhedron* **2006**. *25*, 859.

[232] Zhu, T.; Wambach, T. C.; Fryzuk, M. D. *Inorg. Chem.* **2011**. *50*, 11212.

[233] Batke, S.; Sietzen, M.; Merz, L.; Wadepohl, H.; Ballmann, J. *Organometallics* **2016**. *35*, 2294.

[234] OShaughnessy, P. N.; Gillespie, K. M.; Morton, C.; Westmoreland, I.; Scott, P. *Organometallics* **2002**. *21*, 4496.

[235] Cortright, S. B.; Huffman, J. C.; Yoder, R. A.; Coalter-III, J. N.; Johnston, J. N. *Organometallics* **2004**. *23*, 2238.

[236] Riley, P. N.; Fanwick, P. E.; Rothwell, I. P. *J. Chem. Soc. Dalton Trans.* **2001**. 181.

[237] Gehrmann, T.; Fillol, J. L.; Wadepohl, H.; Gade, L. H. *Angew. Chem. Int. Ed.* **2009**. *48*, 2152.

[238] Herrmann, H.; Fillol, J. L.; Wadepohl, H.; Gade, L. H. *Angew. Chem. Int. Ed.* **2007**. *46*, 8426.

[239] Normand, A. T.; Daniliuc, C. G.; Wibbeling, B.; Kehr, G.; Gendre, P. L.; Erker, G. *J. Am. Chem. Soc.* **2015**. *137*, 10796.

[240] Gehrmann, T.; Lloret-Fillol, J.; Herrmann, H.; Wadepohl, H.; Gade, L. H. *Organometallics* **2013**. *32*, 3877.

[241] Schrock, R. R.; Casado, A. L.; Goodman, J. T.; Liang, L.-C.; Bonitatebus, P. J.; Davis, W. M. *Organometallics* **2000**. *19*, 5325.

[242] Lee, C. S.; Park, J. H.; Hwang, E. Y.; Park, G. H.; Go, M. J.; Lee, J.; Lee, B. Y. *J. Organomet. Chem.* **2014**. *772-773*, 172.

[243] Tonzetich, Z. J.; Lu, C. C.; Schrock, R. R.; Hock, A. S.; Peter J. Bonitatebus, J. *Organometallics* **2004**. *23*, 4362.

[244] Horton, A. D.; de With, J.; van der Linden, A. J.; van de Weg, H. *Organometallics* **1996**. *15*, 2672.

[245] Yang, X.; Stern, C. L.; Marks, T. J. *J. Am. Chem. Soc.* **1991**. *113*, 3623.

[246] Bochmann, M.; Lancaster, S. J.; Hursthouse, M. B.; Malik, K. M. A. *Organometallics* **1994**. *13*, 2235.

[247] Gómez, R.; Green, M. L. H.; Haggitt, J. L. *J. Chem. Soc. Dalton Trans.* **1996**. 939.

[248] Beck, S.; Prosenc, M.-H.; Brintzinger, H.-H.; Goretzki, R.; Herfert, N.; Fink, G. *J. Mol. Catal. A: Chem.* **1996**. *111*, 67.

[249] Bazan, G. C.; Cotter, W. D.; Komon, Z. J. A.; Lee, R. A.; Lachicotte, R. J. *J. Am. Chem. Soc.* **2000**. *122*, 1371.

[250] Beck, S.; Lieber, S.; Schaper, F.; Geyer, A.; Brintzinger, H.-H. *J. Am. Chem. Soc.* **2001**. *123*, 1483.

[251] Liu, Z.; Somsook, E.; Landis, C. R. *J. Am. Chem. Soc.* **2001**. *123*, 2915.

[252] Chen, M.-C.; Roberts, J. A. S.; Marks, T. J. *J. Am. Chem. Soc.* **2004**. *126*, 4605.

[253] Li, H.; Li, L.; Schwartz, D. J.; Metz, M. V.; Marks, T. J.; Liable-Sands, L.; Rheingold, A. L. *J. Am. Chem. Soc.* **2005**. *127*, 14756.

[254] Yang, X.; Stern, C. L.; Marks, T. J. *J. Am. Chem. Soc.* **1994**. *116*, 10015.

[255] Al-Humydi, A.; Garrison, J. C.; Mohammed, M.; Youngs, W. J.; Collins, S. *Polyhedron* **2005**. *24*, 1234.

[256] Bondi, A. *J. Phys. Chem.* **1964**. *68*, 441.

[257] Nag, S.; Banerjee, K.; Datta, D. *New J. Chem.* **2007**. *31*, 832.

[258] Batsanov, S. S. *Inorg. Mater.* **2001**. *37*, 871.

[259] Mantina, M.; Chamberlin, A. C.; Valero, R.; Cramer, C. J.; Truhlar, D. G. *J. Phys. Chem. A* **2009**. *113*, 5806.

[260] Bouwkamp, M. W.; de Wolf, J.; del Hierro Morales, I.; Gercama, J.; Meetsma, A.; Troyanov, S. I.; Hessen, B.; Teuben, J. H. *J. Am. Chem. Soc.* **2002**. *124*, 12956.

[261] Bouwkamp, M. W.; Budzelaar, P. H. M.; Gercama, J.; Morales, I. D. H.; de Wolf, J.; Meetsma, A.; Troyanov, S. I.; Teuben, J. H.; Hessen, B. *J. Am. Chem. Soc.* **2005**. *127*, 14310.

[262] Basuli, F.; Aneetha, H.; Huffman, J. C.; Mindiola, D. J. *J. Am. Chem. Soc.* **2005**. *127*, 17992.

[263] Chapman, A. M.; Haddow, M. F.; Wass, D. F. *J. Am. Chem. Soc.* **2011**. *133*, 18463.

[264] Metters, O. J.; Forrest, S. J. K.; Sparkes, H. A.; Manners, I.; Wass, D. F. *J. Am. Chem. Soc.* **2016**. *138*, 1994.

[265] Michiue, K.; Jordan, R. F. *J. Mol. Catal. A: Chem.* **2008**. *282*, 107.

[266] Stephan, D. W.; Stewart, J. C.; Guérin, F.; v. H. Spence, R. E.; Xu, W.; Harrison, D. G. *Organometallics* **1999**. *18*, 1116.

[267] Yue, N.; Hollink, E.; Guérin, F.; Stephan, D. W. *Organometallics* **2001**. *20*, 4424.

[268] Shi, X.-C.; Jin, G.-X. *Organometallics* **2012**. *31*, 7198.

[269] Burger, B. J.; Bercaw, J. E. Vacuum Line Techniques for Handling Air-Sensitive Organometallic Compounds. In *Experimental Organometallic Chemistry: A Practicum in Synthesis and Characterization*, vol. 357 (American Chemical Society, Washington, D.C., **1987**).

[270] Matson, E.; Forrest, W.; Fanwick, P.; Bart, S. *Organometallics* **2012**. *31*, 4467.

[271] Crimmin, M. R.; Arrowsmith, M.; Barrett, A. G. M.; Casely, I. J.; Hill, M. S.; Procopiou, P. A. *J. Am. Chem. Soc.* **2009**. *131*, 9670.

[272] Pohlmann, J.; Brickmann, F. *Z. Naturforsch* **1965**. *B20*, 5.